UNIVERSITÀ DEGLI STUDI DI PALERMO
DIPARTIMENTO DI INGEGNERIA INDUSTRIALE

INVESTIGATION OF THE INDENTATION BEHAVIOUR OF FOAM CORED LIGHTWEIGHT COMPOSITE SANDWICHES

Tesi di Dottorato di Ricerca

di

João Pedro GUIMARÃES AMORIM

February 2010

XXI CICLO - DOTTORATO DI RICERCA IN PROGETTAZIONE MECCANICA

Settore scientifico disciplinare: ING-IND/14

UNIVERSITÀ DEGLI STUDI DI PALERMO
DIPARTIMENTO DI INGEGNERIA INDUSTRIALE

INVESTIGATION OF THE INDENTATION BEHAVIOUR OF FOAM CORED LIGHTWEIGHT COMPOSITE SANDWICHES

Tesi di Dottorato di Ricerca

di

João Pedro GUIMARÃES AMORIM

Tutor
Ing. Giuseppe PITARRESI

Coordinatore del Dottorato
Prof. Gabriele VIRZÍ MARIOTTI

XXI CICLO - DOTTORATO DI RICERCA IN PROGETTAZIONE MECCANICA

Settore scientifico disciplinare: ING-IND/14

ACKNOWLEDGEMENTS

The following words are of gratitude to those who in different ways and moments shared with me the road to complete the work here presented.

To my supervisor, Dr. Giuseppe Pitarresi for his orientation, patience and encouragement throughout all these years, even in moments where things seemed far away from a promising result. For his scientific dedication, for having transmitted me the values of excellence, critical sense and having always trusted in my capacities to accomplish my doctoral work. Lastly but not less important, for his valuable friendship.

To Professor Gabriele Virzì Mariotti, Ph.D. coordinator, for his guidance throughout the project.

To my friends from the University of Palermo for the cheerful environment and for the pleasure and enjoyable moments lived during my staying periods in Sicily. A special acknowledgement to Dr. Davide Tumino and Dr. Michele Scafidi.

To my colleagues and Professors from the Marie Curie Research Training Network MOMENTUM. My gratitude to European Union for the Marie Curie fellowship, giving me the opportunity to grow professionally and personally.

To my colleagues in CRF, with a special thanks to Eng. Giuseppe Ieropoli and Davide Fulcheri for their advising on meshing and numerical simulation.

To my friends from Turin: Paolo, Raquel, Raul, Alessandro, Joana, Rute, Michele, Rui, Maria João, Carolina, Mario, Sara, Filipa, Andrea...for their good spirit and for making me feel a bit more “at home”.

To my long-lasting friends from Portugal, Nuno, Celeste, Patrícia, Cila, Marco, Luísa, Zé Miguel, Julinho, Miguel, Ricardo, Baião, Lalo, Eduardo,...who always received “o emigra” with the happiness and enthusiasm of the genuine friendship.

To my Mother and my Father, to my Sister Maria Luís and my Brother Zé Manel, for their love, encouragement and strength to carry on my Ph.D. and successfully complete this life cycle.

To Elisa my love, for her dedication and comprehension, and for having been at my side in the most critical period of my Ph.D.

To my Grandmother Ana, passed away in 2010, and to Whom this Thesis is dedicated.

ABSTRACT

The present thesis work has been performed within the framework of research activities of a Marie Curie Research Training Network: MOMENTUM - Multidisciplinary Research and Training on Composite Materials Applications in Transport Modes. This network has been funded by the EU under the Framework Programme 6 (Contract Number: MRTN-CT-2005-019198). The author of this thesis in particular has received a Marie Curie grant to serve as an Early Stage Researcher (ESR) at Centro Ricerche FIAT (CRF) in Orbassano (Torino, Italy).

The involvement of CRF in MOMENTUM was in particular allocated in the work-package 1 (WP1), focused on the development of "New Materials Concepts Suitable for high volume production". According with the MOMENTUM project plan (outlined in the Annex 1 of the project), this research activity has been also carried out in cooperation with the University of Palermo (UniPa), with UniPa acting as leader of the MOMENTUM WP1. One of the purposes of this cooperation was to perform part of the research towards the award of the PhD title in "Progettazione Meccanica" to the ESR author of this thesis.

In light of the above mentioned context, an important preliminary part of the activity performed at CRF was focused on the R&D of suitable lightweight composite sandwich panel solutions for Body in White applications in general, and for the realisation of hoods structures in particular. The strict constraints introduced by high volume mass production on the one side, and by End of Life vehicle regulations on the other, have sensibly restricted the range of sandwich constituent materials and manufacturing solutions with potentials in fulfilling the

automotive sector requirements. In particular it was found that thermoplastic polymer based sandwich constituents offer the most advantageous compromises in terms of processability and end-of-life disposal. Fully thermoplastic sandwich concepts employing thermoplastic foam cores and glass fibre reinforced thermoplastic matrix skins have then been selected as a favourable potential combination for automotive body-in-white sandwich applications.

Some most important structural design issues regarding hoods applications in particular comprise the achievement of sufficient torsional and flexural stiffness, and the achievement of good indentation strength under localised loading. Since foam cored sandwich panels in general and thermoplastic foam cores in particular have low stiffness in the through-thickness direction, a main issue in the use of these materials is then represented by the modelling of their indentation behaviour.

The research work comprised in this thesis has focused on the study of the indentation failure mode on foam cored sandwich structures. A thorough literature review on analytical and numerical approaches to model the indentation behaviour in foam cored sandwich structures is proposed highlighting the role of the different constitutive behaviours exhibited by different commercial foam core materials. It has been found that indentation is an important failure mode typical of sandwiches with transversely flexible core materials, such as low density polymer foams. Furthermore localised loading can be a rather common occurrence at joining sites, or by external events such as low velocity impacts, and indentation induced permanent damages can have many important implications on the residual load bearing capabilities of a sandwich structure.

In this work a generalised analytical approach is presented based on the Winkler foundation theory, to investigate the development of permanent indentation damage in sandwich beams under concentrated loads. A Segment-Wise model is implemented to the case of fully backed sandwich beams with polymeric foam cores exhibiting generic non-linear compressive behaviours, as typically observed in low density thermoplastic foams. The non-linear load *vs.* displacement uniaxial compression curve of the foam is discretised by a succession of linear segments, providing the material constitutive behaviour and

the boundary conditions needed to solve the general fourth order differential equation expressing the equilibrium of the indented face skin. The study presents some closed form analytical solutions to derive the indentation curve for simplified foam compression behaviours: elastic-perfectly-plastic, bilinear and bilinear-perfectly-plastic, extending the prediction capabilities of actual indentation models and working itself as an organic compendium of all those approaches based on the implementation of the Winkler theory to study indentation. A general analytical solution is also derived for the prediction of the critical load at which flexural failure of the sandwich skins is expected to occur.

Experimental validation of the method is performed on industrial materials, exhibiting peculiar non-linear compressive behaviours most of which employing thermoplastic based materials, demonstrating the potentials of the method to deal with actual and interesting sandwich solutions, appealing to those industrial sectors which always seek the use of lightweight sustainable materials. The proposed models are found to give a better match of the experimental data than the classic elastic-perfectly-plastic model and significantly improve the indentation curve prediction whenever the foam compression behaviour presents an hardening, softening or a marked non-linear trend in the post-elastic high deformation range of the foam uniaxial compression curve.

A final chapter of this thesis is also devoted to present a FEA modelling strategy to study the structural behaviour of sandwiches adopting low density fully thermoplastic foam cores. The behaviour of the considered foam materials has in particular been resembled to a hyperelastic behaviour. The ABAQUS code was then chosen and non-linear analyses performed exploiting the availability of a hyperelastic constitutive model suitable for foams: HYPERFOAM. The developed FEA models in particular simulate three behaviours: the indentation of a fully backed sandwich beam, the deformation of a beam under a three point bending configuration, the behaviour of a foam block under repeated uniaxial compression at various load levels. All simulated cases and the tuning of the numerical models have been supported and compared with experimental data.

THESIS OUTLINE

This doctoral thesis is organized into seven chapters described as follows:

Chapter I, **Introduction**, proposes a literature review covering all fundamental aspects related to indentation of composite sandwich structures, focusing on analytical models. The main contributions in past literature and the state of the art are presented in a straightforward and schematic manner highlighting virtues and disadvantageous for the different theoretical approaches.

Chapter II addresses the **Analytical developments** using the theoretical approach proposed on this research. A generalised method, able to consider foam cores with generic non-linear behaviours, to analytically model the indentation behaviour of fully backed sandwich beams under local loading is implemented and confronted with some of the theories reviewed in chapter I. Furthermore a generalised procedure to predict bending skin failure is also presented whose results compare well with those obtained in the literature with similar but less general procedures.

Chapter III describes the **Laminates and foams experimental characterization** performed in this work to evaluate the effectiveness of the analytical approach proposed. In this chapter only the sandwich constituent parts are described and characterised, i.e. the laminate and foam materials used as sandwich face sheets and cores. Tensile and flexural mechanical tests for the

laminates and compressive and shear tests for the foams are implemented and measured properties analysed.

Chapter IV presents the **Sandwich experimental characterization**. The manufacturing and characterisation of sandwich beams adopting different materials is evaluated via three-point bending tests, and experimental indentation curves are assessed for a fully backed configuration. In addition a correction method is proposed to account for the local indentation displacement in the evaluation of the flexural and shear rigidity of sandwich beams performed with variable span three-point bending tests.

Chapter V is devoted to **Results and discussion** validating the method proposed in chapter II with experimental observations from chapter IV. Foam core *Segment-Wise* (SW) constitutive parameters are calculated by fitting of the experimental uniaxial compressive curves performed on foam materials. Theoretical predictions for sandwiches presenting different core behaviours are confronted with experimental indentation curves. Top face sheet failure load predictions developed for elastic-perfectly-plastic and bilinear pattern behaviours are as well confronted with experimental results.

Chapter VI proposes a **Numerical simulation with highly non-linear foam cores** of the indentation process in sandwich beams. Constitutive models from a commercially available finite element analysis code (ABAQUS) are calibrated with the experimental results from chapter III and validated for predicting the indentation behaviour of samples tested in chapter IV employing a non-linear foam core.

Chapter VII, **Concluding remarks**, draws the major findings of the thesis and outlines future research topics on this area.

Appendix A is an overview to some of the main expressions used in classical beam theory on sandwich beams subjected to flexural loads and presents the development steps for the differential governing equation for indentation modelling on fully backed and simply supported sandwich beams. Through

Appendix B, an extensive collection with the general solutions for the indentation governing equation, boundary conditions and final systems of equations is provided. **Appendices C** and **D** contain part of the most important MATLAB® and ABAQUS® routines compiled during this research study.

ABBREVIATIONS AND NOTATIONS

The following list contains some of the principal abbreviations and notations used throughout this thesis. Other abbreviations and notations less cited and not mentioned here are defined in the text when appearing.

Abbreviations:

2D	Two Dimensional
3D	Three Dimensional
ASTM	American Society of Testing and Materials
BC	Boundary Conditions
BL	Bilinear
BL_h	Bilinear with Hardening
BL_s	Bilinear with Softening
BS	British Standards
BLPP	Bilinear-Perfectly-Plastic
CAD	Computer Aided Design
CFCs	Chlorofluorocarbons
DIN	German Institute for Standardization
E	Pure Linear Elastic
EPP	Elastic-perfectly-plastic
EPS	Expanded Polystyrene
EVA	Ethylene Vinyl Acetate

FB	Fully Backed
FE	Finite Element
FEA	Finite Element Analysis
FPB	Four Point Bending
GFRP	Glass Fibre Reinforced Polymer
HOSPT	Higher Order Sandwich Panels Theory
ISO	International Organisation for Standards
NAEC	Naval Air Engineering Center
PA	Polyamide
PBT	Polybutylene Terephthalate
PEI	Polyetherimide
PMI	Polymethacrylimide
PP	Polypropylene
PS	Polystyrene
PU	Polyurethane
PVC	Polyvinyl Chloride
RPP	Rigid-Perfectly-Plastic
RTM	Resin Transfer Molding
SMCs	Sheet Moulding Compounds
SW	Segment-Wise
USFPL	U.S. Forest Products Laboratory
TPB	Three-Point Bending
VARTM	Vacuum-assisted Resin Transfer Moulding
VDA	*Verband der Automobilindustrie*
VOC	Volatile Organic Compound
XPS	Extruded Polystyrene

Notations:

In some parts of the text or images it may occurs that the same symbol is applied to different descriptions or that for the same description a different symbol is used. Those local situations will be always mentioned in the text.

Symbol	Description	Unit
a, s	Half-length of plastic core region	[mm]
b	Width of the beam	[mm]
δ, α	Vertical mid-point deflection or indentation	[mm]
d	Distance between the centroids of the faces ($d=t_c+t_f$)	[mm]
D	Sandwich flexural stiffness	[N.m^2]
D_f	Face sheet or skin flexural stiffness	[N.mm^2]
ε_c	Strain value at the onset of core plastic deformation	[mm/mm]
E_c	Compression Young's modulus of the core	[MPa]
E_f	Young's modulus of the face sheet	[MPa]
G_c	Shear modulus of the core	[MPa]
h	Sandwich total thickness	[mm]
I_f	Second moment of inertia of top face sheet	[mm^4]
k	Foundation stiffness	[MPa]
l	Length	[mm]
L	TPB outer span	[mm]
M_s	Top skin bending moment	[N.mm]
P	Load	[N]
q	Foundation load reaction per unit length	[N/mm]
ρ_c	Density (mass/unit volume)	kg/m^3
σ_c, σ_p	Compressive strength or yield stress of the core (*plateau*)	[MPa]
σ_f	Flexural strength of the top face-sheet	[MPa]
τ_c	Shear strength of the core	[MPa]
t_c	Core thickness	[mm]
t_f	Face sheet or skin thickness	[mm]

T_s	Top skin shear force	[N]
U	Sandwich shear rigidity	[N]
w_e	Elastic vertical face sheet deflection	[mm]
w_p	Plastic vertical face sheet deflection	[mm]

TABLE OF CONTENTS

ACKNOWLEDGEMENTS ..... **i**

ABSTRACT ..... **iii**

THESIS OUTLINE ..... **vii**

ABBREVIATIONS AND NOTATIONS ..... **xi**

CHAPTER I – Introduction **7**

1.1 Sandwich structures: The concept 7

1.2 Sandwich structures: Historical review 8

1.3 Sandwich structures: most common constituent materials 12

1.4 Collapse mechanisms in sandwich structures 15

1.4.1 Face microbuckling failure 18

1.4.2 Face wrinkling failure 18

1.4.3 Core shear failure 18

1.4.4 Core indentation failure 19

1.5 Literature review of indentation analytical models 19

1.6 Indentation of sandwich beams using the Winkler approach 21

1.6.1 *Fully-backed* sandwich beam and concentrated load 22

1.6.2 Simply supported sandwich beams loaded in *three-point bending* 27

1.6.3 Edge clamped sandwich beams loaded in *three-point bending* 29

1.6.4 Winkler theories synopsis 30

1.7 Scope of the research 32

CHAPTER II - Analytical developments 35
2.1 Introduction 35
2.2 The *Segment-Wise* model 35
2.2.1 Pure-elastic and elastic-perfectly-plastic solutions 45
2.2.2 Bilinear solution 47
2.2.3 Bilinear-perfectly-plastic solution 49
2.3 Failure load at face sheet fracture 52

CHAPTER III - Laminates and foams experimental characterization 55
3.1 Introduction 55
3.2 Sandwich constituent materials 56
3.2.1 Laminate materials for the skins 56
3.2.1.1 *In-house* laminate panels 57
3.2.1.2 Commercial laminate panels 58
3.2.2 Foam materials for the core 60
3.3 In-plane tensile laminate properties 64
3.3.1 Experimental apparatus and test coupons 64
3.3.2 Results and discussion 67
3.4 Flexural laminate properties 69
3.4.1 Experimental apparatus and test coupons 69
3.4.2 Results and discussion 70
3.5 Flatwise compressive foam properties 71
3.5.1 Experimental apparatus and test coupons 71
3.5.2 Results and discussion 72
3.6 Shear foam properties 76
3.6.1 Experimental apparatus and test coupons 76
3.6.2 Results and discussion 78

CHAPTER IV - Sandwich experimental characterization 81
4.1 Introduction 81
4.2 Sandwich beams preparation 81
4.3 Three-point bending test 83
4.3.1 Experimental method and test specimens 84

4.3.2 On the influence of elastic indentation in sandwich TPB tests 87
4.3.3 TPB tests: results and discussion.....90
4.4 Indentation tests 95

CHAPTER V - Validation of the *"Segment-Wise"* model: results and discussion 99
5.1 Introduction.....99
5.2 Evaluation of the foam core *SW* constitutive parameters.....99
5.2.1 Discretisation of the PMI 31 compression curve 100
5.2.2 Discretisation of the PA Zotek® N B50 compression curve 101
5.2.3 Discretisation of the ThermoTec® XPS compression curve 103
5.3 Evaluation of the analytical indentation curves 105
5.3.1 Sandwich specimen w/ a classical crushable core presenting a plateau.105
5.3.2 Sandwich specimen with an hyperelastic core 106
5.3.3 Sandwich specimen w/ a crushable core presenting an hardening behaviour 107
5.4 Evaluation of the failure load at face sheet fracture.....109
5.4.1 Solution for an elastic-perfectly-plastic core behaviour.....110
5.4.2 Solution for a bilinear generic core behaviour 114

CHAPTER VI – Numerical simulation with highly non-linear foam cores .117
6.1 Introduction.....117
6.2 Modelling of polymeric foams behaviours with ABAQUS.....118
6.3 Ogden's strain energy model 120
6.4 Hyperfoam fitting parameters 122
6.5 Case studies using the ABAQUS hyperfoam formulation.....125
6.5.1 Simulation of an indented fully-backed beam sandwich.....126
6.5.1.1 Model and analysis definitions.....126
6.5.1.2 Output results and discussion 128
6.5.2 Numerical simulation of a TPB test on a beam sandwich employing a non-linear foam core 131
6.5.2.1 Model and analysis definitions.....131
6.5.2.2 Output results and discussion 133

6.5.3 Modelling Mullins effect in elastomeric foams with ABAQUS 136
6.5.3.1 Mullins concept and experimental proofing 136
6.5.3.2 Simulation of Mullins effect on a PA Zotek® foam slab model 139
6.5.3.2.1 Model and analysis definitions 139
6.5.3.2.2 Results and discussion 140

CHAPTER VII - Concluding remarks 143

APPENDIX A - Classical beam theory 149
A1. Differential equation modelling indentation on *FB* sandwich beams 150
A2. Differential equation modelling indentation on simply supported sandwich beams 152
A3. Stiffness of simply supported sandwich beams 154
A4. Moment equation in a beam with mid-plane symmetry subjected to a transverse load 157

APPENDIX B - *Segment-Wise* Model Configurations 159
B1. General Solutions for the indentation governing equation 160
B1.1 Pure elastic segment 160
B1.2 Elasto-plastic segments with hardening 160
B1.3 Elasto-plastic segments with softening 161
B1.4 Perfectly-plastic segment 161
B2. Boundary Conditions for the n^{th} *Segment-Wise* segments 162
B2.1 Pure elastic segment 162
B2.2 Elastic-perfectly-plastic segments 163
B2.3 Bilinear segments with hardening 165
B2.4 Bilinear segments with softening 167
B2.5 Bilinear-perfectly-plastic segments 170
B3. Systems of Equations for the n^{th} *Segment-Wise* segments 173
B3.1 Pure elastic segment 173
B3.2 Elastic-perfectly-plastic segments 173
B3.3 Bilinear segments with hardening 174
B3.4 Bilinear segments with softening 175

B3.5 Bilinear-perfectly-plastic segments 176

APPENDIX C - MATLAB® scripts 181

C1. Modelling of an indented fully-backed beam sandwich.....182

C1.1 Definition of the sandwich material properties and *SW* parameters.....182

C1.2 Linear and bilinear load-deflection curves and face sheet bending failure load prediction.....182

C1.3 Elastic-perfectly-plastic load-deflection curve and face sheet bending failure load prediction 183

C1.4 Bilinear-perfectly-plastic load-deflection curve.....184

C1.5 Comparison of critical load predictions at face bending skin failure 185

C2. Defining the compression foam behaviour.....187

C2.1 Elastic Perfectly Plastic function (MATLAB M-file *EPPmodel.m*) 187

C2.2 Bilinear function (MATLAB M-file *EEmodel.m*).....188

C2.3 Bilinear Perfectly Plastic function (MATLAB M-file *EEPPmodel.m*)..189

APPENDIX D - ABAQUS® scripts 191

D1. Indentation on a fully-backed beam sandwich.....192

D1.1 Main file: Sandwich indentation input file (*2Dindentation.inp*).....192

D1.2 Include file: Face sheet material definition (*material.inp*).....195

D1.3 Include file: Flat support analytical surface definition (*supportAS.inp*) 195

D1.4 Include file: Cylindrical indenter analytical surface definition (*indenterAS_D25.inp*).....195

D1.5 Include file: Contact definitions (*contact-02.inp*) 196

D2. *TPB* test on a beam sandwich employing a non-linear foam core 196

D2.1 Main file: Sandwich beam model (*model_03.inp*) 196

D2.2 Include file: Cylindrical indenter and supports (*supports_impactorTPB-L230.inp*) 198

D2.3 Include file: Contact definitions (*contact-01.inp*) 198

D3. Mullins effect on a PA Zotek® foam slab model 199

D3.1 Main file: Polyamide foam input file (*PA_uniaxial_compress.inp*) 199

D3.2 Include file: Mullins test data - 1x3 cycles (*Mullins_calibrate_testdata.inp*).....201

D3.3 Include file: Contact definitions (*contact.inp*) 202
D3.4 Include file: Flat indenter and flat support (*impactor.inp*) 202

PUBLICATIONS 205
BIBLIOGRAPHIC REFERENCES 207

CHAPTER I

Introduction

1.1 Sandwich structures: The concept

Paraphrasing the American Society of Testing and Materials (ASTM) definition of sandwich:

"A structural sandwich is a special form of laminated composite comprising of a combination of different materials that are bonded to each other so as to utilise the properties of each separate component to the structural advantage of the whole assembly".

In a sandwich two thin, stiff and strong faces are separated by a thick, light and weaker core. The faces, which can be of different thickness on each side, take up the most of the normal stresses in the structure and are attached to the core, assuring a load transfer between the components and counteracting the external bending moment. The core resists most of the shear stresses and stabilises the faces against global and local instabilities (e.g. buckling or wrinkling). In order for the sandwich concept work and the two skins effectively cooperate, a perfect attach between the skins and the core is needed. A sandwich beam adopts the same principle of an I-Beam to save weight by using the material in a more effective way. In a sandwich the faces take the place of the flanges and the core takes the place of the web. A high bending stiffness is obtained by placing the stiff material in the faces far from the neutral axis. The scheme in figure 1.1 compares stiffness and weight for different configurations of a sandwich panel obtained by varying the core thickness and leaving the other parameters unchanged. It is verified that a substantial increase in the panel stiffness can be obtained by

increasing the core thickness with only a slight increment in the panel weight. In figure 1.1 is also interesting to observe the incremental stiffness and strength by using a sandwich construction in comparison with a monocoque (thin walled) construction with the same face weight (i.e. the same face sheet material but with a face thickness double of each face sheet used in the sandwich). It is therefore clear that a sandwich beam of the same width and similar weight as a solid beam has remarkably higher stiffness due to its higher moment of inertia [1-5, 6].

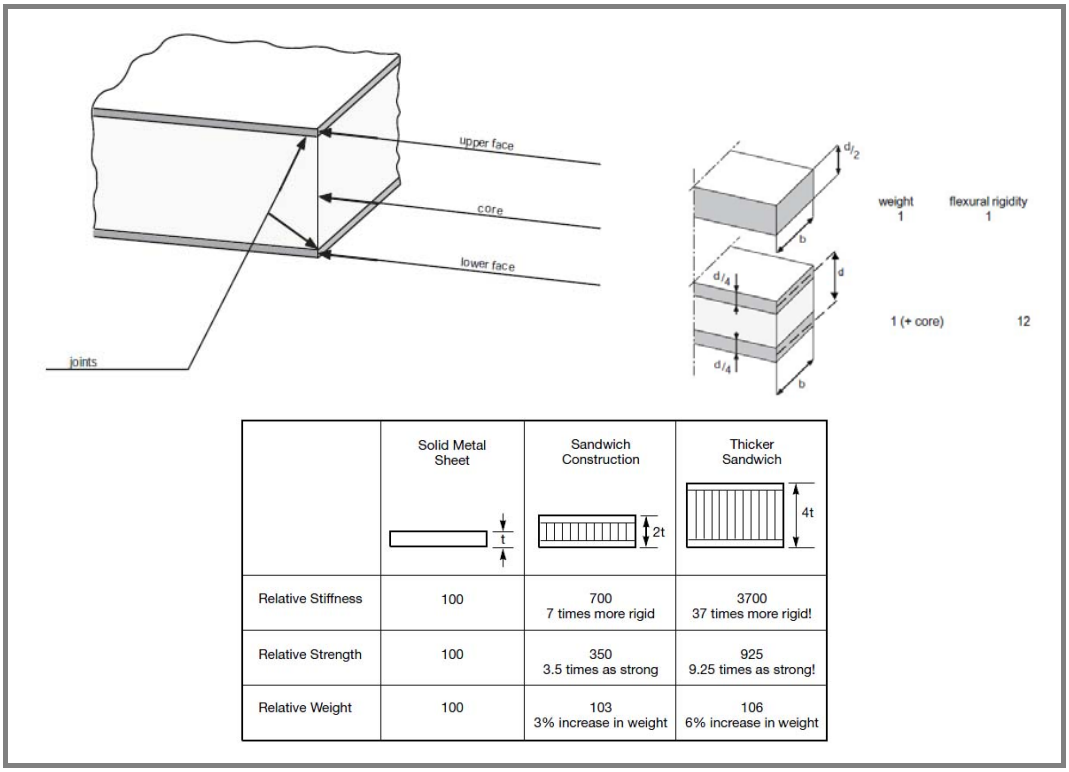

	Solid Metal Sheet	Sandwich Construction	Thicker Sandwich
	t	2t	4t
Relative Stiffness	100	700 7 times more rigid	3700 37 times more rigid!
Relative Strength	100	350 3.5 times as strong	925 9.25 times as strong!
Relative Weight	100	103 3% increase in weight	106 6% increase in weight

Figure 1.1 Influence of the core thickness on stiffness and weight of a sandwich panel [7].

1.2 Sandwich structures: Historical review

A general consensus about when sandwich construction was first used is not easy to find in the literature. More consensual is that first results of research presented in a unified manner and with a coherent system of notation were reported in the late ‘60s with the publication of the two reference books: Allen [1] and Plantema [2] and later on in 1974 by Stamm and Witte [3]. Another milestone in sandwich publications was the publication by Zenkert [4] in 1995, covering most of the classical theory aspects treated by Allen [1] and Plantema [2] but

employing a more practical and problem solving approach. In 1999, Vinson [5] publishes another important book where he applies the laminate theory to sandwich structures. Up to date these works continue to be the reference manuals to those engineers, designers and analysts who seek the advantages of the concept of combining different materials as in a sandwich. Even though the ‘60s are considered the “boom decade” in terms of sandwich applications and publications regarding sandwiches structures, it was towards the completion of the Second World War that some of the first theoretical works on sandwich constructions were published. Among the pioneers, Zenkert [4] mentions the work of Gough, Elam and de Bruyne from 1940 [8] about “The Stabilization of a Thin Sheet by a Continuous Supporting Medium”, and that of Williams, Leggett and Hopkins about “Flat Sandwich Panels under Compressive end loads” in 1941 [9]. According to Vinson [5,10] the first research paper concerning sandwich construction was due to Marguerre [11], in 1944 and it dealt with in-plane compressive loads. This illustrates how difficult is to produce a general consensus about who was the first person to publish a work on sandwich structures. What should be relevant is that many others followed such as the article from Hoff [12] in 1950 where he derives the differential equations and boundary conditions for bending and buckling of sandwich plates using the principle of virtual displacements and the case studies presented in 1949 by Flügge [13] with solutions for (1) the geometric dimension and the core properties for a given compression load and minimum weight; (2) the geometrical dimension and core properties for a given weight and maximum compressive load; and (3) the ultimate strength of a given sandwich [5].

During the early post World War Two period, the U.S. Forest Products Laboratory (USFPL) was the primary group in the development of analysis and design methods for sandwich structures, being the promoter for some of the most significant publications on sandwich research during that period [14-19]. Also from this period, and thanks to Reissner [20], was developed the theory on sandwich plates which derives the differential equation for deflection of a sandwich panel. Libove and Batdorf [21] derived differential equations for the deflection and shear forces in orthotropic panels with thin faces, and Mindlin [22]

derived the governing equation of motion for an isotropic plate accounting for both transverse shear deflections and rotary inertia.

By the mid '60s, the Naval Air Engineering Center (NAEC) sponsored research to develop a fibreglass-sandwich construction to compete in weight with conventional aluminium construction for aircraft structures [5, 8]. Much of its effort was in minimum-weight optimization of the sandwich to weight less than the aluminium construction for the same load conditions [23-28]. In Vinson and Shore [23] it is provided a bibliography describing over 250 publications regarding sandwich construction before 1966. More recently, was published in 1986 a test containing many of the landmark papers on sandwich construction written by Hoff's [29]; in 1989 Ha [30] provided a review on finite element analysis applied to sandwich plates; in 1991 Bert [31] provides a review of sandwich plate analysis and in 1996 Bert co-published with Noor and Burton [32] a review providing over 800 references discussed and another 599 references as a supplemental bibliography where they report the concept of sandwich construction back to Fairbairn in 1849 [33]. Indeed, the first known applications of sandwich panels reverse to the World War One and World War Two period. In the World War One sandwich panels of asbestos faces with a fibreboard core were used and prior to World War Two some use was made of sandwich panels in small planes. However, it was the invention and widespread acceptance of structural adhesives in England and the United States in the 1930s that allowed the application of bonded sandwich composites. The pre-war Havilland Albatross airplane designed for an experimental transatlantic service had a sandwich fuselage and with the Mosquito aircraft, produced in England during the World War Two, sandwich panels were for the first time produced in a mass scale production, using veneer faces with a balsa core to fulfil the shortage of the standard build materials [4]. Vinson [5, 10] states that already in 1943, Wright Patterson Air force Base designed and fabricated the Vultee BT-15 fuselage using fiberglass-reinforced polyester as faces and glass-fabric honeycomb and balsa-wood as core. This way, in the middle of the 20^{th} century the use of sandwich materials increased substantially, in part merit of the military and civil aeronautic sector and aerospace applications that were the first ones to show interest on these

concept. The first honeycomb cores and face sheet made of laminate composites were used in parts of the fuselage, floors, side panels and ceiling of some of the most known commercial aircrafts build in the second half of the last century and many of them still in use up to date.

Military naval honeycomb-sandwich bulkheads, deck houses and helicopter hangars by the US Navy or even complete hulls of large navy ships such as the TV171/TV172 built for the Swedish Coast Guard and the Landsort mine sweeper class from the Royal Swedish Navy are excellent examples of sandwich application in critical structures. Further more recent examples are the 72-meter Swedish Navy YP2000 Visby, whose hull is completely made in carbon-epoxy sandwich panels, or the ferry boats used in the Scandinavian countries. Showing an increasing interest on these materials is also the mass transport sector for the lightweight design of large ground transportation vehicles such as trains and passengers or cargo vehicles. The XPT locomotives in Australia, the ETR500 in Italy, the 2000 Swiss locomotive and the French TGV substantially reduced their weights by adopting parts made of sandwich structures, and in Japan the Nozomi 500 bullet train uses a honeycomb sandwich for some of its primary structure components. Less known but with good perspectives of development is the use of sandwich structures in civil engineering applications, such as rehabilitation of bridge decks, wall and roof isolating cladding panels and low cost or emergency housing [5, 10]. The better knowledge of the sandwich concept and of its mechanical behaviour has led to a strong development in the last 20 years resulting on an increasing number of sandwich concept solutions and applications. Wind and green energy industry, packaging, leisure and sporting industry (e.g. sailboats, snow and water skis, canoes, tennis rackets, bicycles, etc), racing competitions (e.g. race boats, racing cars) and medical area are all sectors offering ground and market potentials for the further exploitment of this material concept.

1.3 Sandwich structures: most common constituent materials

A real turning point for the success and more widespread adoption of sandwich structures was represented by the use of polymer composite materials, allowing significant weight savings while providing a high degree of design flexibility. In the same way the variety of core solutions proposed nowadays, adopting different types of structures, geometries and innovative materials is a stimulus for the optimisation of sandwich structural applications (see figure 1.2).

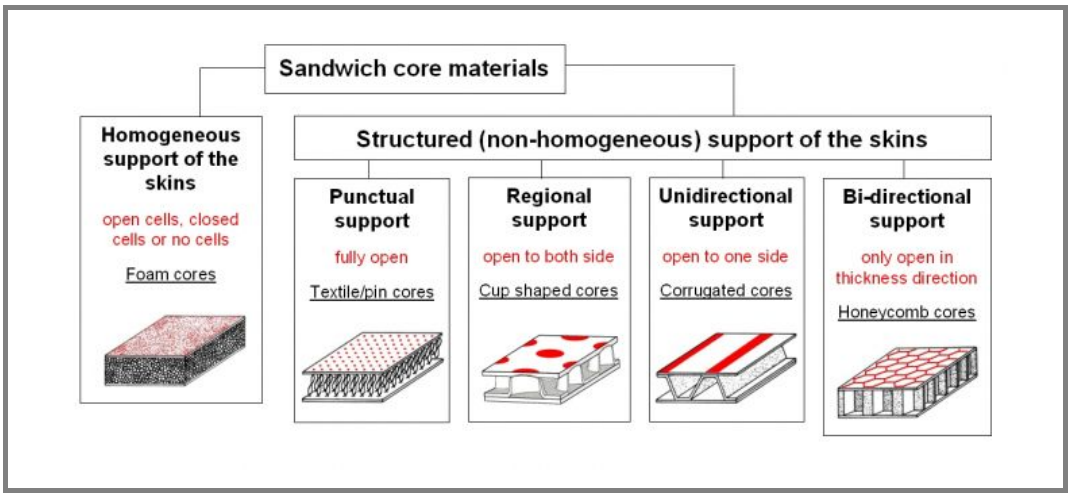

Figure 1.2 Sandwich concept depending on the type of core applied [34].

New honeycombs made of thermoplastic polymers, rather than oriented cell structure foams are just a few examples of the wide variety of core material options available for design. In light of this rich variety of material solutions, the successful design of sandwich structures is highly dependent on the feasibility of manufacturing methods. In fact the proper assembling of materials in a sandwich structure is the key aspect influencing costs, environmental and wear resistance, surface finish, interaction with external loads, damage tolerance and strength, etc. Generically, the properties of primary interest for the faces can be resumed to high stiffness and high flexural rigidity, high tensile and compressive strength, impact resistance, surface finish, resistance to chemical, weather agents and wear resistance. For the core the properties of primary interest are low density, high

shear rigidity and strength, high compression stiffness and strength and thermal insulation of the core material [4].

A first criterion for choosing the sandwich materials is the severity of the final application, depending if it is considered as a *primary* or *secondary structure*. Primary or load carrying structures are those whose principal function is to guarantee stiffness and strength performance in severe mechanical solicitations and overall an important structural function. Examples of primary structures are vehicle frames, vessels hulls and aeronautic profiles. These applications require lightweight materials that guarantee at least the same level of performance when using the traditional materials. Commonly composite face materials used in primary structure sandwiches are long fibre reinforced carbon/epoxy, glass/epoxy or kevlar/epoxy laminates with high fibre volume fractions (e.g. autoclave cured pre-pregs) coupled with cores made of aluminium or kevlar/phenolic (Nomex®) honeycombs or high density foams.

Secondary or non-structural applications are those related to non critical functions, such as low bearing applications, aesthetic or insulating functions, panelling, etc. These applications require low cost cores and face sheet materials in parallel with low cost and high productivity sandwich manufacturing methods. Common composite face materials used in secondary structure sandwiches are low fibre volume fraction GRP (glass reinforced plastic) laminates, glass chopped strand mats and SMCs (sheet moulding compounds). Common less expensive cores generally comprise low density polymer foams (thermoplastic or thermosetting) or solid cores e.g. balsa wood. Thermosetting foams such as cross-linked polyvinyl chloride (PVC) and polyurethane (PU) foam cores are known since the ‘50s but not commercially used until 30 years later due to the softness of these early cores. Nowadays they are commonly used in low and medium cost applications. More recent foam cores are the cellular thermoplastic cores, such as expanded (EPS) and extruded polystyrene (XPS), linear PVC where properties can be tailored by orienting the cell structure and presenting enormous advantageous when thermoformed with thermoplastic face materials [4, 6].

Depending on the uniaxial compression behaviour, foams can be classified in two different ways: *crushable* foams exhibiting an *elastic-perfectly-plastic* behaviour and *hyperelastic* foams exhibiting a *non-linear* behaviour. Figure 1.3 depicts the stress *vs*. strain curve from an uniaxial compression test on a PVC foam exhibiting a classical crushable behaviour.

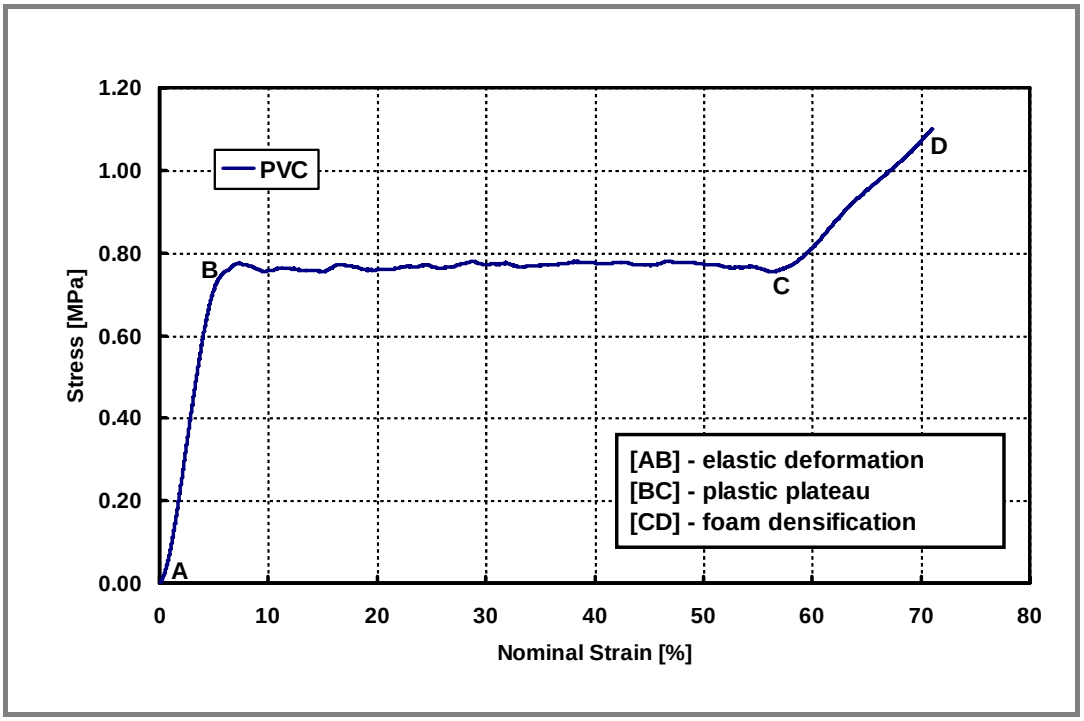

Figure 1.3 Stress *vs.* strain curve from uniaxial flatwise compression tests on a PVC AIREX® C70.55 foam exhibiting a classic three-regime crushable behaviour: [AB] *linear-elastic*; [BC] *plateau*; [CD] *densification*.

The *crushable* compression behaviour is in general described by three distinct regimes in the stress *vs*. strain curve, as exemplified with figure 1.3: in the first regime, the foam undergoes a *linear-elastic* deformation up to an elastic strain limit value (segment A-B) corresponding to the onset of core plastic deformation. At point *B* from starts the second regime or *plateau* characterized by the crushing of the foam at almost constant stress (segment B-C) up to the third regime or *densification*. Here, the foam crushed core cells start to come in contact and being compacted with a rapid increase in stiffness (segment C-D). After a complete unloading, these foams always present a significant residual strain [35].

Figure 1.4 depicts the stress *vs*. strain curve from an uniaxial compression test on a polyamide (PA) foam.

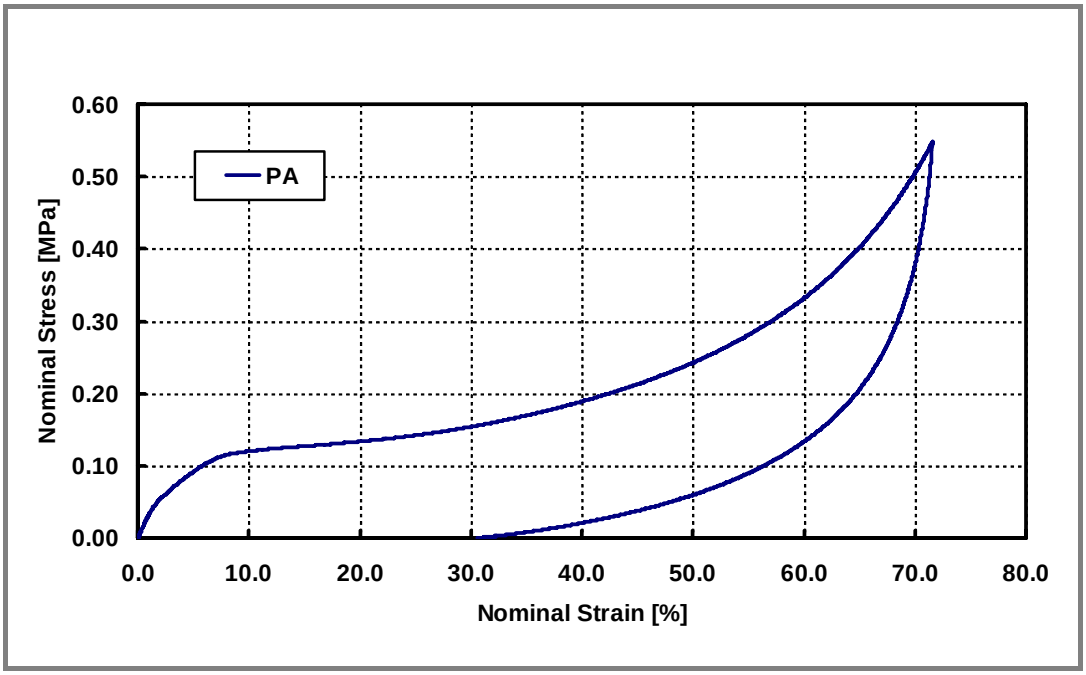

Figure 1.4 Stress *vs.* strain curve from uniaxial flatwise compression tests on a PA Zotek® foam exhibiting a non-linear hyperelastic behaviour.

As observed in figure 1.4, the hyperelastic foams exhibit a highly non-linear compression behaviour. These foams can deform elastically to large strains, up to 90% strain in compression and due to their viscoelastic properties they are able to recover almost totally its original shape, even if immediately after the compression might present some strain [36, 37].

During this work, the two types of foam behaviours here described will be recurrently mentioned and applied to several situations.

1.4 Collapse mechanisms in sandwich structures

Some typical advantages of sandwich structures include high stiffness and strength to weight ratios, vibration damping and high energy absorption capability, good thermal and acoustic insulation, etc. A main common drawback is though represented by the relatively low transverse flexibility of most core materials such as low density polymer foams. So localised loadings in particular tend to favourite some peculiar initial failure modes such as face wrinkling and

local core indentation. This requires a careful evaluation by designers since there are some typical situations where a sandwich material can experience severe concentrated forces, which include the complex loading conditions at joining sites in complex structures, the occurrence of highly concentrated loads during handling or in the rather common event of a low velocity impact with external objects, experienced by most transportation structures.

Indentation damage induced by localised loads in foam cored sandwich structures is the main topic of this work. Since it represent one of a few typical damage mechanisms, it is first of all useful to give a general review of the most recurrent failure modes in sandwich structures. Depending on the geometry of the sandwich, external loading and boundary conditions, the critical limits for the activation of some form of initial failure can be reached, compromising in that way the residual load bearing capacity of the whole structure. The most common competing failure mechanisms in sandwich beam structures are schematically sketched in figure 1.5 and some of them will be briefly analysed in the next coming sections.

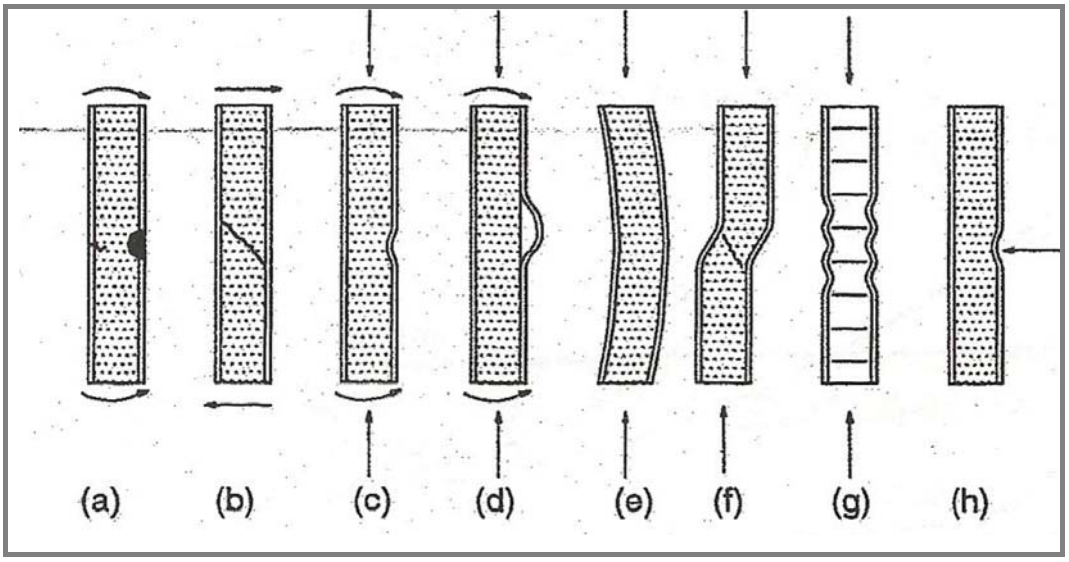

Figure 1.5 Some typical failure modes in sandwich beams. **(a)** Face yielding/fracture, **(b)** core shear failure, **(c, d)** face wrinkling, **(e)** general buckling, **(f)** shear crimping, **(g)** face dimpling, **(h)** local indentation [4].

Some researchers in the last years have tried to investigate in some systematic way the conditions leading to the activation of such collapse mechanisms, by generally choosing some reference loading conditions and

structures. For instance a beam in three-point bending is one most common basic benchmark on which to develop failure models and from which to build parametric failure maps. Steeves and Fleck [38] have investigated the three-point bending (TPB) response of simply supported sandwich beams made from glass fibre/epoxy face sheets and a polymeric foam core. Analytical predictions are derived for the TPB strength due to core shear, face microbuckling, face winkling and indentation (see figure 1.6) and applied on the construction of collapse mechanism maps and minimum weight design as a function of an appropriate structural load index and properties of the constituent materials. Experimental and numerical validation of the developed analytical expressions is shown in Steeves and Fleck, Part II [39].

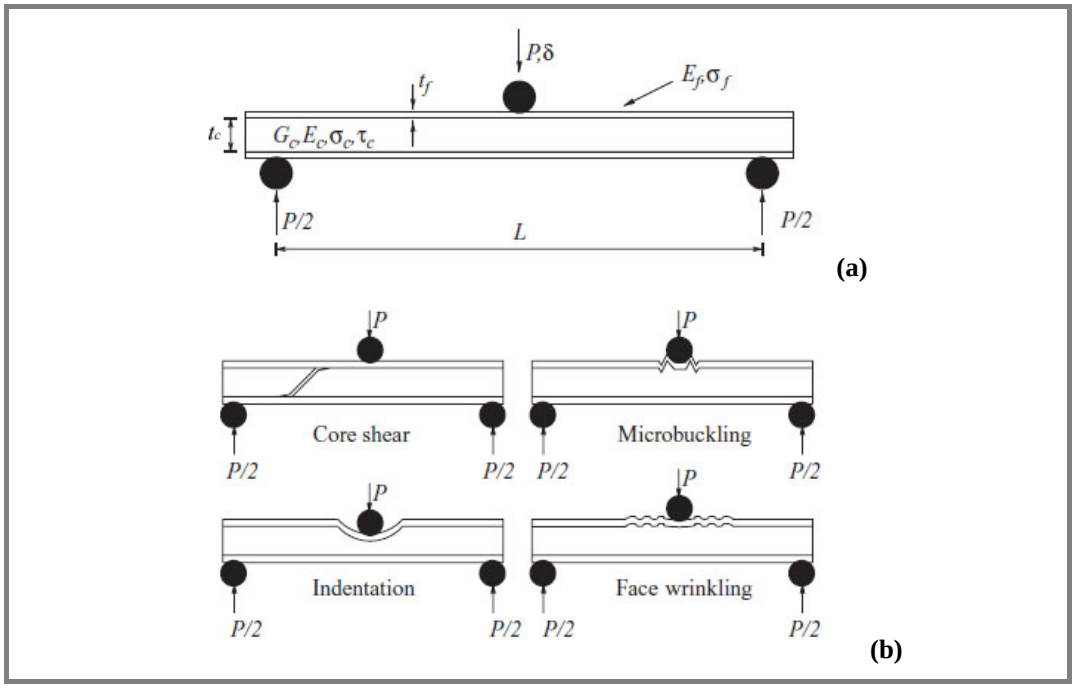

Figure 1.6 (a) Geometry of sandwich beam **(b)** Failure modes in sandwich beams subjected to three-point bending [38].

Tagarielli, Fleck and Deshpande [40] extended the work of Steeves and Fleck [38] to the case of clamped supported beams tested in three-point bending. Analytical expressions are derived and good agreement is found with experimental tests and finite element predictions. Normalised initial collapse mechanism maps are built for simply supported and clamped woven glass face sheets and PVC foam core sandwich beams.

As referred in [38], other investigators confirmed these failure modes for sandwich beams in three point and four point bending, such as Gibson and Ashby [41], Triantafillou and Gibson [42, 43], Lingaiah and Suryanarayana [44], Theotokoglou [45], Zenkert [4] and Chen et al. [46].

1.4.1 Face microbuckling failure

Sandwich beam failure by microbuckling of the upper face sheet occurs when the axial compressive stress in this face sheet attains the face sheet microbuckling strength, σ_f. Neglecting the core contribution to the bending strength, moment equilibrium across the central section of the sandwich beam implies that the collapse force P is for,

i. simply supported TPB beams [38]:

$$P_{ss} = \frac{4bdt_f\sigma_f}{L} \tag{1.1}$$

ii. clamped TPB beams [40]:

$$P_{cl} = \frac{8bdt_f\sigma_f}{L} \tag{1.2}$$

1.4.2 Face wrinkling failure

Face wrinkling is a local elastic instability of the faces involving short wavelength elastic buckling of the upper face sheet, resisted by the elastic core. By treating the core as an elastic half-space, Hoff and Mautner [47] gave a conservative and generic estimate for the face wrinkling load P as [38],

$$P = \frac{2bt_f d}{L}\sqrt[3]{E_f E_c G_c} \tag{1.3}$$

1.4.3 Core shear failure

For sandwich beams with relatively thin faces compared with that of the core, it may be assumed that the core material collapses at a uniform shear

strength τ_c, neglecting the strength effect of the composite faces. This shear stress produces a positive direct stress at 45 degree angle from the face sheet plane which causes cracks inclined 45 degrees. Such cracks are typical of shear failure and are usually called as shear cracks. The load P required to initiate the core shear mechanism is given by the general expression [38, 40],

$$P = 2bd\tau_c \tag{1.4}$$

1.4.4 Core indentation failure

This can become a favourite failure mode under certain geometrical and loading conditions. Furthermore a permanent indentation and yielding of the core can significantly deteriorate the residual load bearing capabilities of a sandwich structure [35, 48, 50] or determine other concerns in terms of aesthetic and functionality. In the present work and from this point forward, our attention will be mainly focused on investigating the development of permanent indentation damage under static concentrated loads.

1.5 Literature review of indentation analytical models

Classical basic sandwich theories usually consider the core as transversely incompressible, and can predict the global flexural and shear rigidity of sandwich beams and panels with simple explicit analytical relationships which are well known and much used for gross design and characterisation purposes (see Appendix A, section A3) [1, 2]. They though lack of any capability for designing against local loading effects [38, 40, 51, 52]. Different and more sophisticated analytical approaches have been proposed to model the indentation behaviour in order to: a) determine the indentation law, i.e. the load versus displacement indentation curve, possibly including both the elastic and plastic ranges of core compressive behaviour; b) determine the critical load at core yielding onset, and its interaction with other competing failure modes by building up parametric failure maps; c) determine the extent of the residual dent, the extension of the core plastic zone and the load value at which local skin bending failure occurs. Three

main analytical approaches have been used to predict some of the above behaviours: higher order sandwich panel theories (HOSPT), models based on the Winkler elastic foundation theory and superposition models.

Approaches based on the HOSPT were first proposed by Frostig et al. [53] and Frostig [54]. The higher order approach allows and predicts the non-linear through-the-thickness core-compression behaviour up to core yielding onset. Although not simple, the higher order approach has demonstrated many strengths such as the ability to consider local loading distributions in Petras and Stutcliffe [55], the influence of geometric non-linearities in Sokolinsky et al. [56], and the interaction between indentation deformation with bending and shear deformation. Solutions of simply supported sandwich beams loaded in three-point bending have been obtained in particular, and used to build up failure maps of competing damage modes [53-57]. The complexity of the HOSPT approach has though rarely led to sufficiently simple final analytical solutions correlating the mechanical behaviour with design and material parameters, so limiting its practical adoption. Shen et al. [58] have used HOSPT results to determine the mid-span deflection in sandwich beams in TPB, interpolated results with a relationship formally similar to that given by the sandwich beams classic theory. This allowed the definition of HOSPT derived correction factors which could improve the classic prediction while using the same simple formalism. Another interesting result in terms of simplification was recently presented by Saadati and Sadighi [59] who derived an explicit relationship of the indentation stiffness for fully-backed and edge-supported sandwich beams.

Another popular approach to the study of the indentation behaviour consists in solving the equilibrium equations of the point loaded sandwich skin face modelled as a beam or plate on a compressible Winkler type foundation [35, 48]. A main drawback of this approach is that it is able to model only the local skin-core interaction, neglecting the influence of the bottom skin, while its major strength compared with the HOSPT is the ability to derive simpler analytical solutions of the elastic indentation stiffness, the critical load at core yielding onset and the indentation damage progression after core yielding. Simple explicit solutions within the elastic compression behaviour of the foundation have been

provided for sandwich beams [35, 38, 48, 60, 61] and plates [61, 62-65]. In Thomsen [62, 63], Yaing and Qiao [65] a two parameters elastic foundation approach is used and able to include also shear forces at the skin-core interface while a justification for neglecting them in the case of sandwich beams, thus considering only normal forces (assumption found in the in the majority of works) is provided in Steeves and Fleck [38]. Solutions are most frequently provided for the fully backed sandwich configuration where the unloaded face is resting against a rigid foundation [35, 48, 60, 61, 65, 66, 67, 68]. Solutions for edge supported beams are provided by using superposition approaches, e.g. by simply adding the indentation displacement contribution to the mid span bending and shear displacements measured with the classic approach [54, 69, 70]. A more rigorous approach is proposed by Steeves and Fleck [38] in which a solution for an *elastic-perfectly-plastic* foundation is derived. Tagarielli et al. [40] extended these results to edge clamped beams. Failure by indentation onset was also employed to derive failure maps for edge constrained sandwich beams in TPB [38, 40, 51]. In Thomsen [62, 63], Lee and Tsotis [64] solutions for edge supported and edge clamped panels with the core behaving as an elastic foundation are also provided, and the influence of a locally distributed load, as opposed to the point load assumption, is discussed in Yang and Qiao [65].

The indentation behaviour beyond the elastic limit of the foundation has been generally treated by representing the yielding behaviour of foam cores as *perfectly-plastic*, which is a reasonable assumption for the wide class of popular foam materials addressed to as *"Crushable"* foams [35, 38, 48, 61, 66, 69, 71]. Solutions for the important estimation of residual dents, resulting from unloading after core yielding, are more rare to find for both foam [35, 50] and honeycomb cores [68].

1.6 Indentation of sandwich beams using the Winkler approach

The earlier and most comprehensive approach to study local indentation in sandwiches implements the Winkler theory based on the equilibrium of a beam or plate perfectly attached to a compressible foundation. A number of solutions

regarding the indentation behaviour have been found for several load scenarios and core behaviours. Some of the most relevant models are briefly described here.

1.6.1 *Fully-backed* sandwich beam and concentrated load

Concentrated (line) load on sandwich beams where the bottom skin is resting on a rigid surface, i.e. a *fully-backed* sandwich beam (FB) has been the adopted geometry in several works to study the indentation mechanisms [35, 48, 60, 61, 66, 67, 68], for its simplicity and to suppress other competitive modes of failure. The case of the contact between a sandwich beam and a cylindrical indenter with the back face supported by a rigid base (see figure 1.7) is in particular studied by Zingone [72], Shuaeib and Soden [67], Abrate [48] and Zenkert [35]. The common approach used in these works is to model the indentation problem as that of a beam attached on a compliant (elastic or elasto-plastic) foundation. The upper sandwich skin laminate is in particular the indented beam or plate in the model, and the foam core the compressible foundation, whose constitutive parameters determine the distributed reactions forces at the interface with the top skin laminate (see figure 1.7).

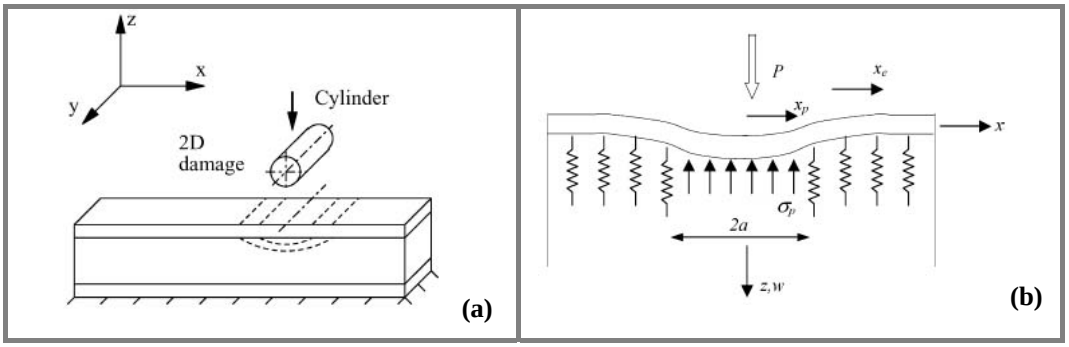

Figure 1.7 (a) Fully backed sandwich beam indentation test set-up [35]; **(b)** Schematic sandwich beam indentation for an elastic-perfectly-plastic core (EPP) [35].

Two main assumptions are in particular made in the previously referred works: a) the beam material is linear elastic and brittle, with local brittle bending failure occurring without the onset of plastic yielding (this is a reasonable assumption for brittle FRP skin laminates); b) only normal stress components in the core transverse direction are considered at the skin-core interface, requiring

only one foundation elastic stiffness parameter (see [38] for a more in-depth discussion of this assumption).

Solutions for the fourth order differential equation describing the bending of a fully backed beam resting on a Winkler type foundation (consult Appendix A, section A1, equation A1.8) are presented in Abrate [48] and Zenkert [35]. The model assumes an elastic Winkler foundation for the elastic core, and a perfectly plastic foundation for the part of the core that undergoes crushing, as schematically shown in figure 1.7b. For small concentrated loads, the entire foundation denotes an elastic response and the governing equation results from equation A1.8, without considering the plastic response given by the reaction term q.

$$D_f \frac{d^4 w_e}{dx_e^4} + k w_e = 0 \tag{1.5}$$

where w_e is the elastic vertical face sheet deflection, x_e the longitudinal axis coordinate for the part of the core within the elastic range, D_f is the face sheet flexural stiffness, equal to the product of the Young's modulus E_f and the second moment of inertia I_f of the beam section. The value k is the elastic foundation modulus or stiffness of the foundation and related to the compression modulus of the core E_c, the width of the beam b and the thickness of the core t_c, defined by:

$$k = \frac{E_c b}{t_c} \tag{1.6}$$

The general solution for equation (1.5) describing the elastic indentation behaviour is,

$$w_e(x_e) = e^{-\lambda x_e} \cdot \left[A \cdot \sin(\lambda x_e) + B \cdot \cos(\lambda x_e)\right] + e^{\lambda x_e} \cdot \left[C \cdot \sin(\lambda x_e) + D \cdot \cos(\lambda x_e)\right] \tag{1.7}$$

where $\lambda = \sqrt[4]{\frac{k}{4D_f}}$ and results in an explicit linear relationship between the indentation load P and deflection α (consult sub-section 2.2.1, chapter II):

$$P = \left(8 \cdot D_f \cdot \lambda_1^3\right) \cdot \alpha \tag{1.8}$$

The elastic equation (1.8) is valid for a deflection α before the core crushing, i.e. occurring at the condition $\alpha = \varepsilon_c t_c$, where ε_c is the strain value at the onset of core plastic deformation.

Considering the values of λ, α at the onset of core crushing and equations (1.6) and (1.8) it is possible to derive the maximum contact force, P_c, prior to core plastic deformation:

$$\lambda P = 8 D_f \lambda^4 \alpha \Leftrightarrow \lambda P = \frac{2 E_c b}{t_c} \alpha \Leftrightarrow P_c = \frac{2 b E_c \varepsilon_c}{\lambda} \tag{1.9}$$

The same result is described in Abrate [48] and Zenkert [35].

With the progressive increase of the concentrated load, part of the core (starting from the mid-center part of the beam) undergoes plastic deformation. From this point onward the core reaction is no longer proportional to transverse displacement, but equal to the constant value $q=\sigma_c b$ where σ_c is the *plateau* stress or compressive yield stress of the *crushable* core material, implying that the core progressive deformation proceeds at a constant stress in the absence of any hardening or softening phenomena (perfectly-plastic behaviour). Hence considering a perfectly-plastic foundation the elastic core response to the concentrated load is neglected and equation (A1.8) turns to,

$$D_f \frac{d^4 w_p}{dx_p{}^4} + q = 0 \tag{1.10}$$

The general solution for equation (1.10) describing the perfectly-plastic indentation behaviour is,

$$w_p(x_p) = -\frac{q_n}{24 D_f} x_p^4 + A \frac{x_p^3}{3} + B \frac{x_p^2}{2} + C_n x_n + D_n \tag{1.11}$$

Imposing the adequate boundary conditions to the elastic and plastic general solutions (see chapter II for a fully detailed and generalised solution procedure) and combining both particular solutions (the elastic and the plastic), the indentation law, i.e. the vertical displacement *w* vs. concentrated load *P*, for a fully backed sandwich beam on an *elastic-perfectly-plastic* (EPP) foundation is

found, as described in [48] and [35]. Furthermore, the plastic length *2a* can be calculated for a given indentation load *P*.

Others assumptions and models have been proposed during the years for the study of the indentation phenomenon in sandwich beams, and all of them presenting improvements or less accurate predictions, depending always on the initial premises. Even before [48] and [35], Green [73] investigated the penetration of an elastic beam resting on a *rigid-perfectly-plastic* foundation (RPP). He assumed the ends of the beam as free to lift up and derived an expression for the critical load at which the beam penetrated the foundation,

$$P_{cr} = 3.63 \cdot \sqrt[3]{q^2 E_f I_f} \tag{1.12}$$

In the same way, Soden [66] applied Green's approach for the case of an elastic beam firmly attached to a crushable, RPP foundation and derived an expression for the critical load at which the top face sheet of a sandwich beam fails due to local bending,

$$P_{cr} = \frac{4}{3} b t_f \cdot \sqrt{\sigma_f \sigma_c} \tag{1.13}$$

where b is the beam width, t_f is the skin thickness, σ_f is the bending strength of the face sheet and σ_c is the core yielding stress. Moreover, expressions for calculating the deflection at failure for the beam (equation 1.14), the length of the crushed zone (equation 1.15) and the load-indenter displacement relationship (equation 1.16) have been derived in the work of Soden (see also figure 1.8).

$$y_f = \frac{1}{6} \frac{\sigma_f^2}{E_f \sigma_c} t_f \tag{1.14}$$

$$l_p^* = \frac{3}{2} \frac{P_f}{q} = 2 t_f \sqrt{\frac{\sigma_f}{\sigma_c}} \tag{1.15}$$

$$P(x) = \left(\frac{4}{\sqrt{3}} \right) \cdot \left(\frac{2}{3} \right)^{\frac{1}{4}} b t_f^{\frac{3}{4}} \sigma_c^{\frac{3}{4}} E_f^{\frac{1}{4}} y(x)^{\frac{1}{4}} \tag{1.16}$$

One advantage in Soden's approach is the derivation of the above indentation parameters by means of explicit equations very appealing for design purposes. It

remains though the limit of considering a RPP model which can significantly underestimate the indentation at given low loading values, due to the neglected contribution of the elastic core deformation. This will be shown in the next chapter V when the Soden's model will be implemented to compare the more sophisticated indentation models predictions and the experimental results.

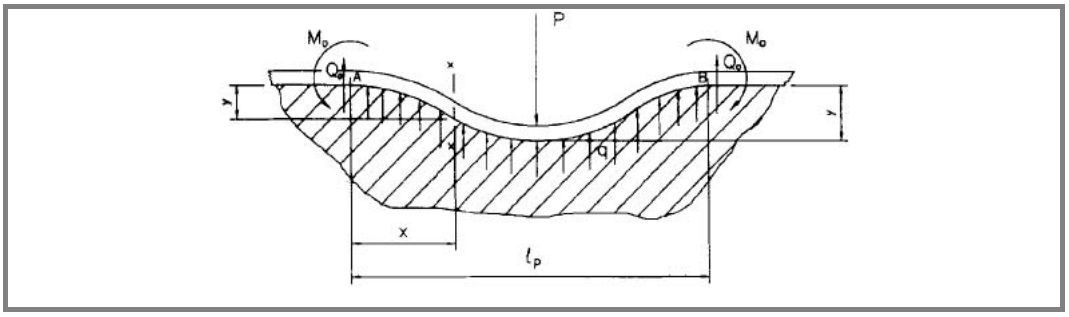

Figure 1.8 Beam firmly attached to a crushable RPP foundation [66].

In Shuaeib and Soden [67], a more refined solution under the elastic-perfectly-plastic (EPP) model assumption is proposed. In particular, based on the work of Zingone [72], Shuaeib and Soden [67] proposed an elastic indentation curve which consider also the influence of the beam length *L*. Accordingly, the expression that predicts the load at core yielding onset is given by:

$$P_{yielding} = \frac{2\sigma_c b}{\lambda} \cdot \frac{sinh(\lambda L) + sin(\lambda L)}{cosh(\lambda L) + cos(\lambda L) + 2} \approx \frac{2\sigma_c b}{\lambda} \; for L >> 1/\lambda \qquad (1.17)$$

Shuaeib and Soden [67] also extended their approach to the plastic core deformation range. By opportune assumptions on boundary conditions, the following equation was derived relating the external load *P* and the length *s* (extension of the core portion under plastic deformation for half beam length, see figure 1.9):

$$\left(\frac{3\lambda}{2\sigma_c b}\right)P = \frac{2z^3\left(\sinh^2 z' + \sin^2 z'\right) + 3\left(\sinh z' \cosh z' - \sin z' \cos z'\right)\left(2z^2 - 1\right) - 6z}{z^2\left(\sinh^2 z' + \sin^2 z'\right) + 2z\left(\sinh z' \cosh z' - \sin z' \cos z'\right) - \left(\cosh^2 z' + \cos^2 z'\right)} \qquad (1.18)$$

where $z = \lambda s,\ z' = \lambda s'$ and $\lambda = \sqrt[4]{\frac{k}{4D_f}}$.

A second relationship is derived by imposing equilibrium of moments on the portion of beam over the plastically deformed core (portion A in figure 1.9) and

considering the maximum moment at beam failure, computed under the assumption that the beam material is perfectly elastic up to failure. The following equation relating P and s is then obtained:

$$\left(\frac{\lambda}{\sigma_c b}\right)P = \frac{\dfrac{2M_f\lambda^2}{\sigma_c b} + z^2 + 2zA + B}{z + A} \tag{1.19}$$

The two previous simultaneous equations can be numerically solved to find the values of P and s at which bending failure of the top skin occurs.

This procedure will be implemented in chapter V to compare the analytical prediction with experimental values determined in this work. Furthermore this procedure from Shuaeib and Soden [67] based on the moments equilibrium of a portion of beam will be extended to derive a more general relationship giving the load P at skin failure when the core compression behaviour is generically non-linear.

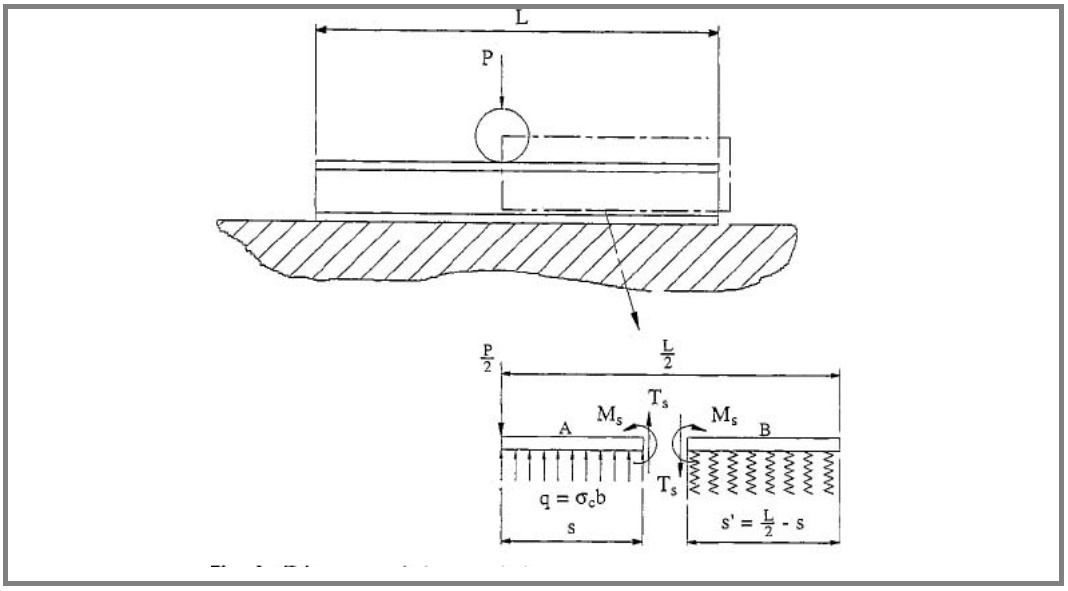

Figure 1.9 Fully backed sandwich beam and upper face sheet modelled as a beam firmly attached to an EPP foundation [67].

1.6.2 Simply supported sandwich beams loaded in *three-point bending*

As mentioned before, Steeves and Fleck [38] proposed a solution to predict indentation on a sandwich beam loaded in three-point bending for the cases of

elastic face sheets and a rigid-perfectly-plastic (RPP) foundation core (figure 1.10) and elastic face sheets and an elastic-perfectly-plastic (EPP) foundation core.

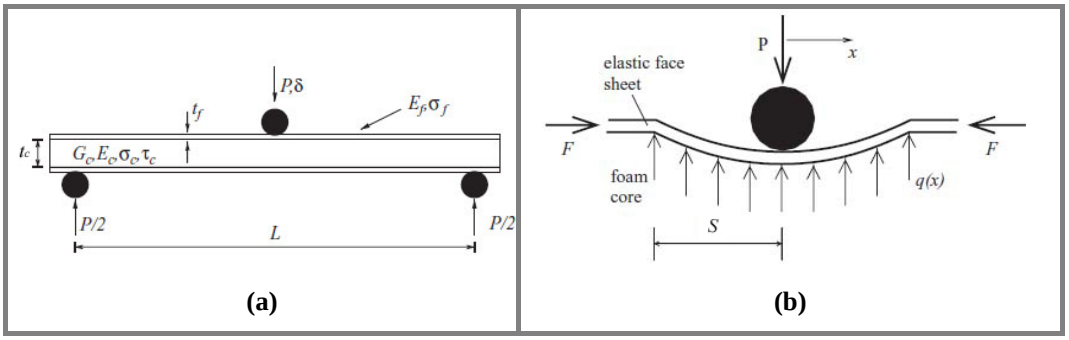

Figure 1.10 (a) TPB sandwich beam indentation geometry [38]; **(b)** Schematic simply supported sandwich beam indentation for a rigid-perfectly-plastic (RPP) core [38].

The transverse load *P* at mid-span induces a bending moment *M=PL/4* on the mid-span sandwich cross section (see figure 1.10a) and carried by the face sheets, in the form of a compressive axial load for the upper face sheet and tensile axial load for the lower face sheet. Thus, the magnitude of both loads is given by:

$$F = \frac{M}{t_c + t_f} \Leftrightarrow F = \frac{PL}{4(t_c + t_f)} \tag{1.20}$$

In the indentation zone of length *2s* (see figure 1.10b), the core is compressed and will exert a force per unit equal to $q = \sigma_c \cdot b$ on the upper face sheet for the case of a *rigid-perfectly-plastic* (RPP) behaviour, or $r(x) = kw(x) + q$ for the case of an *elastic-perfectly-plastic* (EPP) behaviour.

Steeves and Fleck [38] proposed two governing equations for RPP and EPP core behaviours in simply supported TPB sandwich beams (see also Appendix A, section A2). According to this approach the plastic response, present in the RPP and EPP, is governed by the equation:

$$\frac{d^4u}{dx^4} + \frac{F}{E_f I_f}\frac{d^2u}{dx^2} = -\frac{q}{E_f I_f} \tag{1.21}$$

which presents a general solution of the type:

$$u(x) = A_1 \cos(kx) + A_2 \sin(kx) + A_3 x + A_4 - \frac{\sigma_c b x^2}{2F} \tag{1.22}$$

where A_1, A_2, A_3 and A_4 are constants to be determined by imposition of boundary conditions and $k = \sqrt{\frac{F}{E_f I_f}}$.

In [38] an expression for the maximum load that the simply supported beam can withstand is also derived:

$$P_{\max} = bt_f \left(\frac{\pi^2 d E_f \sigma_c^2}{3L} \right)^{1/3} \tag{1.23}$$

The elastic response, only present in the EPP model, is governed by the equation:

$$\frac{d^4 u}{dx^4} + \frac{F}{E_f I_f} \frac{d^2 u}{dx^2} + kw = 0 \tag{1.24}$$

and has a general solution of the type,

$$u(x) = \left(B_1 e^{\beta x} + B_2 e^{-\beta x} \right) \cos(\alpha x) + \left(B_3 e^{\beta x} + B_4 e^{-\beta x} \right) \sin(\alpha x) \tag{1.25}$$

where B_1, B_2, B_3 and B_4 are constants to be determined by imposition of boundary conditions and the parameters α and β depend on the axial load F. Yield of the core occurs at the load value predicted by:

$$P_c = \frac{4\sigma_c b \beta}{\alpha^2 + \beta^2} \tag{1.26}$$

1.6.3 Edge clamped sandwich beams loaded in *three-point bending*

As mentioned before, Tagarielli et al. [40] extended the results of Steeves et al for a RPP foundation to the case of edge clamped beams (figure 1.11). The beam is loaded centrally by a force P and the clamped support rig provides a resisting bending moment $M=PL/8$ in the central section and an axial force carried on by the face sheets. This force is compressive on the upper face sheet and has magnitude of

$$F = \frac{M}{t_c + t_f} \Leftrightarrow F = \frac{PL}{8(t_c + t_f)} \tag{1.27}$$

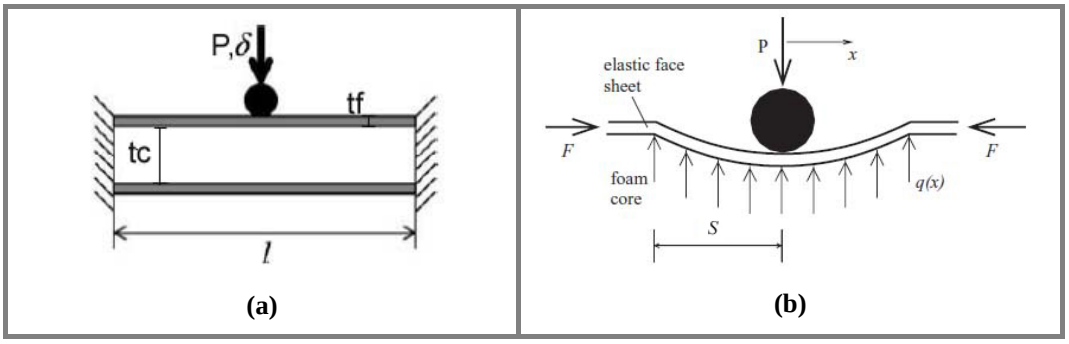

Figure 1.10 (a) Clamped sandwich beam indentation geometry; **(b)** Schematic clamped sandwich beam indentation for a rigid-perfectly-plastic (RPP) core [40].

For clamped beams, Tagarielli et al. [40] arrived to the same governing equation and general solution of a simply supported sandwich beam loaded in TPB and with a RPP core behaviour deduced in [38] (see equations 1.21 and 1.22). They also derived an expression for the maximum load that the clamped beam is able to stand before failure,

$$P_{\max} = bt_f \left(\frac{2\pi^2 dE_f \sigma_c^2}{3L} \right)^{1/3} \tag{1.28}$$

1.6.4 Winkler theories synopsis

A general expression for the equilibrium equation of the beam, which comprises all cases listed above, can be written as a fourth order linear differential equation [35, 48, 68], whose coefficients are functions of the core and skin geometry, elastic and constitutive properties. For further detail on how equation (1.29) is derived consult Appendix A, sections A1 and A2.

$$l \cdot \frac{d^4 w(x)}{dx^4} + m \cdot \frac{d^2 w(x)}{dx^2} + k \cdot w(x) = c \tag{1.29}$$

As shown in figure 1.7, x is the beam axis coordinate centred on the loading point and w the transverse deflection orthogonal to the beam axis. The presence of coefficients l, k, c depends on the particular core constitutive behaviour (i.e. on the foundation parameters), while coefficient m appears only in the case of a TPB loading configuration (see table 1.1 for which coefficients are present in the various models, and table 1.2 for their definition).

In particular the normal reaction force from the core is proportional to the indentation displacement through the elastic foundation parameter *k*. A relationship of *k* is provided in [35, 48] for a finite core thickness (see also table 1.2), and in [59, 60] for an infinite core thickness. A second foundation parameter *q* is considered to account for a constant normal reaction force from the core. This is the only reaction force when core compression is rigid-perfectly-plastic [35]. Both foundation parameters depend on the core Young's modulus in compression E_c and the yield stress σ_c, which are usually provided by material suppliers, or measured from standardised uniaxial compression tests [35, 68].

Table 1.1. Sandwich beam indentation features in sandwich beams predicted by different analytical models based on the Winkler approach.

Contributions	Type of support	Mid-span displ. *vs* load curve				Load at core yielding onset	Load at skin bending fracture
		RPP	***E***	***EPP***	***SW***		
Soden [66]	*FB*	×	-	-	-	-	×
Shuaeib and Soden [67]	*FB*	-	×	-	-	×	×
Abrate [48], Zenkert et al. [35]	*FB*	-	*l, k*	*l,c*	-	×	-
Steeves et al. [38]	TPB_{ss}	*l,m,c*	*l,m,k*	*l,m,c*	-	×	×
Tagarielli et al. [40]	TPB_{cl}	*l,m,c*	-	-	-	-	×
Minakuchi et al. [68]	*FB*	×	×	×	*l,k,c*	-	-

Table 1.2. Definition of equation (1.29) coefficients.

Coeff.	Definition	notes
l	$E_f I_f$	Flexural rigidity of the beam (E_f longitudinal Young's modulus of beam, I_f inertia moment);
m	$\frac{PL}{4(t_c + t_f)}$	Membrane axial force *F* on the beam skin for simply supported *tpb* beams (*P* applied point load, *L tpb* span length, t_c core thickness, t_f face sheet thickness)
	$\frac{PL}{8(t_c + t_f)}$	Membrane axial force *F* on the beam skin for clamped *tpb* beams (*P* applied point load, *L tpb* span length, t_c core thickness, t_f face sheet thickness)
k	$E_c b / t_c$	Foundation Elastic modulus (E_c Core compressive stiffness, b sandwich beam width);
c	$-b \cdot q_i$	Constant stress applied to the beam
	$-b \cdot \sigma_c$	Where σ_c is the core yield stress (value of plastic plateau in EPP behaviour).

Minakuchi et al. [68] have proposed to represent the measured uniaxial core compression curve through a series of line segments, each described by two values of k_i and q_i. The top skin beam is then discretised into a succession of segments, where each segment delimits a portion of the beam where the core reaction forces are described by the same foundation parameters k_i and q_i. As indentation deflection progresses, each beam segment will move outward from the loading point and change its length, while new segments with new couples of foundation parameters will turn up. This incremental procedure is referred to as *"segment-wise"* model (abbreviated *SW* in table 1.1) and was introduced in Minakuchi et al. [68, 74] to model the complex compression behaviour of honeycomb cores. In [68] it was demonstrated that the discretised beam segments had all the same length, which allowed to simplify the analytical treatment. In this work the SW model is extended to foam core materials, and the discretised representation of the uniaxial compression behaviour of the core is exploited to consider non-linear foam core compressive behaviours.

1.7 Scope of the research

In this study an incremental procedure using the Winkler foundation approach is proposed to evaluate the indentation law on foam cored sandwich beams, with the foam material exhibiting a generic non-linear compressive behaviour. Very few works have been found in the literature which include non-linear elastic or plastic behaviour of constituent materials in the modelling of the indentation problem. In fact the above mentioned solutions are at least valid only for a perfectly-plastic post-yielding behaviour [35, 38, 48], which may not satisfactorily model foam materials with a post-yield hardening or other non linear behaviours (e.g. hyperelastic foams). Gdoutos and Daniel [75] have considered non-linear tensile-compressive behaviour of the skins and Joon Yoon et al. [76] have considered non-linear shear behaviour of the foam to correct the mid-span deflection on sandwich beams in four-point bending (FPB). In both cases though the compressive behaviour of the core was not modelled and the indentation deformation component not considered.

For this purpose, the segment-wise model proposed by Minakuchi et al. [68, 74] to study the indentation behaviour of honeycomb cores is extended to the case of foam cores and used to model some typical non-linear behaviours of foam materials. The work shows how the resulting analytical approach is a generalisation of the procedures based on the Winkler foundation model. In fact a generic non-linear foam core compressive behaviour is considered which includes the pure-elastic and elastic-perfectly-plastic as particular cases. Analytical solutions to derive the indentation law are in particular obtained for three simplified foam compression behaviours: elastic-perfectly-plastic, bilinear and bilinear-perfectly-plastic. A general analytical solution is also derived for the prediction of the critical load at which flexural failure of the sandwich skin occurs. These analytical predictions are then compared with experimental results measured on sandwich beams adopting foam materials with different compressive behaviours.

CHAPTER II

Analytical developments

2.1 Introduction

This chapter addresses the analytical developments formulated on the current research to model the indentation behaviour of fully backed sandwich beams under local loading. A single model capable of uniformize the specificities of some of the theories presented in chapter I as well as extend it to the case of sandwiches employing foams with a non-linear behaviour at compression is here proposed. The model is based on the Winkler foundation assumptions and is denominated as "*Segment Wise*" model (SW), since it discritises the foam stress *vs.* strain curve of a uniaxial compression test as a succession of segments.

Furthermore a generalised procedure to predict bending skin failure is also presented whose results compare well with those obtained in the literature with similar but less general procedures.

2.2 The *Segment-Wise* model

As seen before, most of the theories found in literature to describe the indentation behaviour in foam sandwiches are valid to foams exhibiting an elastic-perfectly-plastic compression behaviour, such as the one described in figure 1.3, section 1.3 from the previous chapter.

Though, there are a consistent number of foam materials exhibiting more or less marked non-linearities under uniaxial compression. Even some PVC or PU,

which are popular polymer foam core materials, classified as crushable foams, may exhibit some post-yield hardening or pre-yield elastic non-linearity which cannot be taken into account by the elastic-perfectly-plastic assumption. As outlined at the end of the first chapter, in this work a model is proposed, developed and implemented, which aims at predicting the indentation behaviour of fully backed composite sandwich beams where the foam core material employed exhibits a generically non-linear behaviour. In particular the compressive behaviour of the foams considered for the new model is not well represented by an EPP behaviour. Since the proposed model will represent the foam stress *vs.* strain curve of a uniaxial compression as a succession of segments, the general model proposed in this thesis is shortly addressed as the "Segment-wise" model (SW).

In order to define the SW procedure in the most general case, a non-linear monotonically increasing uniaxial compression curve is considered as shown in figure 2.1.

The curve is approximated by a succession of line segments, whose number in theory can grow as much as needed to better fit the original curve. In order to refer the constitutive behaviour of the foam (e.g. the values of k_i, q_i and δ_i as introduced in figure 2.1), evaluated from a foam block with a generic cross section (e.g. a square section, or others, according to standards such as ASTM C365-03 [77]), to the geometry or the indented sandwich beam, it is convenient to opportunely rescale the normalised stress-strain uniaxial compression curve obtained from the compression of the foam block. In particular it is convenient to rescale the vertical axes multiplying the compression stress by the sandwich beam width b, and report the vertical compression displacement w on the horizontal axis. A correction factor t_c/t_p is multiplied to w if the height t_p of the foam specimen used in the compression test is different from the sandwich foam core thickness t_c. Considering $t_c=t_p$ for simplicity, then each line segment in figure 2.1 is represented by the equation:

$$b \cdot \sigma\left(w(x)\right) = k_i w(x) + q_i \quad \text{where } \delta_{\mathrm{i}} < w(x) < \delta_{\mathrm{i+1}} \tag{2.1}$$

which allows the direct evaluation of the foundation parameters k_i and q_i as the slopes and y-axis intercepts of each segment i. The x variable in equation (2.1) is referred to the longitudinal axis of the sandwich beam. If x is fixed at a generic point along the longitudinal axis of the beam, equation (2.1) predicts the total amount of vertical reaction force that the foam applies on the skin at the coordinate x for a given vertical displacement w. The model consists in dividing the beam length into a number of sections [68].

During the indentation loading each section of the beam is defined by having vertical deflections comprised between δ_i and δ_{i+1}, i.e. within the displacement range of a segment in the core compression curve of figure 2.1. So δ_i is the vertical deflection at the unknown position along the beam axis at which the foam material changes his compressive behaviour from k_i, q_i (outer part) to k_{i+1}, q_{i+1} (inner part), and each segment section of the sandwich maintains constant foundation parameters. A scheme of the segment-wise discretisation is given in figure 2.2 where only one half of the beam is represented. It is noticed that the case of a fully-backed sandwich is being considered.

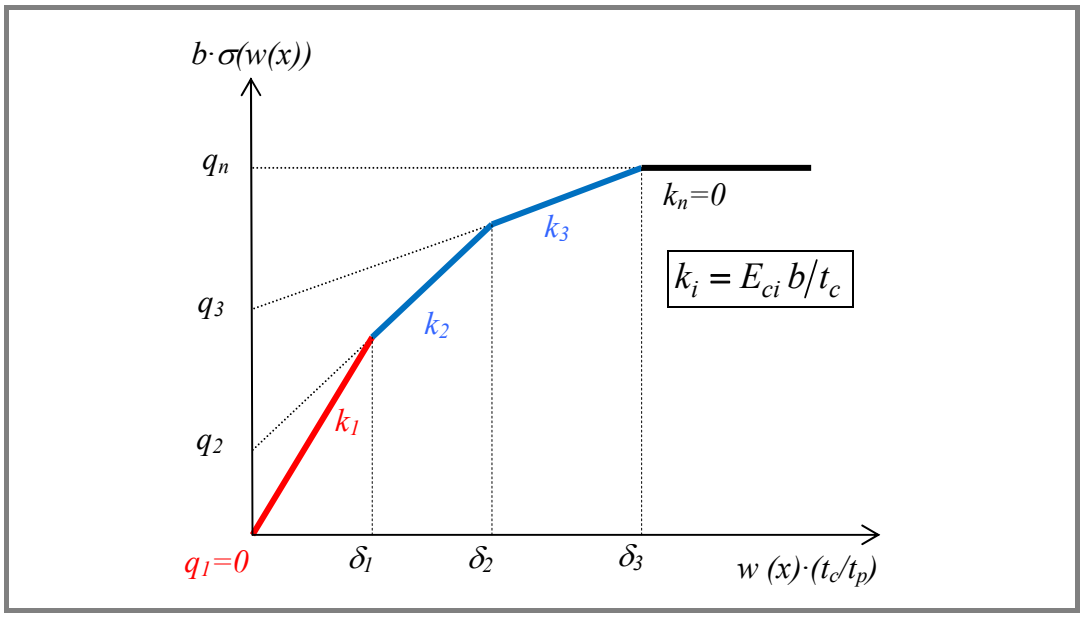

Figure 2.1 Multi-linear discretisation of the foam uniaxial compression curve.

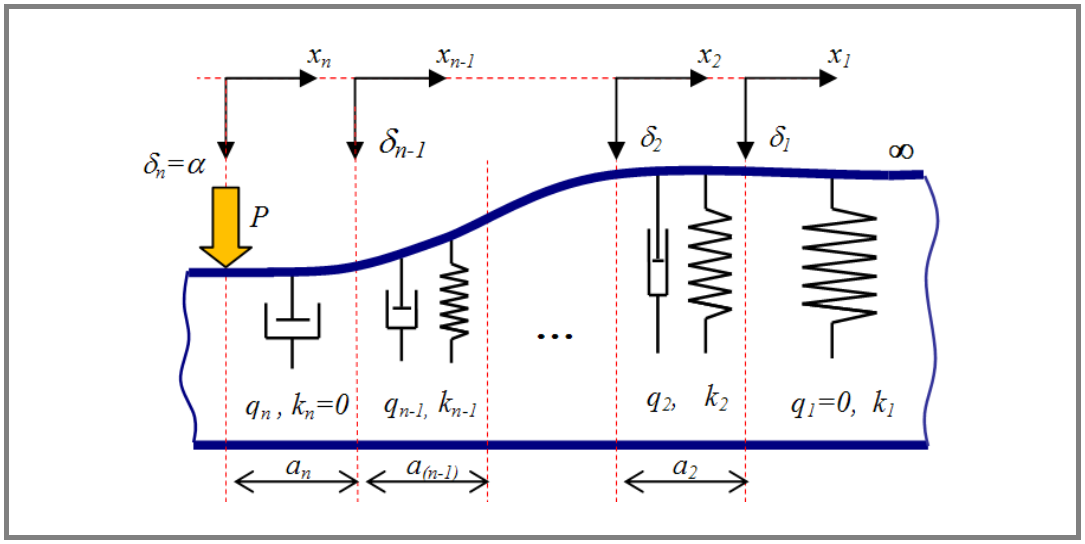

Figure 2.2 Schematic representation of the segment-wise model on a fully-backed point loaded half beam.

Also figure 2.1 shows the case where the last line segment in the core compression curve is horizontal ($k_n=0$, i.e. perfectly-plastic behaviour), although this is not necessarily the general case.

Equation (2.1) gives the distributed normal reaction forces, which the core applies to the skin within each beam segment. At a generic x coordinate of the beam, the normal force given by equation (2.1) is the only force component at the skin-core interface, and comprises two terms: one proportional to the global vertical displacement $w(x)$ through the stiffness parameter k_i, and one constant q_i, as illustrated in figure 2.3.

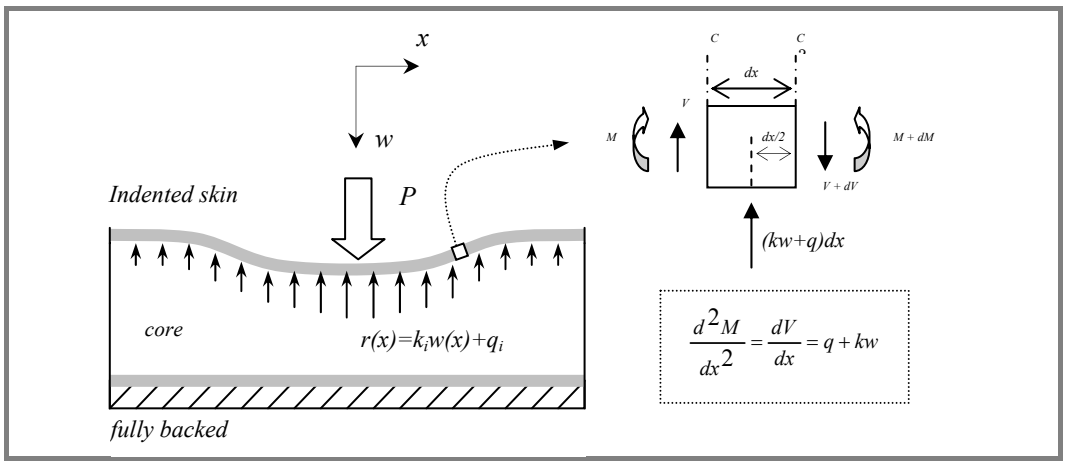

Figure 2.3 Schematic representation of a *fully-backed* indented sandwich beam and free-body diagram of an infinitesimal beam element of the upper skin (see also Figure A1.1 in Appendix A, section A1).

From the equilibrium of moments applied to an infinitesimal beam length, a general fourth order differential equation is obtained for each beam segment (see Appendix A, section A1):

$$E_f I_f \frac{d^4 w(x)}{dx^4} + k_i \cdot w(x) + q_i = 0 \tag{2.2}$$

As exposed in chapter I, general solutions for equation (2.2) are in particular reported in [35, 48, 68]. If for simplicity the compression curve is considered monotonically increasing (as represented in figure 2.1), only three general solutions are needed, each referred to the following three cases: **a)** for $k_i > 0$ and $q_i = 0$ (e.g. when $i=1$), **b)** for $k_i > 0$ and $q_i \neq 0$, **c)** for $k_i = 0$ and $q_i \neq 0$ (e.g. when $i=n$ and the last segment is a plateau).
A different case may arise where the post yielding behaviour ($i>1$) exhibit a linear softening rather than hardening, for which a forth case arise: **d)** $k_i < 0$ and $q_i \neq 0$. The four general solutions of equation 2.2 addressing the previous cases are:

$$\begin{aligned}
&a)\ w_1(x_1) = e^{-\lambda_1 x_1}\left[A_1 \sin(\lambda_1 x_1) + B_1 \cos(\lambda_1 x_1)\right] + e^{\lambda_1 x_1}\left[C_1 \sin(\lambda_1 x_1) + D_1 \cos(\lambda_1 x_1)\right] \\
&b)\ w_i(x_i) = -\frac{q_i}{k_i} + e^{-\lambda_i x_i}\left[A_i \sin(\lambda_i x_i) + B_i \cos(\lambda_i x_i)\right] + e^{\lambda_i x_i}\left[C_i \sin(\lambda_i x_i) + D_i \cos(\lambda_i x_i)\right] \\
&c)\ w_n(x_n) = -\frac{q_n}{24 E_f I_f} x_n^4 + A_n \frac{x_n^3}{3} + B_n \frac{x_n^2}{2} + C_n x_n + D_n \\
&d)\ w_i(x_i) = -\frac{q_i}{k_i} + A_i e^{-\lambda_i x} + B_i e^{\lambda_i x} + C_i \sin(\lambda_i x) + D_i \cos(\lambda_i x)
\end{aligned} \tag{2.3}$$

where

$$\lambda_i = \sqrt[4]{\frac{k_i}{4 E_f I_f}} \ \text{for } k_i > 0 \quad \text{and} \quad \lambda_i = \sqrt[4]{\frac{-k_i}{E_f I_f}} \ \text{for } k_i < 0 \tag{2.4}$$

The problem has assigned a number of $5 \times n$ total boundary conditions, B.C., summarised in figure 2.4.

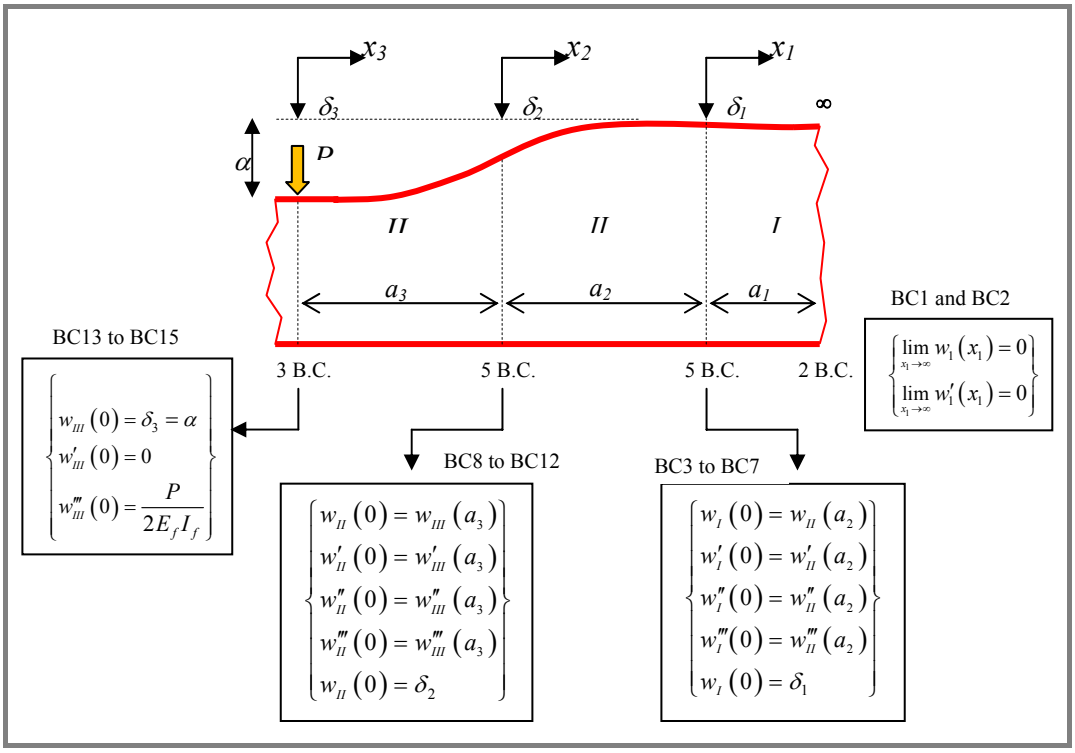

Figure 2.4 Boundary conditions for three segments segment-wise discretisation.

In particular if an infinite beam length is considered there are always two B.C. requiring that the beam does not deform at the outermost end [35, 48, 68]. Solutions for finite length beams are derived in [67]:

$$\lim_{x_1\to\infty} w_1(x_1)=0;\quad \lim_{x_1\to\infty} w'_1(x_1)=0 \tag{2.5}$$

Three further B.C. apply at the loading point:

$$w_n(0)=\alpha;\quad w'_n(0)=0;\quad w'''_n(0)=\frac{P}{2E_fI_f} \tag{2.6}$$

in which α is the indentation displacement at $x=0$ (i.e. maximum indentation). The second of equations (2.6) impose a zero slope at mid beam section due to symmetry, and the third of equations (2.6) results from the equilibrium of vertical forces of the infinitesimal beam at the loading point (equilibrium of shear forces, V), with P being the external load on the top skin. The shear force on the mid-section of the beam at $x=0$ is expressed by $V=-\frac{P}{2}$. Using the expressions for the moment and shear force deduced from the beam theory in Appendix A:

$$\left.\begin{array}{l} M = -EI\dfrac{\partial w^2}{\partial x^2} \quad \text{(A4.4)} \\ \dfrac{dM}{dx} = V \quad \text{(A1.4)} \end{array}\right\}, \qquad \text{results that} \quad \frac{P}{2} = EI\frac{\partial w^3}{\partial x^3} \Leftrightarrow w_n'''(0) = \frac{P}{2E_f I_f}$$

Finally a total $5\times(n-1)$ B.C. apply from imposing continuity of the displacements, slopes, bending moments and shear forces at the interface between adjacent beam segments, and knowing the core displacement at which a new set of material parameters k_i and q_i is set:

$$\left.\begin{array}{c} w_i(a_i) = w_{i-1}(0);\quad w_i'(a_i) = w_{i-1}'(0);\quad w_i''(a_i) = w_{i-1}''(0); \\ w_i'''(a_i) = w_{i-1}'''(0);\quad w_i(a_i) = \delta_{i-1} \end{array}\right\} \text{ where } i = 2,3,...,n \quad (2.7)$$

Imposing the boundary conditions to the n solutions (taken from equations 2.3) yields a system of $5\times n$ non linear equations with $(5\times n+1)$ unknowns: $4\times n$ consisting in A_i, B_i, C_i and D_i (with $i=1$ to n), $(n-1)$ values of a_i (with $i=2$ to n), and finally the last two unknowns consisting in P and α (from which the indentation curve is obtained). The system is reduced to $5\times n$ equations in $5\times n$ unknowns by assigning a value to a_2 and deriving a solution. Iterating the solution for a range of chosen a_2 values yields the entire curve P,α.

The generic final system of simultaneous $5\times n$ equations from the application of all B.C. is non-linear whenever $n>2$. In [68] the previous model is applied to honeycomb core sandwich beams. In this case it is shown that the beam segments described by the same foundation parameters have also all the same extension, $a_i=const$ (for $i=2$ to n). This is due to the regular repeating cellular structure of honeycombs. So the segmentation of sandwich beams is easily established by dimensioning all values of a_i with the same length of the repeating cell unit. This allows a reduction of unknowns and a more straightforward solution of the problem. With foam cores no such information is provided for a_i.

The described segment-wise approach lends itself well as a general modelling approach to the study of indentation in sandwiches with foam cores. By following this scheme different solutions based on different assumptions on the foam uniaxial compressive behaviour can be derived in a straightforward way. In the next subsections the solving systems giving the indentation curve are derived for the basic cases of elastic (E) and elastic-perfectly-plastic (EPP) foundations.

Two further closed-form analytical solutions are then derived which are able to consider generic bilinear (BL, $n=2$ and $k_2 \neq 0$) and bilinear-perfectly-plastic (BLPP, $n=3$ and $k_3=0$) core compressive models, which can significantly extend the application of this indentation model to some peculiar non-linear foam behaviours.

The bi-linear model in particular provides a closed form solution for the indention curve of foam cores which have a linear hardening behaviour in the post-elastic region. This is for instance the case of some popular foam materials such as XPS, EPS or some PMI foam grades [71, 78, 79, 80].

In order to report a concise form of the solving systems for the various foam behaviours, figure 2.4 and tables 2.1 and 2.2 will be much referred. Figure 2.4 in particular shows the notation adopted for a beam segmentation with $n=3$ and $k_3=0$. Tables 2.1 and 2.2 collect all definitions of coefficients and constant terms of the solving systems.

A description of the notation adopted and an example showing how such coefficients are derived is briefly summarised downwards.

Table 2.1 Definition of coefficients in equation 2.16 (E model) and equation 2.20 (EPP model).

Boundary	E model	EPP model
BC1; BC2	$C1 = D1 = 0$	
BC3	$b13 = 1;\ r13 = \alpha$	$b13 = 1;\ r23 = -\frac{q_2}{24Df} \cdot a_2^4;\ a23 = \frac{a_2^3}{3};\ b23 = \frac{a_2^2}{2};\ c23 = a_2;\ d23 = 1$
BC4	$a14 = \lambda_1; b14 = -\lambda_1; r14 = 0$	$a14 = \lambda_1;\ b14 = -\lambda_1;\ r24 = -\frac{q_2}{6Df} \cdot a_2^3;\ a24 = a_2^2;\ b24 = a_2;\ c24 = 1$
BC5	$a15 = b15 = 2\lambda_1^3$	$a15 = -2\lambda_1^2; r25 = -\frac{q_2}{2Df} \cdot a_2^2;\ a25 = 2a_2;\ \ b25 = 1$
BC6	-	$a16 = b16 = 2\lambda_1^3;\ r26 = -\frac{q_2}{Df} \cdot a_2;\ \ a26 = 2$
BC7 to BC10	-	$b17 = d28 = c29 = 1; a210 = 2$

Table 2.2 Definition of coefficients in equation 2.22 (bilinear hardening BL_h model), Equation 2.25 (bilinear softening BL_s model) and equation 2.27 (BLPP model). Abbreviated notation: $m=exp(\lambda_2 a_2)$; $n= exp(-\lambda_2 a_2)$; $s=\sin(\lambda_2 a_2)$; $c=\cos(\lambda_2 a_2)$.

Boundary	BLPP model (equal to either BL_h or BL_s for BC1 to BC7)		
	BL_h model		**BL_s model**
BC1/2	$C1 = D1 = 0$		
BC3	$b13 = 1;\ r23 = -q_2/k_2$ $a23 = ns\ ;\ b23 = n; c23 = ms;\ d23 = mc$		$b13 = 1;\ r23 = -q_2/k_2$ $a23 = n\ ;\ b23 = m; c23 = s;\ d23 = c$
BC4	$a14 = \lambda_1;\ b14 = -\lambda_1$ $a24 = -\lambda_2 n(s-c);\ b24 = -\lambda_2 n(s+c);$ $c24 = \lambda_2 m(s+c);\ d24 = -\lambda_2 m(s-c)$		$a14 = \lambda_1;\ b14 = -\lambda_1$ $a24 = -\lambda_2 n;\ b24 = \lambda_2 m;\ \ c24 = \lambda_2 \cdot c;\ d24 = -\lambda_2 \cdot s$
BC5	$a15 = -2\lambda_1^2$ $a25 = -2\lambda_2^2 nc;\ b25 = 2\lambda_2^2 ms;$ $c25 = 2\lambda_2^2 mc;\ d25 = -2\lambda_2^2 ms$		$a15 = -2\lambda_1^2$ $a25 = \lambda_2^2 n;\ b25 = \lambda_2^2 m; c25 = -\lambda_2^2 s;\ d25 = -\lambda_2^2 c$
BC6	$a16 = b16 = 2\lambda_1^3;$ $a26 = 2\lambda_2^3 n(s+c); b26 = -2\lambda_2^3 n(s-c);$ $c26 = -2\lambda_2^3 m(s-c);\ d26 = -2\lambda_2^3 m(s+c)$		$a16 = b16 = 2\lambda_1^3;$ $a26 = -\lambda_2^3 n;\ b26 = \lambda_2^3 m; c26 = -\lambda_2^3 \cdot c;\ d26 = \lambda_2^3 \cdot s$
BC7	$b17 = 1$		
	BL_h model	**BL_s model**	**BLPP model**
BC8	$r28 = -q_2/k_2\ ;\ a28 = 0$ $b28 = d28 = 1$	$r28 = -q_2/k_2\ ;$ $a28 = b28 = d28 = 1$	$r28 = -q_2/k_2\ ;\ b28 = d28 = 1;\ a28$ from BL_s or BL_h $e38 = -q_3/24D_f\ ;\ d38 = c38 = 1;\ a38 = 1/3;\ b38 = 1/2$
BC9	$a29 = d29 = \lambda_2;$ $b29 = -\lambda_2; c29 = \lambda_2$	$a29 = -\lambda_2;\ b29 = \lambda_2$ $c29 = \lambda_2;\ d29 = 0$	$a29, b29, c29, d29$ from BL_s or BL_h $e39 = -q_3/6D_f\ ;\ b39 = c39 = a39 = 1$
BC10	$a210 = b210 = c210 = 2\lambda_2^3;$ $d210 = -2\lambda_2^3$	$a210 = c210 - \lambda_2^3;$ $b210 = \lambda_2^3$	$a210 = -2\lambda_2^2;\ c210 = 2\lambda_2^2;\ e310 = -q_3/2D_f\ ;$ $a310 = 2; b310 = 1$
BC11	-	-	$a211 = b211 = c211 = 2\lambda_2^3;\ d211 = -2\lambda_2^3;\ e311 = -q_3/D_f\ ;\ a311 = 2;$
BC12-15	-	-	$r212 = -q_2/k_2\ ;\ b212 = d212 = 1;\ d313 = d314 = 1;\ a315 = 2$

Coefficients in tables 2.1 and 2.2 are obtained from applying all boundary conditions (see figure 2.4) to equations (2.3). Systems of equations are obtained where in general the unknowns are A_1, B_1, A_2, B_2, C_2, D_2, A_3, B_3, C_3, D_3, P, α, a_3.

The first ten unknowns come from the differential equations (2.3) and the coefficients associated to these unknowns are called using the same letter in lower-case. Constant terms use the letter r and the first number after the coefficient letter refers to the beam segment ($n=1,2,3$). The second number refers to the applied boundary condition. So the coefficient c_{311} for instance is the

coefficient from collecting all terms in C_3 and imposing the boundary condition BC11: $w_2'''(0) = w_3'''(a_3)$.

The equations resulting from applying BC6 are fully reported here as an example of the procedure to obtain all coefficients summarised in tables 2.1 and 2.2.

The derivatives of the solution equations (2.3b) and (2.3c), for segment $n=1$ ($k_1 > 0$ and $q_1=0$) and segment $n=2$ ($k_2 > 0$ and $q_2 \neq 0$), are derived as:

$$\begin{aligned} w_1'''(x_1) &= 2\lambda_1^3 \cdot e^{-\lambda_1 x_1} \cdot \left[(A_1 - B_1)sin(\lambda_1 x_1) + (A_1 + B_1)cos(\lambda_1 x_1)\right] + \ldots \\ &- 2\lambda_1^3 \cdot e^{\lambda_1 x_1} \cdot \left[(C_1 + D_1)sin(\lambda_1 x_1) - (C_1 - D_1)cos(\lambda_1 x_1)\right] \end{aligned} \tag{2.8}$$

$$\begin{aligned} w_2'''(x_2) &= 2\lambda_2^3 \cdot e^{-\lambda_2 x_2} \cdot \left[(A_2 - B_2)\sin(\lambda_2 x_2) + (A_2 + B_2)\cos(\lambda_2 x_2)\right] + \ldots \\ &- 2\lambda_2^3 \cdot e^{\lambda_2 x_2} \cdot \left[(C_2 + D_2)\sin(\lambda_2 x_2) - (C_2 - D_2)\cos(\lambda_2 x_2)\right] \end{aligned} \tag{2.9}$$

equations (2.8) for $x_1=0$ and (2.9) for $x_2=a_2$ become

$$w_1'''(0) = 2\lambda_1^3 \cdot (A_1 + B_1) + 2\lambda_1^3 \cdot (C_1 - D_1) \tag{2.10}$$

$$\begin{aligned} w_2'''(a_2) &= 2\lambda_2^3 \cdot e^{-\lambda_2 a_2} \cdot \left[\sin(\lambda_2 a_2) + \cos(\lambda_2 a_2)\right]A_2 - 2\lambda_2^3 \cdot e^{-\lambda_2 a_2}\left[\sin(\lambda_2 a_2) - \cos(\lambda_2 a_2)\right]B_2 \ldots \\ &- 2\lambda_2^3 \cdot e^{\lambda_2 a_2} \cdot \left[\sin(\lambda_2 a_2) - \cos(\lambda_2 a_2)\right]C_2 - 2\lambda_2^3 \cdot e^{\lambda_2 a_2} \cdot \left[\sin(\lambda_2 a_2) + \cos(\lambda_2 a_2)\right]D_2 \end{aligned} \tag{2.11}$$

equations (2.10) (for $C_1=D_1=0$) and (2.11) can also be written as:

$$w_1'''(0) = a16 \cdot A_1 + b16 \cdot B_1 \tag{2.12}$$

$$w_2'''(a_2) = a26 \cdot A_2 + b26 \cdot B_2 + c26 \cdot C_2 + d26 \cdot D_2 \tag{2.13}$$

By comparing equation (2.12) with equation (2.10), and (2.13) with (2.11) it is found:

$$\begin{cases} a16 = b16 = 2\lambda_1^3 \\ a26 = 2\lambda_2^3 e^{-\lambda_2 a_2} \cdot \left[sin(\lambda_2 a_2) + cos(\lambda_2 a_2)\right] \\ b26 = -2\lambda_2^3 e^{-\lambda_2 a_2} \cdot \left[sin(\lambda_2 a_2) - cos(\lambda_2 a_2)\right] \\ c26 = -2\lambda_2^3 e^{\lambda_2 a_2} \cdot \left[sin(\lambda_2 a_2) - cos(\lambda_2 a_2)\right] \\ d26 = -2\lambda_2^3 e^{\lambda_2 a_2} \cdot \left[sin(\lambda_2 a_2) + cos(\lambda_2 a_2)\right] \end{cases} \tag{2.14}$$

The boundary condition equation for BC6 is finally obtained from equation (2.12) and (2.13):

$$w_1'''(0) = w_2'''(a_2) \rightarrow -a16 \cdot A_1 - b16 \cdot B_1 + a26 \cdot A_2 + b26 \cdot B_2 + c26 \cdot C_2 + d26 \cdot D_2 = 0 \quad (2.15)$$

The complete procedure for deriving all coefficients summarised in tables 2.1 and 2.2 is extensively reported in the Appendix B.

2.2.1 Pure-elastic and elastic-perfectly-plastic solutions

Most structural foams in general exhibit an initial pure linear-elastic behaviour under uniaxial compression. This stage is then more or less gradually interrupted by the onset of permanent local damage of the cell walls, which increases the material compliance. In this second stage of big deformations the internal voids are gradually filled by the collapsing cell walls until eventually a rapid increase of the compressive stiffness is determined due to material densification.

During the very first linear elastic stage of foam compression the whole length of the sandwich top skin is resting on a pure elastic foundation characterised by the stiffness parameter $k_1>0$, and the segment-wise discretisation consider only one segment coinciding with the whole beam half length. The only governing differential equation is given by equation 2.3a, which has four unknowns (A_1,B_1,C_1,D_1). Two further unknowns are given by P and α. By imposing the 5 B.C. (3 at the loading point and 2 at the outermost beam end as in figure 2.4) the following simplifications are obtained:

$$\begin{cases} \underline{BC1/2:}\ C_1 = D_1 = 0 \\ \underline{BC3:}\ b13 \cdot B_1 = \alpha \\ \underline{BC4:}\ a14 \cdot A_1 + b14 \cdot B_1 = 0 \\ \underline{BC5:}\ a15 \cdot A_1 + b15 \cdot B_1 = \dfrac{P}{2D_f} \end{cases} \rightarrow \left\{ \begin{array}{l} C_1 = D_1 = 0 \\ B_1 = \alpha \\ \lambda_1(A_1 - B_1) = 0 \\ 2\lambda_1^3(A_1 + B_1) = \dfrac{P}{2 \cdot D_f} \end{array} \right| \rightarrow A_1 = B_1 = \alpha \left| \rightarrow 4\lambda_1^3 \alpha = \frac{P}{2 \cdot D_f} \right. \quad (2.16)$$

It is seen that a direct linear relationship is found in explicit form, between the indentation load P and deflection α, which coincides with the expressions given in [35, 48, 67].

$$P = \left(8 \cdot D_f \cdot \lambda_1^3\right) \cdot \alpha \quad (2.17)$$

This solution is valid until the maximum indentation reach the value $\alpha=\delta_1$ (figure 2.1).

The most common behaviour considered in the literature after the first linear elastic stage is perfectly-plastic, modelled with $k_2=0$ and $q_2=\sigma_c*b$ where σ_c is the compressive yield stress usually obtained from tests. The corresponding δ_1 value at yield onset is then evaluated by considering the strain at yield, σ_c / E_c and the foam core thickness t_c:

$$\delta_1 = \frac{\sigma_c}{E_c} t_c \tag{2.18}$$

After the onset of the perfectly-plastic-behaviour, the sandwich beam is split in two parts (or segments according with the segment-wise nomenclature): the outermost where the foam is linear elastic and the inner part (having half length a_2, see figure 2.2) where the foam compressive behaviour is perfectly plastic. In this case there will be 10 B.C. (2 at the outermost beam end, 5 at the transition section between the elastic and plastic core, and 3 at the loading point, see figure 2.4) and 10 unknowns (P, α, A_i, B_i, C_i, D_i with $i=1,2$).

Assigning a value to a_2, a system of linear simultaneous equation is obtained, whose straightforward solution provides the corresponding values for P and α after yield onset.

In particular application of the boundary conditions yields (see table 2.1):

$$\begin{cases} \underline{BC3:}\ a23\cdot A_2 - b13\cdot B_1 + b23\cdot B_2 + d23\cdot D_2 = -r23 \\ \underline{BC4:}\ -a14\cdot A_1 + a24\cdot A_2 + b24\cdot B_2 + c24\cdot C_2 = b14\cdot B_1 - r24 \\ \underline{BC5:}\ r25 - a15\cdot A_1 + a25\cdot A_2 + b25\cdot B_2 = 0 \\ \underline{BC6:}\ -a16\cdot A_1 + a26\cdot A_2 = b16\cdot B_1 - r26 \\ \underline{BC7:}\ B_1 = \delta_1 \\ \underline{BC8:}\ D_2 = \alpha \\ \underline{BC9:}\ C_2 = 0 \\ \underline{BC10:}\ A_2 = \dfrac{P}{2\cdot a210\cdot D_f} \end{cases} \tag{2.19}$$

These reduce to a sub-system of four linear equations:

$$\begin{bmatrix} 0 & a23 & b23 & d23 \\ -a14 & a24 & b24 & 0 \\ -a15 & a25 & b25 & 0 \\ -a16 & a26 & 0 & 0 \end{bmatrix} \cdot \begin{Bmatrix} A_1 \\ A_2 \\ B_2 \\ \alpha \end{Bmatrix} = \begin{Bmatrix} \delta_1 + \dfrac{q_2 \cdot a_2^4}{24Df} \\ -\lambda_1 \cdot \delta_1 + \dfrac{q_2 a_2^3}{6Df} \\ \dfrac{q_2}{2Df} \cdot a_2^2 \\ 2\lambda_1^3 \cdot \delta_1 + \dfrac{q_2 \cdot a_2}{Df} \end{Bmatrix} \tag{2.20}$$

Equation (2.20) shows also that the system can be reduced to a sub-system of three equations in the unknowns A_1, B_2 and A_2 (or P, if BC10 relationship from equation (2.19) is used), and then evaluate α with a fourth explicit equation. The entire P-α curve after core yielding is then obtained by varying the value of a_2, and solving the system at each step. The whole elastic-perfectly-plastic (EPP) indentation curve is then obtained by combining equation (2.17) with the results of the iterative solution of equation (2.20).

2.2.2 Bilinear solution

A generalisation of the elastic-perfectly-plastic (EPP) behaviour is obtained by considering a generic bilinear behaviour where the second segment of the foam core uniaxial compression curve is not a plateau, $k_2 \neq 0$. This extension could usefully model hardening ($k_2 > 0$) or softening ($k_2 < 0$) phenomena accompanying the compression behaviour of the foam after its first linear elastic stage (see figure 2.5).

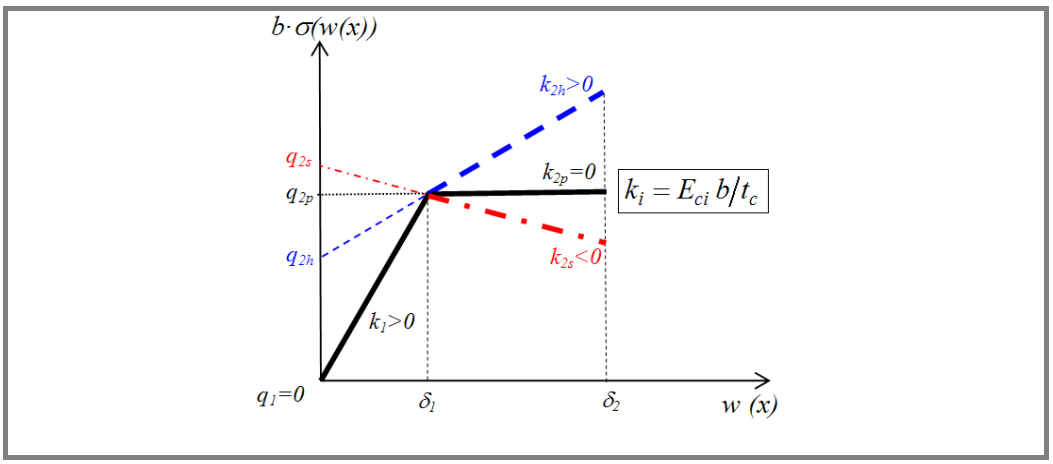

Figure 2.5 Generic bilinear discretisation of the foam uniaxial compression.

Likewise the EPP solution there will be 10 B.C. and 10 unknowns (P, α, A_i, B_i, C_i, D_i with $i=1,2$). The difference is that the general differential equation for the beam segment a_2 is now equation 2.3b (to model hardening) or equation 2.3d (to model softening) instead of equation (2.3c). Although equation (2.3b) is more complex due to the presence of trigonometric and exponential terms in a_2, this is still not a major concern since only two segments are considered ($n=2$). Assigning values to a_2 all non-linear terms becomes constants. In particular the application of all boundary conditions now yields (see table 2.2):

$$\begin{cases} \underline{BC3:}\ \ a23\cdot A_2 - b13\cdot B_1 + b23\cdot B_2 + c23\cdot C_2 + d23\cdot D_2 = -r23 \\ \underline{BC4:}\ \ a14\cdot A_1 - a24\cdot A_2 + b14\cdot B_1 - b24\cdot B_2 - c24\cdot C_2 - d24\cdot D_2 = 0 \\ \underline{BC5:}\ \ -a15\cdot A_1 + a25\cdot A_2 + b25\cdot B_2 + c25\cdot C_2 + d25\cdot D_2 = 0 \\ \underline{BC6:}\ \ -a16\cdot A_1 - b16\cdot B_1 + a26\cdot A_2 + b26\cdot B_2 + c26\cdot C_2 + d26\cdot D_2 = 0 \\ \underline{BC7:}\ \ B_1 = \delta_1 \\ \underline{BC8:}\ \ b28\cdot B_2 + d28\cdot D_2 - \alpha = -r28 \\ \underline{BC9:}\ \ a29\cdot A_2 + b29\cdot B_2 + c29\cdot C_2 + d29\cdot D_2 = 0 \\ \underline{BC10:}\ \ a210\cdot A_2 + b210\cdot B_2 + c210\cdot C_2 + d210\cdot D_2 = \dfrac{P}{2D_f} \end{cases} \tag{2.21}$$

A system of five linear simultaneous equations is obtained in the unknowns A_1, A_2, B_2, C_2 and D_2:

$$\begin{bmatrix} 0 & a23 & b23 & c23 & d23 \\ a14 & -a24 & -b24 & -c24 & -d24 \\ -a15 & a25 & b25 & c25 & d25 \\ -a16 & a26 & b26 & c26 & d26 \\ 0 & a29 & b29 & c29 & d29 \end{bmatrix} \cdot \begin{Bmatrix} A_1 \\ A_2 \\ B_2 \\ C_2 \\ D_2 \end{Bmatrix} = \begin{Bmatrix} \delta_1 + q_2/k_2 \\ -b14\cdot\delta_1 \\ 0 \\ b16\cdot\delta_1 \\ 0 \end{Bmatrix} \tag{2.22}$$

Two explicit equations are then obtained from BC8 and BC10 (see equation (2.21) and table 2.2), which give the values of P and α:

$$\alpha = B_2 + D_2 - q_2/k_2 \tag{2.23}$$

$$P = 4\cdot D_f \cdot \lambda_2^3 \cdot \left[A_2 + B_2 + C_2 - D_2\right] \tag{2.24}$$

The iterative solution of equations (2.22-2.24) at varying a_2 will then provide values of (P, α), i.e. the indentation curve after the onset of the second linear

compressive behaviour (k_2, q_2), while for the first linear portion of the indentation curve equation (2.17) is still valid up to a value of $\alpha=\delta_1$ (figure 2.1). If a post elastic linear softening ($k_2<0$) behaviour is to be modelled, then the three solving equations (2.22-2.24) now become:

$$\begin{bmatrix} 0 & a_{23} & b_{23} & c_{23} & d_{23} \\ a_{14} & -a_{24} & -b_{24} & -c_{24} & -d_{24} \\ -a_{15} & a_{25} & b_{25} & c_{25} & d_{25} \\ -a_{16} & a_{26} & b_{26} & c_{26} & d_{26} \\ 0 & a_{29} & b_{29} & c_{29} & 0 \end{bmatrix} \cdot \begin{Bmatrix} A_1 \\ A_2 \\ B_2 \\ C_2 \\ D_2 \end{Bmatrix} = \begin{Bmatrix} b_{13}\cdot\delta_1 - r_{23} \\ -b_{14}\cdot\delta_1 \\ 0 \\ b_{16}\cdot\delta_1 \\ 0 \end{Bmatrix}$$
$$\alpha = a28\cdot A_2 + b28\cdot B_2 + d28\cdot D_2 + r28 \qquad (2.25)$$
$$P = 2D_f \cdot a210\cdot\left(A_2 + C_2 - B_2\right)$$

2.2.3 Bilinear-perfectly-plastic solution

The previous solutions all use two linear segments at most. A generalisation of this discretising procedure would involve a generic $n>2$ number of linear segments, with the possibility to better approximate highly non-linear curves. When $n\geq 3$ the system of equations, obtained from applying the boundary conditions to equations (2.3), can always be split into a linear subsystem (coinciding with equations (2.27) shown below), and a non-linear subsystem whose number and nature of the equations depends on n and the foundation parameters representing each n^{th} segment with $n>2$. As shown in the previous section, linearization of the first subsystem is made possible by assigning values to the unknown a_2. The non-linear subsystem will in general contain equations with trigonometric and exponential terms in the unknowns $\lambda_i a_i$ ($i>2$), and their most straightforward solution will be through numerical methods.

One further case for which a simple closed form analytic solution is derived is proposed here. This is represented by a foam compression curve discretised with three linear segments with $k_1>k_2>k_3=0$ and $0<q_2<q_3$. This is the case where the third segment is a plateau as in the EPP solution, but with a generic bilinear discretisation preceding the plateau. The segment-wise discretisation for this case is schematically represented in figure 2.4. A total number of 15 B.C. is applicable, while the differential equation for the beam segment a_1 is equation (2.3a), for

beam segment a_2 is equation (2.3b) and for beam segment a_3 is equation (2.3c). If values of a_2 are assigned as done before, the remaining unknowns are A_1, B_1, A_2, B_2, C_2, D_2, A_3, B_3, C_3, D_3, a_3, α, P with $C_1=D_1=0$ determined as usual after applying the sandwich beam outermost boundary conditions. The application of all boundary conditions for this case yields (see table 2.2):

$$\begin{cases} \underline{BC3:}\ a23A_2 - b13B_1 + b23B_2 + c23C_2 + d23D_2 = -r23 \\ \underline{BC4:}\ a14A_1 - a24A_2 + b14B_1 - b24B_2 - c24C_2 - d24D_2 = 0 \\ \underline{BC5:}\ -a15A_1 + a25A_2 + b25B_2 + c25C_2 + d25D_2 = 0 \\ \underline{BC6:}\ -a16A_1 - b16B_1 + a26A_2 + b26B_2 + c26C_2 + d26D_2 = 0 \\ \underline{BC7:}\ B_1 = \delta_1 \\ \underline{BC8:}\ e38(a_3)^4 + a38(a_3)^3 A_3 + b38(a_3)^2 B_3 + c38a_3C_3 + d38D_3 = \delta_2 \\ \underline{BC9:}\ a29A_2 + b29B_2 + c29C_2 + d29D_2 - e39(a_3)^3 - a39(a_3)^2 A_3 - b39a_3B_3 - c39C_3 = 0 \\ \underline{BC10:}\ a210A_2 + c210C_2 - e310(a_3)^2 - a310a_3A_3 - b310B_3 = 0 \\ \underline{BC11:}\ a211A_2 + b211B_2 + c211C_2 + d211D_2 - e311a_3 - a311A_3 = 0 \\ \underline{BC12:}\ r212 + b212B_2 + d212D_2 = \delta_2 \\ \underline{BC13:}\ D_3 = \alpha \\ \underline{BC14:}\ C_3 = 0 \\ \underline{BC15:}\ A_3 = P/4D_f \end{cases} \tag{2.26}$$

The solution in terms of indentation curve values P,α, is found in three steps. The first step consists in solving the linear sub-system in the unknowns A_1, A_2, B_2, C_2, D_2:

$$\begin{bmatrix} 0 & a23 & b23 & c23 & d23 \\ a14 & -a24 & -b24 & -c24 & -d24 \\ -a15 & a25 & b25 & c25 & d25 \\ -a16 & a26 & b26 & c26 & d26 \\ 0 & 0 & 1 & 0 & 1 \end{bmatrix} \cdot \begin{Bmatrix} A_1 \\ A_2 \\ B_2 \\ C_2 \\ D_2 \end{Bmatrix} = \begin{Bmatrix} \delta_1 + q_2/k_2 \\ -b14 \cdot \delta_1 \\ 0 \\ b16 \cdot \delta_1 \\ \delta_2 + q_2/k_2 \end{Bmatrix} \tag{2.27}$$

The unknowns left are five: a_3, A_3, B_3, α with the fifth unknown P directly given by a fifth explicit equation (see BC15 in equation 2.26).

These four remaining unknowns are solved by the following non-linear system of four equations:

$$\begin{cases} e38\cdot(a_3)^4+1/3\cdot(a_3)^3\cdot A_3+1/2\cdot(a_3)^2\cdot B_3+\alpha=\delta_2 \\ e39\cdot(a_3)^3+(a_3)^2\cdot A_3+a_3\cdot B_3=H39 \\ e310\cdot(a_3)^2+2\cdot a_3\cdot A_3+B_3=H310 \\ e311\cdot a_3+2\cdot A_3=H311 \end{cases} \tag{2.28}$$

where

$$\begin{aligned} H39&=a29\cdot A_2+b29\cdot B_2+c29\cdot C_2+d29\cdot D_2 \\ H310&=a210\cdot A_2+c210\cdot C_2 \\ H311&=a211\cdot A_2+b211\cdot B_2+c211\cdot C_2+d211\cdot D_2 \end{aligned} \tag{2.29}$$

The system in equation (2.28) is linearised after solving the following third order equation in the unknown a_3:

$$e39\cdot(a_3)^3-\frac{1}{2}\cdot H311\cdot(a_3)^2+H310\cdot a_3-H39=0 \tag{2.30}$$

The coefficients of equation (3.30) are obtained by assigning values to a_2 and solving the system (2.27). In general, the part of indentation curve solution corresponding to the plateau follows the solutions of the preceding linear elastic and bilinear cases. The bilinear case in particular ends when $\alpha=\delta_2$. The final value of a_2 at which $\alpha=\delta_2$ is also the starting value when solving the system (2.27). In general a_2 may vary towards growing or decreasing values while a_3 will gradually grow with the proceeding of indentation. The correct trend of variation of a_2 will be dictated by the solutions of equation (2.30). In general a pair of complex conjugate roots are obtained which have no physical meaning. If the third real root is positive then it has physical meaning and this is considered for the further solution of the remaining unknowns. If the real root is negative it has no physical meaning, and this is possibly due to a wrong choice of the trend of variation (growing or decreasing) chosen for a_2. One application to experimental data, verifying the above considerations, is reported in the chapter V.

2.3 Failure load at face sheet fracture

Skin flexural failure can occur after core yielding with the progression of indentation, before the onset of significant foam densification under the loading point. This is in particular the case for brittle FRP laminas with high bending stiffness (e.g. thick laminate skins). In this paragraph the skin face material is supposed to be ideally brittle, with a uniaxial tensile/compression behaviour which is linear elastic up to fracture failure (absence of any plastic or non-linear elastic deformation stages). This assumption is reasonable when considering FRP face skins made of brittle thermoset matrices. Analytical models to predict the external load at the onset of the face skin flexural failure are proposed in [66] and [67] respectively for a RPP and an EPP core behaviour. In this work the analytical procedure proposed in [67] is readapted for a generic BL core behaviour, which comprises the EPP case. The same procedure though can be easily extended in principle and adapted to cases of more generic non-linear core compressive behaviours.

The equilibrium of forces and moments on the beam segment II for a BL compressive behaviour of the foam core material is schematically represented figure 2.6.

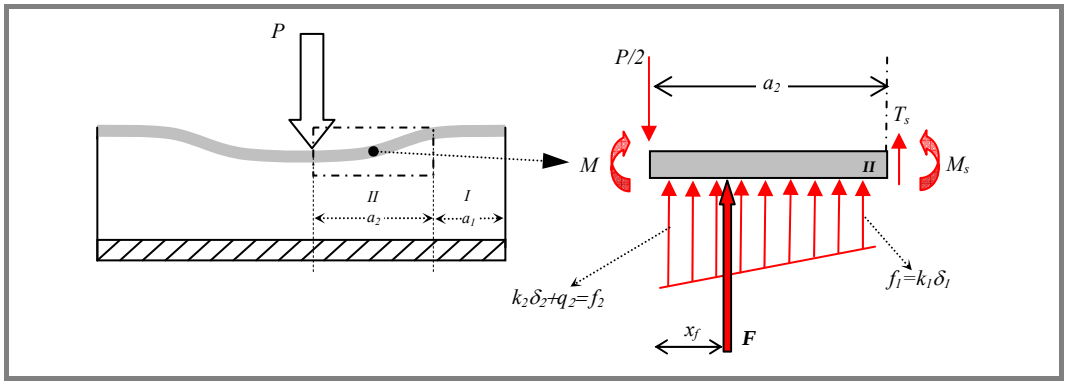

Figure 2.6 Equilibrium scheme for the beam segment a_2 in a bilinear segment-wise discretisation (T_s – top skin shear force; M_s – top skin bending moment).

Core reaction forces on the beam segment will be continuously distributed and linearly growing from the value $f_1=k_1\delta_1$ to $f_2=k_2a_2+q_2$. A trapezoid

distribution is obtained whose resulting F force and centroid coordinate x_f are given by:

$$F = \frac{a_2}{2}(f_1 + f_2); \quad x_f = \frac{a_2}{3}\left(\frac{f_1 + 2f_2}{f_1 + f_2}\right) \tag{2.31}$$

Equilibrium of forces and moments gives:

$$M = M_s + T_s \cdot a_2 + F \cdot x_f \quad \rightarrow \quad M = M_s + \frac{P}{2} \cdot a_2 + F \cdot (x_f - a_2) \tag{2.32}$$

The boundary condition BC5 for the BL or EPP models (see tables 2.1 and 2.2) states that:

$$M_s = -D_f \cdot w_1''(0) = -D_f \cdot a15 \cdot A_1 = 2D_f \cdot \lambda_1^2 \cdot A_1 \tag{2.33}$$

Assuming a linear elastic behaviour of the skin laminate up to brittle failure, with σ_f maximum tensile stress, the bending moment at failure M_f, which is the maximum value of M in equation (2.32), is given by:

$$M_f = \sigma_f \cdot \frac{b \cdot t_f^2}{6} \tag{2.34}$$

By equating equations (2.32) and (2.34) the critical flexural failure load is found as :

$$P = \sigma_f \cdot \frac{b \cdot t_f^2}{3a_2} - \frac{4D_f \cdot \lambda_1^2 \cdot A_1}{a_2} - 2F \cdot \left(\frac{x_f}{a_2} - 1\right) \tag{2.35}$$

Adaptation of equation (2.35) to the EPP case is straightforward by considering $F=\sigma_c \cdot b \cdot a_2$ *and* $x_f=a_2/2$. Equation (2.35) gives the critical flexural load as a function of a_2. In fact A_1 in the formula is also a function of a_2, determined by solving equations (2.20) or (2.22). The exact value of the critical load is then found by considering also the relationship between P and a_2 obtained by solving the indentation problem, e.g. equations (2.19, 2.20) for the EPP model and equations (2.22-2.24) for the BL hardening model.

The above procedure has been applied to evaluate the failure load using material and specimen data given in [67] (consult table 2 in [67]). The values of the calculated critical loads are compared in table 2.3 with those from [67]

(consult chapter I, section 1.6.1, equations (1.18, 1.19)) and those calculated using formula 18 described in [66] (consult chapter I, section 1.6.1, equation (1.13)).

Table 2.3 Comparison of critical load predictions at face skin bending failure (sample data from [67]).

t_c [mm]	t_f [mm]	E_f [MPa]	σ_f [MPa]	***P* (skin failure) [kN]**		
				Shuaeib and Soden [67]	**Soden [66]**	**Present work**
3	25	18000	250	5.33	4.43	4.16
3	25	18000	500	6.92	6.26	6.14
6	25	18000	250	10.15	8.85	8.60
3	50	18000	250	5.70	4.43	3.99
3	25	10000	250	5.09	4.43	4.28
3	25	20000	250	5.39	4.43	4.19

It is observed that the critical loads predicted with the present procedure (using the EPP model for the foam) are in general comparable with predictions in [66] and [67], and in particular lower than those predicted in [67] and very close to those from [66]. Developed MATLAB® scripts for predicting the load value at face skin bending failure with the present procedure for the EPP and BL behaviour, as well as scripts to model the literature load approach from [66] and [67] are reported in Appendix C.

CHAPTER III

Laminates and foams experimental characterisation

3.1 Introduction

The present chapter, as well as the next chapters IV and V, describes the experimental activity carried out with the aim to validate the closed form solutions derived in chapter II and associated with the proposed *segment-wise* approach. In this first chapter, in particular the choice of the constituent materials used to assemble the indented sandwich specimen is presented, together with the description of the experimental tests carried out to characterize the constitutive material parameters required. The implementation of standard testing methods to measure compressive, tensile and shear properties of FRP skin faces and foam cores is then described.

In particular, in-plane and flexural properties of the laminate material used as sandwich skin face are to be used as input data both in the analytical (chapter V) and numerical simulations (chapter VI). Moreover, Young's modulus of the foam materials in compression, yield strength, i.e. the stress *plateau* at core plastic crushing for crushable foams, and the foam's stress *vs.* strain curve under uniaxial compression are measured and used to find the foam compression parameters (k_i and q_i) explained in the SW formulation. In addition to foam stress *vs.* strain curve under uniaxial compression, shear stress *vs.* strain curves will be also measured to be used as input data in the numerical simulation of a non-linear polyamide foam (chapter VI).

3.2 Sandwich constituent materials

In general five sandwich beam types have been manufactured and tested in this work. Each sandwich type comprised different skin and core materials in order to obtain a complete range of different expected behaviours, with a particular attention to the performances of the employed cores in compression, in order to reproduce different indentation behaviours. Constituent materials employed as skin or core on the sandwiches analysed for this study, were in part commercial products provided by industrial suppliers, and in part manufactured *in-house* for the purposes of the analysis. Before describing the tests performed for the mechanical characterization, a brief comment of the employed materials is reported.

3.2.1 Laminate materials for the skins

All sandwiches assembled and tested in this work (see table 3.1) employed fibre reinforced plastic face skins.

In one case the sandwich panel was provided in a complete assembled form by its commercial manufacturer (sandwich *3S* in table 3.1). In all other cases the sandwich specimen were assembled by adhesively joining the skin laminates to a foam core material with the application of an epoxy glue.

The skins were in one case manufactured *in-house* (sandwich *4S* in table 3.1) and in all other cases obtained as finite industrial products. A more detailed description follows in the next sub-sections.

Table 3.1 Sandwich beams tested in this work.

Sandwich ID	Skin laminate	Foam Core
1S	Glass/PA6 $[0°/90°]_{s\ twill}$	PMI31
2S		PA
3S	PBT1212-50	XPS40
4S	Glass/Epoxy $[0_{50}°/90_{50}°]_s$	PVC C70.55
5S	Glass/PA6 $[0°]_{s\ unid.}$	PMI31

3.2.1.1 *In-house* laminate panels

A symmetric cross ply $[0^o/90]_s$ glass fibre/epoxy resin laminate was manufactured with the hand lay-up technique obtaining a fibre volume fraction of 40%. The panel was fabricated with stacking up six layers of a glass fibre woven fabric with a nominal thickness of 2 mm and areal weight of 200 kg/m^3. To avoid excessive data scatter during experimental tests, good practices during panel fabrication, such as control of proper fibres alignment is essential. The manufacturing steps obeyed to the following sequence:

1. Cutting of the fabric layers to the desired dimensions and protection of the borders with a paper tape to avoid strapping of warp and weft fibres during handling (figure 3.1a-b);
2. Cleaning of the working-bench surface (consisting of a glass platter) and disposal of a releasing film of Mylar to avoid the permanent attachment of the panel (figure 3.1a-b);
3. Preparation of the matrix by adding the two commercial components, epoxy resin and a reaction catalyst agent and mixing for about 3 min in order to get a good homogenization of both components (figure 3.1c). The pot life of the catalysed resin was not inferior to 15 min, which allowed impregnation of all stacked plies before the onset of gelification;
4. Apply a small portion of resin directly over the transparent film and immediately start the lay-up of the first layer of fabric;
5. Wet the first layer very well using a “cylindrical roller” to spread the resin all over the fabric surface (figure 3.1d);
6. Alternate matrix layers with fibre layers, wetting all the fibre area with the resin; (figure 3.1e-g);
7. Finally place a peel ply tissue over the last layer of fabric. These film leaves the panel with a rough surface finish which will favourite a stronger grip of the glue layer when gluing the skin to the foam core to assemble the sandwich (figure 3.1h);
8. The cure reaction of the employed epoxy grade is completed after 24 hours resting at room temperature (figure 3.1i).

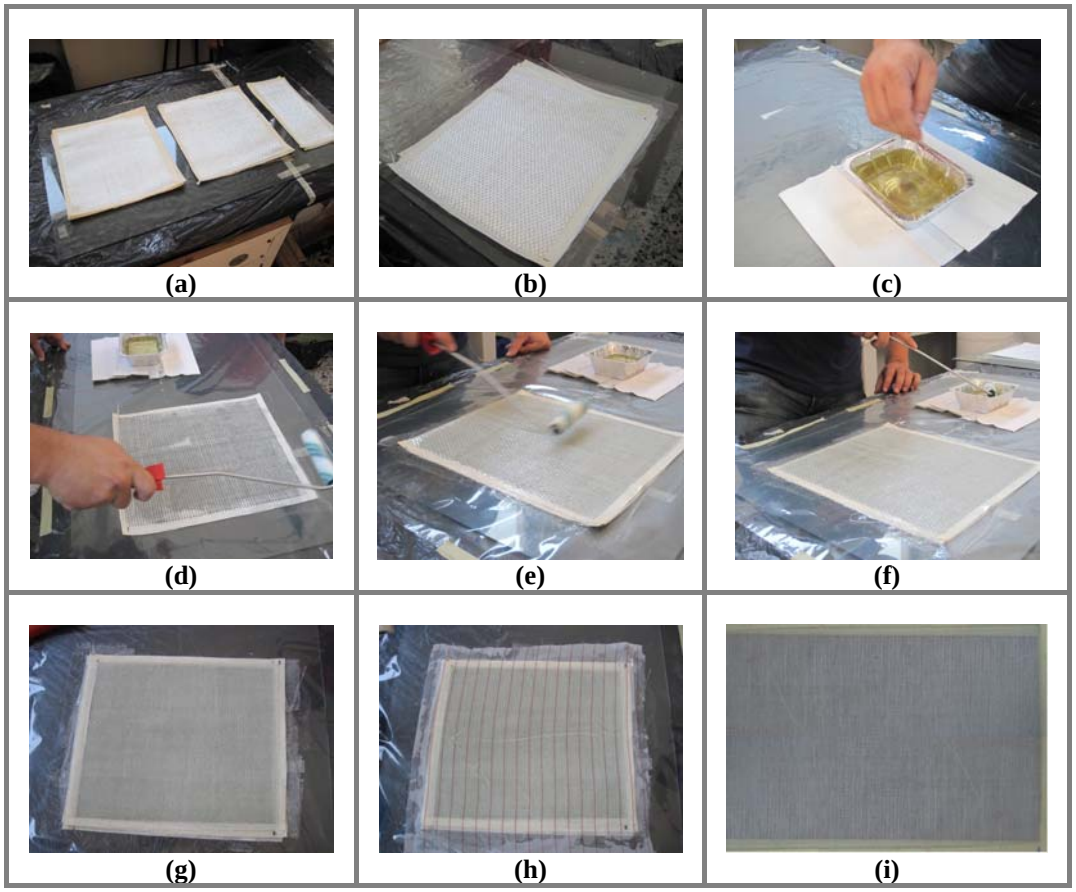

Figure 3.1 Preparation of $[0^o/90^o]_s$ glass fibre/epoxy resin panel by the hand lay-up technique.

3.2.1.2 Commercial laminate panels

All commercial panels selected in this work and used as face skins were made of glass fibres reinforced thermoplastic matrices. These materials were supplied on their final cured state by industrial producers. A description provided from suppliers follows:

i) TEPEX® dynalite102 (figure 3.2a), consists of multiple layers of continuous fibre reinforcements in a Polyamide-6 (PA6) matrix.

These panels use continuous fibres providing this way an improved strength and stiffness and are available with different fibre volume contents, fabrics and thickness.

Due to its thermoplastic nature, TEPEX® is perfectly adjustable to be used on continuous industrial production process and formed into components in extremely short cycle times (between 15 and 60s, depending on component

thickness) with a highly consistent quality throughout the entire production process and excellent cost-effective results.

The fundamental stages involved are heating the composite sheet, forming and cooling in the mould, then removing and possibly finishing the product. Heating by means of infrared radiation is the preferred method, but contact heating is also possible. Depending on the complexity of the component, and according to the supplier BondLaminates, forming techniques using rubber and metal moulds or just a rubber diaphragm pressurised are available.

Commercial applications for these laminates are often sports articles, automotive (e.g. bumper beams) and anti-ballistics. Having a melting temperature of 220°C, forming temperature of approximately 240°C and continuous use temperature of 120°C, this product enables very good forming properties and surfaces with a *Class A*[1] appearance [81].

***ii*)** SkinTec® PBT (figure 3.2b), is a laminate made of continuous glass fibres and a polybutylene terephthalate (PBT) thermoplastic matrix. Tailor-made combinations of glass fabrics and stitched mats are available with different lengths and thickness. According to the supplier IQ Tec Germany GmbH, these panels are suitable to be thermoformed (PBT melting temperature is 204 ºC) and press molded with the same technology employed in steel materials, for similar productivity and performance. Unfinished or coated surfaces are also accessible [82].

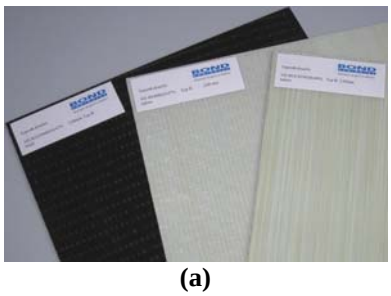

(a)

(b)

Figure 3.2 Supplied laminated panels: **(a)** Polyamide TEPEX® *dynalite* 102; **(b)** Skin Tec® PBT.

[1] ***Class A***: automotive and CAD design terminology for a surface that conforms to a set of tolerances for continuity to surrounding surfaces and smoothness within the surface. In terms of the end-user a *Class A* appearance will traduce into a visual and touch quality perception for a physical surface of some component.

Table 3.2 Laminate materials used as face sheet in the sandwich specimens.

ID	Laminate (fibre/matrix)	Fibre content [%vol]	Thickness t_f [mm]	Supplier	Commercial name
1L	Glass/epoxy $[0_{50}°/90_{50}°]_{s\ plain}$	40%	2	manufactured by hand lay-up	
2L	Glass/PA6 $[0_{50}°/90_{50}°]_{s\ twill}$	47%	2	Bond Laminates ®	TEPEX® *dynalite* 102-RG600(x)/47%
3L	Glass/PA6 $[0°]_{s\ unid.}$	60%	2	Bond Laminates ®	TEPEX® *dynalite* 102-RGUD385(x)/60%
4L	PBT1212-50-0	60%	0.8	IQ Tec Germany GmbH ®	Skin Tec® PBT

3.2.2 Foam materials for the core

In the recent decades, research and development of high density and high quality cellular foams endorsed an increase of these as sandwich core materials. Almost any polymer, either thermoset or thermoplastic, may be expanded and the density range available is suitable for a great number of applications [4, 41]. Although cellular foams do not have the same high stiffness and strength to weight ratio as honeycombs, they do offer other appealing properties. They are in general less expensive, surface preparation and shaping is simple and the foam surface is easy to bond to, making the process of assembling the skins easier than with honeycomb cores. Besides, cellular foams offer high thermal insulation, acoustical damping, and the closed cell structure of most foams ensure that the structure will be buoyant and resistant to water penetration [4].

Polymers are foamed using physical or chemical foaming agents. Physical blowing agents are gases that are dispersed in the liquid polymer and expand to form voids when the temperature increases or the pressure decreases. Chlorofluorocarbons (CFCs) used to be the most popular, but are being phased out due to their harmful effects on the environment. Typically physical foaming agents require a continuous foam extrusion into ambient atmosphere.

Chemical blowing agents are mixed into the polymer and decompose into gases, often nitrogen or carbon dioxide, when the processing temperature reaches the decomposition temperature of the blowing agent. The foam expansion is done in a batch process in closed moulds. A sheet is cast from the

polymer which already contains a chemical blowing agent and follows a solidification or gelation of the sheet, free-hanging in a hot air oven or lying in a heated water, in order to expand it. The expanded structure is finally set through cooling or steam treatment [83].

Some low density foam materials have been investigated in this work, including a thermoplastic matrix whose main appeal is in the possibility of this class of polymers to better comply with *end-of-life* regulations. All the foams were kindly provided by industrial manufactures. A brief description of properties and applications for each employed foam is here reported:

***i*)** Polymethacrylimide (PMI) foams are manufactured by hot forming of methacrylic acid/methacrylonitrile copolymer sheets. They are lightly crosslinked and have very thin rigid closed cells with densities available from 30 to 300 kg/m^3. Even if brittle with an ultimate elongation at break of approximately 3% in tension, the mechanical properties are quite good and the temperature tolerance allows PMI cores to be used with some high-temperature crosslinking epoxies, making them a suitable core option in autoclave manufacturing. PMI cores are also among the most expensive foam solutions commercially available [4, 83].

Rohacell® (figure 3.3a) is one commercial brand of PMI foams. It is halogen free, using alcohol as a blowing agent during the foaming process. Due to its thermoplastic nature (reduced cross linked nature) it is able to be thermoformed and easy to shape and machine. According to the manufacturer, Evonik, it presents excellent mechanical properties, high dimensional stability under heat, solvent resistance and, particularly at low temperature, a low thermal conductivity allowing its use on a range of areas such as aerospace industry (e.g. Bulkhead A340, bulkhead A380, helicopter rotor blades, etc); medicine technology (e.g. x-ray tables); high performance sporting goods (Corima frame bicycles and wheels, formula 1 flaps and wing parts, racing skis, etc.); rail vehicles; shipbuilding; interior panelling of motor vehicles; wind energy and defence (e.g. radomes), among others [84].

***ii*)** Polyamide (PA) foams are among a new generation of thermoplastic foams resulting from either environmental and recycling restrictions, either from process cycle and cost optimization industrial milestones. In the last decade, automotive industry has been the major impellor for the research and study of these foam materials. Zotefoams proposes the Zotek® N B50 (figure 3.3b), a lightweight, closed cell and cross-linked polyamide-6 (PA6) foam. It is produced by an ecological friendly process of expansion of the base polymer using azotes as blowing agent in an autoclave high pressure and temperature controlled environment. Connected to the absence of VOCs (Volatile Organic Compounds) during the foaming process are the reduced levels of *Fogging*[2] and *Odour*[3], in concordance with several automotive standards (VDA 270 and DIN 75201). Based on manufacturer information some good properties of PA6 include: the intrinsic outstanding high temperature tolerance and excellent resistance to a range of chemicals (hydrocarbons, such as oils, fuels, alcohols and ketones), the low weight, flexural response, buoyancy, thermal and acoustic insulation. Zotek® N B50 has also a significantly higher upper operating temperature limit and presents excellent patterns of durability and longevity. Commonly used on high temperature resistant seals, gaskets, industrial packaging, and finding also application on demanding energy absorbing semi structural parts, and as thermal insulation material such as in engine compartments of automobiles [85].

***iii*)** Polystyrene (PS) foam is produced either by extrusion (XPS) or by expansion (EPS) in closed moulds. PS has closed cells and is available in densities ranging from 15 to 300 kg/m^3. It denotes fairly good mechanical and thermal insulation properties but its incompatibility with styrene solvents forbidden it to be used with ester-based adhesives. PS is also one of the cheapest foam core materials available in market. ThermoTec® XPS-PBT (figure 3.3c), is the commercial term adopted by IQ Tec Germany GmbH for a sandwich based on the combination of an extruded polystyrene (XPS) foam core attached to two polybutylene terephthalate (PBT) face sheets, SkinTec® PBT, through a

[2] ***Fogging***: automotive terminology to indicate windscreen fogging by chemical contamination in new cars;

[3] ***Odour***: attempt from car manufacturers to quantify what is essentially a subjective judgement of the negative effects of "new car smell" caused by new materials.

technology based on thermo adhesives. According to the supplier, excellent mechanical properties can be reached because of the glass fibre reinforcement and the high glass fibre content of the face sheets, leading to a weight reduction potential, as the face sheet thickness can be reduced compared to traditional FRP laminates. The continuous production line guarantees a consistent high quality of the product. Panel size dimensions are limited up to 13.6 x 3.0 x 0.2 [m] and easy to machine. Adhesive bonding and riveting is also possible. Application in building construction due to its good insulation properties is quite common [82].

iv) Polyvinyl chlorides (PVC) are the most common foam cores used in structural composite applications and are available both in thermoplastic (linear PVC) and thermoset (cross-linked) versions. The major difference between thermoplastic and thermoset PVC cores are that the latter generally have better mechanical properties and temperature tolerance, but are less ductile.

Even though, cross-linked PVC has an ultimate elongation of about 10% in tension which is significantly better than polyurethane (PU) and Polystyrene (PS) foams. PVC foams are available with densities from 30 to 400 kg/m^3 and are the most widely used among all foams, and perhaps all other core materials, even if more expensive than PU and PS cores. Low density PVC present around 5% of open cells, whereas the higher densities have exclusively closed cells, being for this reason very appreciated in naval applications. In some cases, low crosslink densities may be thermoformed [4, 83].

The commercial brand AIREX® C70.55 (figure 3.3d), is a closed cell, cross-linked PVC foam produced by a foaming process using almost exclusively air as blowing agent.

According to the supplier, Alcan, it provides a good impact strength, good sound and thermal insulation, an excellent resistance to chemicals and good fire performance (self-extinguishing).

Its fine cell structure offers an excellent bonding surface that is compatible with most resins and manufacturing processes, in parallel with low resin absorption volumes. Suitable manufacturing processes are contact moulding (hand/spray), pre-peg processing, adhesive bonding and thermoforming. Main application fields are aerospace (helicopter rotor blades, radomes, cockpit doors, insulating

panels, interiors, etc.), road and rail (roof panels, interiors, front-ends, etc), marine (radomes, fire resistant interiors), among others [86].

Table 3.3. Foam materials used as core in the sandwich specimens.

ID	Foam	Matrix	Density ρ [kg/m^3]	Thickness t_c [mm]	Supplier	Commercial name
1F	PMI 31	Polymethacrylimide	32	10	Evonik Röhm GmbH	Rohacell® 31 IG
2F	PA	Polyamide-6	52	10	Zotefoams	Zotek® N B50
3F	XPS	Polystyrene	40	28	IQ TecGermany GmbH	ThermoTec® XPS-PBT[1]
4F	PVC	Polyvinylchloride	60	15	Alcan Airex AG	AIREX® C70.55

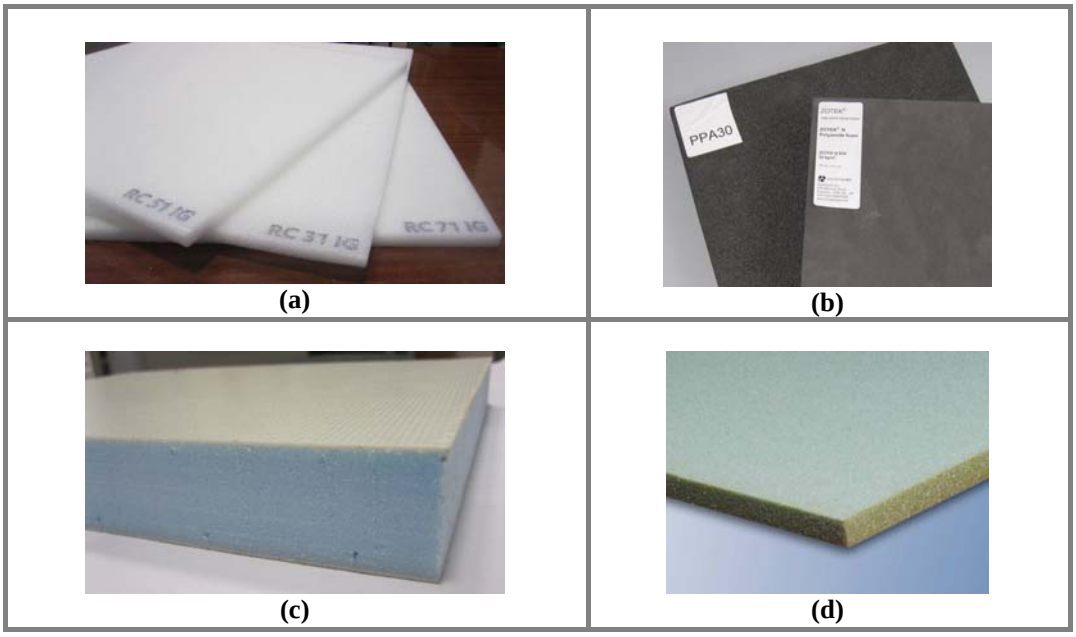

(a) **(b)** **(c)** **(d)**

Figure 3.3 Supplied foam: **(a**) Rohacell®; **(b)** Zotek®; **(c)** ThermoTec®; **(d)** AIREX®.

3.3 In-plane tensile laminate properties

3.3.1 Experimental apparatus and test coupons

Tensile tests were conducted on two universal testing machines: an electro-mechanical Hounsfield equipped with a load cell of 20 kN and on a servo-hydraulic MTS with a 100 kN load cell.

With the Hounsfield, tests were done in displacement control mode (0.5 and 1 mm/min) and an external data logger unit (HBM UPM100) conditioned and synchronously acquired the load data from the load cell and the strain data from the gauge length extensometer placed between the grips at the mid-center of the specimen.

All data is collected with the software HBM CATMAN by connecting UMP100 and the PC through a USB GPIP board from National Instruments. The MTS was employed whenever predicted failure loads were higher than 20 kN. Data received from the machine load cell and from a MTS extensometer is collected to an external PC via the MTS digital control unit. Tests have been done in load control mode, imposing a rate of 2 kN/min for specimen from laminate *1L* and 5 kN/min for specimens from laminate *3L*.

In-plane quasi-static tensile tests were performed according to ASTM D3039M-00 [87], calculating the tensile modulus for both in-plane orthogonal principal material directions (axes of orthotropy), except for the case of balanced fabrics for which measures were obtained in a single direction.

Following the recommendation from the standard whenever testing unidirectional materials (or strongly unidirectional dominated laminates) to failure in the fibre direction, or whenever testing unidirectional materials in the perpendicular direction of the warp fibres (or matrix direction), tabs were applied to the specimens cut from laminate *3L* to prevent early fracture in the grip zone.

Tab configuration was selected accordingly table 2 of [87] in order to produce acceptable failure modes in the gage section. These were made of woven E-glass fibre reinforced composite and glued in the specimen at ±45º to the loading direction. In addition, to prevent gripping slippage, sandpaper patches were placed between specimen faces and the grip jaws whenever needed.

Special care was taken to ensure a proper specimen/system alignment in order to eliminate excessive spurious bending as a result of misaligned grips, incorrect specimens positioning or poor specimen preparation. At least 5 specimens per laminate panel were cut to the recommended standard dimensions (see table 3.4) and tested.

Table 3.4 Tensile coupons dimensions.

Panel material	ID	Width *b* [mm]	Length *l* [mm]	Thickness *t* [mm]
Glass/Epoxy	1L	25.39	250	1.96
Glass/PA6 $_{twill}$	2L	23.97	250	2.03
Glass/PA6 $_{unid.(long.\ direction)}$	3L	15.19	250	2.04
Glass/PA6 $_{unid.(transv.\ direction)}$	3L	24.41	250	2.01
PBT	4L	not tested due to shortage of material		

(a)

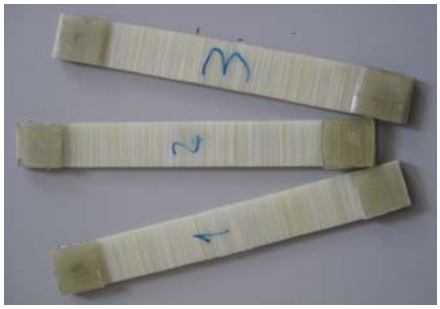

(b)

Figure 3.4 In-plane test specimens: **(a)** Tepex® dynalite 102 coupons - $[90°]_s$ unid , $[0°]_s$ unid , $[0°_{50}/90°_{50}]_s$ twill; **(b)** Tepex® dynalite 102 coupons w/tabs $[90°]_s$ unid.

(a)

(b)

Figure 3.5 In-plane test apparatus: **(a)** Hounsfield universal testing machine equipped with a 20 kN load cell; **(b)** MTS universal testing machine equipped with a 100 kN load cell.

3.3.2 Results and discussion

Table 3.5 reports the average values and variation (based on standard deviation) of all measured parameter from the tensile test performed.

Table 3.5 Laminate Tensile Properties. The *M* superscript values have been measured with uncertainty equal to standard deviation from 5 tested samples (acc. ASTM D 3039/D 3039M-00 [87]). Superscript *S* is used for data provided by the supplier [82].

ID	E_{xx} [*GPa*]^{I}	E_{yy} [*GPa*]^{II}	$\sigma_{r\,xx}$ [*MPa*]^{III}	$\sigma_{r\,yy}$ [*MPa*]^{IV}	$\varepsilon_{r\,xx}$ (%)^{V}	$\varepsilon_{r\,yy}$ (%)^{VI}
1L	19.42±1.0^{M}	-	300.4±15^{M}	-	-	-
2L	20.21±0.63^{M}	-	396.2±21^{M}	-	2.27±0.06^{M}	-
3L	45.98±1.51^{M}	9.10±0.21^{M}	949.6±26^{M}	29.2±1.1^{M}	1.99±0.31^{M}	0.44±0.005^{M}
4L	16.9^{S}	-	434^{S}	-	-	-

Note: ^{I} Young modulus measured on the fibre direction; ^{II} Young modulus measured on the transverse direction; ^{III} Tensile strength on the fibre direction; ^{IV} Tensile strength on the transverse direction; ^{V} Elongation break on the fibre direction; ^{VI} Elongation break on the transverse direction.

The measured properties for the commercial laminate TEPEX® *dynalite* 102-RG600(x)/47%, denominated here as *2L*, are in conformity with the declared values in the manufacturer datasheet with discrepancies around 10% for the Young's modulus, 2% for the tensile strength and 3% for the tensile elongation [81]. For the case of the TEPEX® *dynalite* 102-RGUD385(x)/60% (*3L*), supplier datasheet is not available, but as expected for unidirectional fabrics, mechanical performance on the longitudinal or fibre direction is much superior to mechanical performance obtained on the transverse or matrix direction, being in evidence the remarkable 46 GPa value measured for the Young's modulus and the 950 MPa measured for the tensile strength.

For the Skin Tec® PBT laminate (*4L*), a discrepancy of 38% was measured in the Young's modulus and of 17% for the tensile strength value when confronted with the values presented in the manufacturer datasheet [82].

Furthermore, and as expected for FRP materials, the observed tensile failure mode was typically brittle. In figure 3.7, pictures of the observed failure modes and the respective codification (see the failure code suggested by ASTM D3039) are depicted for some of the tested coupons produced from the laminate panels.

(a) Fibre bridge LGM (P2,P3)

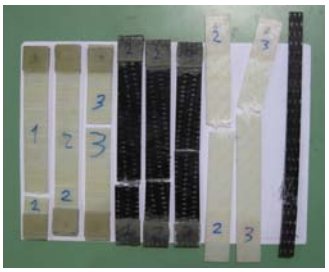

(b)

(c) SIT (P2)

(d) LAB (P1)

(e) SIT (P2)

(f)

SMV (P3)

Figure 3.7 Ultimate tensile failure modes: **(a)** Tepex® PA twill (coupons P2 and P3); **(b)** Tepex® coupons $[90°]_s$ unid; **(c)** Tepex® PA $[0°]_s$ unid (coupon P2); **(d)** Tepex® PA $[0°]_s$ unid (coupon P1); **(e)** Tepex® PA $[0°]_s$ unid (coupon P2); **(f)** Tepex® PA $[0°]_s$ unid (coupon P3).

Figure 3.7a, illustrates the situation of *fibre-bridge* occurred in two coupons of the twill fabric TEPEX® dynalite 102-RG600(x)/47%. On this case the failure occurred laterally on the middle gage area for both coupons (failure code LGM). For the unidirectional TEPEX® dynalite 102-RGUD385(x)/60%, different failure modes were observed when tested on the fibre direction, depending on the tested coupon. Hence, for coupon P1 (figure 3.7d) a lateral failure mode at the bottom tab area was observed (failure code LAB), while for coupon P2 (figure 3.7c and 3.7e) a long splitting inside the top tab area was observed (failure code SIT). Testing coupon 3 (figure 3.7f) of the same laminate, again a long splitting occurred, but this time on multiple areas of the coupon (failure code SMV). In all the three coupons of the unidirectional TEPEX fabric

the failure could be considered as more “explosive” than the failures occurred in the balanced twill TEPEX® fabric.

3.4 Flexural laminate properties

3.4.1 Experimental apparatus and test coupons

As expected in the case of composite laminates, differences between tensile and flexural properties tend to be significant, thus the need to measure the flexural Young’s modulus and flexural strength in order to use it in the Winkler bending theory employed for the indentation model investigated.

Flexural properties of the fibre-reinforced plastic composite skins are determined by means of a three-point bending (TPB) test according to the international standard EN ISO14125:1998 [88]. All TPB tests have been performed on an universal electro-mechanical Instron 3367 testing machine controlled via PC with the software *Instron Bluehill-2* (see figure 3.8a).

The test machine was equipped with a load cell of 1 kN. All sample dimensions and the testing machine cross-head speed (1 mm/min) were selected according with the standard recommendations. An Instron TPB “loading rig” was used, consisting of two supports with 4 mm diameter each and a 10 mm diameter indenter (figure 3.8b).

(a)

(b)

Figure 3.8 (a) Universal Instron 3367; **(b)** Three-point bending (TPB) set-up.

At least 5 specimens were tested. Specimen nominal dimensions and span values, reported on table 3.6, are in agreement with material Class III suggested by the standard [88].

Table 3.6 Flexural coupon nominal dimensions and test span.

Panel ID	Width *b* [mm]	Length *l* [mm]	Thickness *t* [mm]	Outer span *L* [mm]
1L,2L,3L	15	60	2	40
4L	not tested due to shortage of material			

3.4.2 Results and discussion

Measured values are reported in table 3.7:

Table 3.7 Laminate flexural properties.

Panel material	ID	Flexural Young´s Modulus E_f [GPa]		Flexural Strength σ_f [MPa]
Glass/Epoxy	1L	14.74 ± 0.8^{M}		415.78 ± 31^{M}
Glass/PA6 $_{twill}$	2L	15.70 ± 0.39^{M}		585^{S}
Glass/PA6 $_{unid.}$	3L	*Longitudinal (0º)* 42.35 ± 0.63^{M}	*Transverse (90º)* 8.25 ± 0.14^{M}	--
PBT	4L	15.80^{S}		434^{S}

Note: Properties with the *M* superscript were experimentally obtained acc. BS EN ISO1425 [88]; *S* superscript were provided by the supplier [81, 82].

The measured flexural modulus for the commercial laminate TEPEX® *dynalite* 102-RG600(x)/47% (2*L*), compares well with the one declared in the manufacturer's datasheet, with a maximum discrepancy as high as 18% [81]. Flexural strength was not measured and the manufacturer's value was used as input data in the developed models.

For the case of the TEPEX® *dynalite* 102-RGUD385(x)/60% (*3L*), a supplier datasheet is not available.

For the Skin Tec® PBT laminate (*4L*) flexural tests were not performed. Instead, values presented in the manufacturer datasheet were used as input data in the developed models [82].

3.5 Flatwise compressive foam properties

3.5.1 Experimental apparatus and test coupons

Compressive behaviour of each foam type in the transverse direction (normal to the sandwich plane) is assessed according to the guidelines given in ASTM C365-03 [77]. Tests are conducted on an Instron 3367 testing rig equipped with a 1 kN load cell in displacement control with a crosshead speed of 1mm/min. Test apparatus consists on a rigid flat support where lays the specimen to be compressed and another metallic flat platen between the specimen and the load cell. A spherical bearing was placed between the load cell and the flat compressing platen in order to distribute the load uniformly across all the specimen area, compensating for small misalignment errors. For the type of materials studied, the ASTM C365-03 standard [77] recommends specimens having square or circular cross section with an area between 625 mm^2 and 10000 mm^2. All coupons analysed had a square section with a nominal area of 900 mm^2. At least five specimens per foam type were prepared and a special care to cutting operations was essential to assure that loaded ends of specimens were parallel to each other and perpendicular to the sides of the specimen.

As mentioned on the ASTM C365-03 standard [77], in some cases, specially for honeycomb cores, it is recommended to reinforce the loaded ends with thin facings bonded to the core. This is called a stabilized compression test in opposition to the bare compression test whenever the edges are not stabilized. At the beginning of this study both tests were considered, but acquaintance with the experimental method and critical assessment guided to the decision of just carrying on with the stabilized test, performing the flatwise compression of a sandwich block which already includes the bonded skin faces. In this way the skin-foam reciprocal constraint is included in the assessed foam material characterisation, which is reckoned beneficial since the same constraint is present in the indentation loading of the sandwich. In figure 3.9 it is shown the experimental apparatus for three of the tested foam specimens.

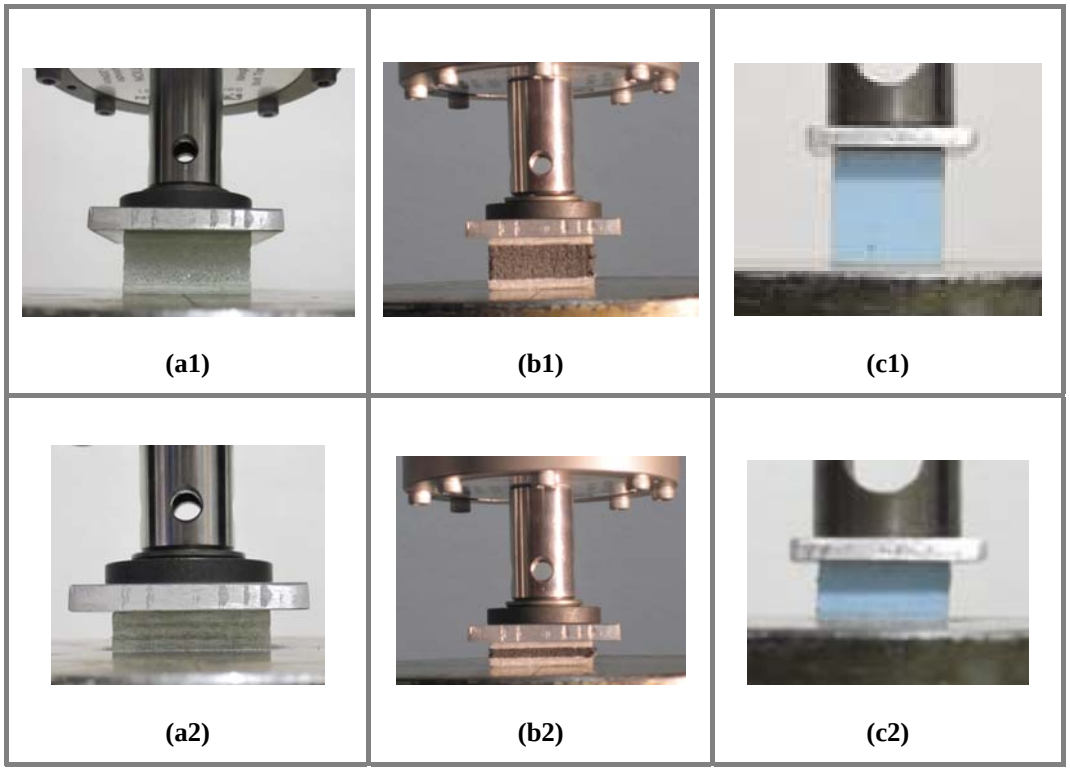

Figure 3.9 Flatwise foam compression test: **(a)** PMI 31 IG Rohacell® (stabilized test); **(b)** PA Zotek® N B50 (stabilized test); **(c)** XPS ThermoTec® (stabilized test).

3.5.2 Results and discussion

The measured stress-strain curves from the flatwise compression tests are shown in figure 3.10 and figure 3.11.

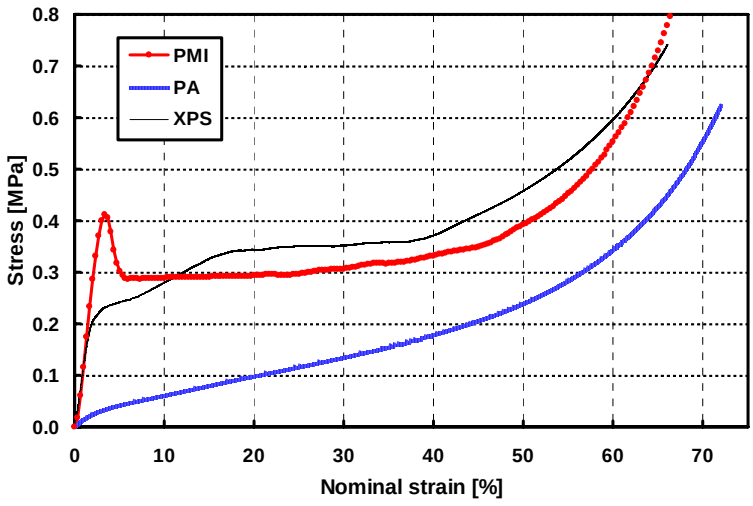

Figure 3.10 Stress vs. strain curves from uniaxial flatwise compression tests on the foam cores: PMI 31 IG Rohacell®; PA Zotek® N B50; XPS ThermoTec®.

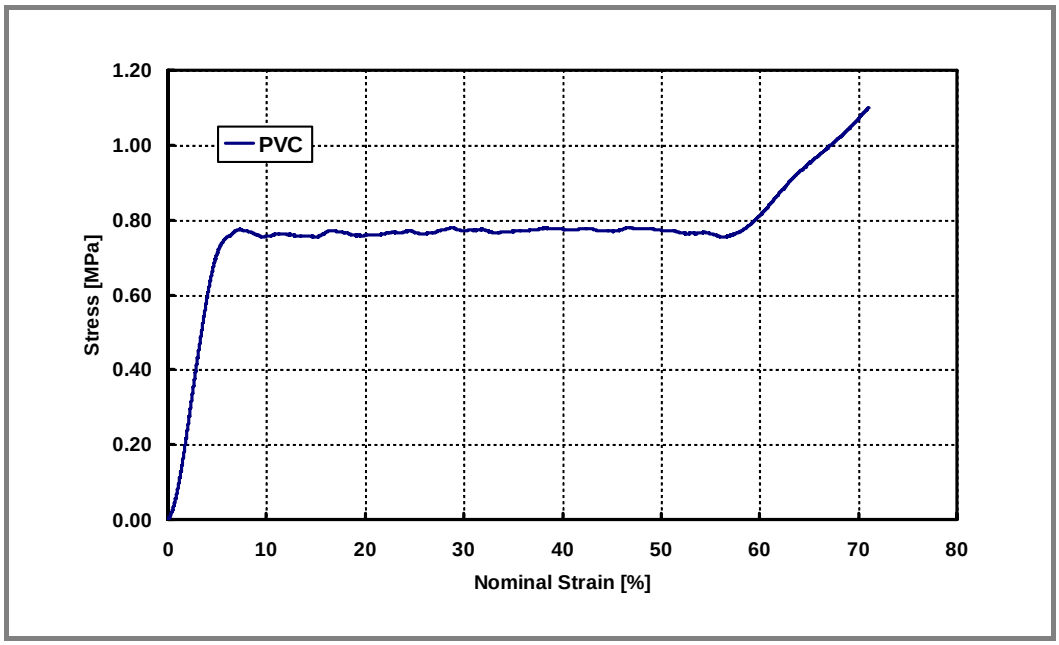

Figure 3.11 Stress vs. strain curve from uniaxial flatwise compression tests on a PVC AIREX® C70.55 foam.

It is first of all observed that PVC, XPS and PMI had a much higher stiffness than the pure thermoplastic PA foam and exhibited a crushable behaviour after yield onset. A somewhat peculiar behaviour was observed with XPS. In fact it was found that there is an intermediate second stage between the first purely elastic stage and the third plastic plateau stage, where a linear hardening behaviour is detected with a quite steep trend although not as steep as in the elastic stage. The compression curve measured with the XPS foam core in figure 3.10 shows a first zone up to about 18% compression which exhibits a bilinear hardening trend. This zone is then followed by a plateau which extends up to about 40% strain, after which densification starts to take place. This behaviour was repeatedly observed on all samples of the same material, so that its occurrence could not be explained as an occasional internal damage of the specimen or bad positioning. An attempt to find some data in the literature reporting on the compressive behaviour of XPS foams was also made but none was found. The presence of an intermediate hardening phase between the linear elastic and the perfectly plastic zones provides a good case study to evaluate the BL and BLPP indentation models presented in sections 2.1.2 and 2.1.3, as it will be discussed in chapter V.

As expected, the PA foam exhibited a hyperelastic behaviour with a highly non-linear smooth trend all the way from early elastic strains up to densification, hence providing a good case study to evaluate the BL indentation model as it will be discussed in chapter V.

The compression behaviour of the PMI and PVC foam cores showed a marked crushable behaviour, with the post-elastic phase between yielding and densification that is very well approximated by a plateau. In fact, a progressive crushing mechanism is triggered.

After an initial pure linear elastic behaviour, the collapse of the cell walls with filling of the foam internal voids gradually proceeds till the material is all compacted (densification stage). The elastic and plastic stages are then well modelled with the classical EPP behaviour for this class of foam materials.

The observed "*crushable*" behaviour also implies that crushing of foam is initiated in one particular cell layer, usually the "weakest" layer, rather than in a whole volume of the foam.

This cell layer is crushing at almost constant stress, *plateau*, while increasing the strain up to the densification value. When this layer is fully crushed, the opposite cell walls get in contact causing an increase in stiffness and stress which triggers crushing of the next cell layer [35].

In the case of the PMI foam, and as observed in figure 3.10, there is a peak yield stress followed by a steep decrease until a plateau stress value is reached. This behaviour is believed to be due to the absorption of epoxy resin by the PMI at the skin-core interface, favoured by the very low density value of this grade of PMI foam used. In fact the epoxy glue used to bond the skins showed a rather low viscosity, and the PMI 31 is on the contrary a very porous material due to the low density.

So it is likely that the epoxy glue penetrated for some depth inside the foam, strengthening this same part of the foam. The effect was an initial higher yield onset, while the yield stress decreases to lower values once the crushing mechanism starts to involve the inner foam layers, not affected by the epoxy glue.

A summary reporting the measured flatwise compression properties from the tested foams is found in table 3.8.

Table 3.8 Compressive properties of the foams materials.

Foam ID	Commercial name	Compressive Young's Modulus E_c [MPa]	Compressive Strength σ_c [MPa]
1F	Rohacell® PMI 31 IG	$16.3^{M}/36^{S}$	$0.31^{M}/0.4^{S}$
2F	Zotek® PA N B50	0.80^{M}	0.10^{M}
3F	ThermoTec® XPS	11.62^{M}	0.36^{M}
4F	AIREX® PVC C70.55	$17.56^{M}/58^{S}$	$0.75^{M}/0.85^{S}$

Note: Properties with the *M* superscript were experimentally measured acc. ASTM C365-03 [77] and with *S* superscript were provided by the supplier [84, 86].

In addition, a mention to the sensitive of the method during characterization of these low density foam materials. Even in the case of foam materials with a typical crushable behaviour, discrepancies between the measured Young's modulus and the manufacturer's data were observed. This is observed for the case of the Rohacell® PMI (*1F*) and AIREX® PVC (*4F*) materials. In fact, reported results for a Rohacell® PMI 51 WF foam in an experimental characterization study performed by Li et al. [89] refers some discrepancies between experimental and manufacturer's data.

It is finally interesting to observe that a few other standards are also available to perform uniaxial foam compression characterisations: ASTM D1621-73 (*Standard test methods for compressive properties of rigid cellular plastics*) used in [90], ASTM D3574-91 (*Standard test methods for flexible urethane foams*) used in [89] or EN ISO 3386-1 [91]. These standards present slight differences between them, essentially based on the recommended specimen dimensions and geometry, type of material to be characterized and its density, the adopted mechanism to guarantee a uniform pressure on the specimen, use or not of an extensometer for the Young's modulus calculation, among others. It remains valid though the observation already made about the preference of the ASTM C365 in this work, since it recommends foam specimens for the flatwise compression including the bonded upper and lower skins.

3.6 Shear foam properties

3.6.1 Experimental apparatus and test coupons

Besides the uniaxial compressive properties of the foams described in the previous section by a flatwise compression test, a shear test is performed in the case of the Zotek® PA foam. The experimental shear stress *vs.* shear strain curve is therefore used in chapter VI on the simulation of non-linear foams using the hyperfoam model available in the numerical software ABAQUS [92].

The Instron 3367 testing machine was employed to implement a test method for the determination of pure shear properties of the core materials, according to the standard ASTM C273-00 [92]. Although the implemented test does not mimic a pure shear effect, it is reported to be reliable for what concerns the determination of the shear strength and the shear modulus parallel to the plane of the sandwich, as long as the line of action of the direct tensile or compressive force pass through the diagonally opposite corners of the foam block. Therefore, a special care should be taken into account in order to use loading plates of the suitable length. Shear tests were conducted using the experimental setup from figure 3.12.

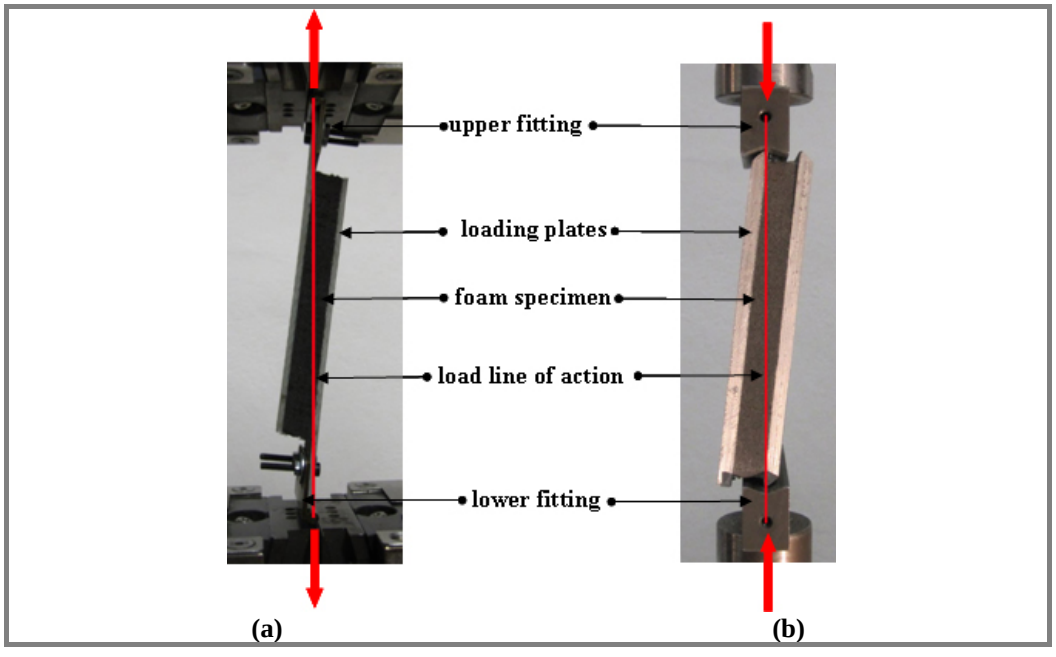

Figure 3.12 Loading plates and load line of action during the shear foam test of the PA Zotek® N B50 foam: **(a)** fixtures used in the tension setup; **(b)** fixtures used in the compression setup.

In figure 3.12a, a tensile line of action pass through the opposite corners of the foam specimen and the shear test is performed in tension. On the contrary in figure 3.12b, a compressive line of action pass through the opposite corners of the foam specimen and the shear test is performed in compression.

The specimen depicted in figures 3.12a and 3.13a uses a PA Zotek® N B50 foam combined with Tepex $PA_{twill.}$ skins which are fixed to metallic hinges in both ends. This way, the metallic hinges contact with the load cell and transfers the tensile load to the foam. On the other hand, the specimen depicted in figures 3.12a and 3.13a uses a PA Zotek® N B50 foam combined with two aluminium plates. In this case the loading plates contact the load cell, transferring the compressive load to the foam.

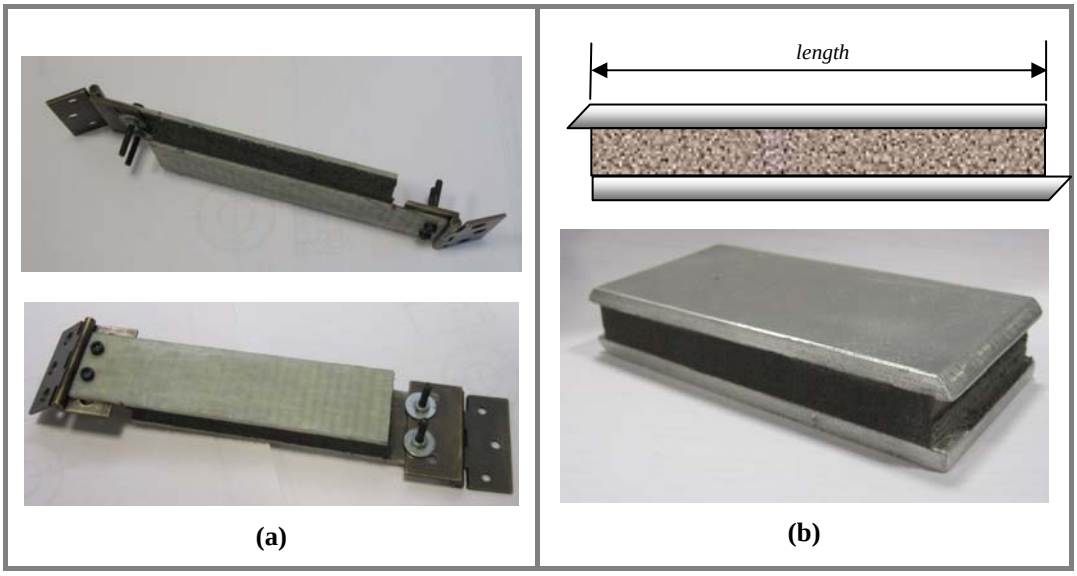

Figure 3.13 Shear foam specimens: **(a)** PA Zotek® N B50 foam bonded to Tepex PA_{twill} skins for tensile shear test; **(b)** PA Zotek® N B50 foam bonded to metallic plates for compressive shear test.

Table 3.9 reports both specimen dimensions.

Table 3.9 Shear test nominal specimen dimensions.

Shear test setup	Width *b* [mm]	Length *l* [mm]	Core thickness *t* [mm]	Skin or aluminium plate thickness [mm]
In tension	30	100	10	2
In compression	53	107	10	5

3.6.2 Results and discussion

Figure 3.14 shows the shear stress *vs.* shear strain curve for both compressive and tensile test setup.

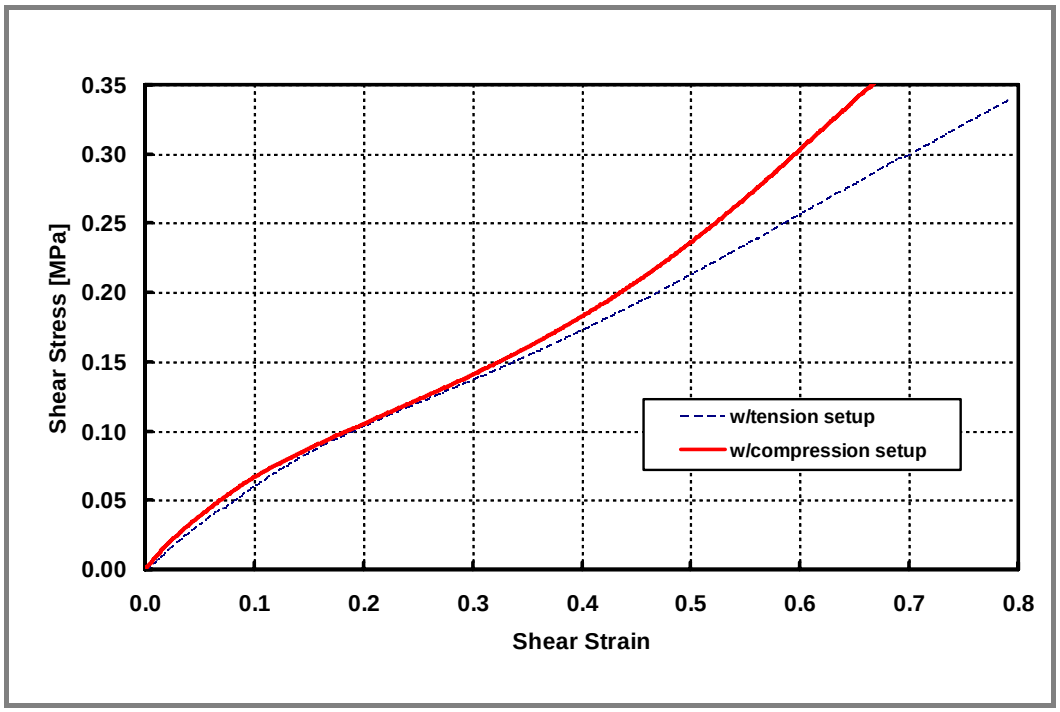

Figure 3.14 Stress vs. strain curve from shear test (using tension and compression setup) for the Zotek® PA N B50 foam core.

As observed in figure 3.14, although both curves initially denote a linear trend, they quickly change to a rather marked non-linear behaviour.

Shear curves are very much similar up to about a 40% shear strain, regardless of the tension or compression testing setup used.

Above this value the two experimental curves diverge probably due to the experimental technical hitches in maintaining a correct line of load for higher strains.

The shear curve data obtained with the compression setup will be applied to the fitting of the hyperelastic ABAQUS foam model, so called hyperfoam (see chapter VI).

The shear modulus was calculated based on the slope of the initial elastic trend (up to 5% strain).

Table 3.10 Core shear modulus for Zotek® PA N B50 foam, acc. ASTM C273-00 [92].

Shear test setup	Shear modulus [MPa]
In tension	0.70
In compression	0.84

Both measured values are similar but lower than the manufacturer reported value of 1.19 MPa[4].

[4] information kindly emailed by supplier on 16.06.2008.

CHAPTER IV

Sandwich experimental characterisation

4.1 Introduction

The laminates and foam materials described in the previous chapter are bonded to each other to produce sandwich specimens with the scope of characterizing the flexural and indentation behaviour under a localised load. In view of that, this chapter describes the sandwich specimens tested and the implemented experimental analyses.

Some of the results in particular, such as the indentation experimental curves, will be confronted in chapter V with the analytical predictions based on the models developed in chapter II, and with the predictictions of numerical models in chapter VI.

4.2 Sandwich beams preparation

Five sandwich beam types have been considered in this work, whose combination of skin and core materials is summarised in table 4.1. Of these sandwiches, only one (the *3S*) was an industrial product supplied by its producer in its final assembled form under the trade name of ThermoTec®. All others were obtained by gluing the laminates onto the foam panels by using a commercial epoxy resin Cecchi C-System 10-10 (see figure 4.1).

Table 4.1 Summary of the sandwich beams analysed with their principal mechanical and geometric parameters. Properties with the *M* superscript have been measured (uncertainty equal to standard deviation from 5 tested samples), and superscript *S* is used for data provided by the supplier. Samples *3S* and *3Sbis* were cut from the same panel and hence have identical constituent properties. Sample *3S* was used for the TPB characterisation and sample *3Sbis* for the full evaluation of the indentation behaviour (see chapter V), so they will always be referred to as *3S*.

Sandwich ID	Skin				Core			
	laminate	t_f [mm]^{I}	E_f [GPa]^{II}	σ_f [MPa]^{III}	Foam	t_c [mm]^{IV}	E_c [MPa]^{V}	σ_c [MPa]^{VI}
1S	Glass/PA6 $[0°/90°]_{s\ twill}$	2	15.70 ± 0.39^{M}	585^{S}	PMI31	10	16.3^{M}	0.31^{M}
2S					PA	10	0.8^{M}	0.10^{M}
3S	PBT1212-50	0.8	15.8^{S}	434^{S}	XPS40	28	11.62^{M}	0.36^{M}
3Sbis								
4S	Glass/epoxy $[0_{50}°/90_{50}°]_s$	2	14.74 ± 0.8^{M}	415.78 ± 31^{M}	PVC C70.55	15	58^{S}	0.75^{M}
5S	Glass/PA6 $[0°]_{s\ unid.}$	2	42.35 ± 0.63^{M}	$^{VII}49.6\pm26^{M}$	PMI31	10	16.3^{M}	0.31^{M}

Note: ^{I} Face sheet thickness; ^{II} Face sheet flexural modulus; ^{III} Face sheet flexural strength; ^{IV} Core thickness; ^{V} Core compression Young's modulus; ^{VI} Core compression strength; ^{VII} Tensile strength was used because bending/flexural strength was not available.

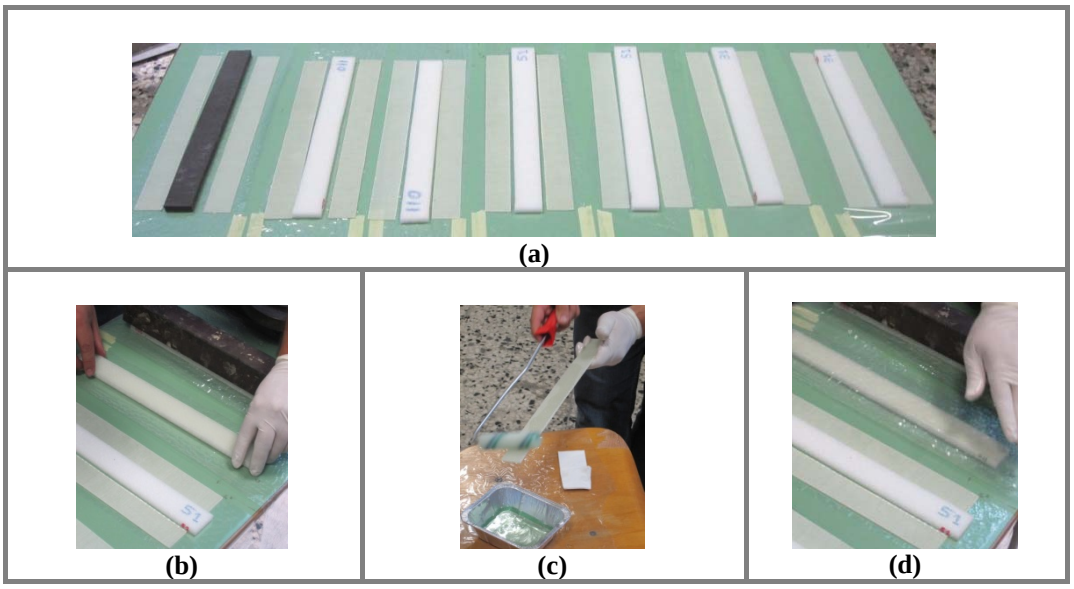

(a) **(b)** **(c)** **(d)**

Figure 4.1 Preparation of sandwiches coupons: **(a)** PMI, PA core and GF/Epoxy skins; **(b)** gluing and positioning of core to lower skin; **(c)** wetting a skin with epoxy resin; **(d)** positioning of top skin to core and placement of a protecting transparent film.

The epoxy glue completed its curing after 15 hours at room temperature, after which the sandwich beam samples were cut and brought to a constant width by using a band saw (see figure 4.2 for the specimens final appearance).

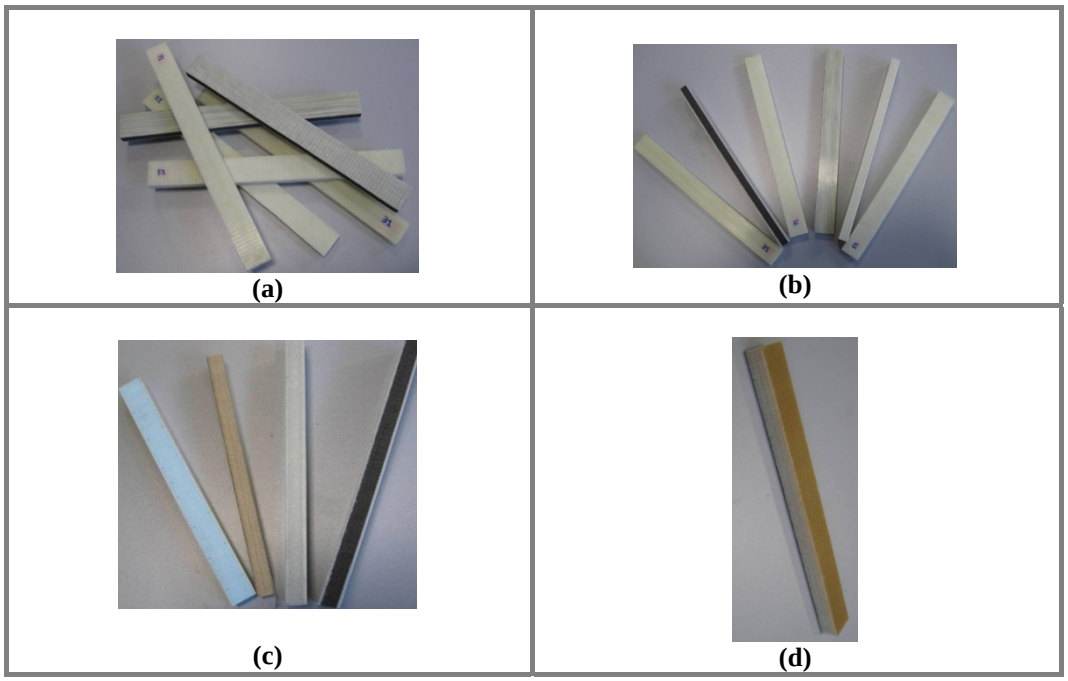

Figure 4.2 (a),(b) PMI, PA core with Tepex® skins; **(c)** from left to right: ThermoTec® XPS-PBT, PVC core with GF/epoxy skins, PMI core with Tepex® skins, PA core with Tepex® skins; **(d)** PVC core with GF/epoxy skins.

4.3 Three-point bending test

The five sandwich beam types considered in this work employ four different foam materials with different compressive behaviours as commented in chapter III (e.g. see figure 3.10). It is observed that the four foam materials have similar and rather low values of densities (ranging between 32 to 60 kg/m^3 as reported in table 3.3)[1]. Furthermore one foam, the PA, exhibits a rather strongly non-linear behaviour comparable to a hyperelastic material, while PVC and PMI have a pure crushable, and hence elastic-perfectly-plastic behaviour, and XPS exhibits a quite peculiar bilinear-perfectly-plastic and hence ultimately crushable behaviour. Although the main focus of the present thesis is on the evaluation of the

[1] Structural PMI or PVC foams can also be provided with higher density values, up to about 150-200 kg/m^3. It is though evident that indentation damage is more favoured in low density foam grades, hence the choice to test in this work low density foams.

indentation behaviour, three-point bending tests have also been performed in order to evaluate the flexural stiffness of the sandwich beam types, and assess the influence of the different foam materials. In fact the role of the foam core is fundamental for the sandwich concept to work, i.e. for ensuring a proper load transfer from the upper to the lower skin, and hence allowing the expected enhancement of bending stiffness. The Three-Point Bending (TPB) test has been implemented to assess the flexural behaviour. In this setup localised loads are applied on the supports and on the specimen mid-span, so that one further investigated aspect has been the influence of local indentation during the TPB on the calculated bending stiffness. This influence is possibly made stronger by the low density and low Young's modules in compression exhibited by the adopted foam materials.

4.3.1 Experimental method and test specimens

The TPB tests implemented and carried out followed only in part the recommendations given by the reference standard ASTM C393-00 [93], suggested for the determination of flexural properties of sandwich beam constructions. One main difference with the standard prescriptions was the use or repeated TPB tests on the same specimen, where each test employed a different span and a maximum applied load such that no permanent damages in the skins and foam could be introduced (i.e. the flexural load did stress each material within its linear elastic range)[2]. Tests were conducted on an electro-mechanical Hounsfield universal testing machine equipped with a load cell of 5 kN at a crosshead speed of 2 mm/min. The TPB rig consists on a 10 mm diameter cylindrical nose loading the specimen at mid-span length between two roller supports with 25 mm diameter each (figure 4.3a). The applied load was measured by the load cell of the test machine and the vertical deflections of top and bottom face sheets were respectively measured by the test machine displacement transducer and by a half inductive displacement transducer placed at mid-span (figure 4.3b). The inductive transducer assures that the displacement measured at bottom face sheet is not

[2] The main scope of the TPB tests in this work is the assessment of the flexural stiffness. Since no strength data in TPB are needed, each TPB test was performed within the linear elastic range of the material.

influenced by the occurrence of local indentation likely to occur in the upper face sheet. The conditioning and synchronous sampling of the load cell and displacement transducers signals was carried-out by using an HBM UPM-100 data logger.

In figures 4.3b it is shown that the probe of the inductive transducer is rested against the loading nose moved by the machine crosshead. A Preliminary test was carried out in this way to assess that the two displacement signal were similar within a resolution useful to neglect any direct influence in the calculations of the flexural stiffness.

(a)

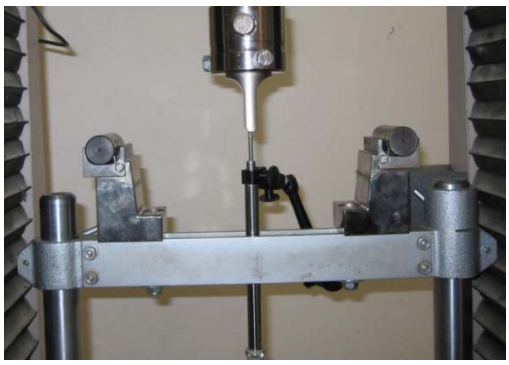

(b)

Figure 4.3 (a) Hounsfield universal testing machine (5 kN load cell); **(b)**Three-point bending jig.

The main geometric parameters related with the cross section of the tested sandwich beams are summarised in table 4.2.

Table 4.2 Sandwich beam specimen data used on TPB tests.

ID	Width b [mm]	Skin thickness t_f [mm]	Core thickness t_c [mm]
1S (PMI)	29.77	2.03	10
2S (PA)	29.74	2.03	10
3S (XPS)	29.74	0.80	30
4S (PVC)	30.51	1.99	15

Different span lengths were used to perform TPB tests These spans usually ranged from 250 mm to as low as 130 mm. Some pictures taken during the tests at different outer-span values are shown in figure 4.4.

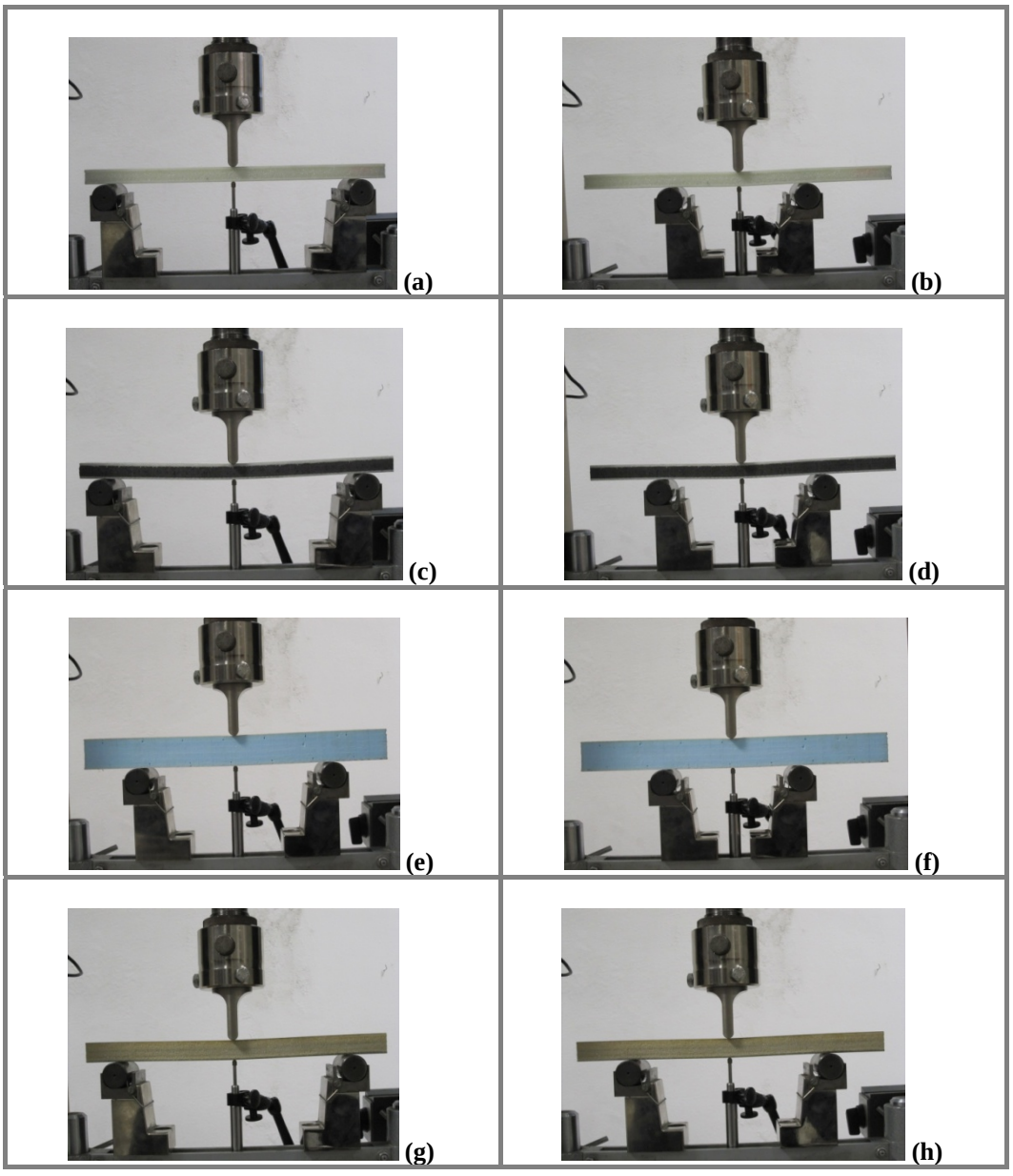

Figure 4.4 TPB tests on sandwich beams. **Specimen 1S**: **(a)** span L=250 mm, **(b)** span L=130 mm; **specimen 2S**: **(c)** span L=190, **(d)** span L=130; **specimen 3S**: **(e)** span L=230, **(f)** span L=190; **specimen 4S**: **(g)** span L=250, **(h)** span L=130.

In order to derive the flexural stiffness from several TPB tests performed at variable span a linear regression procedure is performed on the equation correlating the mid-span vertical displacement with the applied load. The equation, derived from classical beam theory, as well as the linear regression

procedure are suggested for sandwich beams characterisation in many different reference books on sandwiches [1, 2, 4]. The reference equation is in particular reported in Appendix A (section A.3, equation A3.1), and is here rewritten as:

$$\frac{\Delta}{PL} = \frac{1}{48D} \cdot L^2 + \frac{1}{4U} \rightarrow y = m \cdot x + b \tag{4.1}$$

The proper grouping of terms in equation (4.1) gives a linear equation in x and y where the angular coefficient m is function of the bending stiffness D and the y-axis intercept is a function of the shear rigidity U. So equation (4.1) suggests that by using data from different load *vs.* displacement curves, each measured with different values of L (i.e. different span lengths), a series of x,y coordinates is found. The linear regression of these points allows to derive the bending and shear stiffness of the beam from the regression parameters slope and intercept. This procedure which is not standardised, has the evident advantage to consider also the vertical shear displacement component together with the pure bending component. This is fundamental when beams with relatively low span to thickness ratios are tested. In this work the tested sandwich beams indeed have rather low length-to-thickness ratios and furthermore their low density foam cores results also in quite low shear rigidities, so it is expected that shear deformation cannot be neglected and flexural rigidity measured with only one TPB test at relatively low span (as suggested by ASTM C393) is not reliable.

4.3.2 On the influence of elastic indentation in sandwich TPB tests.

In a TPB test the external applied loads will act as point loads at the supports and the loading nose sites. If the sandwich is made of a core material with low transverse rigidity and also the skin has a low flexural rigidity (e.g. thin skins), then there is a risk that a consistent local indentation is developed which is measured by the displacement transducers together with the overall beam displacement induced by flexural and shear deformation. The local force at the loading nose in particular has the higher value and it could cause a local indentation of the upper skin on the core which is measured by the displacement transducer of machine cross head. A transducer probing on the lower skin and

measuring the lower skin vertical mid-span displacement will not be affected by the indentation of the loading nose on the upper skin location. Results of TPB tests reported in the next section are generally evaluated by using the data measured by the lower inductive transducer.

A method is here described which uses the analytical prediction of elastic indentation to correct the displacement data measured by the machine crosshead transducer [94]. This consists in using the linear relationship predicting the elastic indentation on a fully backed sandwich beam under a localised load. This is the equation 2.17 which is here rewritten as:

$$P = \left(8 \cdot D_f \cdot \lambda_1^3\right) \cdot \Delta_{ind} \tag{4.2}$$

The linear proportionality between the load and the indentation displacement is expressed by a stiffness term which is function of the skin flexural stiffness D_f and the foam Young's modulus in compression[3]. A more complete TPB midspan displacement equation can be written including the local indentation term:

$$\Delta = \Delta_{bending} + \Delta_{shear} + \Delta_{ind} = \frac{PL^3}{48D} + \frac{PL}{4U} + \frac{P}{8 \cdot D_f \cdot \lambda_1^3} \tag{4.3}$$

It is then possible to reshape the previous equation in order to obtain a new linear curve where the slope and intercept are still defined as before:

$$\underbrace{\left(\frac{\Delta}{P} - \frac{1}{8 \cdot D_f \cdot \lambda_1^3}\right)\frac{1}{L}}_{\mathrm{y}} = \underbrace{\frac{1}{48D}}_{m} \cdot \underbrace{L^2}_{x} + \underbrace{\frac{1}{4U}}_{q} \tag{4.4}$$

The previous equation implements the correction for the local elastic indentation at the loading nose contact zone, allowing the correct flexural stiffness and shear rigidity to be calculated using the data from the crosshead transducer.

The proposed correction procedure uses the elastic indentation prediction for a fully backed sandwich configuration, while the specimen is loaded in TPB.

In order to investigate the influence of this, a comparison is proposed between the prediction made through equation 4.2 and that made by using the elastic

[3] It is here recalled that $\lambda^4 = k/(4D_f)$ where k is the foundation modulus referred to the foam core $k = E_c b/c$. For the meaning of all geometrical symbols see also figure A3.1.

indentation solution obtained by Steeves et al. [38] for a simply supported beam in TPB.

The solution derived in [38] in the case of an elastic skin and elastic foam is a non-linear relationship between the applied load and mid-span displacement:

$$\Delta_{ind} = \frac{P\left(\alpha^2 + \beta^2\right)}{4k\beta} \quad \text{with} \quad \begin{cases} \alpha^2 = \lambda^2 + \dfrac{PL}{16d \cdot D_f} \\ \beta^2 = \lambda^2 - \dfrac{PL}{16d \cdot D_f} \end{cases} \tag{4.5}$$

It is observed that equation (4.5) reduces to equation (4.2) when the span length L reduces to zero. It is also observed that equation (4.5) is non linear in P so that it is not immediate to accommodate it in equation (4.3) and do the same data reduction procedure to obtain a linear relationship. By using equations (4.2) and (4.5) it is possible to predict and compare the load *vs.* displacement elastic curves for a sandwich beam type.

This is done here (see figure 4.5) by using data relative to the sandwich sample *3S* (XPS foam).

All plotted curves obtained form equation (4.5) consider different span lengths growing from zero.

All curves are also delimited at a maximum mid-span displacement $\Delta_c = \sigma_c \cdot c/E_c$, where σ_c is the yielding stress (corresponding to the plastic plateau for a crushable foam)[4].

It is seen from figure 4.5 that the difference in the extent of mid-span elastic indentation between the cases of a fully backed versus a simply supported beam is negligible.

This is particularly so at low load values and for small span lengths.

In light of this finding, in this work an example of correction of crosshead data is proposed only for sandwich *3S*, by using equation (4.4) (see next section for the presentation of these results).

[4] In the case of the XPS foam σ_c is taken as the critical stress at the end of the first linear elastic segment in the compression curve.

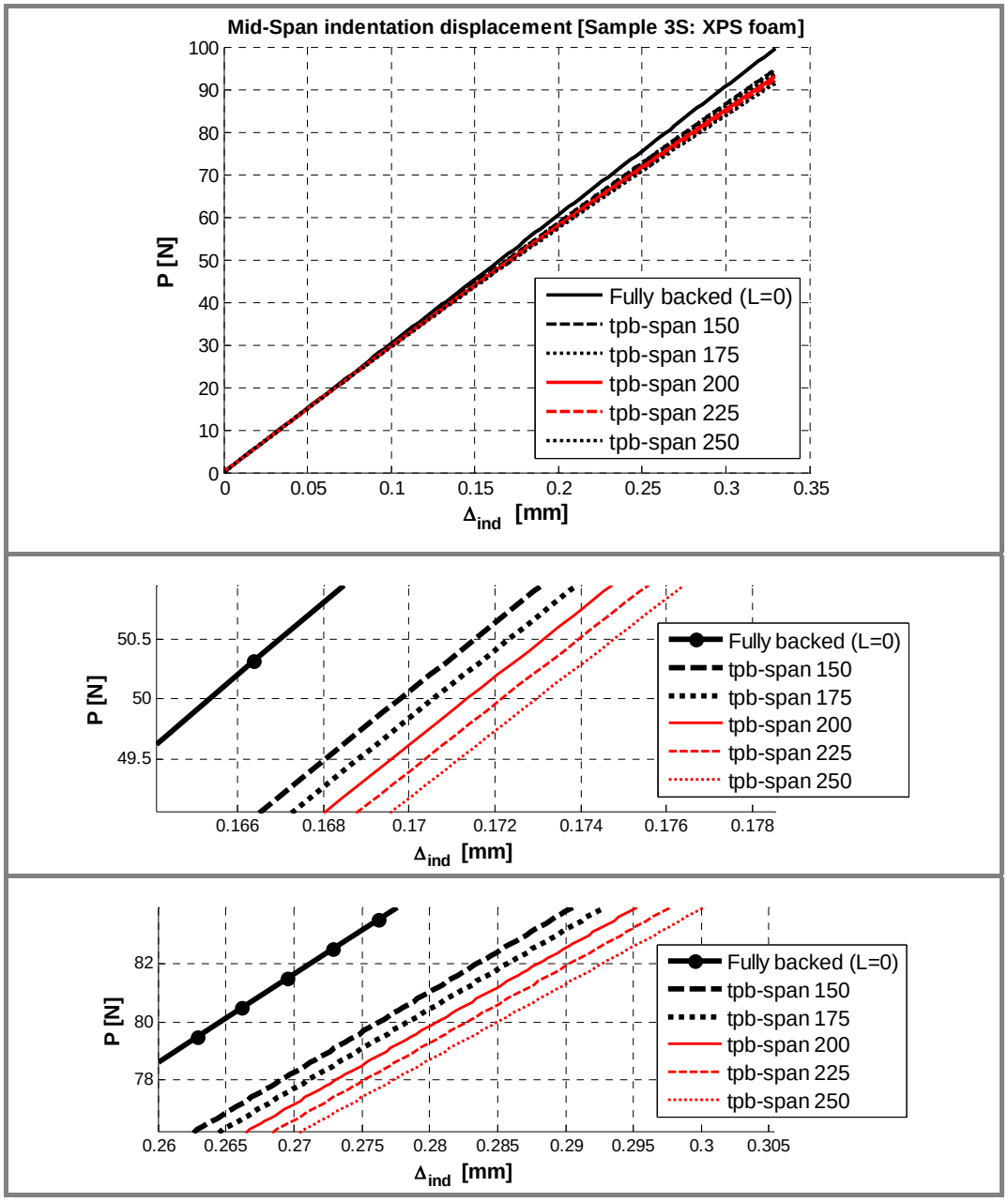

Figure 4.5 Theoretical prediction of force vs. mid-span indentation displacement results in TPB tests at different span lengths (sandwich *3S*).

4.3.3 TPB tests: results and discussion

Figure 4.6 shows the load *vs.* displacement curves at various spans, measured by the inductive transducer probing on the lower skin of sample *4S* (PVC foam) during TPB tests.

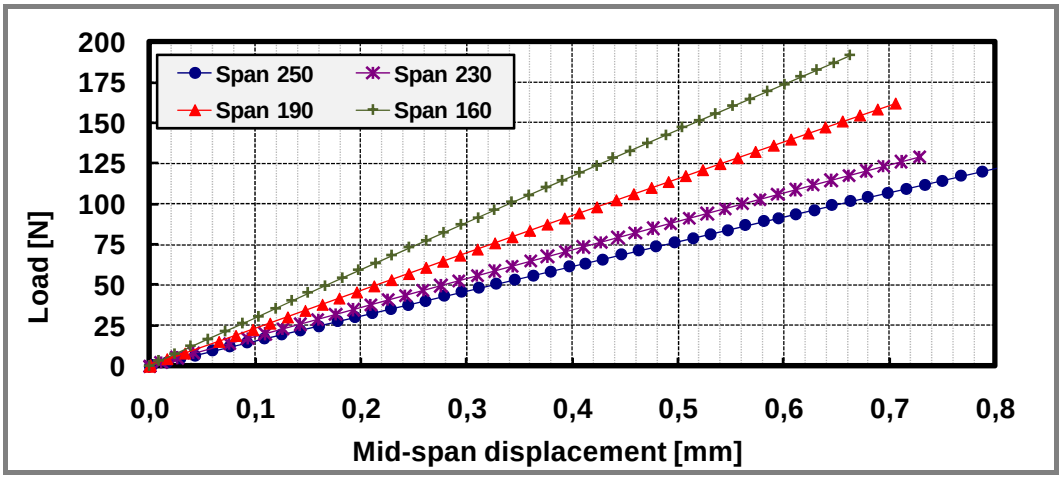

Figure 4.6 Load vs. displacement results in TPB tests at different spans (sandwich *4S*).

The Load *P vs*. total mid-span displacement δ curves are measured (figure 4.6) and the slope of each curve is calculated by interpolating data with a linear regression fitting.

As expected, at the same applied load, vertical mid-span displacement is higher for larger spans

Considering equation (4.1) as defining a linear line segment where the *y-axis* values are given by δ/PL and the *x-axis* values by L^2 , a linear regression is made in order to calculate the slope and intercept of that data (figure 4.7).

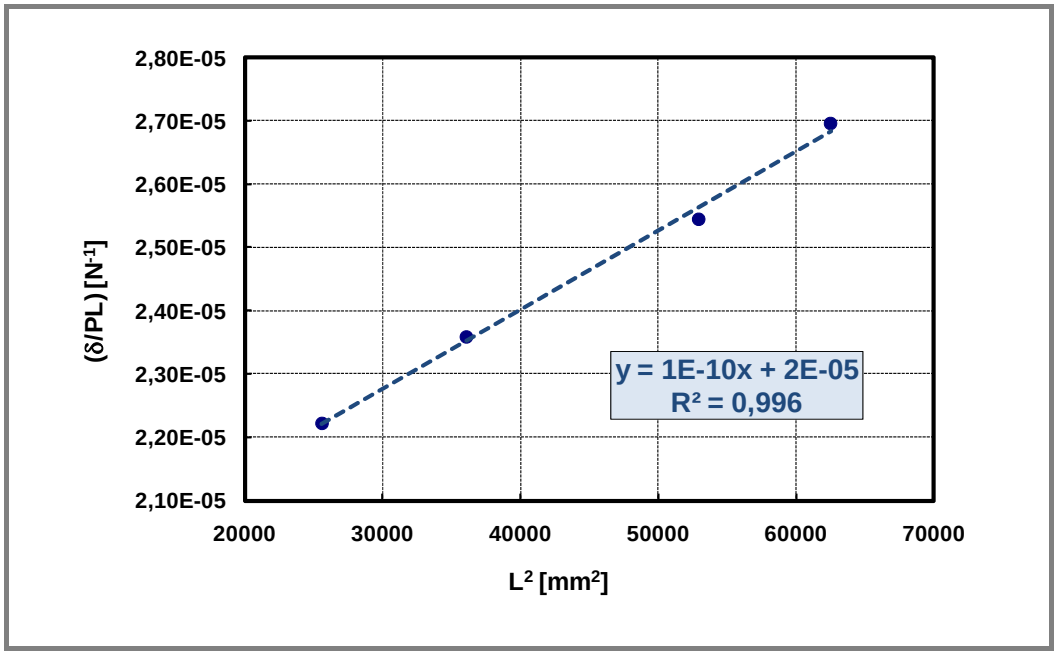

Figure 4.7 Linear regression for δ/PL *vs.* L^2 data (sandwich *4S*).

Thus, experimental flexural stiffness D and shear rigidity U are calculated:

$$Slope: m = \frac{1}{48D} \tag{4.6}$$

$$Intercept: b = \frac{1}{4U} \tag{4.7}$$

Table 4.3 collects the stiffness results for the sandwich specimens tested in TPB.

Table 4.3 Three-point bending sandwich specimen results

ID	D [N.m^2] Exp. eq. (4.6)	D [N.m^2] Eq. (A3.4)	D [N.m^2] (single skin $h=2t$)	U [N] Exp. eq. (4.7)
1S (PMI)	87.5	90.2	3.2	8005
2S (PA)	4.60	104	3.2	2291
3S (XPS)	204	168	0.17	6740
4S (PVC)	166	168	3.11	13260

The experimental estimation of beams flexural rigidity by means of variable span TPB tests reported in table 4.3 used the displacement data from the inductive transducer probing the lower skin displacement. It is found that for the two samples adopting pure crushable foams of PMI and PVC, i.e. samples *1S* and *4S*, the determined flexural stiffness is very close to the stiffness predicted with equation (A3.4). Furthermore, both values of D_f are significantly higher than the flexural rigidity of a single monolithic skin having $h=2t_f$, i.e. the equivalent situation of neglecting the sandwich concept by eliminating the core thickness.

The prediction for sample *3S* is also satisfying. The flexural stiffness of sample *3S* was also evaluated by implementing the data reduction method described in the previous section [94], which is able to correct displacement data from the testing machine crosshead movement by predicting the mid-span elastic indentation displacement component. The application of this procedure to sample *3S* is particularly meaningful since this sandwich exhibits a marked elastic indentation (see also figure 4.8a).

The bending stiffness of sample *3S*, D_f, is calculated with different formulas all summarised and commented in table 4.4. Figure 4.8b shows the linear regression curves resulting from the application of equations 4.1 and 4.4.

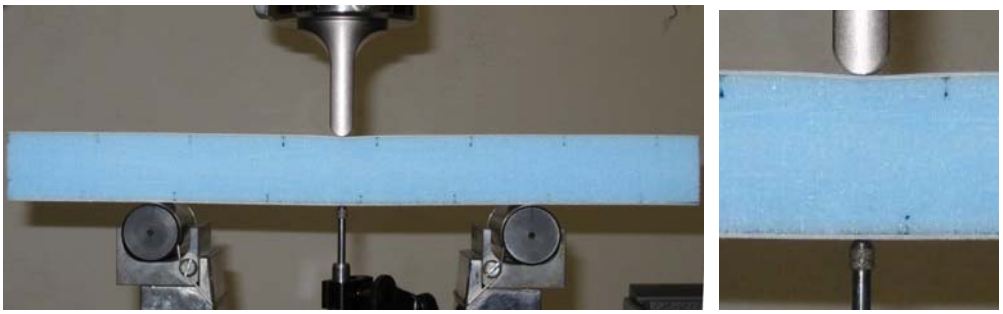

(a)

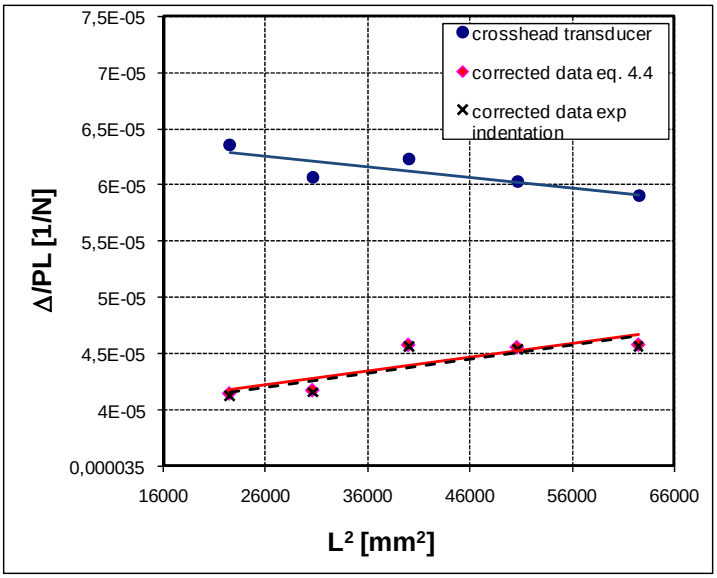

(b)

Figure 4.8 a) image of sample 3S under TPB with L=150 mm and close up of the mid-span loading contact evidencing the local indentation; **b)** linear regression curves from using equations 4.1 and 4.4.

Results in table 4.4 evidence that it is essential to consider the shear contribution through a series of tests at various span lengths. The tested beam is in fact too short to neglect the shear deformation contribution, so that using the approach outlined in ASTM C393 results in a far too low bending stiffness. More significantly it is shown also that using the crosshead displacement in the multiple span procedure is still insufficient since the measured displacement is highly corrupted by the local elastic indentation. The bending stiffness evaluated from the testing machine crosshead displacement has even a negative value which has no physical sense at all. It is very satisfying the measured value with the multiple span procedure when the crosshead displacement is corrected for the indentation

displacement component, through the use of equation 4.4. The last row in table 4.4. shows the same calculation of equation 4.4 but this time the slope of the elastic indentation is obtained experimentally rather then using equation 4.2.

Table 4.4 Values of bending stiffness calculated for sample *3S*.

Bending Stiffness D [N.m^2]	**Evaluation method**
168.2	Theoretical value according with classic beam theory approach (eq. A3.4)
22	Value obtained from using ASTM C393 formula (i.e. neglecting the shear deformation contribution) and using the maximum span (L=250 mm, aspect ratio L/h=8.5) data measured from the crosshead transducer.
28.4	As before but applying the elastic indentation correction, i.e. subtracting Δ_{ind} to the measured displacement.
-223.2	Multiple spans linear regression method using equation 4.1.
171.6	Multiple spans linear regression method using equation 4.4
168.9	Multiple spans linear regression method using the experimental elastic indentation slope measure from an indentation test on sample *3S*.

Data from table 4.3 related to sample *2S* are somewhat very surprising. It is found that the sandwich adopting the hyperelastic PA foam core is markedly underperforming in terms of flexural rigidity. It is found that the sandwich effect of flexural rigidity enhancement is severally affected by the hyperelastic behaviour. Although the real flexural stiffness is very much lower than the theoretical one predictable by the sandwich concept, its magnitude is still higher than the value of the equivalent monolithic beam. It is then suggested that the very low shear and compression stiffness values of the PA foam, together with its marked non-linear behaviour, determine a not very effective load transfer between the upper and lower skin, with a severe detrimental effect on the flexural rigidity enhancement expected from the sandwich configuration.

Also the shear rigidity values measured and reported in table 4.3 confirm how *structurally weak* can be the hyperelastic foam based sandwich beam when compared to the classical crushable foams such as PVC and PMI, or low density and low cost foams with a near crushable behaviour such as XPS foams.

4.4 Indentation tests

The sandwich beams described in section 4.2 have been also tested under quasi-static indentation loading with the purpose to compare the measured indentation curves with those predicted using the analytical models developed in chapter II.

Tests were carried out in displacement control with a constant cross head speed of 1 mm/min on the same Universal Instron 3367 testing machine used for the foam uniaxial compression characterization.

A cylindrical roller with 25 mm diameter was used as indenter and the sandwich specimens were positioned on a flat and rigid surface (*fully-backed* indentation, see figure 2.3 in section 2.2, chapter II). Specimens and their dimensions are listed in table 4.5.

For the *in-house* assembled sandwiches, the total sandwich thickness is higher than the simple addition of singular core and skins thickness due to the glue layer in-between.

Table 4.5 Sandwich beam specimen data used on indentation tests

ID	Width *b* [mm]	Length *l* [mm]	Total thickness *h* [mm]
1S (PMI)	29.77	150	14.24
2S (PA)	29.74	150	15.14
3S (XPS)	29.74	208	29.88
4S (PVC)	30.51	145	19.24
5S (PMI)	29.99	150	14.32

Photographs of these sandwich specimens taken before and during the indentation tests are shown in figure 4.9.

Experimental curves and evaluation of the analytical indentation curves are discussed in chapter V, though some considerations about the observed experimental behaviour are reported here.

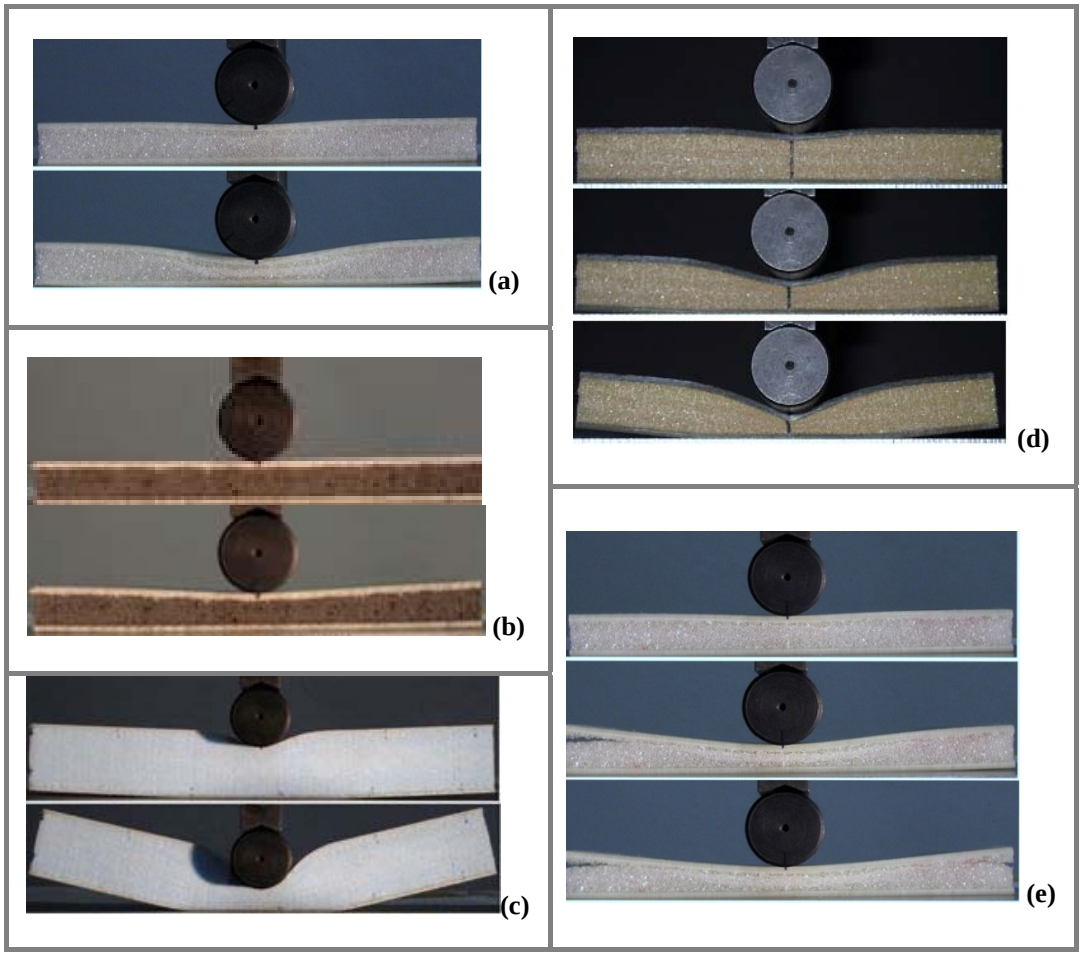

Figure 4.9 Indentation test: **(a)** coupon *1S* (PMI core + Tepex® PA $_{twill}$ skins); **(b)** coupon *2S* (PA core + Tepex® PA twill skins); **(c)** coupon *3S* (ThermoTec® XPS40 PBT1212-50-0); **(d)** coupon *4S* (PVC core + GF/epoxy skins); **(e)** coupon *5S* (PMI core + Tepex® PA $_{unid.}$skins).

A strong influence related with the employed foam type was observed on the extent of residual dent after complete load removal. In fact all indentation tests were performed applying a total displacement far bigger than the yield point of the foam, and usually such to induce densification on the foam material under the loading site. Using the same skin material, specimen *2S* with the hyperelastic PA foam core, almost fully recovered to its originally state after load removal and specimen *1S* with a smaller density PMI core presents a marked residual dent after load removal.

Specimens *1S* and *5S*, both employing the same PMI grade of foam core, and identical skin thickness, did give rise to some quite different indentation behaviours as evidenced by comparing figures 4.9a and 4.9e. This has to do with the use of stiffer Glass/PA6 unidirectional skins in sandwich *5S.* The higher

flexural stiffness of the skins in sample *5S*, due to a higher longitudinal Young's modulus, determines a wider dent with a smaller radius of curvature than sample *1S*, at equal extent of roller penetration. Besides, core failure in traction has occurred in sandwich specimen *5S* at the beam ends.

In specimen *3S* the indenter penetrated through the soft XPS foam core and both sandwich extremities lifted up at the point of maximum indentation (see figure 4.9c). At the end of the test no failure marks were visible in the core and skins, as well as no residual indentation was observed.

Sandwich specimen *4S*, employing a crushable PVC foam core and very brittle Glass/Epoxy skins, clearly presented an initial core yielding followed by top face skin failure (see also chapter V, section 5.4.1, figure 5.9).

CHAPTER V

Validation of the "Segment-Wise" model: results and discussion

5.1 Introduction

In this chapter the predicted indentation laws from the adoption of the "Segment-Wise" (SW) indentation model are compared with the experimental indentation curves from the sandwich specimens described in chapter IV.

In section 5.2, the experimental foam compression curves presented in chapter III are used for the determination of the SW constitutive parameters for the different foam behaviours. These data is further processed in section 5.3 to perform the comparison with the experimental results.

A final section, 5.4, evaluates the ability of the proposed model (see also section 2.3 from chapter II) to predict the maximum indentation load at which skin flexural failure occurs in sandwiches employing EPP and BL foam types.

5.2 Evaluation of the foam core *SW* constitutive parameters

The experimental foam compression curves measured as described in chapter III, are now used for the determination of the foundation SW constitutive parameters (k_i,q_i), adopting the procedure previously explained in chapter II, section 2.2.

In figures 5.1–5.4 the compression curves for PMI 31, PA Zotek® N B50 and ThermoTec® XPS are rescaled using force-per-unit-length *vs.* vertical

displacement coordinate axes[1], in order to evaluate the constitutive parameters needed to tune the indentation models with direct linear regression procedures on this data.

5.2.1 Discretisation of the PMI 31 compression curve

Figure 5.1 shows the experimental compression curve of the PMI 31 foam discretised with an EPP behaviour according to the segment-wise approach. As expected, the EPP behaviour approximates very well the crushable trend of the PMI foam.

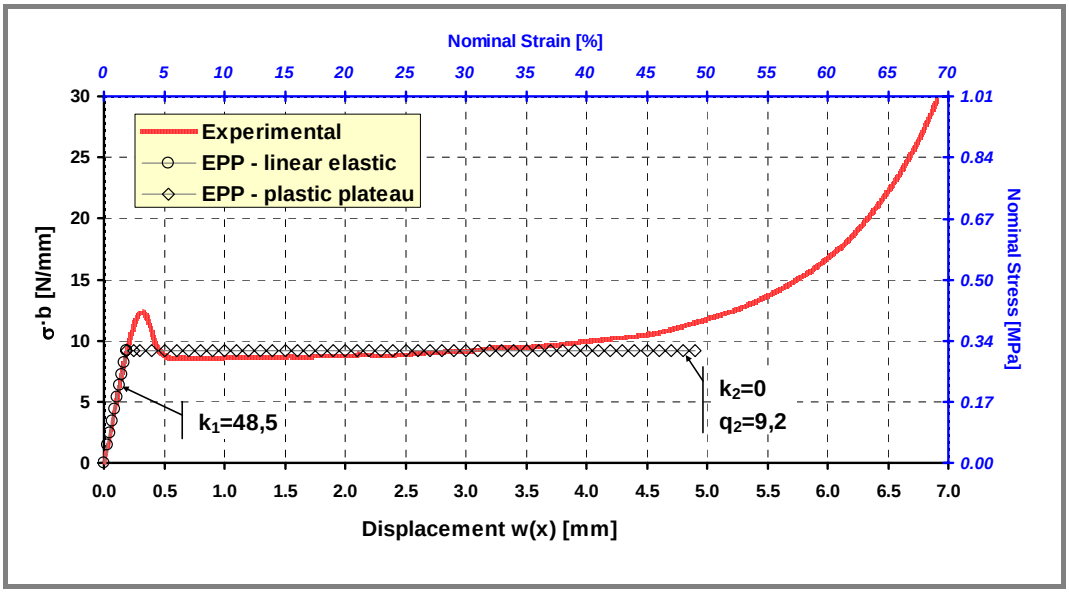

Figure 5.1 Elastic-perfectly-plastic discretisation model for the PMI 31 compression curve.

The EPP model requires two *SW* parameters to characterize the core foundation behaviour. A linear elastic segment defined by the foam stiffness parameter k_1 proceeds up to the point where the compressive stress in the core reaches the plateau value of σ_c, corresponding this to the onset of plastic deformation in crushable foams. The vertical displacement corresponding to the end of the first segment, i.e. when the linear elastic curve reaches the plateau stress value, will be $w_1(0) = \delta_1 = \alpha$, with δ_1 calculated at the core elastic limit or

[1] The sample blocks used for the compression tests had square cross-sections ($b \times b$) with side equal to the sandwich beams width b. The vertical axis of the compression curves is then rescaled to report the applied force per unit width of sample block.

onset plastic strain, ε_c (see equation 2.18, chapter II). Then with the EPP model a constant force per unit length q_2, equal to $\sigma_c \cdot b$, is applied by the core on the upper face sheet of a sandwich specimen after the core has yielded. The calculated constitutive SW parameters in the EPP model, k_1 and q_2 and vertical displacement δ_1 are reported in figure 5.1 and summarised in table 5.1.

5.2.2 Discretisation of the PA Zotek® N B50 compression curve

Figure 5.2 shows the experimental compression curve of the PA Zotek® N B50 foam and two discretised approximations of the measured curve according with the segment-wise approach: one representing an EPP behaviour and the other a much better fitting BL behaviour.

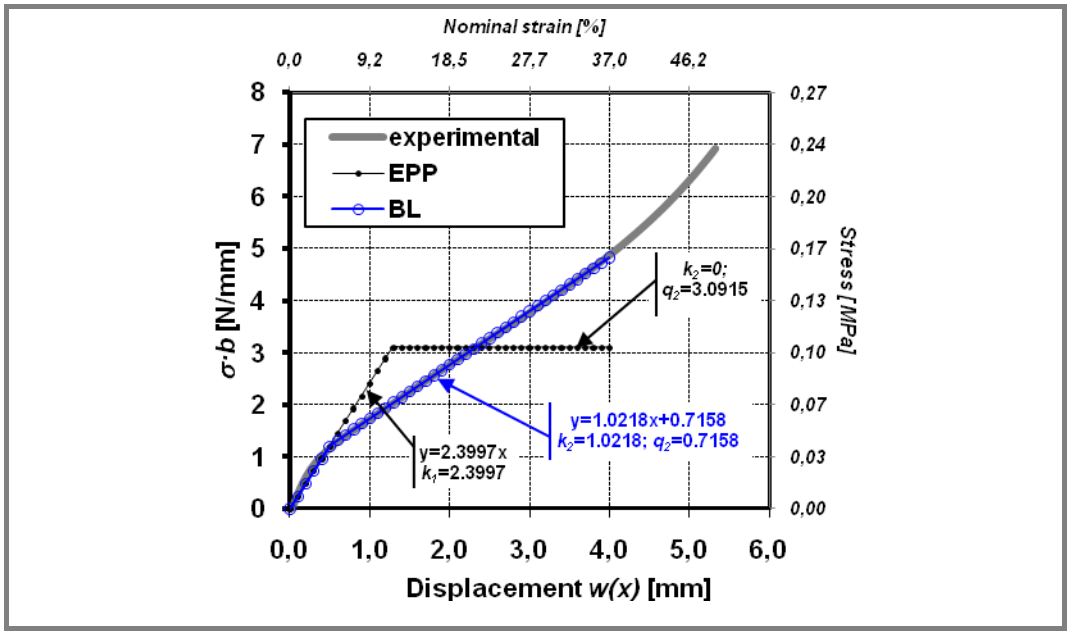

Figure 5.2 Elastic-perfectly-plastic and bilinear discretisation models for the PA Zotek® N B50 compression curve.

Regarding the markedly non-linear compressive behaviour of the polyamide foam this could in theory still be represented by an EPP model which though highly approximate the range of big deformations. A simple bilinear hardening model can already provide a much better fit of the experimental compression curve. A comparison between the EPP model and the BL-hardening model was

then carried out (see figure 5.2) up to about 40% compression strain, just before the onset of a more marked densification behaviour.

Considering the EPP model, two *SW* parameters are required to characterize the core foundation behaviour. Hence an initial linear elastic segment defined by the initial foam stiffness parameter k_1 proceeds up to the point where the compressive stress in the core reaches the plateau value of σ_c, with this usually corresponding to the onset of plastic deformation in crushable foams. The vertical displacement correspding to the end of the first segment, i.e. when the first linear elastic curve reaches the plateau stress value, will be $w_1(0) = \delta_1 = \alpha$ (see B.C.3 in Appendix B, section B2.1), with δ_1 calculated at the core elastic limit or onset plastic strain, ε_c. Thus with the EPP model a constant force per unit length q_2, equal to $\sigma_c \cdot b$, is applied by the core on the upper face sheet of a sandwich specimen after the core has "yielded". The calculated constitutive SW parameters in the EPP model, k_1 and q_2 and vertical displacement δ_1 are reported in figure 5.2 and summarised in table 5.1.

In the case of a BL behaviour of the PA Zotek® N B50 foam, two linear segments are again used to approximate the experimental curve. Likewise the EPP model, the first segment considers a core elastic behaviour defined by the stiffness parameter k_1. This segment extends up to a value of vertical displacement δ_1. In this work this vertical displacement δ_1 is estimated as the inflexion point of the curve and define the initiation of the second segment. Contrary to the EPP behaviour, the second segment of the foam core uniaxial compression curve is not a plateau and takes into account the slope of the growing load experimentally observed for the PA Zotek® N B50 foam. Hence, a new pair of constitutive parameters (k_2, q_2) characterise the second linear segment up to a vertical displacement δ_2 which is usually taken at the verge of a steeper growth of the curve, which usually states the onset of densification of the foam. The constitutive BL parameters k_1, k_2 and q_2 and vertical displacement δ_1 are reported in figure 5.2 and table 5.1. As stated before, even though the PA Zotek® N B50 foam exhibits a quite marked non-linear compressive behaviour, a simple BL hardening model

already provides a much better approximation of the experimental compression curve than the EPP discretisation.

5.2.3 Discretisation of the ThermoTec® XPS compression curve

In the case of the ThermoTec® XPS foam, two bilinear hardening models, BL1 and BL2, (see figure 5.3) have been considered and compared first, and then an EPP model and a BLPP model (figure 5.4) were also considered.

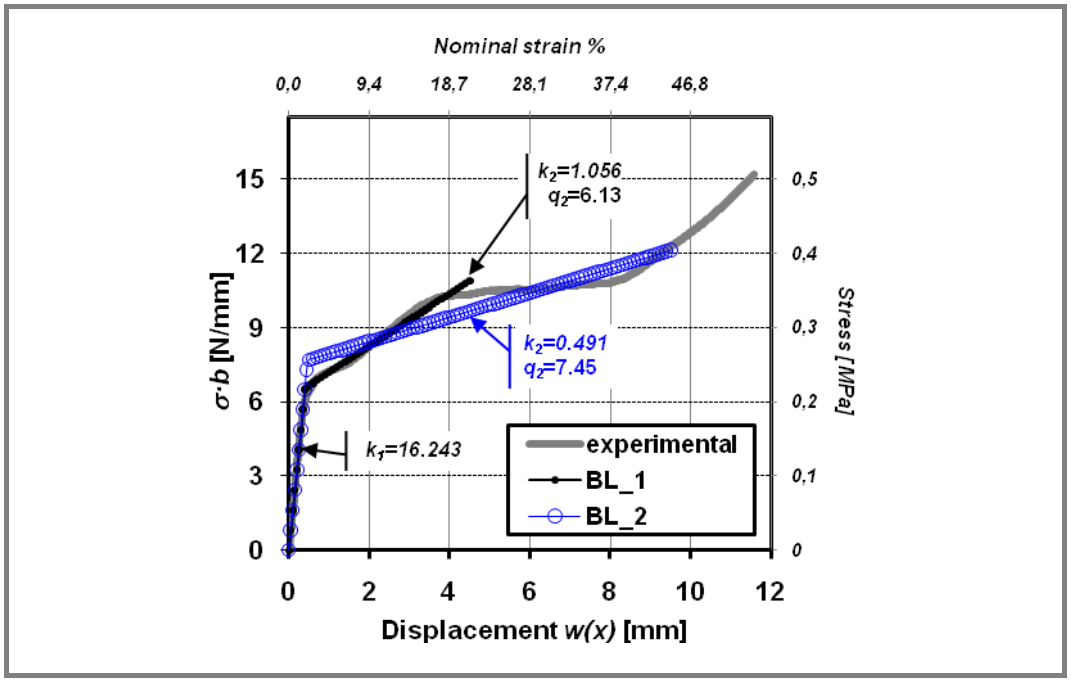

Figure 5.3 Bilinear discretisation models for the ThermoTec® XPS compression curve.

Both BL hardening models have in common the first linear segment extended up to the inflexion point of the curve corresponding to the vertical displacement δ_1 and are characterized by the same k_1 elastic constitutive parameter. The second segment describes the hardening behaviour experimentally observed for the ThermoTec® XPS foam and is characterized by a new pair of constitutive parameters (k_2, q_2), different for each of the BL fittings. The BL1 discretisation is obtained with a finer fitting of the foam compression curve only in the first range of post-yielding compression, this is up to around 18% compression strain; and BL2 uses a linear fitting of a wider range of post-yield

compression data, up to the beginning of foam densification (40 % compression strain).

Again, constitutive parameters k_1, k_2 and q_2 and vertical displacement limits δ_1 and δ_2 calculated for both BL hardening models are reported in figure 5.3 and table 5.1.

In figure 5.4, an EPP and a BLPP discretising models are as well considered for the ThermoTec® XPS foam.

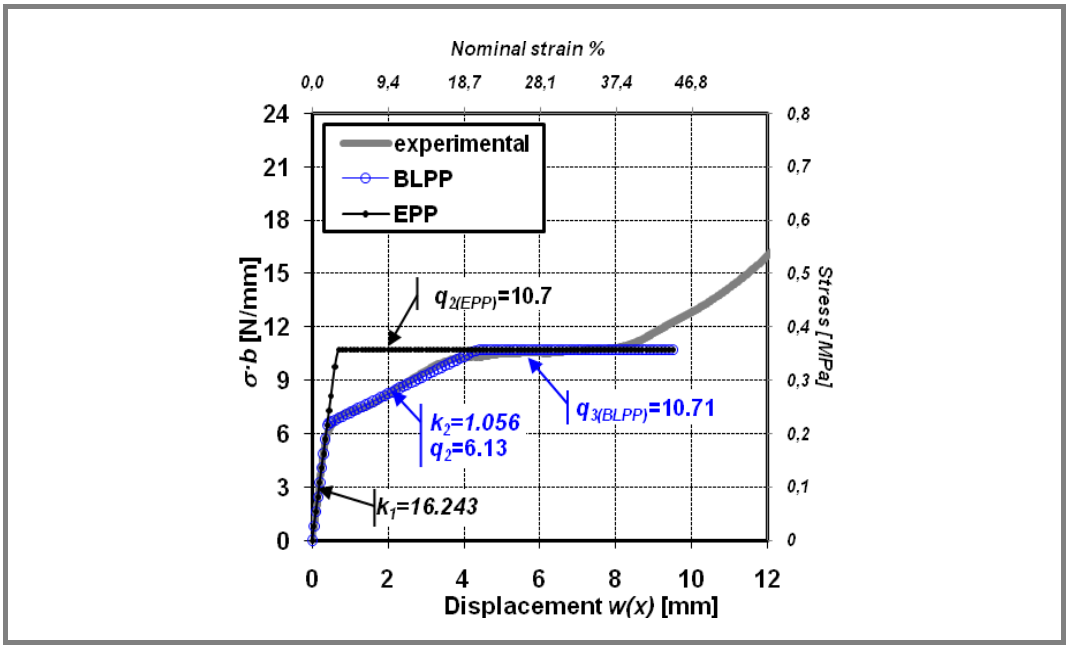

Figure 5.4 Multi-linear discretisation models for the ThermoTec® XPS compression curve.

The experimental foam compression curve was fitted according with an EPP behaviour, still using two segments. The initial elastic segment is defined by the initial foam stiffness parameter k_1 (equal value to the BL models) and extends up to a vertical displacement δ_1 which is fixed at the intersection of the linear elastic curve with the plastic plateau.

The value of σ_c is now the stress value at the plateau which follows the first hardening stage and precedes densification, and amounts to 0.36 MPa (see figure 5.4 and section 3.5.2). So for this EPP discretisation the second segment is just characterized by the constant constitutive parameter $q_2 = \sigma_c \cdot b$.

Finally a three segments discretisation is also proposed providing a bilinear-perfectly-plastic (BLPP) fitting of the experimental compression curve. The first

two segments of the BLPP discretisation coincides with the ones defined for the BL1 disretisation defined above.

A third segment starting at the same δ_2 value is then added, which proceeds as a plateau up to the beginning of densification.

For the XPS curve presented in figure 5.4, the constitutive parameter q_3 used for characterising the last segment coincides with the constitutive parameter q_2 already calculated for the EPP fitting. The constitutive BLPP SW parameters, k_1, k_2, q_2, q_3 and vertical displacement limits δ_1 and δ_2 calculated are once again summarised in table 5.1.

Table 5.1 Summary of implemented discretisation models and SW parameters.

Foam ***(Model)***	k_1 **[MPa]**	δ_1 **[mm]**	k_2 **[MPa]**	δ_2 **[mm]**	q_2 **[N/mm]**	k_3 **[MPa]**	q_3 **[N/mm]**
PMI *(EPP)*	48.5	0.19	0	-	9.23	-	-
PA *(EPP)*	2.4	1.30	0	-	3.09	-	-
PA *(BL)*	2.4	0.65	1.02	3.99	0.72	-	-
XPS *(EPP)*	16.2	0.87	0	-	10.71	-	-
XPS *(BL1)*	16.2	0.38	1.06	4.54	6.13	-	-
XPS *(BL2)*	16.2	0.38	0.49	9.53	7.45	-	-
XPS *(BLPP)*	16.2	0.38	1.06	4.54	6.13	0	10.71

5.3 Evaluation of the analytical indentation curves

5.3.1 Sandwich specimen with a classical crushable core presenting a plateau

In figure 5.5 the experimental and analytical indentation curves are compared for the sandwich specimen employing a PMI31 foam core and Tepex® PA_{twill} skins, identified as *1S* in table 4.1. It is noticed that the graph reports also an analytical prediction made by using the rigid-perfectly-plastic (RPP) model according with the explicit formula given by Soden in [66] (see equation 1.16, chapter I), while the EPP model curve is obtained by implementing the equations 2.19-2.20 presented in chapter II.

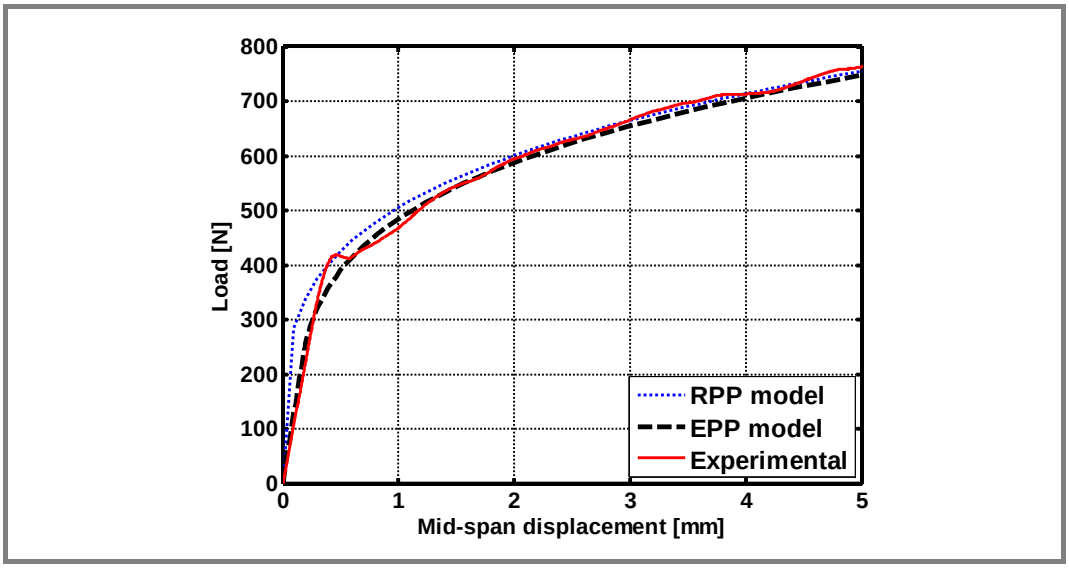

Figure 5.5 Indentation curves from sandwich specimen *1S* (PMI31 core + Tepex® PA $_{twill}$ skins).

It is also noticed that the peak at yielding observed in the pure flatwise compression test on the PMI31 foam (see figure 3.10) is influencing also the onset of yielding in the indentation test.
In fact the yield onset in figure 5.5 is evidenced by a little local peak which is not predicted by the analytical curves.

As expected, the RPP model underperforms in the first elastic range, while both the RPP and EPP models seem to predict well the trend after yield onset, confirming the good performances of the EPP model with foams exhibiting a crushable behaviours, confirming the findings from other works[2] [35, 70]. Furthermore the adoption of a thermoplastic reinforced laminate as skin face material in this work has not affected the effectiveness of the EPP approach.

5.3.2 Sandwich specimen with an hyperelastic core

Figure 5.6 compares the experimental and analytical indentation curves for the sandwich specimen employing a PA Zotek® foam core and Tepex® PA_{twill} skins identified as *2S* in table 4.1.

[2] It is noticed that the quoted works used sandwich beams with PVC foam cores, so the extension of the validity of the EPP model also for PMI foams could be regarded as a finding of this thesis.

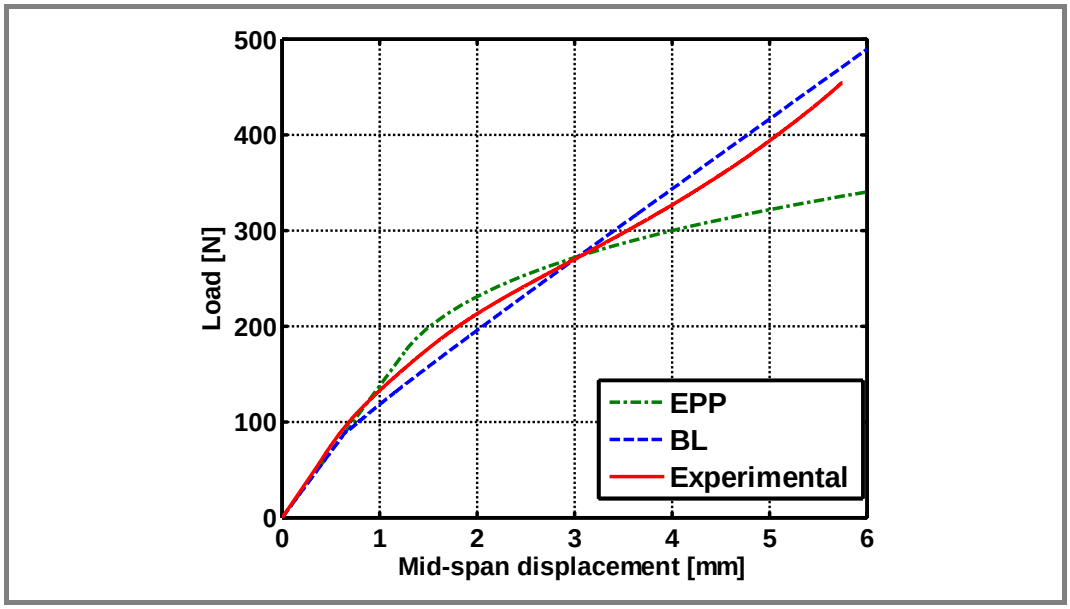

Figure 5.6 Indentation curves from sandwich specimen *2S* (PA core + Tepex® PA $_{twill}$ skins).

The constitutive parameters for the two EPP and BL models are reported in table 5.1. In this case the absence of a plateau in the compressive behaviour of the foam determines a marked mismatch between experimental data and the EPP predictions, which becomes more severe with the progression of indentation (see in particular for displacements α>3 mm). The BL model is able to predict the growing trend of the experimental curve also at big displacements. The highly non-linear behaviour of this PA foam would require a finer discretisation using a higher number of linear segments. The higher computational effort to derive and solve the resulting non-linear equations, is though probably not justified by the margins of improvement over the solution readily provided by the analytical BL solution.

5.3.3 Sandwich specimen with a crushable core presenting an hardening behaviour

Figures 5.7 and 5.8 compare the experimental and analytical indentation curves for the sandwich specimen ThermoTec® XPS40 PBT1212-50-0 identified as *3S* in table 4.1. The comparison in figure 5.7 is performed with the two bilinear hardening models whose features are given in figure 5.3.

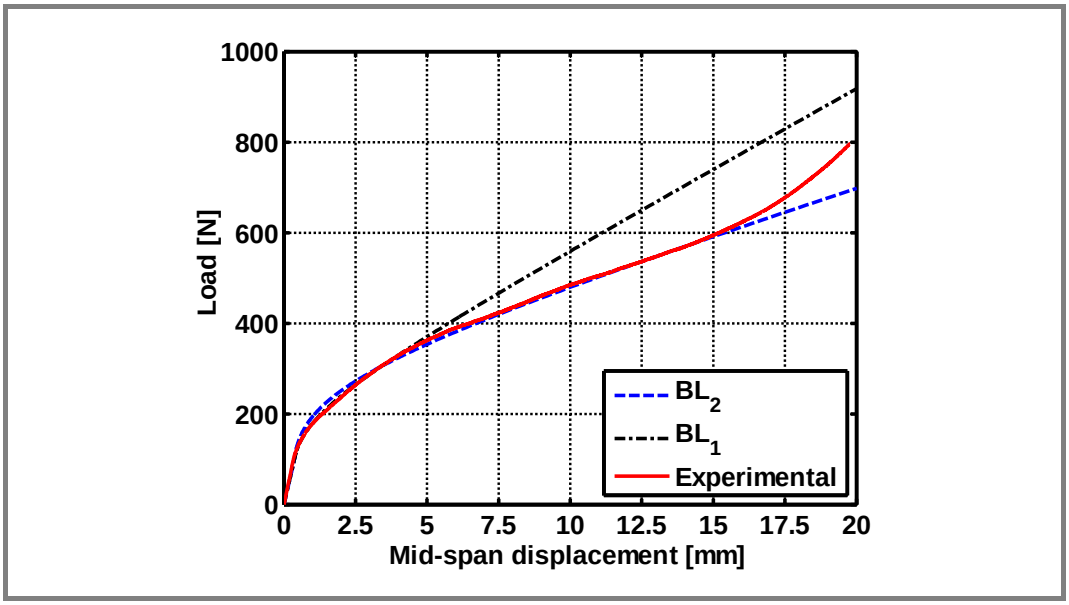

Figure 5.7 Indentation curves from sandwich specimen *3S* (ThermoTec® XPS40 PBT1212-50-0).

In figure 5.7 it is observed that the BL1 predictions are better and very good up to a value of α of about 4 mm, but for higher displacements there is a marked departure from the experimental trend. The BL2 model is not as accurate as the BL1 in the first range of displacements, but on the contrary it provides a good prediction of the overall trend up to foam densification (values of α as high as 15 mm). In figure 5.8 the comparison is made with the EPP and the BLPP models defined in figure 5.4.

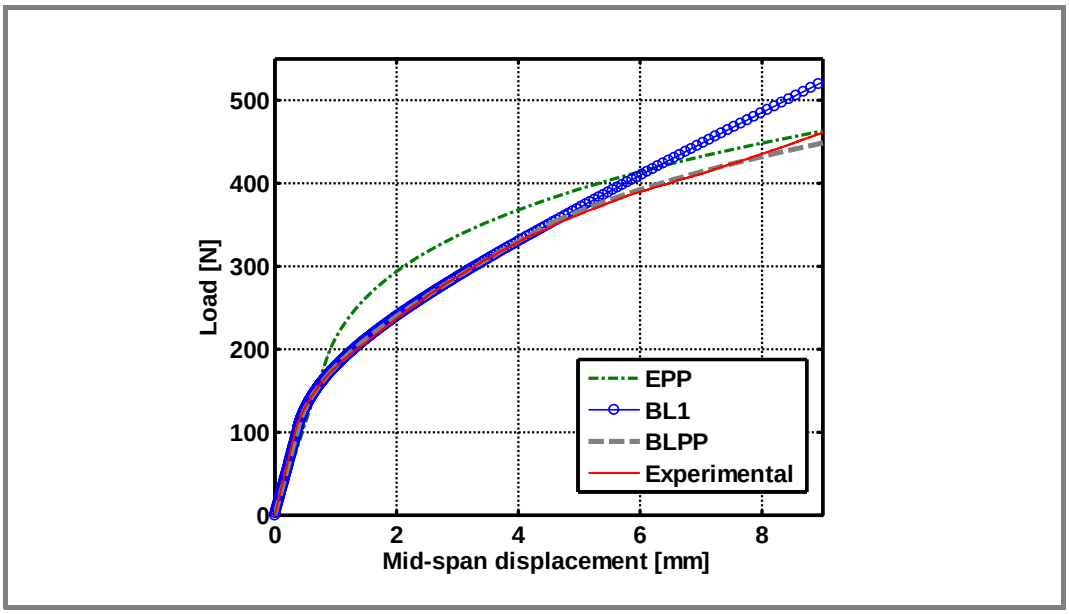

Figure 5.8 Indentation curves from sandwich specimen *3S* (ThermoTec® XPS40 PBT1212-50-0).

The BLPP model is implemented through the consecutive use of equation 2.17 (relative to the elastic segment), equations 2.22-2.24 (relative to the intermediate segment) and equations 2.27-2.30 (relative to the last plateau segment).

To solve equation (2.30) a range of variation for a_2 was chosen starting from the last value obtained from solving equations (2.22-2.24). It was observed that equation (2.30) always gave two complex conjugate solutions with no physical meaning and a third real solution. It also was observed that by increasing a_2 the real solution was negative, and hence not physical. By varying a_2 towards decreasing values the third solution became positive with growing values of a_3.
This choice then gave physically sound results and the consequent indentation curve for the BLPP model is shown in figure 5.8.
It is finally observed that the EPP model prediction is the less accurate while the BLPP prediction is very accurate and better than those from the BL1 and BL2 models for values of indentation up to α=8 mm, which is also the displacement at which the plateau in figure 5.4 ceases and the compression curve starts to grow again due to foam densification. It can be concluded that the BLPP prediction is the most accurate up to α=8 mm but the BL2 prediction gives also a very good match up to α=15 mm thanks to the wide extension of the linear fitting used to define the segment 2 (k_2,q_2).

5.4 Evaluation of the failure load at face sheet fracture

The detailed procedure for prediction of the critical applied load producing bending failure at the top skin in a generic BL model (consult chapter II, section 2.3) is here confronted with experimental observations for some of the sandwich specimens used in the indentation tests (see table 5.2).

Table 5.2 Sandwich beams employed on the top skin failure load study.

Sandwich *ID*	Skin				Core			
	laminate	t_f [mm]^{I}	E_f [GPa]^{II}	σ_f [MPa]^{III}	Foam	t_c [mm]^{IV}	E_c [MPa]^{V}	σ_c [MPa]^{VI}
2S	Glass/PA6 $[0°/90°]_{s\ twill}$	2	15.70 ± 0.39^{M}	585^{S}	PA	10	0.8^{M}	0.10^{M}
4S	Glass/epoxy $[0_{50}°/90_{50}°]_s$	2	14.74 ± 0.8^{M}	415.78 ± 31^{M}	PVC C70.55	15	58^{S}	0.75^{M}
5S	Glass/PA6 $[0°]_{s\ unid}$	2	42.35 ± 0.63^{M}	^{VII} 49.6 ± 26^{M}	PMI31	10	16.3^{M}	0.31^{M}

Note: ^{I} Face sheet thickness; ^{II} Face sheet flexural modulus; ^{III} Face sheet flexural strength; ^{IV} Core thickness; ^{V} Core compression Young's modulus; ^{VI} Core compression strength; ^{VII} Tensile strength was used because bending/flexural strength was not available.

5.4.1 Solution for an elastic-perfectly-plastic core behaviour

a) Sandwich *4S* - PVC C70.55 core and Glass/epoxy skins

Figure 5.9a reports the experimental and analytical indentation curves obtained for sample *4S*. Figure 5.9b also shows photos taken at three different instant of the indentation test, which are also indicated in the graph of figure 5.9a. This sandwich employs a common grade PVC foam core with a marked crushable behaviour, and brittle glass/epoxy skins. It is observed that at the onset of core yielding the experimental curve presented a little wrinkle which clearly identified the start of the permanent plastic crushing of the foam (photo 1 in figure 5.9).

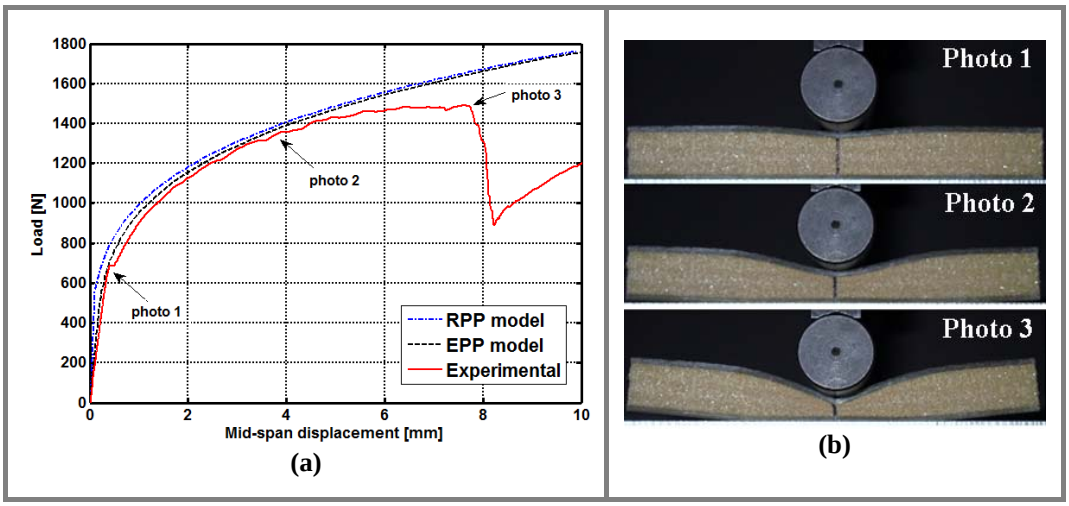

Figure 5.9 (a) Indentation curves from sandwich specimen *4S* (PVC C70.55 core + Glass/epoxy skins); **(b)** Photos illustrating different indentation stages: **photo 1** (on-set core crushing); **photo 2** (on-set top skin failure); **photo3** (top skin collapse).

The photo 2 in figure 5.9b was also taken at the onset of bending failure on the top face skin, while photo 3 was taken at the evidence of a strong damage onset on the face skin.

To predict the external applied load responsible for the initiation of skin flexural failure, the generic BL procedure proposed in chapter II is applied to the particular situation of an EPP core behaviour, as it is in the case of the PVC C70.55 employed in sandwich *4S*.

By adapting the general equation (2.35) to the EPP behaviour, an expression relating the critical flexural load as a function of a_2 is obtained.

The exact value of the critical load is then found by considering also the relationship between P and a_2 obtained by solving the indentation problem, i.e. the equations (2.19, 2.20) for the EPP model. In figure 5.10 both resulting curves are plotted and the interception value identified as the critical flexural failure load of the top skin.

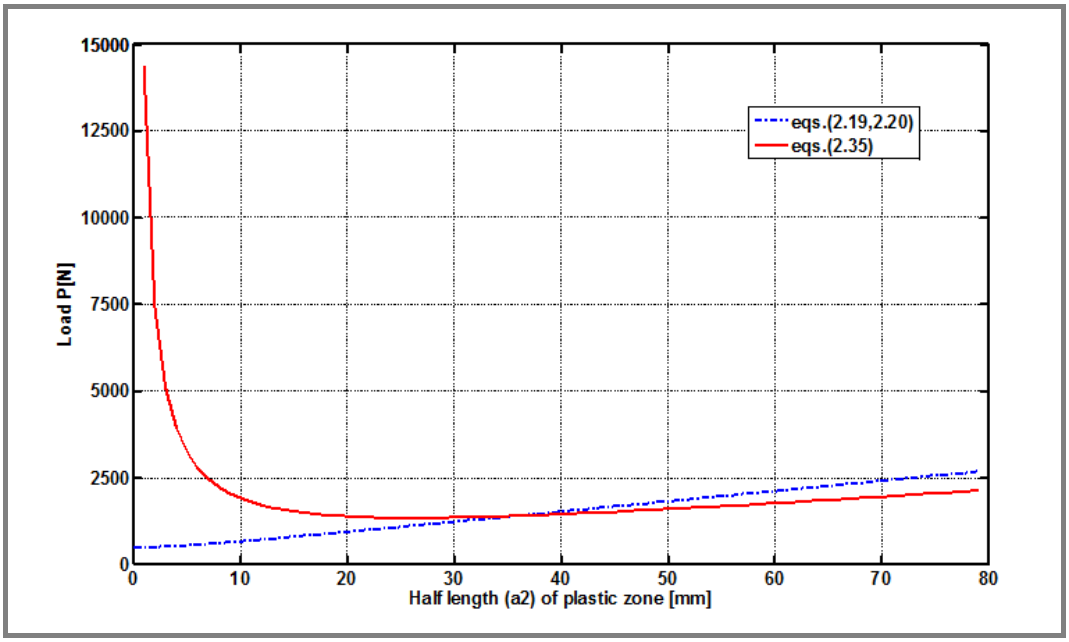

Figure 5.10 Skin flexural critical load prediction for sandwich specimen *4S* (PVC C70.55 core + Glass/epoxy skins).

Table 5.3 compares the experimentally observed failure load with those predicted in Soden [66], Shuaeib and Soden [67] and using the proposed BL generic model.

Table 5.3 Experimental and predicted skin failure load [N] for the sandwich specimen *4S* (PVC C70.55 core + Glass/epoxy skins).

Sandwich ID	Experimental	Soden [66]	Shuaeib and Soden [67]	BL generic model
4S	1390-1450	1403	1474	1397

As observed in the indentation curve from figure 5.9a, identification of a single experimental value is quite ambiguous. For this reason a range of values based on the visual observation of the specimen during the indentation was considered in table 5.3. Furthermore, all the analytically predicted values are within or near the experimental range of values.

b) Sandwich *5S* - PMI31 core and Tepex® PA $_{unid}$ skins

Figure 5.11 reports the experimental and analytical indentation curves for the sandwich specimen employing a PMI31 foam core and Tepex® $PA_{unid.}$ skins, identified as *5S* in table 4.1.

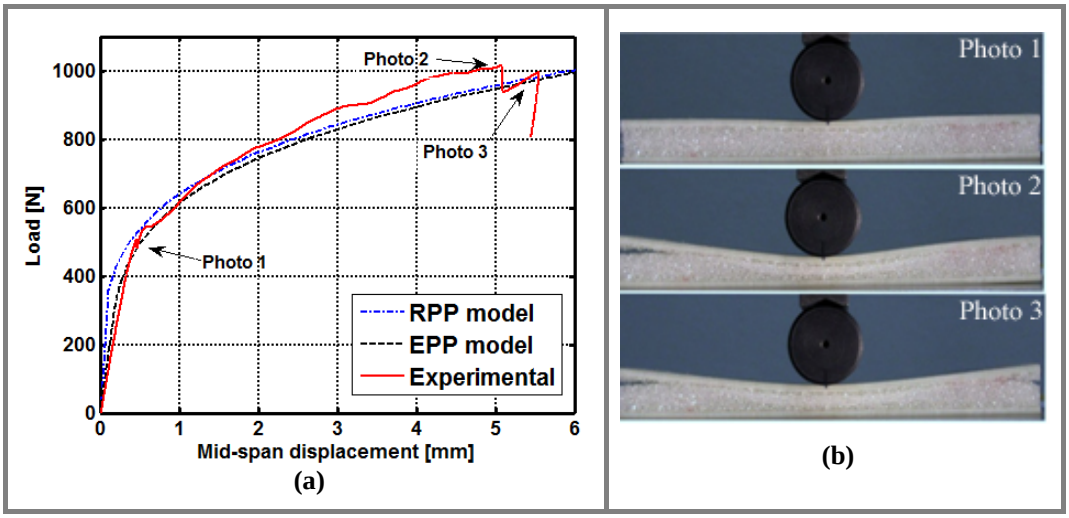

Figure 5.11 (a) Indentation curves from sandwich specimen *5S* (PMI31 core + Tepex® PA $_{unid.}$skins) ; **(b)** Photos illustrating different indentation stages: **photo 1** (on-set core crushing); **photo 2** (1^{s}t failure mode by core traction); **photo 3** (2nd failure mode by core traction).

Likewise the study performed for sandwich *1S*, the RPP model underperforms in the first elastic range but this time both the RPP and EPP models do not properly follow the experimental trend after yield onset.

It is in particular observed that both analytical predictions are lower than the experimental data in the plastic crushing region.

Sample *5S* employs a stiffer skin (since the lay-up is now purely unidirectional compared to the cross ply of sample *1S*), while the length of the indented sample is rather short, as suggested by the detected failure consisting in the debonding of the upper skin at both sample ends.

It is then believed that the higher experimental values are determined by the too short length of the indented sample and early debonding of the top skin. Furthermore, as commented before in section 4.4, the stiffer unidirectional skins do not determine a markedly local indentation of the skin in the core, but rather gives rise to a wide dent which interfere with short length of the beam. The early debonding is then a likely cause for the missing flexural failure mode as predicted by the model.

It is also interesting to observe that the debonding failure at the beam ends was of a cohesive type, within the foam, and adhesive, at the skin to core interface, suggesting that the adhesive bonding employed to manufacture the sandwich samples is reliable and strong enough. The prediction of the flexural skin failure load is anyway reported in table 5.4, and it is also meaningful to observe that the predicted critical loads were expected to be all higher then the failure load at which the debonds have occurred.

Table 5.4 Experimental and predicted skin failure load [N] for the sandwich specimen *5S* (PMI 31 core + Tepex® PA $_{unid.}$skins).

Sandwich ID	Experimental	Soden [66]	Shuaeib and Soden [67]	BL generic model
5S	no occurrence	1372	1880	1371

These results demonstrate that although analytical expressions are in general very useful for predicting failure modes, it is essential not to exclude that different concurrent failure modes can be favoured.

The ability to provide analytical expressions all identified failure possibilities is though very useful to derive global parametric failure maps for serving various design purposes [38, 40, 53-57].

5.4.2 Solution for a bilinear generic core behaviour

a) Sandwich 2*S* - PA core and Tepex® PA twill skins

As seen before, to predict the external load responsible for the initiation of skin flexural failure, the generic BL procedure proposed in chapter II can be applied to the particular situation of a sandwich employing a non linear core behaviour, as it is the case of the PA Zotek® N B50 foam core used in sandwich *2S* (see figure 5.12).

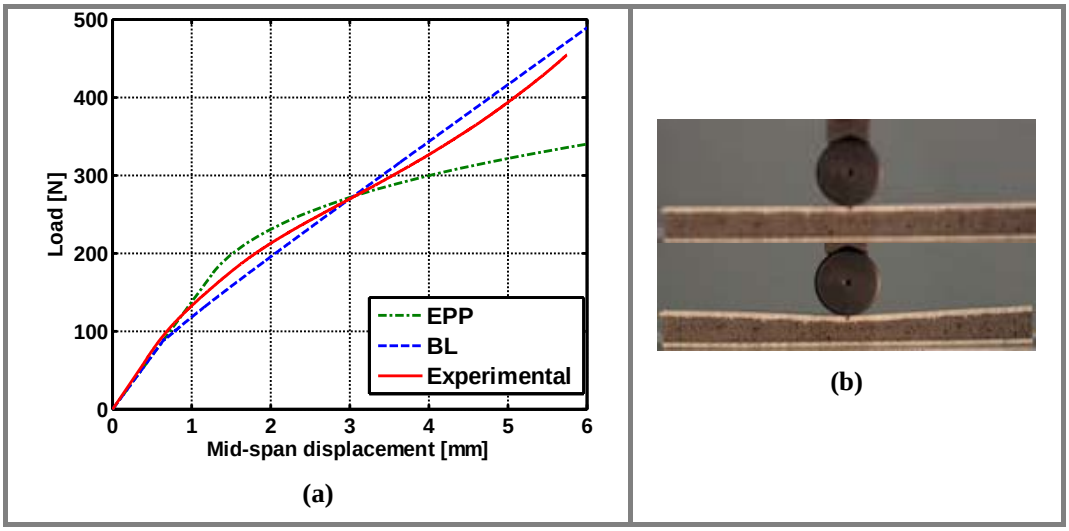

Figure 5.12 (a) Indentation curves from sandwich specimen *2S* (PA core + Tepex® PA $_{twill}$ skins) ; **(b)** Photos illustrating different indentation stages for sandwich *2S*.

Applying equation (2.35) to the BL behaviour an expression relating the critical flexural load as a function of a_2 is obtained.

In the same way a critical load is found by crossing the above expression in function of a_2 with the relationship between P and a_2 obtained when solving the indentation problem using the expressions (2.22 - 2.24) deduced for a BL model. Figure 5.13 shows the resulting curves and the intercept value identified as the critical flexural failure load of the top skin for sandwich *2S*.

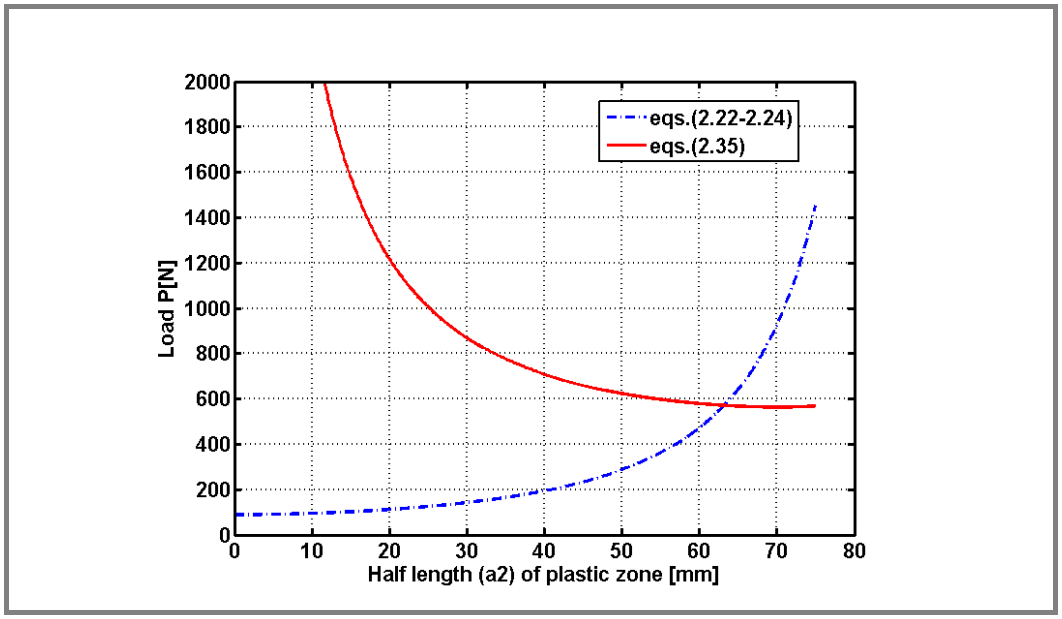

Figure 5.13 Skin flexural critical load prediction for sandwich specimen *2S* (PA core + Tepex® PA $_{twill}$ skins).

Results are compared in table 5.5:

Table 5.5 Experimental and predicted skin failure load [N] for the sandwich specimen *2S* (PA core + Tepex® PA $_{twill}$ skins).

Sandwich ID	Experimental	Soden [66]	Shuaeib and Soden [67]	BL generic model
2S	no occurrence	616	537	571

The load value predicted using the general proposed formula applied to the case of a BL behaviour is similar to the load values obtained using analytical predictions of Shuaeib and Soden [67] and Soden [66], but experimentally there was no occurrence of skin failure. One first explanation is that the GRP skin laminates in sandwich *2S* adopted a thermoplastic PA matrix with a consequent more ductile behaviour, while the failure model introduced in section 2.2 assumes an ideally brittle behaviour more typical of thermoset resin matrices. Furthermore the very low stiffness of the PA foam, the rather short length of the indented beam, the relatively wide extension of the dent on the upper skin, and also the relatively small thickness t_c of the core, all did determine an early onset of foam densification under the loading nose and a smaller top skin bend which in the end was not sufficient to activate any bending failure.

CHAPTER VI

Numerical simulation with highly non-linear foam cores

6.1 Introduction

The focus of this thesis so far has been mainly on the development and implementation of analytical and experimental approaches for the investigation of the indentation behaviour in foam cored sandwiches.

A new analytical method capable of predicting highly non-linear foam compression behaviours has been described and verified in terms of its prediction capabilities for a number of behaviours related with localised loading of sandwich structures.

This chapter reports some results of a numerical investigation of sandwiched structures employing foam cores with a hyperelastic, highly non-linear behaviour.

In particular a commercial numerical code, ABAQUS, has been used with the implementation of the HYPERFOAM formulation from its material library. Three structural cases have been considered in particular by the numerical simulation: indentation of a fully backed sandwich beam, three-point bending of a sandwich beam and repeated compression of a pure foam slab.

Some general information about the polymeric foam constitutive models available in ABAQUS is outlined first. The second part of the chapter will then describe the modelling of the mentioned case studies and the results of the simulations.

6.2 Modelling of polymeric foams behaviours with ABAQUS

A literature review is first proposed with the aim to present some of the main approaches available to model the behaviour of polymeric foams with particular emphasis on the element formulations and constitutive behaviours proposed for this class of materials. A main consideration that can be made at this regard is that the great majority of proposed approaches and studies, in particular from mid nineties onward, adopts the ABAQUS commercial code.

Two constitutive formulations are in particular provided by this software: *Crushable* foams and *Hyperelastic* foams. It is observed that the first crushable formulations appeared towards the end of the nineties, while the introduction of the hyperelastic behaviour as a numerical constitutive model in ABAQUS followed the crushable model of some years. The crushable foam plasticity model implements the features of a typical elastic-perfectly-plastic foam compressive behaviour, in which the plastic phase is associated to a irreversible permanent damage. It must be used in conjunction with the linear elastic material model and enables a post-elastic hardening behaviour. This formulation is particularly suitable for high density and brittle foams, i.e. the majority of the commercial foams, typically used as energy absorption or as sandwich core structures (e.g. PVC, PEI, PMI,…). Since its introduction in ABAQUS it has been used in some scientific works and corroborated with experimental validation by a few authors:

In [80] it is proposed a 2D numerical model in ABAQUS to study the indentation study of rigid PMI foam cores and GFRP face sheets sandwich panels on a fully backed configuration. The CRUSHABLE FOAM HARDENING and NLGEOM features are used to model the foam constitutive behaviour. Good matches between finite element modelling and experimental results were obtained for residual stress and strain prediction, and residual dent magnitude in sandwich panels subject to a static indentation load. In [95] experimental curves from uniaxial compression tests where used to calibrate a crushable foam constitutive model for the study of the elastic-plastic response of two rigid closed-cell PVC foams subjected to quasi-static point and line loads and in [96] the same materials were used in a comparison between experimental and simulation in a low velocity

localized impact. In [71] Rizov extended his work from [80] and combined it with GFRP face sheets to perform experimental and numerical two dimensional studies and in [97] developed a damage model for predicting the local failure in a GFRP composite face sheet under local loading, using a crushable foam model for the sandwich PVC core material. In [98], a multi-axial crushing model of a PVC foam core was implemented to study the progressive collapse of sandwich beams with glass/epoxy pre-preg skins.

The works mentioned confirm the accuracy of the ABAQUS crushable model when applied to foams with a net elastic-perfectly-plastic behaviour.

Another available formulation from ABAQUS to model polymeric foams is given by the *hyperfoam* constitutive material, which consider a hyperelastic behaviour typical of elastomeric materials. Common examples of this kind of foams include PA, PP and some PU foams finding applications as cushions, paddings and packaging materials. The model is valid for foams with open or closed cells and whose porosity permits very large volumetric changes. These materials can deform elastically to large strains up to 90% strain in compression and require that geometric nonlinearity be accounted for during the analysis step. In ABAQUS [36] and MSC Marc [99] elastomers or hyperelastic material models are characterized by different forms of their strain energy (density) polynomial functions. Some of the polynomial strain energy function implemented include *Klesner-Segel*, *Hart-Smith*, *Gent-Thomas* and *Valants-Landel* for modelling the non-linear elastic response, and for materials going through large volumetric deformations several models have been suggested, such as *Blatz-Ko*, *Penn* and *Storaker*. Generalised models, such as *Mooney-Rivlin*, *Ogden* and *Boyce-Arruda* have been successfully applied for elastomers and slightly compressible rubbers in the analysis of o-rings, seals and other industrial products. From these, the *Ogden* model has become quite popular recently, and was adopted by ABAQUS as the material model for highly compressible low density foams. In section 6.3 a description on how ABAQUS adopts the Ogden's strain energy function and applies it on the hyperfoam model (section 6.4) will be given. In view of that, in the last years a few works adopting the ABAQUS hyperfoam constitutive model have been proposed:

in [100] it is used a hyperelastic model to predict the indentation behaviour of PU polymer foams with a good fitting response due to the strong tensile hardening component of the hyperelastic model. Again, remoulded PU foams to be used in head impact protection applications are modelled in [101] as hyperelastic compressible materials. Also in [102] low density PU foams and Ethylene Vinyl Acetate foams (EVA) used on personal protection in cushions, shoes and helmets are modelled as hyperelastic materials.

In [37] it is proposed an inverse FE modelling method to determine the non-linear material parameters during continuous indentation tests, as an alternative to the conventional compression and shear tests used to tune the Ogden's energy function. Closed Cell polymeric foams with a highly nonlinear and viscoelastic properties, such as EVA, where experimentally tested with both approaches and it was found that the inverse method proposed is comparable to the combined compression-shear tests, while uniaxial compression test could not provide accurate material data to simulate complex loading conditions.

A neural network based constitutive model for elastomeric foams is proposed in [103] to be implemented on finite element analysis package software as an alternative to the commercial hyperfoam constitutive formulations. Simulation of a plane-strain foam indentation process using the proposed neural network approach and the hyperfoam constitutive model available in ABAQUS indicated that the neural network model provides a better representation of the test data, specially when tension and simple shear deformation modes are included in the deformation, while finds the performance of the hyperfoam model satisfactory when only or prominent compression deformation is involved.

6.3 Ogden's strain energy model

As seen before, ABAQUS uses a *hyperelastic* model for constitutive modelling elastomeric foam materials, called *hyperfoam* model and based on the Ogden's strain energy function [104]. Ogden's strain energy potential is expressed in terms of the principal stretches or in terms of deviatronic strain invariants and volume ratio. The derivative of the energy function with respect to the strain

direction gives the stress values response. In ABAQUS the following polynomial strain energy formulation is used [36]:

$$U\left(\hat{\lambda}_1\right)=\sum_{i=1}^{N}\frac{2\mu_i}{\alpha_i^2}\left[\hat{\lambda}_1^{\alpha_i}+\hat{\lambda}_2^{\alpha_i}+\hat{\lambda}_3^{\alpha_i}-3+\frac{1}{\beta_i}\left(J_{el}^{-\alpha_i\beta_i}-1\right)\right] \quad (6.1)$$

Where $\hat{\lambda}_i = J_{th}^{-\frac{1}{3}}\lambda_i$ (6.2) and $\hat{\lambda}_1\hat{\lambda}_2\hat{\lambda}_3 = J_{el}$ (6.3)

λ_i are the principal stretches and J^{el} is the elastic volume ratio defined in equation (6.4) and related with the total volume ratio J and the thermal volume ratio J^{th}.

$$J_{el}=\frac{J}{J_{th}} \quad (6.4)$$

The total volume ratio J is the Jacobian measuring the current volume divided by the original volume and defined as the determinant of deformation gradient F (equation 6.5). The thermal volume ratio J^{th} is a function of ε^{th}, the linear thermal expansion strain (equation 6.6).

$$J=\frac{V}{V_0}=\det(F) \quad (6.5) \qquad J_{th}=(1+\varepsilon_{th})^3 \quad (6.6)$$

When the thermal effect is not considered ($\varepsilon^{th}=0$), expressions from (6.1) to (6.6) are simplified, since $J_{th}=1$ and $J_{el}=J$.

The parameter N is the fitting order and the coefficients μ_i, α_i, β_i are temperature-dependent material parameters to be determined by curve fitting the experimental data from simplified and well defined strain states. Each value of N corresponds to a specific strain state, and gives the associated strain energy stored. The coefficients μ_i are related to the initial shear modulus, μ_0 (equation 6.7), and the coefficients β_i determine the degree of compressibility for each term in energy function. β_i is related to the Poisson's ratio, ν_i, by the equation (6.8).

$$\mu_0=\sum_{i=1}^{N}\mu_i \quad (6.7) \qquad \beta_i=\frac{\nu_i}{1-2\nu_i} \quad (6.8)$$

If we consider β_i the same for all terms we have also a single effective Poisson's ratio, thus if $\beta_i=\nu_i=0$ there is no Poisson effect, which is a realistic simplification

at larger strains during compression, since it was experimentally observed during the flatwise compression tests performed with the hyperelastic PA Zotek® N B50 foam (sample *2S* in table 3.1, section 3.2.1, chapter III) that buckling of the foam cell walls did not result in significant lateral deformation.

6.4 Hyperfoam fitting parameters

ABAQUS provides two procedures for assigning the material parameters defined in the strain energy function. The first one is by direct inputting the previous known value of each parameter in the code, and the second one, which is the most common, is by assigning to the script a list of experimental data from several experiments representative of simplified strains states and relevant for the load case studied [37]. With this second approach, the unknown model parameters can be obtained using curve fittings for up to five experimental data tests, each reproducing a specific strain state. The most common deformation states accepted by ABAQUS are: uniaxial (tension or compression), equibiaxial, simple shear, planar and volumetric (tension or compression) tests. The hyperfoam model in ABAQUS allows the use of a fitting order *N*, up to six terms and as many data points as required can be entered from each test, obviously depending on the available computational resources and time consuming expectative. Besides, a correct choice of the number and type of experimental tests to perform has to be well valuated in order to optimize the experimental consuming time and obtain the most rewarding data test for the application case to be simulated. Therefore, in order to choose which characterisation tests are more appropriate and essential for the model characterisation, a preliminary evaluation is advised in order to identify the type of strains expected to arise on the final application that is being analysed. Usually the most relevant data for a correct fitting is that one obtained from uniaxial, biaxial or simple shear tests. Also the other tests usually require very complicated and expensive experimental apparatus (e.g. volumetric compression tests) which can be justified only for few specific applications. Moreover, it is important that the experimental data points for the fitting procedure cover the range of nominal strains expected to arise in the application case. Strain data is given as nominal strain values (per unit of original length) as well as nominal

stress values (force per unit of original cross-sectional area), except for the case of the volumetric tests where stress data is given as pressure values and the deformation as volumetric strain. The principal stretches, λ_i, defined as the ratios of current length to original length in the principal directions, are related to the principal nominal strains, ε_I, by the following relationships:

$$\lambda_i = 1 + \varepsilon_i \tag{6.9}$$

An quick overview on the principal deformation modes, experimentally measured and used as input data for ABAQUS is described below:

***i*) Uniaxial, biaxial and planar test**

The deformation gradient F is expressed in the principal directions of stretch and related to the total volume ratio, J, such as:

$$F = \begin{bmatrix} \lambda_1 & 0 & 0 \\ 0 & \lambda_2 & 0 \\ 0 & 0 & \lambda_3 \end{bmatrix} \quad (6.10) \qquad \text{and} \qquad \det(\mathrm{F}) = J = \lambda_1\lambda_2\lambda_3 \quad (6.11)$$

Since elastomeric foams are not incompressible, the total volume ratio (equation 6.5) always diverges from 1 ($J \neq 1$). For each stress-strain data pair, ABAQUS generates an expression for the stress in terms of the stretches and the unknown hyperfoam constants. The nominal stress-strain for the uniaxial, biaxial and planar test deformation mode is:

$$T_j = \frac{\partial U}{\partial \lambda_j} = \frac{2}{\lambda_j} \sum_{i=1}^{N} \frac{\mu_i}{\alpha_i} \left(\lambda_j^{\alpha_i} - J^{-\alpha_i \beta_i} \right) \tag{6.12}$$

where λ_j, is the stretch in the direction of loading.

- Uniaxial test mode $\lambda_1, \lambda_2(\nu), \lambda_3(\nu)$

  λ_1 is the principal stretch in the uniaxial test direction and λ_2, λ_3 are either independently determined by lateral deformation measurements or defined by a Poisson's ratio.

$$\lambda_1 = \lambda_U ; \lambda_2 = \lambda_3 ; J = \lambda_U \cdot \lambda_2^2 ; \lambda_U = 1 + \varepsilon_U \tag{6.13}$$

- Equibiaxial test mode $\lambda_1=\lambda_2, \lambda_3(\nu)$

  λ_1 and λ_2 are the principal stretches in the biaxial test directions and λ_3 is either independently determined by lateral deformation measurements or defined by a Poisson's ratio.

$$\lambda_1 = \lambda_2 = \lambda_B; J = \lambda_3 \cdot \lambda_B^2; \lambda_B = 1 + \varepsilon_B \tag{6.14}$$

- Planar test mode $\lambda_1, \lambda_2=1, \lambda_3(\nu)$

  Similar to biaxial mode, but with $\lambda_2=1$ (i.e. in this deformation mode the lateral stretch along direction 2 orthogonal to 1 is deliberately constrained). The λ_3 is either independently determined by lateral deformation measurements or defined by a Poisson's ratio.

$$\lambda_1 = \lambda_P; \lambda_2 = 1; J = \lambda_P \cdot \lambda_3 \tag{6.15}$$

***ii*) Simple shear test**

The deformation gradient, F, is expressed in equation (6.16), where γ is the shear strain value:

$$F = \begin{bmatrix} 1 & \gamma & 0 \\ 0 & 1 & 0 \\ 0 & 0 & 1 \end{bmatrix} \tag{6.16}$$

and

$$\det(\mathrm{F}) = J = \lambda_1\lambda_2\lambda_3 = 1 \tag{6.17}$$

This mode deformation is achieved by performing a pure shear test to the foam similar to the one described in chapter III, section 3.6. The nominal stress, is likewise equation 6.12 calculated by derivation of the energy function in the strain direction. In these case the nominal shear stress, T_s is given by:

$$T_s = \frac{\partial U}{\partial \gamma} = \sum_{j=1}^{2} \left\{ \frac{2\gamma}{2\left(\lambda_j^2 - 1\right) - \gamma^2} \sum_{i=1}^{N} \frac{\mu_i}{\alpha_i} \left(\lambda_j^{\alpha_i} - 1\right) \right\} \tag{6.18}$$

where λ_j are the principal stretches in the plane of shearing and related to the shear strain:

$$\lambda_{1,2} = \sqrt{1 + \frac{\gamma^2}{2} \pm \gamma\sqrt{1 + \frac{\gamma^2}{4}}} \tag{6.19}$$

***iii*) Volumetric test**

The deformation gradient, *F*, is the same defined for uniaxial tests, with the difference that all principal stretches are equal. Thus $\lambda_1=\lambda_2=\lambda_3=\lambda_v$ and $J=\lambda_v^3$. The pressure-volumetric relation is:

$$-p=\frac{\partial U}{\partial J}=\frac{2}{J}\sum_{i=1}^{N}\frac{\mu_i}{\alpha_i}\left(J^{\frac{1}{3}\alpha_i}-J^{-\alpha_i\beta_i}\right) \tag{6.20}$$

After performing the test method that better describes the type of deformations presented in the simulation study, the measured material stress *vs.* strain curve is inputted in the ABAQUS script as requested by the *hyperfoam* script command (consult Appendix D). The material constants are determined through a least squares fit procedure. For the *n* nominal stress *vs.* nominal strain data points, the relative error *E* measured is minimized:

$$E=\sum_{i=1}^{n}\left(\frac{1-T_i^{th}}{T_i^{test}}\right)^2 \tag{6.21}$$

Where T_i^{test} is a stress value from the test data and T_i^{th} corresponds to the stress calculations preformed by ABAQUS using equations 6.12 or 6.18. During the data fitting process, ABAQUS searches for the optimum set of material properties that describes the material hyperfoam behaviour until convergence is reached.

6.5 Case studies using the ABAQUS hyperfoam formulation

In this section the ABAQUS hyperfoam constitutive material will be applied on the numerical simulation of sandwich structures employing the PA Zotek® foam already considered in the analytical study presented in the previous chapters. Three behaviours in particular have been considered for numerical simulation: indentation of a fully backed sandwich beam, three-point bending of a sandwich beam and repeated compression of a pure foam slab.

Appendix D reports a collection of the main scripts regarding the ABAQUS numerical simulations here described.

6.5.1 Simulation of an indented fully-backed beam sandwich

6.5.1.1 Model and analysis definitions

The finite element model intends to mimic as much as possible the geometrical properties and the experimental fully backed test setup performed for the sandwich specimen *2S* (table 4.1, chapter IV).

By exploiting the model symmetry with respect to the mid-span vertical axis, only half beam was meshed with two dimensional SOLID (continuum) elements, TYPE=CPE4, for both face sheet and core region, optimizing in such way the computational performance (figure 6.1). These four-node bilinear elements are plane strain elements with active degrees of freedom corresponding to orthogonal plane directions *1* and *2*. Usually they are used for linear and complex nonlinear analyses involving contact and large deformations, as it is the case analysed here. A refinement of the mesh was done on the indentation loading area, and the rich resin layer (from the adhesive bonding procedure to assemble the sandwich) at the interface between face sheets and core was not considered.

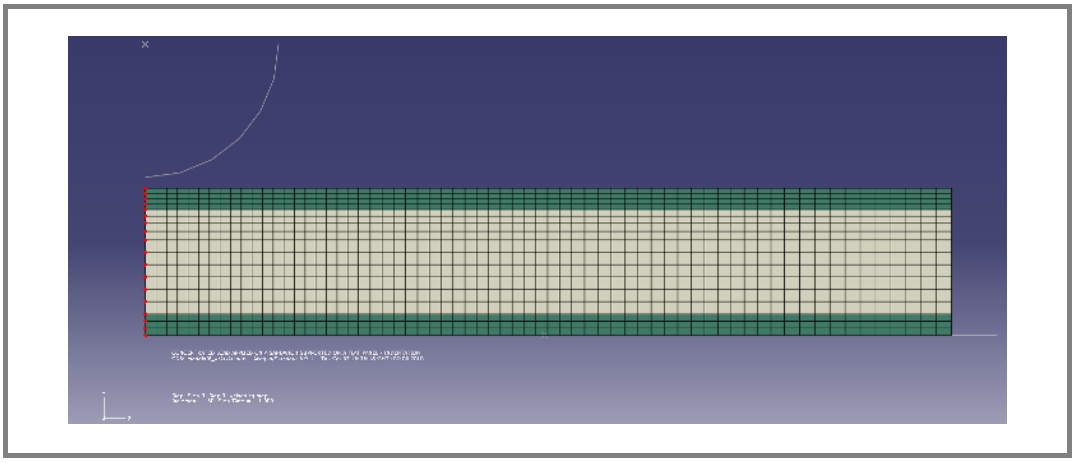

Figure 6.1 2D finite element model for half beam sandwich and analytical surfaces for indenter and flat support.

A *master-slave* contact of TYPE=SURFACE TO SURFACE was implemented between the metallic indenter and the upper face sheet and between the lower face sheet and the metallic flat support. In addition, the model allows separation between the flat support and the sandwich during the analysis,

simulating in a proper way the experimentally observed slight lifting up of the sandwich beam ends.

The cylindrical indenter and the flat support were modelled as RIGID BODIES obtained from analytical surfaces and identified by reference nodes during simulation. The face skin GRP laminate material was modelled as a linear ELASTIC material using TYPE=ENGINEERING CONSTANTS obtained from experimental tests from suppliers datasheets (see chapter III). No damage initiation and growth is considered in the model for the face skin laminates. The foam core material was modelled as hyperfoam material with a fitting order *N=2*. Uniaxial compression test data and uniaxial combined with shear test data were used for the characterisation of the Ogden's parameters. Due to the large deformations introduced by the indenter, a nonlinear geometrical large deformation analysis of the type NLGEOM is defined. Two implicit STATIC steps were used during the simulation. Following a good practice in numerical simulation, an initial first STEP with the restricted function of controlling possible interferences and penetrations in the model that could occur due to wrong elements or contact definitions, is added to the script. Thus, an extra boundary condition preventing horizontal (in axis-*x*) and vertical translations (in axis-*y*) is applied in four nodes (NSET=NBEAM2) from the external part of the half beam model only fort the *step 1* analysis.

A reference node on the flat rigid surface is constrained in all degrees of freedom (1-horizontal translation *x*, 2-vertical translation *y*, 6-rotation θ_z) during all the steps, and symmetry conditions were applied by using the ABAQUS XSYMM boundary condition, restraining in the horizontal direction the nodes located on the vertical axis of symmetry during all the simulation. A reference node belonging to the cylindrical indenter was constrained against horizontal translation and rotation, and assigned a vertical displacement during *step 2* to simulate the indentation loading. HISTORY and FIELD OUTPUT results were requested for nodes and elements at the end of *step 2*. The scripts used in the numerical simulation of the indented fully backed beam sandwich are partially reported in Appendix D, section D1.

6.5.1.2 Output results and discussion

In figure 6.2, it is depicted the FIELD OUTPUT for the vertical displacement, u_2 experienced in all the nodes of the half beam model.

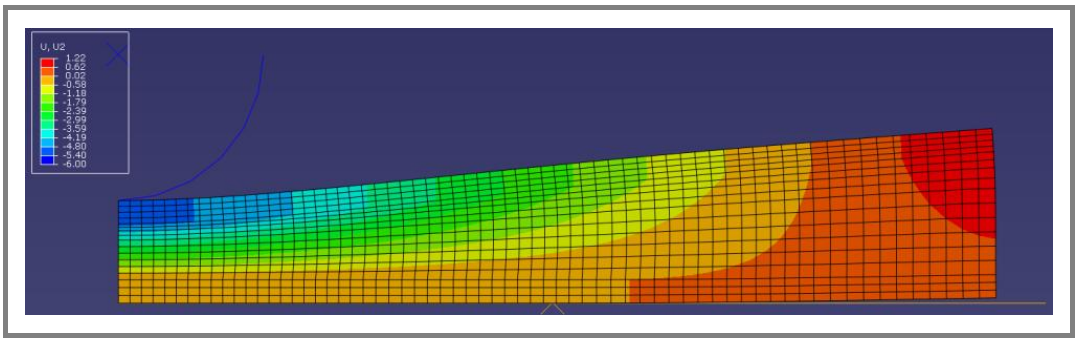

Figure 6.2 Field map of vertical displacements u_2 for an imposed mid-span vertical displacement of the indenter reference node equal to 6 mm (maximum indentation at end of *step 2*).

As expected, the area underneath the indenter roller undergoes the higher vertical displacements.

The nodes belonging to the elements of the lower areas of the beam, near the flat support, practically do not experience any displacement, except for the ones located near the half beam outer end, that slightly lift up at the point of maximum indentation, confirming the observations during the experimental indentation tests on specimen *2S* (elements with positive vertical displacement u_2).

The curves in figure 6.3 were built using data from the HISTORY OUTPUT of vertical displacements and load results obtained from the reference node (REF NODE) of the indenter rigid body, and allowed the construction of the numerical indentation curves which are compared to the experimental curve. Three numerical indentation curves are built up, with each one using a different set of foam experimental data for the tuning of the Ogden's model. In particular one curve is derived from tuning the model with the uniaxial compression test data only, a second curve from using both the uniaxial compression and shear test data, and finally the third curve using just the shear test data.

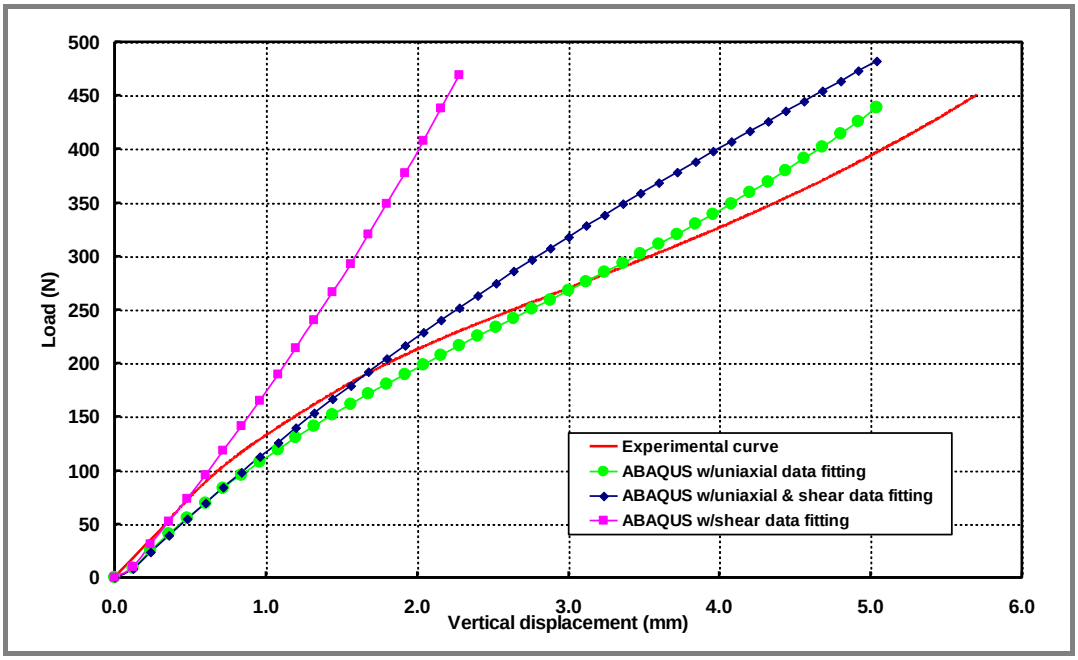

Figure 6.3 Numerical results obtained when using experimental information related with uniaxial compression and pure shear deformation modes compared with the experimental curve for sandwich specimen *2S*.

Based on observation of figure 6.3 some considerations are made:

for small vertical displacements (up to 1 mm) the simulation curves obtained using the uniaxial data fitting and uniaxial data combined with shear test data are very close, probably because at this strain level the *hyperelastic* foam core still deforms in a regular linear elastic manner due to cell wall bending. Afterwards, the simulated curve using both uniaxial and shear test data is less accurate than the simulated curve obtained using just the uniaxial test data, probably indicating that the non-linear compressive behaviour of the polyamide foam core prevails on the overall sandwich indentation behaviour.

It has to be said that the shear stress *vs.* shear strain curve obtained in the pure shear test of the PA foam (see section 3.6) could become less reliable in the range of big deformations, due to the lost correct alignment of the foam slab with the loading direction, which may compromise the pure shear conditions needed for this characterisation.

For the geometry and load case examined in this section, shear effects seem to have a smaller contribution to the overall behaviour of the sandwich beam during the indentation process, justifying the assumption for neglecting shear

components at the skin-core interface made by the one-parameter Winkler approach used by the segment-wise indentation model.

The simulated indentation curve obtained when using the experimental information exclusively related to the pure shear deformation mode are rather poor and do not follow the experimental indentation curve also within the first linear elastic stages of indentation.

In figure 6.4 the simulated indentation curve derived from using the polyamide foam uniaxial compression test data fitting is confronted with the analytical predictions and experimental curve previously reported in figure 5.6 (see also chapter V, section 5.3).

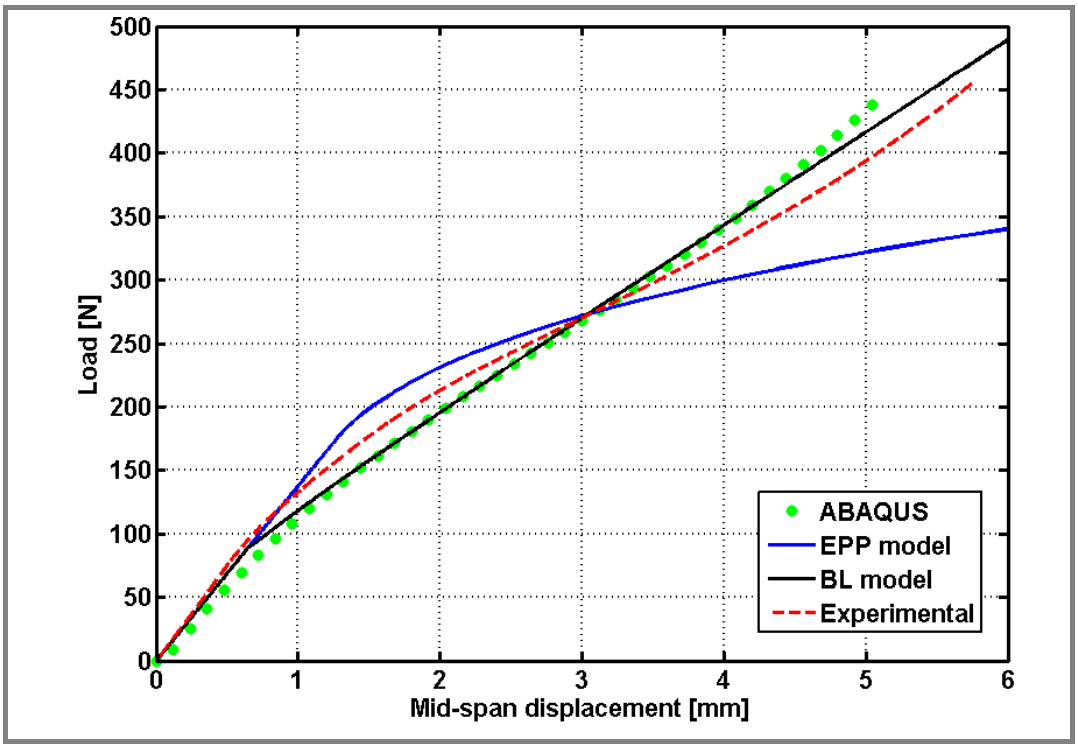

Figure 6.4 Analytical and numerical indentation predictions compared with the experimental indentation law for sandwich beam *2S* employing a highly non-linear behavioural polyamide foam core.

The numerical simulation from ABAQUS and the bilinear model prediction in particular are very closely matched. Both results present a fairly better prediction of the experimental indentation curve than the classical elastic-perfectly-plastic model.

It can be concluded that the above numerical results confirm the adequateness of the option taken in chapter V, of discretising the non-linear foam compression behaviour with just two segments (BL discretisation), avoiding in this way the extra computational effort needed to solve the non-linear equations of the segment-wise model which would arise if a higher number of discretising segments were chosen.

6.5.2 Numerical simulation of a TPB test on a beam sandwich employing a non-linear foam core.

In this section a reproduction of the TPB test setup, already implemented and described in chapter IV, section 4.3, is simulated for a beam sandwich.
The simulation considered a sandwich beam with a 30 mm thickness PA Zotek® hyperelastic foam core and 2 mm Glass/$PA_{unid.}$ laminate skins. Five tests have been simulated, at the variable span value of 100, 130, 160, 190 and 230 mm, in order to determine the flexural stiffness with the same linear regression procedure describe in chapter IV.
The numerical model was then also experimentally reproduced by manufacturing an identical beam specimen, whose main features are summarised in table 6.1.

Table 6.1 Sandwich beam specimen dimensions

Constitutive materials	Width *b* [*mm*]	Length *L* [mm]	Thickness *t* [mm]
PA Zotek® + Glass/PA6 $[0°]_{s\ unid.}$	24.45	245	34.24

6.5.2.1 Model and analysis definitions

For the TPB simulation it was used a three dimensional model of the beam sandwich meshed with SOLID elements TYPE=C3D8R for the core and SHELL elements TYPE=S4 for both skins.
Cylindrical indenter and supports were modelled with RIGID elements TYPE=R3D4 associated to a RIGID BODY by a REFERENCE NODE each.
Figure 6.5 illustrates the FEA model at two different spans and a picture during the experimental test of the PA Zotek® + Glass/PA6 $[0°]_{s\ unid}$ beam specimen.

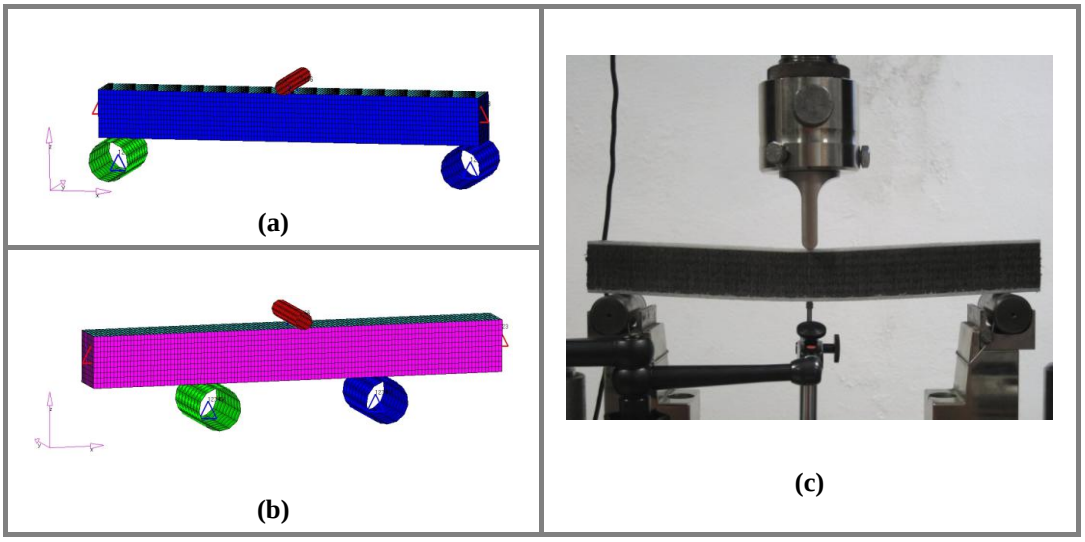

Figure 6.5 TPB of sandwich beam PA Zotek® + Glass/PA6 $[0°]_{s\ unid.}$ **(a)** numerical representation for span 230 mm; **(b**) numerical representation for span 160 mm; **(c)** experimental setup for span 230 mm.

A *master-slave* SURFACE TO SURFACE contact between skins and metallic rollers was applied to model contacts. To guarantee the stability of the model, a surface behaviour with NO SEPARATION was imposed to the CONTACT PAIR between the lower face sheet and the metallic supports.

The face skins material was modelled as linear ELASTIC material using TYPE=ENGINEERING CONSTANTS and foam material was modelled as HYPERFOAM material. Uniaxial compression test data was used for the characterisation of Ogden's parameters.

For each of the spans a non-linear geometrical large deformation analysis, NLGEOM, was performed with two implicit STATIC steps. Like for the analysis of the fully backed model described in section 6.5.1, *step 1* (contact) has exclusively the purpose of controlling possible interferences and penetrations in the model.

Just in this step, extra boundary conditions preventing translations in the longitudinal axis-*x*, transversal axis-*y* and vertical axis-*z* are applied to some node sets (NBEAM1 and NBEAM2) on both ends of the beam model.

Reference nodes from the rigid supports are constrained in all the six degrees of freedom: translations (1-longitudinal translation *x*, 2-transversal translation *y*, 3-vertical translation *z*) and rotations (4-rotation θ_x, 5-rotation θ_y, 6-rotation θ_z) during all the analysis.

A reference node of the rigid cylindrical indenter is free to translate in the third degree, and imposed a vertical displacement during *step 2* (loading). HISTORY and FIELD OUTPUT results were requested for nodes and elements at the end of *step 2*.

The scripts used in the numerical simulation of the TPB test are partially reported in Appendix D, section D2.

6.5.2.2 Output results and discussion

In figure 6.6, an example of the HISTORY OUTPUT results obtained for each of the simulated spans is presented in a single graph combining the load *vs.* mid-span displacement output for the Reference Node of the indenter rigid body (NSET=RB_impactor), simulating the displacement measured by the transducer in the machine cross head.

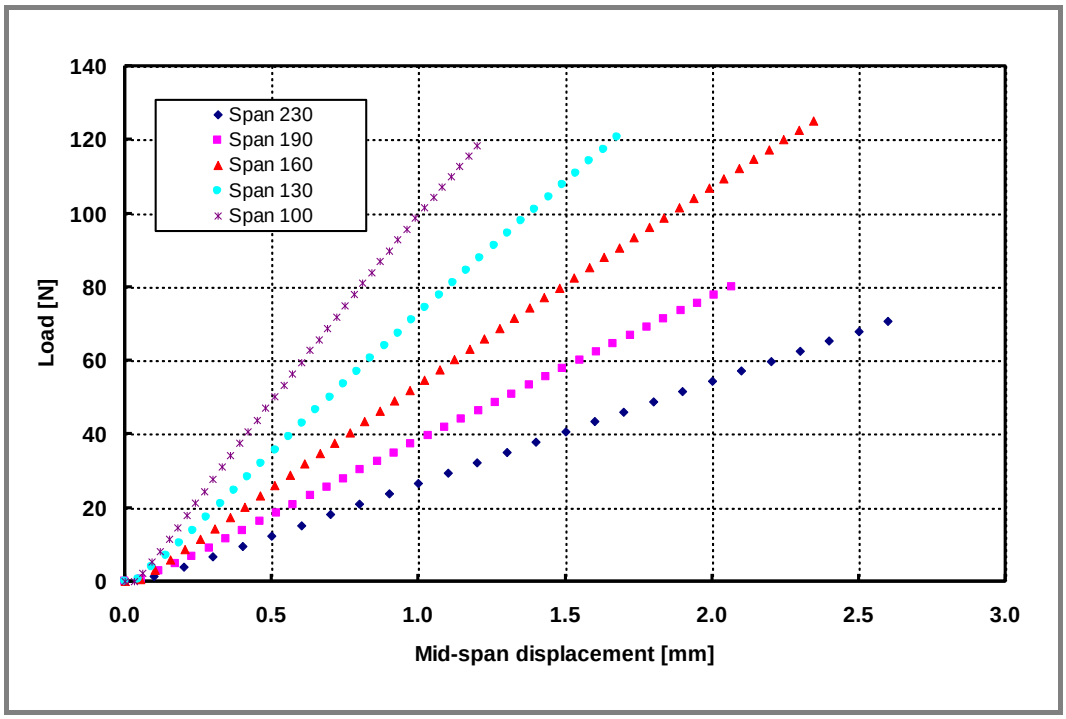

Figure 6.6 TPB Load *vs.* mid-span displacement numerical results in a PA Zotek® + Glass/PA6 $[0°]_{s\ unid}$ sandwich beam model (Output results for upper skin, NSET=RB_impactor).

An identical graph (not depicted) was obtained considering the displacement output at a Reference Node (NSET=N_LVDT) located in the mid-span of the lower skin of the sandwich model. In that case, the analysis reproduces the

experimental transducer probing on the lower skin, hence not affected by the indentation of the loading nose on the upper skin location (see section 4.3.2, chapter IV).

Calculating the inverse of the slope for each of the span results presented in figure 6.6 (which reports the numerical results only for the top skin) and considering equation (4.1) previously described in section 4.3 from chapter IV, a linear regression to the data values δ/PL *vs.* L^2 is performed in order to calculate the slope and intercept (figure 6.7) for the experimental and numerical results.

$$\frac{\Delta}{PL} = \frac{1}{48D} \cdot L^2 + \frac{1}{4U} \rightarrow y = m \cdot x + b \tag{4.1}$$

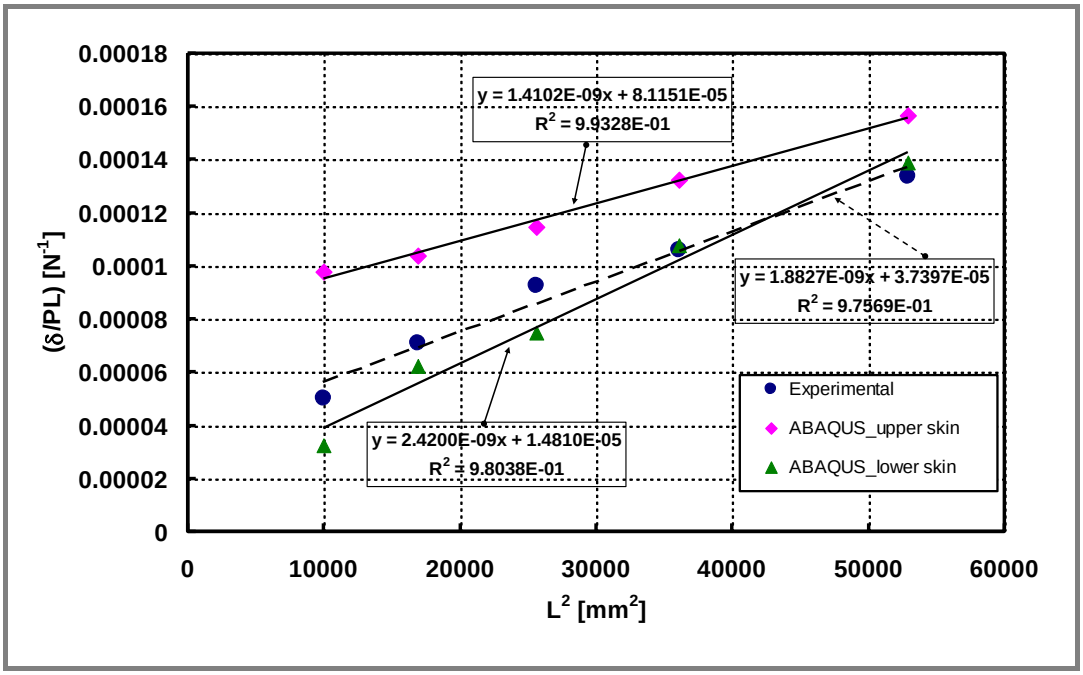

Figure 6.7 Experimental and numerical results for the linear regression δ/PL *vs.* L^2 in a PA Zotek® + Glass/PA6 $[0°]_{s\ unid}$ sandwich beam

In Figure 6.7 is observed that the linear regression obtained using the numerical output in the lower skin, i.e. simulating the displacement measured by the transducer probe is close to the experimental results measured in that way. On the other hand, the linear regression obtained from the numerical output in the upper skin, i.e. equivalent to the displacement measured by the transducer in the machine cross head, is affected by the local indentation due to the loading nose and rather far away from the experimental results.

Therefore, experimental and numerical flexural stiffness *D* are calculated from equation (4.6), here rewritten:

$$Slope: m = \frac{1}{48D} \tag{4.6}$$

Table 6.2 compares the experimental and numerical flexural stiffness results with the one predicted by the classical theory in equation (A3.4) as well as with the flexural stiffness of the single monolithic skins assembly (*h=2t*).

Table 6.2 Comparison of flexural stiffness results

Sandwich beam PA Zotek® + Glass/PA6 $[0°]_{s\ unid.}$				**Monolithic skin** Glass/PA6 $[0°]_{s\ unid}$
***D* [N.m^2] Experimental**	***D* [N.m^2] ABQ upper skin**	***D* [N.m^2] ABQ lower skin**	***D* [N.m^2] Equation (A3.4)**	***D* [N.m^2] (single skin *h=2t*)**
11.1	14.8	8.61	1176.7	5.5

Similar conclusions can be drawn to what said in chapter IV about sandwich *2S*. In fact also the numerical estimation of the flexural rigidity is quite consistently lower than the theoretical flexural rigidity, confirming in this sense the experimental finding.

Also for the sandwich beam tested in this section, which has a much thicker foam core than the specimen *2S*, the numerical and experimental values of flexural rigidity are still higher than the flexural rigidity expected from a single skins monolithic assembly with thickness *h*=2*t*. It is quite clear that the thermoplastic PA foam is not a suitable candidate for structural applications due to its very low structural performances compared to other foam materials which have similar densities.

Having said that, the present numerical study and the previous experimental evaluations still show that a sandwich employing a PA foam has an increase in terms of flexural rigidity, although much smaller than expected on the basis of the sandwich effect. In light of this, PA foams are definitely worth some consideration as candidate foam core materials for specific secondary structure applications.

This is particularly true if other design strengths associated with this material are considered, such as: its lower production costs, its high performances in terms of impact, greatly enhanced by the hyperelastic compressive behaviour, the possibility to combine with composite skins made of thermoplastic matrix forming a fully thermoplastic sandwich structure with alluring end of life disposal potentialities.

6.5.3 Modelling Mullins effect in elastomeric foams with ABAQUS

6.5.3.1 Mullins concept and experimental proofing

Usually low density elastomeric foams are also characterized by a hysteretic phenomenon of energy dissipation and stress softening, commonly called "Mullin's effect" [105].

When an elastomeric test specimen is subjected to simple tension from its virgin state, unloaded, and then reloaded, the stress required on reloading is less than that on the initial loading for stretches up to the maximum stretch achieved during the previous initial loading.

The extent of this stress softening changes according the level of stretch achieved in the first loading cycle, and is interpreted as being due to a continuous damage with microscopic deformation that occurs between bonds in the foam molecular chains [106, 107].

Figure 6.8 represents the experimental curves for a PA Zotek® foam slab which has been cyclically stressed following three different load paths. This graph was obtained by operating the Instron 3367 testing machine in displacement-control[1], defining a load history consisting of three triangular cycles from a zero to a maximum displacement (with this maximum value growing with the progression of cycles).

[1] The loading history was set up by using the Test Profiler function of the Intrson BlueHill 2.0 software which controls the machine.

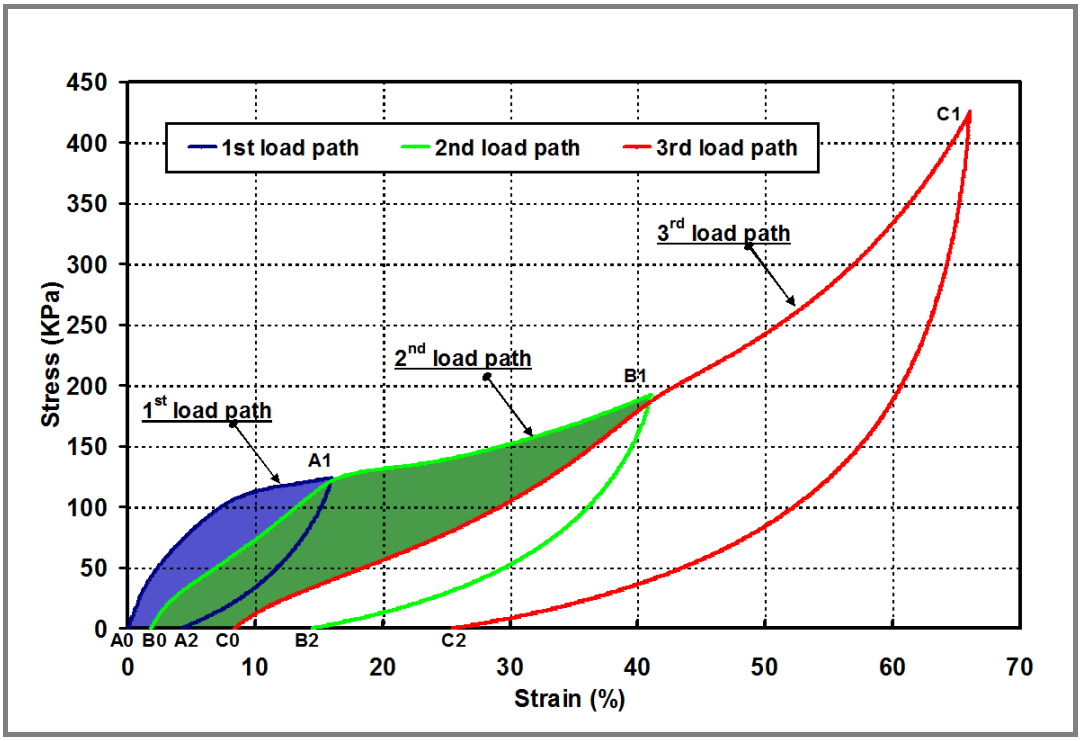

Figure 6.8 Experimental curves and stress softening during Mullins cycles on a PA Zotek® foam slab without skin faces and nominal dimensions 30x30x30 mm.

Lets consider the first load path of the unstressed foam from the point **A0** to the point **A1** and unloading to point **A2**.

The unloaded segment **A2-B0** represents a partial recovering of the material deformation before a new load is applied. When the foam is loaded again, the softened path **B0-A1-B1** is followed, being the path **A1-B1** a continuation of the primary or primitive loading path **A0-A1**, supposing that the unloading path **A1-A2** did not exist. If the foam is again unloaded from **B1** to **B2** it will recover part of its deformation up to the point **C0**. This is the new starting point if the material is loaded again, following the path **C0-B1-C1**, where **B1-C1** is a continuation of the primary loading path **A0-A1-B1**. If no further load is applied at **C1**, material unloads up to the point **C2**, exhibiting a residual strain.

This way, every time a new load path is imposed there is a stress softening represented by the shaded areas in figure 6.8. The shaded area contained on the **A0-A1-B0** curve represents the energy dissipated by material degradation due to a deformation until the point **A1**. The same applies to the shaded area contained in **B0-A1-B1-C0** representing the material degradation when loaded up to the point **B1**.

Another experiment was performed with a different slab of the same material (PA Zotek®) and dimensions (30x30x30 mm) but this time repeatedly compressed in each load path. The cyclic test this time was performed in load control, applying the load values reported in table 6.3.
Each load path was cyclically repeated for five times before applying the next load path, for a total of twenty complete cycles.

Table 6.3 Applied load path set values and maximum resulted strains for twenty cycles in the uniaxial compression test of a PA Zotek® foam slab (experimental data).

Path	Load [N]	Maximum strain (%)				
		cycle 1	cycle 2	cycle 3	cycle 4	cycle 5
1	150	25.31	25.76	26.14	26.42	26.64
2	300	56.76	57.49	57.90	58.21	58.47
3	450	68.13	68.63	68.95	69.19	69.39
4	900	80.17	80.54	80.75	80.91	81.03

Figure 6.9 shows the complete experimental curves applied in load control according with the path values defined in table 6.3.

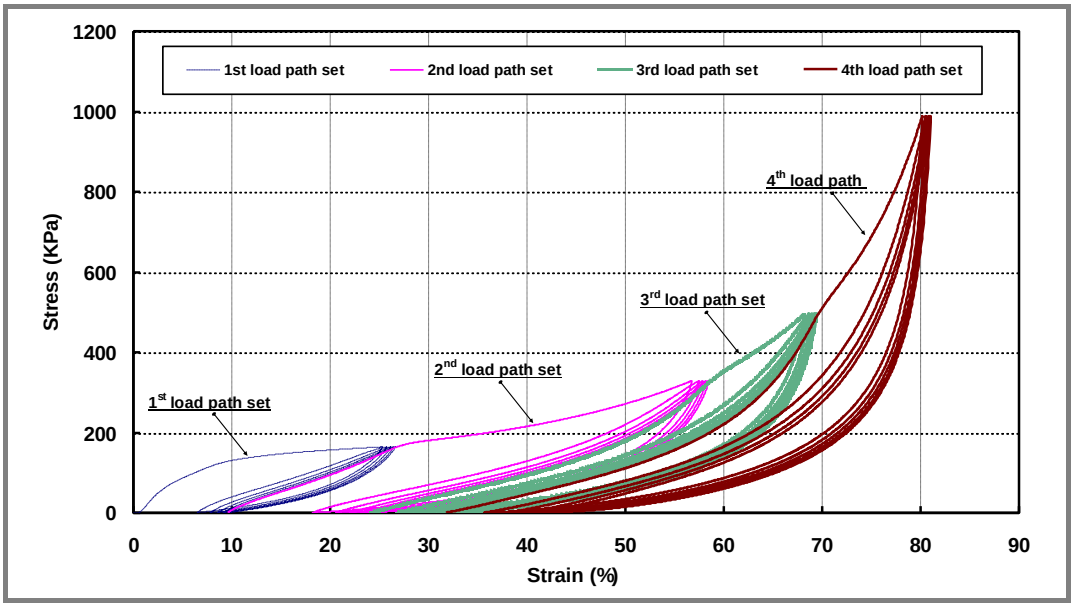

Figure 6.9 Experimental curves and stress softening during Mullins cycles on a PA Zotek® foam slab without skin faces and nominal dimensions 30x30x30 mm.

As observed in figure 6.9, after the first cycle application of each load path a softening effect in the material is determined which is left basically unmodified

during the remaining four cycles which complete each load path set. Additionally, a similar softening effect to what was observed on the simpler Mullins curves described in figure 6.8 is as well observed between different load path sets.

6.5.3.2 Simulation of Mullins effect on a PA Zotek® foam slab model

6.5.3.2.1 Model and analysis definitions

ABAQUS provides a mechanism to model the Mullins effect in elastomeric rubbers that is extended to simulate permanent energy dissipation and stress softening effects in elastomeric foams. When subjected to deformation strain rates higher than the characteristic relaxation time this foams are assumed to be permanently damaged with relevant alterations in the material response [36].

In this way, calibration of experimental data described in figure 6.8 for the PA Zotek® slab is required to determine the material coefficients for the Mullins effect. The primitive loading curve and the loading-unloading data related to different load paths are provided to ABAQUS in the form of nominal stress *vs.* nominal strain data points. In figure 6.10 a three-dimensional model of a cubic foam slab with 30x30x30 mm is meshed with SOLID C3D8R elements. Rigid elements SHELL R3D4 and associated to a RIGID BODY are used to model the lower metallic flat standing surface and the upper metallic contact platen connected with the moving cross head applying the force.

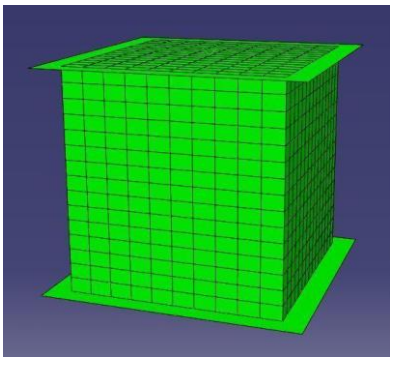

Figure 6.10 3D meshed model of the PA Zotek® foam slab and contact plate surfaces.

SURFACE TO SURFACE contact between the metallic platens and the foam slab is adopted. For each load path considered in the experimental flatwise

compression test, a loading STEP and an unloading step were used, for a total of six steps in the STATIC analysis. Experimental strain measures from table 6.4 were used to calculate the maximum vertical displacement imposed to the single unconstrained degree of freedom of the REFERENCE NODE associated to the upper contact platen in each of the loading steps. Lower metallic flat surface was associated to a reference node constrained in all degrees of freedom during all the analysis. Nonlinear geometrical large deformation analysis (NLGEOM) was used with the HYPERFOAM material card.

The scripts used in the numerical simulation of the Mullins effect in a PA Zotek® foam slab model are partially reported in Appendix D, section D3.

Table 6.4 Applied load path values and maximum resulted strains for three cycles in the uniaxial compression test of a PA Zotek® foam slab (experimental data).

Path	Load [N]	Maximum strain (%)
1	110	15.98
2	170	41.04
3	390	66.10

6.5.3.2.2 Results and discussion

Figure 6.11 shows the FIELD OTPUT results for the displacement *U* at the end of the *step 5*, for an imposed vertical displacement of the loading platen equal to 19.8 mm and equivalent to the experimental strain of 66%. As expected elements from the foam slab in contact with the upper metallic platen experience higher displacements than elements near the lower surface.

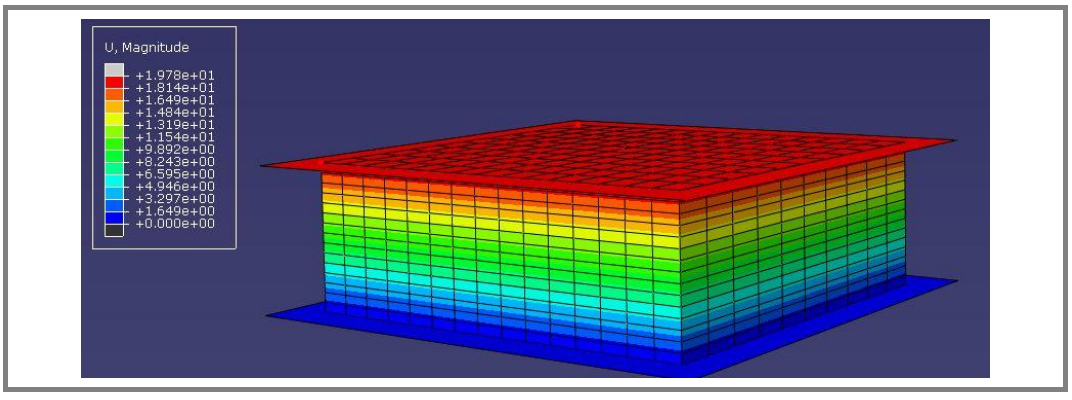

Figure 6.11 Displacement results *U* for an imposed vertical displacement of the contact plate reference node equal to 19.8 mm (66% strain at end of *step 5*).

In figure 6.12 a comparison is shown between the HISTORY OTPUT results in terms of stress *vs.* strain curves, and the experimental data (see figure 6.8).

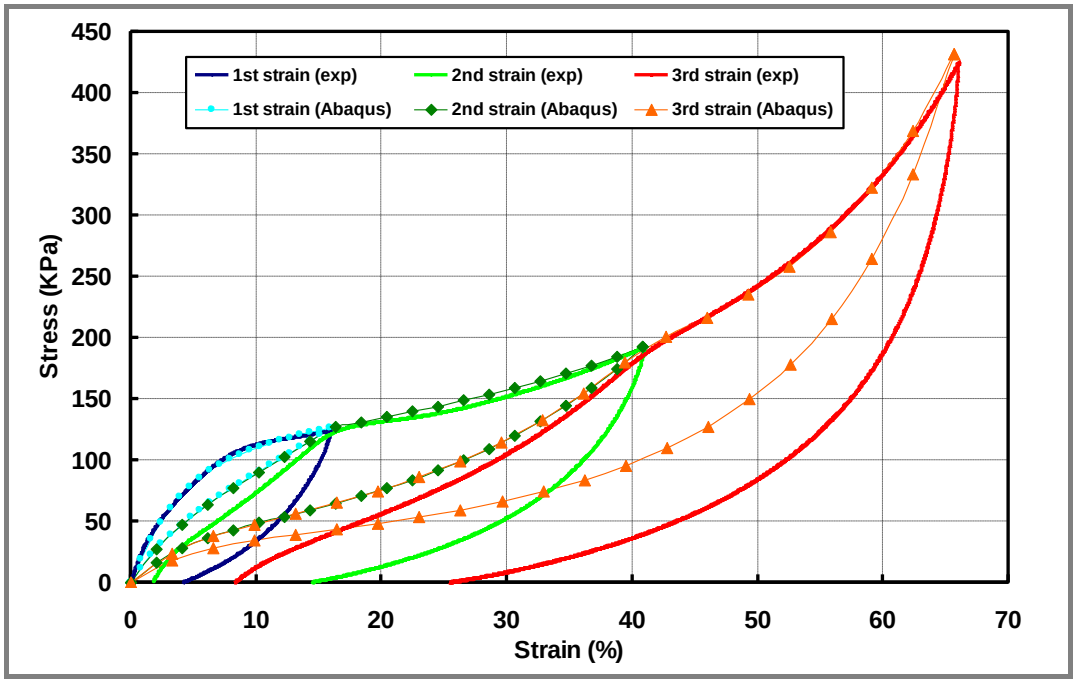

Figure 6.12 Comparison between experimental and numerical *stress vs. strain* results for three different load paths in the Mullins study of a PA Zotek® foam slab.

Curves from figure 6.12 indicate that during the loading phase of the three loading paths, numerical results reproduce quite well the experimental results.

Besides, the experimental primitive loading path **A0-A1-B1-C1** described in figure 6.8 and stress softening between load paths are in agreement with the numerical output results.

The unloading curve obtained by the numerical simulation is though not able to predict the residual strain observed experimentally. The lack of a residual dent is typical and expected for pure hyperelastic fully recoverable elastomers. So it seems that the implemented Mullins effect in the Hyperfoam formulation present in ABAQUS, which is mutuated from the hyperelastic behaviour of elastomers, is not able to predict the residual strain exhibited by hyperelastic foams in the unloading stage. The Technical support[2] from ABAQUS recognizes this limitation of the code that forces the unloading curves to a zero residual strain

[2] Information emailed in 24.11.2009 by ABAQUS Italy technical support, concerning the version ABAQUS/CAE 6.9-1; © Dassault Systemes 2009.

condition at the end of the unloading stage, typical in rubbers and elastomers but not adequate to hyperelastic foams.

CHAPTER VII

Concluding remarks

In this thesis work a unified approach has been presented to analytically model the indentation behaviour of fully-backed sandwich beams employing polymeric foam cores. It has been found that indentation is an important failure mode typical of sandwiches with transversely flexible (soft) core materials, such as low density polymer foams.

The indentation problem is modelled by studying the penetration of an elastic beam (sandwich skin face) on a compressible Winkler type foundation (sandwich core) using a segment-wise model approach. The model discretises the measured uniaxial foam core compression curve through a succession of linear segments, providing the material constitutive behaviour and the boundary conditions needed to solve the general fourth order differential equation expressing the equilibrium of the indented face skin. Experimental validation of the method is performed on industrial materials, exhibiting peculiar non-linear compressive behaviours. The proposed models are found to give a better match of the experimental data than the classic elastic-perfectly-plastic model and significantly improve the indentation curve prediction whenever the foam compression behaviour presents an hardening, softening or a marked non-linear trend in the post-elastic high deformation range of the foam uniaxial compression curve.

Some main topics analysed and reported in this thesis comprise: a literature review of previous analytical theories modelling the indentation of sandwich structures, with a special focus on Winkler based approaches, the development and implementation of the “segment-wise” analytical model for foam core

sandwiches, the implementation of experimental tests on constituent materials and sandwich beam structures for characterisation purposes and for the model validation, the implementation of a numerical model suitable for investigation the behaviour of sandwich structures using non-linear hyperelastic foams.
The results and major findings on these topics are summarized as follows:

Concerning the proposed *Segment-Wise* indentation model:

- Based on the general segment-wise model approach, the work has derived a number of closed form analytical solutions related with simplified constitutive foam behaviours in compression. In particular the pure elastic and elastic-perfectly-plastic (EPP) cases, widely reported in the literature, have been obtained by following the segment-wise schematisation.
- Closed form analytical solutions have been derived for generic bilinear foam compression behaviours, with the possibility to better model post-yield hardening or softening behaviours, and bilinear-perfectly-plastic behaviours which can better fit some highly non-linear trends in the foam compression curve.
- Analytical procedures proposed in the literature to predict the external load at the onset of the face skin flexural failure in a RPP and EPP core behaviour have been readapted for a BL generic non-linear compressive behaviour, comprising the EPP case. Results obtained from the generalised procedure compared well with those obtained in the literature with similar but less general procedures.
- The study extends the prediction capabilities of actual indentation models and works itself as an organic compendium of all those approaches based on the implementation of the Winkler theory to study indentation.

Concerning the constitutive materials experimental characterization:

- Laminate and foam materials used as sandwich face sheets and cores were characterised by means of tensile and flexural mechanical tests for the

laminates, and compressive and shear tests for the foams. Measured properties were used in the analytical and numerical studies.

- In particular, flatwise compression tests were performed on foams exhibiting different compressive behaviours. PMI and PVC foam cores showed a marked crushable behaviour, with the post-elastic phase between yielding and densification very well approximated by a plateau, justifying the EPP assumption. PA foams exhibited a highly non-linear compressive behaviour from early elastic strains up to densification, providing a good case study to evaluate the proposed BL indentation model. The compression curve measured with the XPS foam exhibited a particular bilinear hardening trend followed by a plateau and a final densification stages. The presence of an intermediate hardening phase between the linear elastic and the perfectly plastic zones provided a good case study to evaluate the BL and BLPP indentation models.

Concerning the sandwich beams TPB tests:

- Flexural stiffness and shear rigidity were experimentally calculated by means of TPB tests at different spans for sandwich beams employing foam cores with different compression behaviours. Samples adopting the classic crushable foams of PMI and PVC showed a measured flexural stiffness very close to that predicted by the classical beam theory. The sandwich adopting the PA foam core demonstrated to be markedly underperforming in terms of flexural rigidity. It is then suggested that the very low shear and compression stiffness values of the PA foam, together with its marked non-linear behaviour, determine a not very effective load transfer between the upper and lower skins with a severe detrimental effect on the flexural rigidity enhancement expected from the sandwich configuration.
- An innovative method was implemented using the analytical prediction of elastic indentation to correct the displacement data measured by the machine crosshead transducer in TPB tests. The method was applied to

calculate the bending stiffness value of the sandwich sample adopting the XPS foam with very satisfactory results.

Concerning the validation of the SW indentation model with the experimental indentation curve:

- Predicted indentation laws using the SW model are compared with experimental indentation curves for three sandwich beams employing PMI, PA and XPS foams as core material.
- Experimental foam compression curves were used for the determination of the foundation constitutive parameters using the segment-wise approach to discretise the measured curves: (i) the PMI foam used an EPP model to approximate the uniaxial compression curve; (ii) in the case of the PA Zotek® N B50, an EPP and a BL model have been considered in the fitting of the experimental curve; (iii) in the ThermoTec® XPS foam, two bilinear hardening models, BL1 and BL2 differing on the lengthwise of the second segment have been considered as well as an EPP model and a BLPP model.
- The net crushable behaviour of the PMI foam determined a good correlation between the experimental indentation curve data and the EPP predictions. The non-linear compressive behaviour of the PA foam determined a marked mismatch between the experimental indentation curve data and the EPP predictions, which becomes more severe with the progression of indentation. It was observed that the BL model is very accurate and capable of predicting the indentation law even at higher indentation values. In the case of the XPS sandwich, it was observed that the EPP model prediction is the less accurate while the BLPP prediction is very accurate and better than those from the BL1 and BL2 models up to an indentation penetration of 8 mm (corresponding to a nominal maximum compression strain of about 30%). The BL2 prediction gives also a very good match up to a 50% penetration, thanks to the wide extension of the linear fitting used to define the segment 2.

- In general it has been found that the bilinear approximation of the foam compression behaviour can significantly improve the indentation curve prediction whenever the foam is markedly non-linear.

Concerning the numerical simulation with highly non-linear foams:

- The behaviour of beam sandwiches employing polyamide foams with a highly non-linear compression trend have been numerically modelled using the HYPERFOAM formulation available in ABAQUS for hyperelastic foams. The Ogden strain energy formulation, on which the HYPERFOAM model is based, was characterised by fitting of uniaxial and shear tests performed on the PA foam.
- The implemented FEA models simulate in particular three behaviours: (i) the indentation of a fully backed sandwich beam; (ii) the deformation of a beam under a three-point bending configuration; (iii) the behaviour of a foam block under repeated uniaxial compression at various load levels.

  (i) The numerical simulation from ABAQUS and the bilinear model prediction for the sandwich beam employing the PA foam are very closely matched. Both results provide a fairly good prediction of the experimental indentation curve.

  (ii) The numerical estimation of the flexural rigidity is quite consistently lower than the theoretical flexural rigidity, confirming in this sense the experimental findings for thermoplastic sandwiches adopting PA foam cores.

  (iii) The phenomenon of energy dissipation and stress softening, typical of low density elastomeric foams and commonly called “Mullin’s effect” was experimentally confirmed with repeated uniaxial compression tests in the PA foam and is in agreement with the numerical results. It has been found that the implemented Mullins effect in the Hyperfoam formulation present in ABAQUS is not able to predict the residual strain exhibited by hyperelastic foams in the unloading stage due to a limitation of the code

that forces the unloading curves to a zero residual strain condition at the end of the unloading stage, typical in rubbers and elastomers but not adequate for hyperelastic foams.

Prospects for future research:

Finally a number of issues are briefly summarised which have the potential to improve the analytical approach developed in this work and give a deeper insight into the behaviour of soft core sandwich structures subject to transverse concentrated loads:

- Implementation of numerical procedures in order to derive and solve the non-linear equations resulting from a fitter discretisation (i.e. with a higher number of segments than $n=3$) of the foam compression curve in the presence of highly non-linear behaviour.
- Extend the segment-wise model to the case of beams loaded in TPB, using the approach proposed by Steeves and Fleck [38].
- Use of a two parameters Winkler elastic foundation able to include shear forces at the face-core interface.
- To compare the present analytical approach with the predictions and analysis results provided by the SPHOT (Sandwich Panel Higher Order Theory) proposed in [49], and employed also in sandwich indentation problems [59]. It has been observed that the two approaches have been developed and proposed separately, and have found little interaction in the known literature. While methods based on the Winkler approach seem to provide models which can find easier implementation and which better adapts to the needs of sandwich designers, the methods based on SPHOT are based on more rigorous basic assumptions, at the cost of a more complex computational analysis.

APPENDIX A

Classical beam theory

A1. Differential equation modelling indentation on fully backed sandwich beams

A2. Differential equation modelling indentation on simply supported sandwich beams

A3. Stiffness of simply supported sandwich beams

A4. Moment equation in a beam with mid-plane symmetry subjected to a transverse load

A1. Differential equation modelling indentation on fully backed sandwich beams

Beam theory on a Winkler foundation is applied to a sandwich beam locally loaded and resting on a surface, as sketched on figure A1.1, where the upper face sheet is modelled as a beam bonded to a compliant foundation (the core) and subject to a transverse concentrated line-load, *P*. The Winkler foundation model assumes that the supporting medium can be modelled as continuously distributed linear tension/compression springs.

Considering *r(x)* as the global reaction per unit length provided from the core foundation to the indented skin face as response to the concentrated load *P*, this can be considered as perfectly perpendicular (neglecting shear components) and composed by two terms: one accounting for the elastic response of the core, and one accounting for the plastic. The elastic term in particular is proportional to displacement *w* through an elastic modulus *k*, (Winkler or elastic response, equation A1.1).

$$r(x)_{el} = k_0 w \tag{A1.1}$$

k_0 is the foundation modulus or stiffness of the foundation, with the units [N/m^2/m]. Considering the beam width b and $k=k_0 b$ [N/m^2], comes:

$$r(x)_{el} = kw = k_0 bw \tag{A1.2}$$

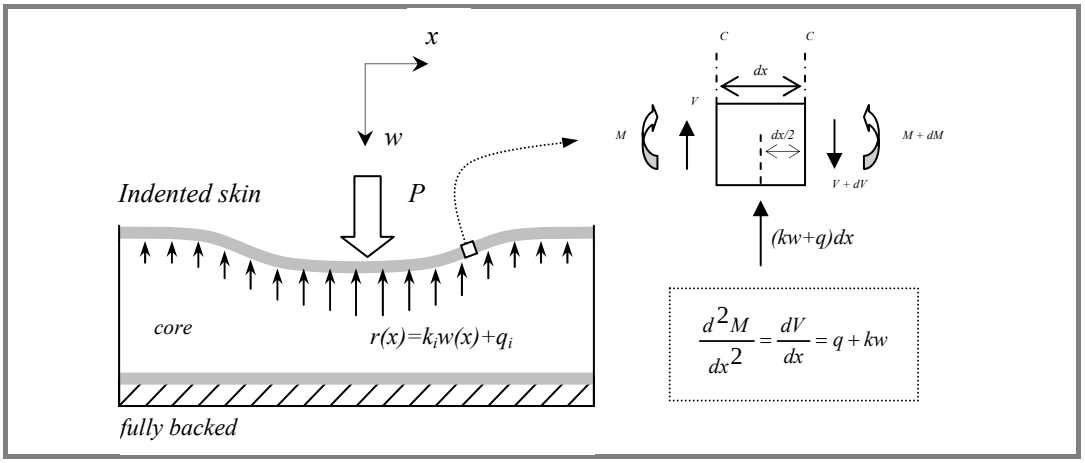

Figure A1.1 Schematic representation of a *fully-backed* indented sandwich beam and free-body diagram of an infinitesimal beam element of the upper skin.

The plastic component will be a constant load term q modelling the reaction of a rigid-perfectly-plastic core foundation.

Applying the equilibrium of vertical forces and moments to the infinitesimal beam element:

$$\sum F_y = 0 \Leftrightarrow V - V - dV + (q + kw)dx = 0 \Leftrightarrow \frac{dV}{dx} = q + kw \qquad \text{(A1.3)}$$

$$\sum M = 0 \Leftrightarrow M + V\frac{dx}{2} + (V + dV)\frac{dx}{2} - M - dM = 0 \Leftrightarrow \frac{dM}{dx} = V \qquad \text{(A1.4)}$$

results

$$\frac{d^2M}{dx^2} = \frac{dV}{dx} = q + kw \qquad \text{(A1.5)}$$

Using the moments governing equation in a beam with midplane symmetry subjected to a transverse load (see sub-section A1.4) gives:

$$M = -EI\frac{d^2w}{dx^2} \qquad \text{(A1.6)}$$

And replacing its second order derivative into equation (A1.5)

$$\frac{d^2M}{dx^2} = -EI\frac{d^4w}{dx^4} = q + kw \qquad \text{(A1.7)}$$

results in the following differential equation for the bending of the beam on a Winkler foundation:

$$EI\frac{d^4w}{dx^4} + kw + q = 0 \qquad \text{(A1.8)}$$

A2. Differential equation modelling indentation on simply supported sandwich beams

In the same way as before, beam theory is applied to a sandwich beam locally loaded and supported on a three-point bending configuration, as sketched in figure A2.1. Again, the upper face sheet is modelled as a beam bonded to a foundation core and subject to a transverse concentrated line-load, *P*.

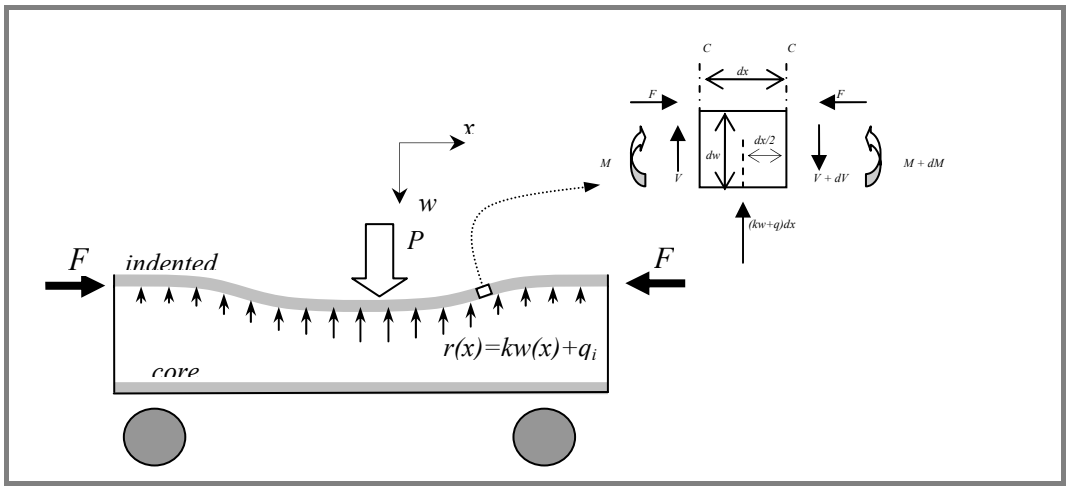

Figure A2.1 Schematic representation of an indented sandwich beam loaded in three-point bending and free-body diagram of an infinitesimal beam element of the upper skin.

In order to account for the modified general TPB constraint of the sandwich, Steeves et al [38] have proposed to consider membrane forces *F* arising from the flexural moments on the sandwich.

These forces will now produce a local flexural moment on the upper skin. So applying the equilibrium of forces and moments to the infinitesimal beam element yields:

$$\sum F_y = 0 \Leftrightarrow V - V - dV + (q + kw)dx = 0 \Leftrightarrow \frac{dV}{dx} = q + kw \qquad \text{(A2.1)}$$

$$\sum M = 0 \Leftrightarrow M + V\frac{dx}{2} + \left(V + dV\right)\frac{dx}{2} - M - dM + Fw - Fw - Fdw = 0 \Leftrightarrow$$

$$\Leftrightarrow \frac{dM}{dx} = V - F\frac{dw}{dx} \qquad \text{(A2.2)}$$

results

$$\frac{d^2M}{dx^2} = \frac{dV}{dx} - F\frac{dw^2}{dx^2} \Leftrightarrow \frac{d^2M}{dx^2} = q + kw - F\frac{dw^2}{dx^2} \tag{A2.3}$$

From the moments governing equation in a beam with midplane symmetry subjected to a transverse load:

$$M = -EI\frac{d^2w}{dx^2} \tag{A2.4}$$

Replacing the second order derivative of equation(A2.4) into equation (A2.3):

$$\frac{d^2M}{dx^2} = -EI\frac{d^4w}{dx^4} = q + kw - F\frac{dw^2}{dx^2} \tag{A2.5}$$

results in the following differential equation for the bending of the beam on a Winkler foundation in three-point bending load:

$$EI\frac{d^4w}{dx^4} - F\frac{dw^2}{dx^2} + kw + q = 0 \tag{A2.6}$$

A3. Stiffness of simply supported sandwich beams

The classical sandwich beam theory provides a simple approach to the characterisation and design of sandwich structures [1, 2, 4]. Although less accurate than more advanced theories, such as HOSPT (higher order sandwich panel theory) or finite element analysis, its simplicity leads to closed form analytical solutions for stress and displacement fields over a wide range of load scenarios, and an effective tool during early stage design for selection of sandwich typologies.

Obviously, the awareness of the assumptions related to this analytical theories is essential for its correct use and critical evaluation of the results. The main assumptions ignore core transverse strains and stresses (core is transversely incompressible and only shear deformation is considered), consider an ideal face-core adhesion and constant shear stresses at any core section [1, 2, 58, 76]. When a sandwich beam is subjected to a flexural load, such as the schematic simply supported three-point bending represented in figure A3.1, the mid-span elastic deflection is the sum of the flexural and shear deflections and is given by [6, 7, 38]:

$$\Delta = \Delta_{bending} + \Delta_{shear} = \frac{PL^3}{48D} + \frac{PL}{4U} \tag{A3.1}$$

where P is the external load, L is the span, D is the bending stiffness and U is the shear stiffness of the sandwich beam.

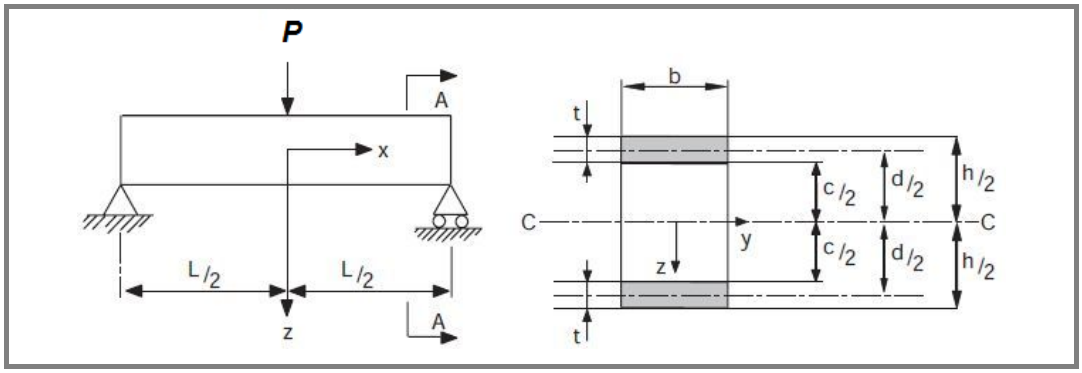

Figure A3.1 Schematic representation of a sandwich beam [7]: **(a)** three-point bending (TPB); **(b)** cross section geometry parameters (b is the beam width, t is the face sheet thickness, c is the core thickness, h is the sandwich thickness, d is the distance between the center line of each face).

Considering the sandwich beam section, the contribution of skins ands core to the overall inertia moment with respect to the central axis-*yy*, the theoretical bending stiffness *D=EI* is expressed as:

$$D = 2 \cdot \left[E_f \left(\frac{bt^3}{12} \right) + E_f \left(\frac{btd^2}{4} \right) \right]_f + \left[E_c \left(\frac{bc^3}{12} \right) \right]_c = E_f \left(\frac{bt^3}{6} \right) + E_f \left(\frac{btd^2}{2} \right) + E_c \left(\frac{bc^3}{12} \right) \quad \text{(A3.2)}$$

where E_f is the elastic modulus of the face sheet material and E_c is the elastic modulus of the foam core. The first term corresponds to the local bending stiffness of the faces about their own centroidal axis and can be neglected for very thin face sheets, whenever $d/t>5.77$ [7]. The second term is the bending stiffness of the faces with respect to the center line of the entire cross section. The third term is the bending stiffness of the foam core and can be ignored if the elastic modulus of the foam core is smaller enough than that of the face sheet material in order to verify the condition:

$$\frac{E_f}{E_c} \cdot \frac{td^2}{c^3} > 16.7 \quad \text{(A3.3)}$$

Therefore, if these conditions are verified, equation (A3.2) is reduced to the form:

$$D = E_f \left(\frac{btd^2}{2} \right) \quad \text{(A3.4)}$$

The sandwich shear rigidity (or shear stiffness) can be calculated if we consider the deformation occurred at the beam cross section due to shear stress when the beam sandwich is loaded in three-point bending.

A simplified approach of the first order shear deformation theory admits a linear shear deformation like the one depicted in figure A3.2. It is assumed that the shear deformation only occurs in the core (weak core with $E_c << E_f$ and thin faces) and that the shear stress is constant for each cross section of the core with value:

$$\tau_{xz} = \frac{T_z(x)}{bd} \quad \text{(A3.5)}$$

and a shear strain expressed by the shear angle γ_{xz}

$$\tau_{xz} = G \cdot \gamma_{xz} \Leftrightarrow \gamma_{xz} = \frac{1}{G} \cdot \frac{T_z(x)}{bd} \quad \text{(A3.6)}$$

where G is the core shear modulus. The shear stiffness, U, is found by calculating the average shear angle of the cross-section [4]:

$$\frac{1}{2}T_z(x)\gamma = \frac{1}{2}\int \tau_{xz}\cdot\gamma_{xz}dz, \text{ where by definition } \gamma = \frac{T_z(x)}{bU} \tag{A3.7}$$

thus,

$$\frac{1}{2}T_z(x)\gamma = \frac{1}{2}\int_{-c/2}^{c/2} \frac{T_z(x)}{bd}\cdot\frac{T_z(x)}{Gbd}dz = \frac{T_z(x)^2\cdot c}{2Gb^2d^2}$$

$$\Rightarrow \frac{T_z(x)^2}{2bU} = \frac{T_z(x)^2\cdot c}{2Gb^2d^2} \Leftrightarrow U = \frac{b\cdot d^2}{c}\cdot G \tag{A3.8}$$

For thin faces with thickness t, and if $d=c+t$ (see figure A3.2), expression (A3.8) simplifies to the form [6, 38, 40]:

$$U = \frac{b\cdot d^2}{c}\cdot G \cong b\cdot c\cdot G \tag{A3.9}$$

Often, and for rectangular sections like the one described here, the shear stiffness U is mentioned as being the product of $A\cdot G$, where A is the transversal area.

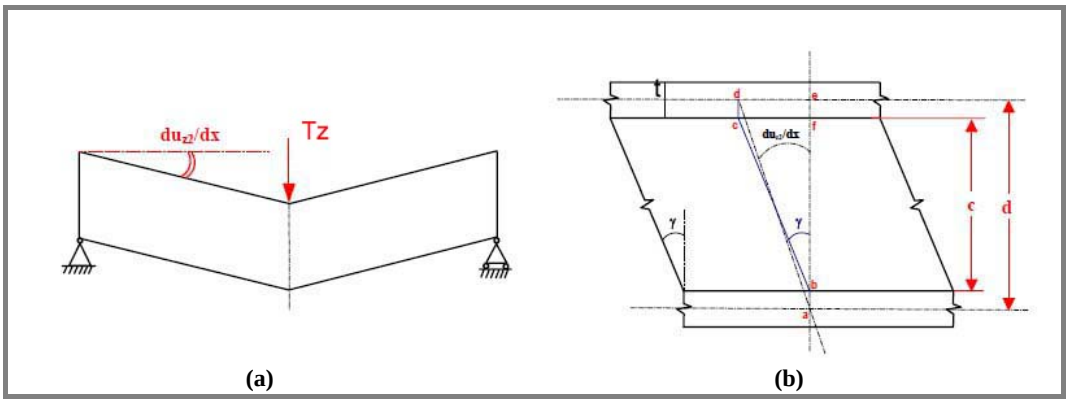

Figure A3.2 (a) Schematic representation of the shear deformation in a *tpb* loaded beam with a pure shear load - transverse force, $T_z(x)$; **(b)** deformation of a structural element subjected to shear forces. [6].

A4. Moment equation in a beam with mid-plane symmetry subjected to a transverse load

The following fundamental assumptions of the Euler-Bernoulli bending theory are recalled for a pure flexural deformation of a beam: (i) the deflection of the beam axis is small compared with the span of the beam; (ii) the slope of the deflection curve is thus very small and its square is negligible in comparison with unit; (iii) plane sections through a beam taken normal to its axis remain plane after the beam is subjected to bending (Bernoulli assumption) [6, 108].

Figure A4.1 schematically represents a beam and one of its infinitesimal elements before and after pure deflection. The angle of rotation, $d\varphi$, or slope of the deflection curve is given by $d\ = -\frac{dw}{dx}$ (negative according to the right-hand rule) and related to the curvature radius, ρ, by means of the expression $dx = \rho d\ $, so that it is also possible to write:

$$\frac{1}{\rho} = \frac{d}{dx} = -\frac{d^2 w}{dx^2} \tag{A4.1}$$

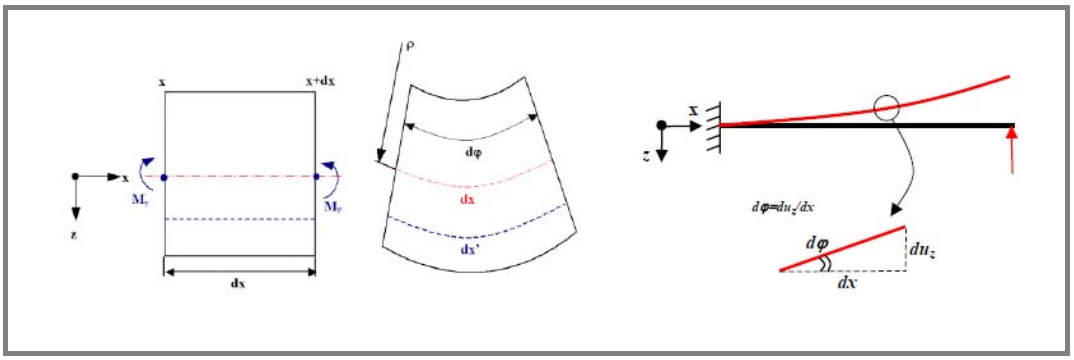

Figure A4.1. Schematic representation of a beam and infinitesimal beam element in pure deflection. [6]

On a cross section such as that represented in figure A4.1, the normal stress σ_x, acting on a longitudinal fiber is provided by the flexure equation:

$$\sigma_x(x,z) = \frac{M_y(x)\cdot z}{I_y} = 12\cdot\frac{M_y(x)\cdot z}{b\cdot h^3} \tag{A4.2}$$

where the bending moment at section x is $M_y(x)$ and I_y represents the moment of inertia of the cross section. The normal stresses vary linearly with the distance z

from the neutral axis, being null at the neutral axis and maximum at the outmost fibres of the beam.

The bending moment $M_y(x)$, obtained from the rotation equilibrium condition is expressed as $M_y = \frac{EI_y}{\rho}$, where $D = EI_y$ is the flexural rigidity term. Considering the inverse of the curvature radius as the beam curvature at a certain x section, $c(x) = \frac{1}{\rho}$, it can be written that:

$$c(x) = \frac{1}{\rho} = -\frac{d^2 w}{dx^2} = \frac{M_y(x)}{EI_y} \tag{A4.3}$$

Combining the expressions (A4.2) and (A4.3) a final equation relating the deflection w to the bending moment in a linearly elastic beam is derived:

$$\frac{d^2 w}{dx^2} = -\frac{M_y(x)}{EI_y} \qquad \text{or} \qquad M_y(x) = -EI_y \frac{d^2 w}{dx^2} \tag{A4.4}$$

APPENDIX B

Segment-Wise model configurations

B1. General Solutions for the indentation governing equation

B1.1 Pure elastic segment

B1.2 Elasto-plastic segments with hardening

B1.3 Elasto-plastic segments with softening

B1.4 Perfectly-plastic segment

B2. Boundary Conditions for the n^{th} *Segment-Wise* segments

B2.1 Pure elastic segment

B2.2 Elastic-perfectly-plastic segments

B2.3 Bilinear segments with hardening

B2.4 Bilinear segments with softening

B2.5 Bilinear-perfectly-plastic segments

B3. Systems of equations for the n^{th} *Segment-Wise* segments

B3.1 Pure elastic segment

B3.2 Elastic-perfectly-plastic segments

B3.3 Bilinear segments with hardening

B3.4 Bilinear segments with softening

B3.5 Bilinear-perfectly-plastic segments

B1. General Solutions for the indentation governing equation

$$E_f I_f \frac{d^4 w(x)}{dx^4} + k_i w(x) + q_i = 0 \qquad \text{(A1.8)}$$

The fourth order differential equation, equation (A1.8) deduced in Appendix A, section A1, admits the following solutions:

B1.1 Pure elastic segment ($k_i > 0$ and $q_i = 0$; $i=1$)

$$\begin{aligned}
w_1(x_1) &= e^{-\lambda_1 x_1}\cdot\left[A_1\cdot\sin(\lambda_1 x_1)+B_1\cdot\cos(\lambda_1 x_1)\right]+e^{\lambda_1 x_1}\cdot\left[C_1\cdot\sin(\lambda_1 x_1)+D_1\cdot\cos(\lambda_1 x_1)\right]\\
w_1'(x_1) &= -\lambda_1\cdot e^{-\lambda_1 x_1}\cdot\left[(A_1+B_1)\sin(\lambda_1 x_1)-(A_1-B_1)\cos(\lambda_1 x_1)\right]+\lambda_1\cdot e^{\lambda_1 x_1}\cdot\left[(C_1-D_1)\sin(\lambda_1 x_1)+(C_1+D_1)\cos(\lambda_1 x_1)\right]\\
w_1''(x_1) &= 2\lambda_1^2\cdot e^{-\lambda_1 x_1}\cdot\left[B_1\sin(\lambda_1 x_1)-A_1\cos(\lambda_1 x_1)\right]-2\lambda_1^2\cdot e^{\lambda_1 x_1}\cdot\left[D_1\sin(\lambda_1 x_1)-C_1\cos(\lambda_1 x_1)\right]\\
w_1'''(x) &= 2\lambda_1^3\cdot e^{-\lambda_1 x_1}\cdot\left[(A_1-B_1)\sin(\lambda_1 x_1)+(A_1+B_1)\cos(\lambda_1 x_1)\right]-2\lambda_1^3\cdot e^{\lambda_1 x_1}\cdot\left[(C_1+D_1)\sin(\lambda_1 x_1)-(C_1-D_1)\cos(\lambda_1 x_1)\right]
\end{aligned} \qquad \text{(B1)}$$

where:

$$\lambda_1 = \sqrt[4]{\frac{k_1}{4D_f}} \qquad \text{(B2)}$$

B1.2 Elasto-plastic segments with hardening ($k_i > 0$ and $q_i \neq 0$)

$$\begin{aligned}
w_i(x_i) &= -\frac{q_i}{k_i}+e^{-\lambda_i x_i}\cdot\left[A_i\cdot\sin(\lambda_i x_i)+B_i\cdot\cos(\lambda_i x_i)\right]+e^{\lambda_i x_i}\cdot\left[C_i\cdot\sin(\lambda_i x_i)+D_i\cdot\cos(\lambda_i x_i)\right]\\
w_i'(x_i) &= -\lambda_i\cdot e^{-\lambda_i x_i}\cdot\left[(A_i+B_i)\sin(\lambda_i x_i)-(A_i-B_i)\cos(\lambda_i x_i)\right]+\lambda_i\cdot e^{\lambda_i x_i}\cdot\left[(C_i-D_i)\sin(\lambda_i x_i)+(C_i+D_i)\cos(\lambda_i x_i)\right]\\
w_i''(x_i) &= 2\lambda_i^2\cdot e^{-\lambda_i x_i}\cdot\left[B_i\sin(\lambda_i x_i)-A_i\cos(\lambda_i x_i)\right]-2\lambda_i^2\cdot e^{\lambda_i x_i}\cdot\left[D_i\sin(\lambda_i x_i)-C_i\cos(\lambda_i x_i)\right]\\
w_i'''(x_i) &= 2\lambda_i^3\cdot e^{-\lambda_i x_i}\cdot\left[(A_i-B_i)\sin(\lambda_i x_i)+(A_i+B_i)\cos(\lambda_i x_i)\right]-2\lambda_i^3\cdot e^{\lambda_i x_i}\cdot\left[(C_i+D_i)\sin(\lambda_i x_i)-(C_i-D_i)\cos(\lambda_i x_i)\right]
\end{aligned} \qquad \text{(B3)}$$

where:

$$\lambda_i = \sqrt[4]{\frac{k_i}{4D_f}} \qquad \text{(B4)}$$

B1.3 Elasto-plastic segments with softening ($k_i < 0$ and $q_i \neq 0$)

$$
\begin{aligned}
w_i(x_i) &= -\frac{q_i}{k_i} + A_i e^{-\lambda_i x_i} + B_i e^{\lambda_i x_i} + C_i \sin(\lambda_i x_i) + D_i \cos(\lambda_i x_i) \\
w_i'(x_i) &= -\lambda_i \cdot e^{-\lambda_i x_i} \cdot A_i + \lambda_i \cdot e^{\lambda_i x_i} B_i + \lambda_i \cdot \left(C_i \cos(\lambda_i x_i) - D_i \sin(\lambda_i x_i)\right) \\
w_i''(x_i) &= \lambda_i^2 \cdot e^{-\lambda_i x_i} \cdot A_i + \lambda_i^2 \cdot e^{\lambda_i x_i} \cdot B_i - \lambda_i^2 \cdot \left(C_i \sin(\lambda_i x_i) + D_i \cos(\lambda_i x_i)\right) \\
w_i'''(x_i) &= -\lambda_i^3 e^{-\lambda_i x_i} \cdot A_i + \lambda_i^3 e^{\lambda_i x_i} \cdot B_i - \lambda_i^3 \cdot \left(C_i \cos(\lambda_i x_i) - D_i \sin(\lambda_i x_i)\right)
\end{aligned}
\tag{B5}
$$

where:

$$
\lambda_i = \sqrt[4]{\frac{-k_i}{D_f}} \tag{B6}
$$

B1.4 Perfectly-plastic segment ($k_i = 0$ and $q_i \neq 0$; $i=n$)

$$
\begin{aligned}
w_n(x_n) &= -\frac{q_n}{24 D_f} {x_n}^4 + A_n \frac{{x_n}^3}{3} + B_n \frac{{x_n}^2}{2} + C_n x_n + D_n \\
w_n'(x_n) &= -\frac{q_n}{6 D_f} {x_n}^3 + A_n {x_n}^2 + B_n x_n + C_n \\
w_n''(x_n) &= -\frac{q_n}{2 D_f} {x_n}^2 + 2 A_n x_n + B_n \\
w_n'''(x_n) &= -\frac{q_n}{D_f} x_n + 2 A_n
\end{aligned}
\tag{B7}
$$

B2. Boundary Conditions for the n^{th} *Segment-Wise* segments

As explained in chapter II, 2 B.C. are imposed to the infinite beam length requiring that the beam does not deform at the outermost end, 3 B.C are applied at the loading point and the remaining $5\times(n-1)$ B.C. impose the continuity of the displacements, slopes, bending moments and shear forces at the interface between adjacent beam segments.

B2.1 Pure elastic segment (*E*, one segment, $q_1=0$)

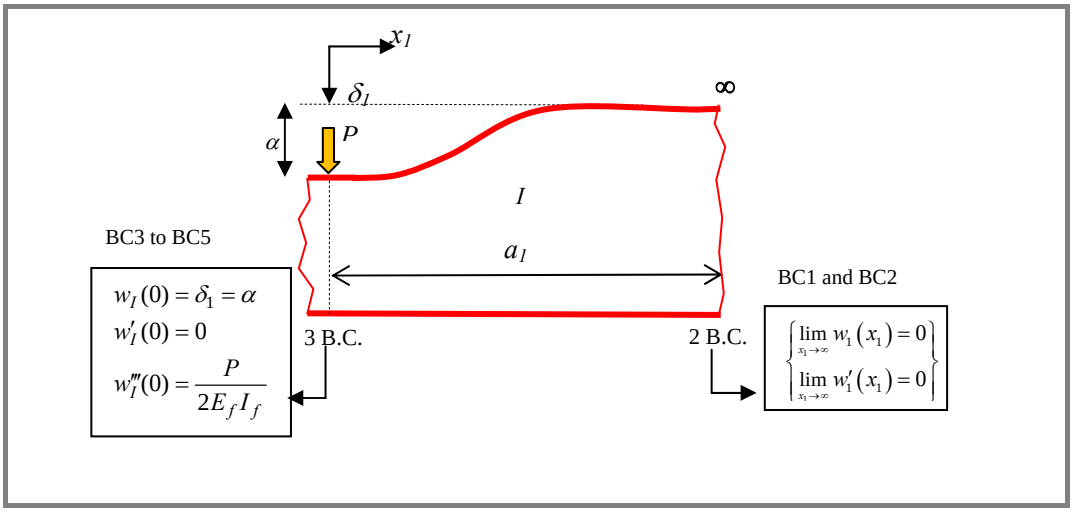

Figure B1. Boundary conditions applicable for one elastic segment.

BC1 and BC2

$$\left\{\begin{matrix}\lim\limits_{x_1\to\infty} w_1(x_1)=0\\ \lim\limits_{x_1\to\infty} w_1'(x_1)=0\end{matrix}\right\}\Rightarrow, \text{ then } C_1=0 \text{ and } D_1=0 \tag{B8}$$

BC3

$$\begin{aligned} &w_1(0)=\delta_1=\alpha\\ &b13\cdot B_1=\alpha\\ &b13=1\end{aligned} \tag{B9}$$

BC4

$$w_1'(0) = 0$$
$$\lambda_1 \cdot (A_1 - B_1) = 0$$
$$w_1'(0) = a14 \cdot A_1 + b14 \cdot B_1$$
$$a14 = \lambda_1; b14 = -\lambda_1 \quad \text{(B10)}$$

BC5

$$w_1''(0) = \frac{P}{2E_f \cdot I_f}$$
$$w_1''(0) = a15 \cdot A_1 + b15 \cdot B_1$$
$$a15 = b15 = 2\lambda_1^3 \quad \text{(B11)}$$

B2.2 Elastic-perfectly-plastic segments (*EPP*, 2 segments, $k_2=0$)

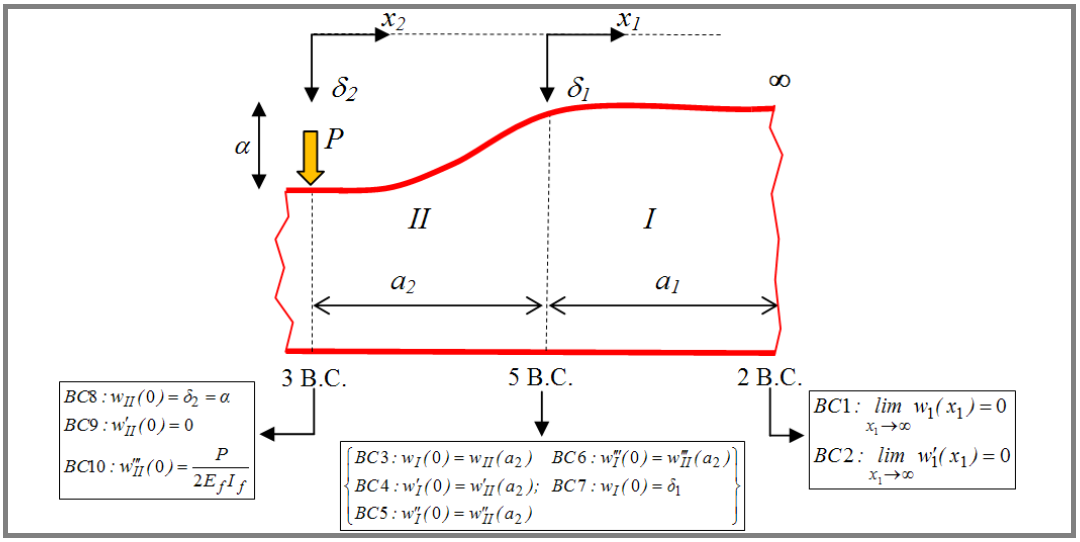

Figure B2. Boundary conditions applicable for two segments.

BC1 and BC2

$C_1=0$; $D_1=0$ (B12)

BC3

$$w_1(0) = w_2(a_2)$$
$$w_1(0) = b13 \cdot B_1$$
$$w_2(a_2) = r23 + a23 \cdot A_2 + b23 \cdot B_2 + c23 \cdot C_2 + d23 \cdot D_2$$
$$b13 = 1;\ r23 = -\frac{q_2}{24Df} \cdot a_2^4;\ a23 = \frac{a_2^3}{3};\ b23 = \frac{a_2^2}{2};\ c23 = a_2;\ d23 = 1 \quad \text{(B13)}$$

$$a23 \cdot A_2 + b23 \cdot B_2 + c23 \cdot C_2 + d23 \cdot D_2 = b13 \cdot B_1 - r23$$

BC4

$$
\begin{aligned}
&w_1'(0) = w_2'(a_2)\\
&w_1'(0) = a14 \cdot A_1 + b14 \cdot B_1\\
&w_2'(a_2) = r24 + a24 \cdot A_2 + b24 \cdot B_2 + c24 \cdot C_2\\
&a14 = \lambda_1; b14 = -\lambda_1;\\
&r24 = -\frac{q_2}{6Df} \cdot a_2^3;\ a24 = a_2^2;\ \ b24 = a_2;\ \mathrm{c}24 = 1\\
&-a14 \cdot A_1 + a24 \cdot A_2 + b24 \cdot B_2 + c24 \cdot C_2 = b14 \cdot B_1 - r24
\end{aligned}
\qquad \text{(B14)}
$$

BC5

$$
\begin{aligned}
&w_1''(0) = w_2''(a_2)\\
&w_1''(0) = a15 \cdot A_1\\
&w_2''(a_2) = r25 + a25 \cdot A_2 + b25 \cdot B_2\\
&a15 = -2\lambda_1^2;\\
&r25 = -\frac{q_2}{2Df} \cdot a_2^2;\ a25 = 2a_2;\ \ b25 = 1\\
&r25 - a15 \cdot A_1 + a25 \cdot A_2 + b25 \cdot B_2 = 0
\end{aligned}
\qquad \text{(B15)}
$$

BC6

$$
\begin{aligned}
&w_1'''(0) = w_2'''(a_2)\\
&w_1'''(0) = a16 \cdot A_1 + b16 \cdot B_1\\
&w_2'''(a_2) = r26 + a26 \cdot A_2\\
&a16 = b16 = 2\lambda_1^3\\
&r26 = -\frac{q_2}{Df} \cdot a_2;\ \ a26 = 2\\
&-a16 \cdot A_1 + a26 \cdot A_2 = b16 \cdot B_1 - r26
\end{aligned}
\qquad \text{(B16)}
$$

BC7

$$
\left.\begin{aligned}
&w_1(0) = \delta_1\\
&w_1(0) = b17 \cdot B_1\\
&b17 = 1;
\end{aligned}\right\} \rightarrow B_1 = \delta_1
\qquad \text{(B17)}
$$

BC8

$$
\left.\begin{aligned}
&w_2(0) = \alpha\\
&w_2(0) = d28 \cdot D_2\\
&d28 = 1
\end{aligned}\right| \rightarrow D_2 = \alpha
\qquad \text{(B18)}
$$

BC9

$$\left.\begin{array}{l} w_2'(0)=0 \\ w_2'(0)=c29\cdot C_2=0 \\ c29=1 \end{array}\right| \rightarrow C_2=0 \qquad \text{(B19)}$$

BC10

$$\left.\begin{array}{l} w_2'''(0)=\dfrac{P}{2D_f} \\ w_2'''(0)=a210\cdot A_2 \\ a210=2 \end{array}\right| \rightarrow A_2=\frac{P}{2\cdot a210\cdot D_f} \qquad \text{(B20)}$$

B2.3 Bilinear segments with hardening (BL_h, 2 segments , $k_2>0$)

BC1 and BC2

C1=0 ; D1=0

BC3

$$\begin{array}{l} w_1(0)=w_2(a_2) \\ w_1(0)=b13\cdot B_1 \\ w_2(a_2)=r23+a23\cdot A_2+b23\cdot B_2+c23\cdot C_2+d23\cdot D_2 \\ b13=1;\ r23=-\dfrac{q_2}{k_2};\ a23=e^{-\lambda_2 a_2}\cdot\sin(\lambda_2 a_2);\ b23=e^{-\lambda_2 a_2}\cdot\cos(\lambda_2 a_2) \\ c23=e^{\lambda_2 a_2}\cdot\sin(\lambda_2 a_2);\ d23=e^{\lambda_2 a_2}\cdot\cos(\lambda_2 a_2) \\ a23\cdot A_2-b13\cdot B_1+b23\cdot B_2+c23\cdot C_2+d23\cdot D_2=-r23 \end{array} \qquad \text{(B21)}$$

BC4

$$\begin{array}{l} w_1'(0)=w_2'(a_2) \\ w_1'(0)=a14\cdot A_1+b14\cdot B_1 \\ w_2'(a_2)=a24\cdot A_2+b24\cdot B_2+c24\cdot C_2+d24\cdot D_2 \\ a14=\lambda_1;b14=-\lambda_1; \\ a24=-\lambda_2 e^{-\lambda_2 a_2}\cdot\left[\sin(\lambda_2 a_2)-\cos(\lambda_2 a_2)\right];\ \ b24=-\lambda_2 e^{-\lambda_2 a_2}\cdot\left[\sin(\lambda_2 a_2)+\cos(\lambda_2 a_2)\right] \\ c24=\lambda_2 e^{\lambda_2 a_2}\cdot\left[\sin(\lambda_2 a_2)+\cos(\lambda_2 a_2)\right];\ \ d24=-\lambda_2 e^{\lambda_2 a_2}\cdot\left[\sin(\lambda_2 a_2)-\cos(\lambda_2 a_2)\right] \\ a14\cdot A_1-a24\cdot A_2+b14\cdot B_1-b24\cdot B_2-c24\cdot C_2-d24\cdot D_2=0 \end{array} \qquad \text{(B22)}$$

BC5

$$
\begin{aligned}
&w_1''(0) = w_2''(a_2)\\
&w_1''(0) = a15 \cdot A_1\\
&w_2''(a_2) = a25 \cdot A_2 + b25 \cdot B_2 + c25 \cdot C_2 + d25 \cdot D_2\\
&a15 = -2\lambda_1^2;\\
&a25 = -2\lambda_2^2 e^{-\lambda_2 a_2} \cdot \cos(\lambda_2 a_2);\quad b25 = 2\lambda_2^2 e^{-\lambda_2 a_2} \cdot \sin(\lambda_2 a_2)\\
&c25 = 2\lambda_2^2 e^{\lambda_2 a_2} \cdot \cos(\lambda_2 a_2);\quad d25 = -2\lambda_2^2 e^{\lambda_2 a_2} \cdot \sin(\lambda_2 a_2)\\
&-a15 \cdot A_1 + a25 \cdot A_2 + b25 \cdot B_2 + c25 \cdot C_2 + d25 \cdot D_2 = 0
\end{aligned}
\tag{B23}
$$

BC6

$$
\begin{aligned}
&w_1'''(0) = w_2'''(a_2)\\
&w_1'''(0) = a16 \cdot A_1 + b16 \cdot B_1\\
&w_2'''(a_2) = a26 \cdot A_2 + b26 \cdot B_2 + c26 \cdot C_2 + d26 \cdot D_2\\
&a16 = b16 = 2\lambda_1^3\\
&a26 = 2\lambda_2^3 e^{-\lambda_2 a_2} \cdot [\sin(\lambda_2 a_2) + \cos(\lambda_2 a_2)];\quad b26 = -2\lambda_2^3 e^{-\lambda_2 a_2} \cdot [\sin(\lambda_2 a_2) - \cos(\lambda_2 a_2)]\\
&c26 = -2\lambda_2^3 e^{\lambda_2 a_2} \cdot [\sin(\lambda_2 a_2) - \cos(\lambda_2 a_2)];\quad d26 = -2\lambda_2^3 e^{\lambda_2 a_2} \cdot [\sin(\lambda_2 a_2) + \cos(\lambda_2 a_2)]\\
&-a16 \cdot A_1 - b16 \cdot B_1 + a26 \cdot A_2 + b26 \cdot B_2 + c26 \cdot C_2 + d26 \cdot D_2 = 0
\end{aligned}
\tag{B24}
$$

BC7

$$
\left.\begin{aligned}
&w_1(0) = \delta_1\\
&w_1(0) = b17 \cdot B_1\\
&b17 = 1;
\end{aligned}\right\} \rightarrow B_1 = \delta_1
\tag{B25}
$$

BC8

$$
\begin{aligned}
&w_2(0) = \alpha\\
&w_2(0) = r28 + b28 \cdot B_2 + d28 \cdot D_2\\
&r28 = -\frac{q_2}{k_2};\ b28 = d28 = 1\\
&r28 + b28 \cdot B_2 + d28 \cdot D_2 = \alpha
\end{aligned}
\tag{B26}
$$

BC9

$$
\begin{aligned}
&w_2'(0) = 0\\
&w_2'(0) = a29 \cdot A_2 + b29 \cdot B_2 + c29 \cdot C_2 + d29 \cdot D_2\\
&a29 = c29 = d29 = \lambda_2;\ b29 = -\lambda_2\\
&a29 \cdot (A_2 - B_2 + C_2 + D_2) = 0
\end{aligned}
\tag{B27}
$$

BC10

$$
\begin{aligned}
&w_2'''(0) = \frac{P}{2D_f} \\
&w_2'''(0) = a210 \cdot A_2 + b210 \cdot B_2 + c210 \cdot C_2 + d210 \cdot D_2 \\
&a210 = b210 = c210 = 2\lambda_2^3; \quad d210 = -2\lambda_2^3 \\
&a210 \cdot \left(A_2 + B_2 + C_2 - D_2\right) = \frac{P}{2D_f}
\end{aligned}
\tag{B28}
$$

B2.4 Bilinear segments with softening (BL_s , 2 segments , $k_2<0$)

BC1 and BC2

$C_1=0$; $D_1=0$

BC3

$$
\begin{aligned}
&w_1(0) = w_2(a_2) \\
&w_1(0) = b13 \cdot B_1 \\
&w_2(a_2) = r23 + a23 \cdot A_2 + b23 \cdot B_2 + c23 \cdot C_2 + d23 \cdot D_2 \\
&b13 = 1; \; r23 = -\frac{q_2}{k_2}; \; a23 = e^{-\lambda_2 a_2}; \; b23 = e^{\lambda_2 a_2} \\
&c23 = \sin\left(\lambda_2 a_2\right); \; d23 = \cos\left(\lambda_2 a_2\right) \\
&a23 \cdot A_2 - b13 \cdot B_1 + b23 \cdot B_2 + c23 \cdot C_2 + d23 \cdot D_2 = -r23
\end{aligned}
\tag{B29}
$$

BC4

$$
\begin{aligned}
&w_1'(0) = w_2'(a_2) \\
&w_1'(0) = a14 \cdot A_1 + b14 \cdot B_1 \\
&w_2'(a_2) = a24 \cdot A_2 + b24 \cdot B_2 + c24 \cdot C_2 + d24 \cdot D_2 \\
&a14 = \lambda_1; b14 = -\lambda_1; \\
&a24 = -\lambda_2 \cdot e^{-\lambda_2 a_2}; \quad b24 = \lambda_2 \cdot e^{\lambda_2 a_2} \\
&c24 = \lambda_2 \cdot \cos\left(\lambda_2 a_2\right); \quad d24 = -\lambda_2 \cdot \sin\left(\lambda_2 a_2\right) \\
&a14 \cdot A_1 - a24 \cdot A_2 + b14 \cdot B_1 - b24 \cdot B_2 - c24 \cdot C_2 - d24 \cdot D_2 = 0
\end{aligned}
\tag{B30}
$$

BC5

$$
\begin{aligned}
&w_1''(0) = w_2''(a_2)\\
&w_1''(0) = a15 \cdot A_1\\
&w_2''(a_2) = a25 \cdot A_2 + b25 \cdot B_2 + c25 \cdot C_2 + d25 \cdot D_2\\
&a15 = -2\lambda_1^2; \qquad (B31)\\
&a25 = \lambda_2^2 e^{-\lambda_2 a_2};\ \ b25 = \lambda_2^2 e^{\lambda_2 a_2}\\
&c25 = -\lambda_2^2 \cdot \sin(\lambda_2 a_2);\quad d25 = -\lambda_2^2 \cdot \cos(\lambda_2 a_2)\\
&-a15 \cdot A_1 + a25 \cdot A_2 + b25 \cdot B_2 + c25 \cdot C_2 + d25 \cdot D_2 = 0
\end{aligned}
$$

BC6

$$
\begin{aligned}
&w_1'''(0) = w_2'''(a_2)\\
&w_1'''(0) = a16 \cdot A_1 + b16 \cdot B_1\\
&w_2'''(a_2) = a26 \cdot A_2 + b26 \cdot B_2 + c26 \cdot C_2 + d26 \cdot D_2\\
&a16 = b16 = 2\lambda_1^3 \qquad (B32)\\
&a26 = -\lambda_2^3 \cdot e^{-\lambda_2 a_2};\ \ b26 = \lambda_2^3 \cdot e^{\lambda_2 a_2}\\
&c26 = -\lambda_2^3 \cdot \cos(\lambda_2 a_2);\ d26 = +\lambda_2^3 \cdot \sin(\lambda_2 a_2)\\
&-a16 \cdot A_1 - b16 \cdot B_1 + a26 \cdot A_2 + b26 \cdot B_2 + c26 \cdot C_2 + d26 \cdot D_2 = 0
\end{aligned}
$$

BC7

$$
\left.\begin{aligned}
&w_1(0) = \delta_1\\
&w_1(0) = b17 \cdot B_1\\
&b17 = 1;
\end{aligned}\right\} \rightarrow B_1 = \delta_1 \qquad (B33)
$$

BC8

$$
\begin{aligned}
&w_2(0) = \alpha\\
&w_2(0) = r28 + a28 \cdot A_2 + b28 \cdot B_2 + d28 \cdot D_2\\
&r28 = -\frac{q_2}{k_2};\ \mathrm{a28} = b28 = d28 = 1 \qquad (B34)\\
&r28 + a28 \cdot A2 + b28 \cdot B_2 + d28 \cdot D_2 = \alpha
\end{aligned}
$$

BC9

$$
\begin{aligned}
&w_2'(0) = 0 \\
&w_2'(0) = a29 \cdot A_2 + b29 \cdot B_2 + c29 \cdot C_2 \\
&a29 = -\lambda_2;\ b29 = \lambda_2;\ c29 = \lambda_2 \\
&a29 \cdot A_2 + b29 \cdot B_2 + c29 \cdot C_2 = 0
\end{aligned}
\tag{B35}
$$

BC10

$$
\begin{aligned}
&w_2'''(0) = \frac{P}{2D_f} \\
&w_2'''(0) = a210 \cdot A_2 + b210 \cdot B_2 + c210 \cdot C_2 \\
&a210 = -\lambda_2^3;\ \ b210 = \lambda_2^3;\ \ c210 = -\lambda_2^3 \\
&a210 \cdot \left(A_2 + C_2 - B_2\right) = \frac{P}{2D_f}
\end{aligned}
\tag{B36}
$$

B2.5 Bilinear-perfectly-plastic segments (*BLPP*, 3 segments, $k_3=0$)

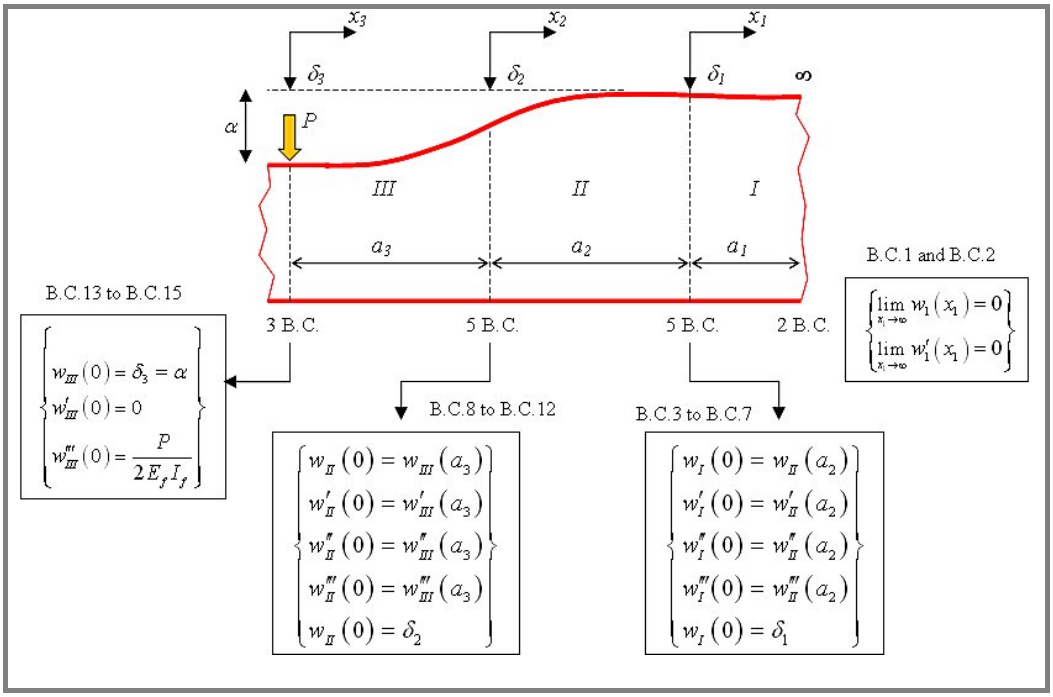

Figure B3. Boundary conditions applicable for three segments.

BC1 to BC7

Equal to either BL_h or BL_s model

BC8

$$w_2(0) = w_3(a_3)$$
$$w_2(0) = r28 + b28 \cdot B_2 + d28 \cdot D_2$$
$$w_3(a_3) = e38 \cdot (a_3)^4 + a38 \cdot (a_3)^3 \cdot A_3 + b38 \cdot (a_3)^2 \cdot B_3 + c38 \cdot a_3 \cdot C_3 + d38 \cdot D_3 = \delta_2$$
$$r28 = -\frac{q_2}{k_2};\ b28 = d28 = 1 \qquad \text{(B37)}$$
$$e38 = -\frac{q_3}{24 D_f};\ d38 = c38 = 1;\ a38 = 1/3;\ b38 = 1/2;$$
$$e38 \cdot (a_3)^4 + a38 \cdot (a_3)^3 \cdot A_3 + b38 \cdot (a_3)^2 \cdot B_3 + c38 \cdot a_3 \cdot C_3 + d38 \cdot D_3 = \delta_2$$

BC9

$$
\begin{aligned}
&w_2'(0) = w_3'(a_3)\\
&w_2'(0) = a29 \cdot A_2 + b29 \cdot B_2 + c29 \cdot C_2 + d29 \cdot D_2\\
&w_3'(a_3) = e39 \cdot (a_3)^3 + a39 \cdot (a_3)^2 \cdot A_3 + b39 \cdot a_3 \cdot B_3 + c39 \cdot C_3\\
&a29 = c29 = d29 = \lambda_2;\ b29 = -\lambda_2\\
&e39 = -\frac{q_3}{6D_f};\ b39 = c39 = a39 = 1\\
&a29 \cdot A_2 + b29 \cdot B_2 + c29 \cdot C_2 + d29 \cdot D_2 - e39 \cdot (a_3)^3 - a39 \cdot (a_3)^2 \cdot A_3 - b39 \cdot a_3 \cdot B_3 - c39 \cdot C_3 = 0
\end{aligned}
\tag{B38}
$$

BC10

$$
\begin{aligned}
&w_2''(0) = w_3''(a_3)\\
&w_2''(0) = a210 \cdot A_2 + c210 \cdot C_2\\
&w_3''(a_3) = e310 \cdot (a_3)^2 + a310 \cdot a_3 \cdot A_3 + b310 \cdot B_3\\
&a210 = -2\lambda_2^2;\ c210 = 2\lambda_2^2;\\
&e310 = -\frac{q_3}{2D_f};\ a310 = 2; b310 = 1;\\
&a210 \cdot A_2 + c210 \cdot C_2 - e310 \cdot (a_3)^2 - a310 \cdot a_3 \cdot A_3 - b310 \cdot B_3 = 0
\end{aligned}
\tag{B39}
$$

BC11

$$
\begin{aligned}
&w_2'''(0) = w_3'''(a_3)\\
&w_2'''(0) = a211 \cdot A_2 + b211 \cdot B_2 + c211 \cdot C_2 + d211 \cdot D_2\\
&w_3'''(a_3) = e311 \cdot a_3 + a311 \cdot A_3\\
&a211 = b211 = c211 = 2\lambda_2^3;\ d211 = -2\lambda_2^3;\\
&e311 = -\frac{q_3}{D_f};\ a311 = 2;\\
&a211 \cdot A_2 + b211 \cdot B_2 + c211 \cdot C_2 + d211 \cdot D_2 - e311 \cdot a_3 - a311 \cdot A_3 = 0
\end{aligned}
\tag{B40}
$$

BC12

$$
\begin{aligned}
&w_2(0) = \delta_2\\
&w_2(0) = r212 + b212 \cdot B_2 + d212 \cdot D_2\\
&r212 = -\frac{q_2}{k_2};\ b212 = d212 = 1\\
&r212 + b212 \cdot B_2 + d212 \cdot D_2 = \delta_2
\end{aligned}
\tag{B41}
$$

BC13

$$\begin{aligned} w_3(0) &= \alpha \\ w_3(0) &= D_3 = \alpha \end{aligned} \tag{B42}$$

BC14

$$\begin{aligned} w_3'(0) &= 0 \\ w_3'(0) &= C_3 = 0 \end{aligned} \tag{B43}$$

BC15

$$\left.\begin{aligned} w_3'''(0) &= \frac{P}{2D_f} \\ w_3'''(0) &= a315 \cdot A_3 \\ a315 &= 2 \end{aligned}\right| \rightarrow A_3 = \frac{P}{2 \cdot a315 \cdot D_f} \tag{B44}$$

B3. Systems of equations for the n^{th} *Segment-Wise* segments

B3.1 Pure-elastic segment (*E*, one segment, $q_1=0$)

Unknowns: $A_1, B_1, C_1, D_1, \alpha, P$

$$\begin{cases} \underline{BC1/2:}\ C_1 = D_1 = 0 \\ \underline{BC3:}\ b13 \cdot B_1 = \alpha \\ \underline{BC4:}\ a14 \cdot A_1 + b14 \cdot B_1 = 0 \\ \underline{BC5:}\ a15 \cdot A_1 + b15 \cdot B_1 = \dfrac{P}{2D_f} \end{cases} \rightarrow \left\{ \begin{array}{l} C_1 = D_1 = 0 \\ B_1 = \alpha \\ \lambda_1 (A_1 - B_1) = 0 \\ 2\lambda_1^3 (A_1 + B_1) = \dfrac{P}{2 \cdot D_f} \end{array} \right| \rightarrow A_1 = B_1 = \alpha \rightarrow 4\lambda_1^3 \alpha = \frac{P}{2 \cdot D_f} \quad \text{(B45)}$$

and

$$P = \left(8 \cdot D_f \cdot \lambda_1^3\right) \cdot \alpha \quad \text{(B46)}$$

B3.2 Elastic-perfectly-plastic segments (*EPP*, 2 segments, $k_2=0$)

Unknowns: $A_1, B_1, A_2, B_2, C_2, D_2, \alpha, P$

$$\begin{cases} \underline{BC3:}\ a23 \cdot A_2 - b13 \cdot B_1 + b23 \cdot B_2 + d23 \cdot D_2 = -r23 \\ \underline{BC4:}\ -a14 \cdot A_1 + a24 \cdot A_2 + b24 \cdot B_2 + c24 \cdot C_2 = b14 \cdot B_1 - r24 \\ \underline{BC5:}\ r25 - a15 \cdot A_1 + a25 \cdot A_2 + b25 \cdot B_2 = 0 \\ \underline{BC6:}\ -a16 \cdot A_1 + a26 \cdot A_2 = b16 \cdot B_1 - r26 \\ \underline{BC7:}\ B_1 = \delta_1 \\ \underline{BC8:}\ D_2 = \alpha \\ \underline{BC9:}\ C_2 = 0 \\ \underline{BC10:}\ A_2 = \dfrac{P}{2 \cdot a210 \cdot D_f} \end{cases} \quad \text{(B47)}$$

Comes,

$$\begin{cases} a23\cdot A_2 + b23\cdot B_2 + d23\cdot \alpha = b13\cdot \delta_1 - r23 \\ -a14\cdot A_1 + a24\cdot A_2 + b24\cdot B_2 + c24\cdot C_2 = b14\cdot B_1 - r24 \\ -a15\cdot A_1 + a25\cdot A_2 + b25\cdot B_2 = -r25 \\ -a16\cdot A_1 + a26\cdot A_2 = b16\cdot B_1 - r26 \\ A_2 = \dfrac{P}{2\cdot a210\cdot D_f} \end{cases} \tag{B48}$$

And finally,

$$\begin{bmatrix} 0 & a23 & b23 & d23 \\ -a14 & a24 & b24 & 0 \\ -a15 & a25 & b25 & 0 \\ -a16 & a26 & 0 & 0 \end{bmatrix} \cdot \begin{Bmatrix} A_1 \\ A_2 \\ B_2 \\ \alpha \end{Bmatrix} = \begin{Bmatrix} \delta_1 + \dfrac{q_2\cdot a_2^4}{24Df} \\ -\lambda_1\cdot\delta_1 + \dfrac{q_2 a_2^3}{6Df} \\ \dfrac{q_2}{2Df}\cdot a_2^2 \\ 2\lambda_1^3\cdot\delta_1 + \dfrac{q_2\cdot a_2}{Df} \end{Bmatrix} \tag{B49}$$

B3.3 Bilinear segments with hardening (BL_h , 2 segments , $k_2>0$)

Unknowns: $A_1, B_1, A_2, B_2, C_2, D_2, \alpha, P$

$$\begin{cases} \underline{BC3}: \ a23\cdot A_2 - b13\cdot B_1 + b23\cdot B_2 + c23\cdot C_2 + d23\cdot D_2 = -r23 \\ \underline{BC4}: \ a14\cdot A_1 - a24\cdot A_2 + b14\cdot B_1 - b24\cdot B_2 - c24\cdot C_2 - d24\cdot D_2 = 0 \\ \underline{BC5}: \ -a15\cdot A_1 + a25\cdot A_2 + b25\cdot B_2 + c25\cdot C_2 + d25\cdot D_2 = 0 \\ \underline{BC6}: \ -a16\cdot A_1 - b16\cdot B_1 + a26\cdot A_2 + b26\cdot B_2 + c26\cdot C_2 + d26\cdot D_2 = 0 \\ \underline{BC7}: \ B_1 = \delta_1 \\ \underline{BC8}: \ b28\cdot B_2 + d28\cdot D_2 - \alpha = -r28 \\ \underline{BC9}: \ a29\cdot A_2 + b29\cdot B_2 + c29\cdot C_2 + d29\cdot D_2 = 0 \\ \underline{BC10}: \ a210\cdot A_2 + b210\cdot B_2 + c210\cdot C_2 + d210\cdot D_2 = \dfrac{P}{2D_f} \end{cases} \tag{B50}$$

Comes,

$$\begin{cases} a23\cdot A_2 + b23\cdot B_2 + c23\cdot C_2 + d23\cdot D_2 = \delta_1 - r23 \quad \text{where } b13 = 1 \text{ and } B_1 = \delta_1 \\ a14\cdot A_1 - a24\cdot A_2 - b24\cdot B_2 - c24\cdot C_2 - d24\cdot D_2 = -b14\cdot \delta_1 \\ -a15\cdot A_1 + a25\cdot A_2 + b25\cdot B_2 + c25\cdot C_2 + d25\cdot D_2 = 0 \\ -a16\cdot A_1 + a26\cdot A_2 + b26\cdot B_2 + c26\cdot C_2 + d26\cdot D_2 = b16\cdot \delta_1 \\ B_2 + D_2 - \alpha = -r28 \quad \text{where } b28 = d28 = 1 \\ a29\cdot A_2 + b29\cdot B_2 + c29\cdot C_2 + d29\cdot D_2 = 0 \end{cases} \tag{B51}$$

$$P = 2D_f \cdot \left[a210\cdot A_2 + b210\cdot B_2 + c210\cdot C_2 + d210\cdot D_2\right]$$

And finally,

$$\begin{bmatrix} 0 & a23 & b23 & c23 & d23 \\ a14 & -a24 & -b24 & -c24 & -d24 \\ -a15 & a25 & b25 & c25 & d25 \\ -a16 & a26 & b26 & c26 & d26 \\ 0 & a29 & b29 & c29 & d29 \end{bmatrix} \cdot \begin{Bmatrix} A_1 \\ A_2 \\ B_2 \\ C_2 \\ D_2 \end{Bmatrix} = \begin{Bmatrix} \delta_1 + q_2/k_2 \\ -b14\cdot\delta_1 \\ 0 \\ b16\cdot\delta_1 \\ 0 \end{Bmatrix} \tag{B52}$$

$$P = 2D_f \cdot a210\cdot\left[A_2 + B_2 + C_2 - D_2\right]$$
$$\alpha = B_2 + D_2 - q_2/k_2$$

B3.4 Bilinear segments with softening (BL_s , 2segments , $k_2<0$)

Unknowns: $A_1, B_1, A_2, B_2, C_2, D_2, \alpha, P$

$$\begin{cases} \underline{BC3:}\ a23\cdot A_2 - b13\cdot B_1 + b23\cdot B_2 + c23\cdot C_2 + d23\cdot D_2 = -r23 \\ \underline{BC4:}\ a14\cdot A_1 - a24\cdot A_2 + b14\cdot B_1 - b24\cdot B_2 - c24\cdot C_2 - d24\cdot D_2 = 0 \\ \underline{BC5:}\ -a15\cdot A_1 + a25\cdot A_2 + b25\cdot B_2 + c25\cdot C_2 + d25\cdot D_2 = 0 \\ \underline{BC6:}\ -a16\cdot A_1 - b16\cdot B_1 + a26\cdot A_2 + b26\cdot B_2 + c26\cdot C_2 + d26\cdot D_2 = 0 \\ \underline{BC7:}\ B_1 = \delta_1 \\ \underline{BC8:}\ a28\cdot A_2 + b28\cdot B_2 + d28\cdot D_2 - \alpha = -r28 \\ \underline{BC9:}\ a29\cdot A_2 + b29\cdot B_2 + c29\cdot C_2 = 0 \\ \underline{BC10:}\ a210\cdot\left(A_2 + C_2 - B_2\right) = \dfrac{P}{2D_f} \end{cases} \tag{B53}$$

Comes,

$$\begin{cases} a23\cdot A_2 + b23\cdot B_2 + c23\cdot C_2 + d23\cdot D_2 = b13\cdot\delta_1 - r23 \\ a14\cdot A_1 - a24\cdot A_2 - b24\cdot B_2 - c24\cdot C_2 - d24\cdot D_2 = -b14\cdot\delta_1 \\ -a15\cdot A_1 + a25\cdot A_2 + b25\cdot B_2 + c25\cdot C_2 + d25\cdot D_2 = 0 \\ -a16\cdot A_1 + a26\cdot A_2 + b26\cdot B_2 + c26\cdot C_2 + d26\cdot D_2 = b16\cdot\delta_1 \\ a29\cdot A_2 + b29\cdot B_2 + c29\cdot C_2 = 0 \end{cases} \quad \text{(B54)}$$

And finally,

$$\begin{bmatrix} 0 & a_{23} & b_{23} & c_{23} & d_{23} \\ a_{14} & -a_{24} & -b_{24} & -c_{24} & -d_{24} \\ -a_{15} & a_{25} & b_{25} & c_{25} & d_{25} \\ -a_{16} & a_{26} & b_{26} & c_{26} & d_{26} \\ 0 & a_{29} & b_{29} & c_{29} & 0 \end{bmatrix} \cdot \begin{Bmatrix} A_1 \\ A_2 \\ B_2 \\ C_2 \\ D_2 \end{Bmatrix} = \begin{Bmatrix} b_{13}\cdot\delta_1 - r_{23} \\ -b_{14}\cdot\delta_1 \\ 0 \\ b_{16}\cdot\delta_1 \\ 0 \end{Bmatrix} \quad \text{(B55)}$$

$$\begin{aligned} &B_1 = \delta_1 \\ &a28\cdot A_2 + b28\cdot B_2 + d28\cdot D_2 + r28 = \alpha \\ &P = 2D_f\cdot a210\cdot\left(A_2 + C_2 - B_2\right) \end{aligned} \quad \text{(B56)}$$

B3.5 Bilinear-perfectly-plastic segments (*BLPP*, 3 segments, $k_3=0$)

Unknowns: $A_1, B_1, A_2, B_2, C_2, D_2, A_3, B_3, C_3, D_3, a_3, \alpha, P$

$$\begin{cases} \underline{BC3}: & a23\cdot A_2 - b13\cdot B_1 + b23\cdot B_2 + c23\cdot C_2 + d23\cdot D_2 = -r23 \\ \underline{BC4}: & a14\cdot A_1 - a24\cdot A_2 + b14\cdot B_1 - b24\cdot B_2 - c24\cdot C_2 - d24\cdot D_2 = 0 \\ \underline{BC5}: & -a15\cdot A_1 + a25\cdot A_2 + b25\cdot B_2 + c25\cdot C_2 + d25\cdot D_2 = 0 \\ \underline{BC6}: & -a16\cdot A_1 - b16\cdot B_1 + a26\cdot A_2 + b26\cdot B_2 + c26\cdot C_2 + d26\cdot D_2 = 0 \\ \underline{BC7}: & B_1 = \delta_1 \\ \underline{BC8}: & e38\cdot(a_3)^4 + a38\cdot(a_3)^3\cdot A_3 + b38\cdot(a_3)^2\cdot B_3 + c38\cdot a_3\cdot C_3 + d38\cdot D_3 = \delta_2 \\ \underline{BC9}: & a29\cdot A_2 + b29\cdot B_2 + c29\cdot C_2 + d29\cdot D_2 - e39\cdot(a_3)^3 - a39\cdot(a_3)^2\cdot A_3 - b39\cdot a_3\cdot B_3 - c39\cdot C_3 = 0 \\ \underline{BC10}: & a210\cdot A_2 + c210\cdot C_2 - e310\cdot(a_3)^2 - a310\cdot a_3\cdot A_3 - b310\cdot B_3 = 0 \\ \underline{BC11}: & a211\cdot A_2 + b211\cdot B_2 + c211\cdot C_2 + d211\cdot D_2 - e311\cdot a_3 - a311\cdot A_3 = 0 \\ \underline{BC12}: & r212 + b212\cdot B_2 + d212\cdot D_2 = \delta_2 \\ \underline{BC13}: & D_3 = \alpha \\ \underline{BC14}: & C_3 = 0 \\ \underline{BC15}: & A_3 = P/4D_f \end{cases}$$

(B57)

Problem solved in three steps:

Step 1:

Solve the linear sub system to find $A_1, B_1, A_2, B_2, C_2, D_2$

$$\begin{cases} a23\cdot A_2 + b23\cdot B_2 + c23\cdot C_2 + d23\cdot D_2 = b13\cdot \delta_1 - r23 \\ a14\cdot A_1 - a24\cdot A_2 - b24\cdot B_2 - c24\cdot C_2 - d24\cdot D_2 = -b14\cdot \delta_1 \\ -a15\cdot A_1 + a25\cdot A_2 + b25\cdot B_2 + c25\cdot C_2 + d25\cdot D_2 = 0 \\ -a16\cdot A_1 + a26\cdot A_2 + b26\cdot B_2 + c26\cdot C_2 + d26\cdot D_2 = b16\cdot \delta_1 \\ b212\cdot B_2 + d212\cdot D_2 = \delta_2 - r212 \end{cases} \quad \text{(B58)}$$

$$\begin{bmatrix} 0 & a23 & b23 & c23 & d23 \\ a14 & -a24 & -b24 & -c24 & -d24 \\ -a15 & a25 & b25 & c25 & d25 \\ -a16 & a26 & b26 & c26 & d26 \\ 0 & 0 & 1 & 0 & 1 \end{bmatrix} \cdot \begin{Bmatrix} A_1 \\ A_2 \\ B_2 \\ C_2 \\ D_2 \end{Bmatrix} = \begin{Bmatrix} \delta_1 + q_2/k_2 \\ -b14\cdot \delta_1 \\ 0 \\ b16\cdot \delta_1 \\ \delta_2 + q_2/k_2 \end{Bmatrix} \quad \text{(B59)}$$

Step 2:

The unknowns left are five: a_3, A_3, B_3, α with the fifth unknown P directly given by a fifth direct equation (BC15) and solved by mean of a non linear system of four equations:

$$\begin{cases} e38\cdot (a_3)^4 + a38\cdot (a_3)^3\cdot A_3 + b38\cdot (a_3)^2\cdot B_3 + d38\cdot \alpha = \delta_2 \\ e39\cdot (a_3)^3 + a39\cdot (a_3)^2\cdot A_3 + b39\cdot a_3\cdot B_3 = a29\cdot A_2 + b29\cdot B_2 + c29\cdot C_2 + d29\cdot D_2 \\ e310\cdot (a_3)^2 + a310\cdot a_3\cdot A_3 + b310\cdot B_3 = a210\cdot A_2 + c210\cdot C_2 \\ e311\cdot a_3 + a311\cdot A_3 = a211\cdot A_2 + b211\cdot B_2 + c211\cdot C_2 + d211\cdot D_2 \end{cases} \quad \text{(B60)}$$

$$A_3 = P/4D_f$$

Which, grouping all constants can be written in the easier form:

$$\left.\begin{cases} e38\cdot (a_3)^4 + 1/3\cdot (a_3)^3\cdot A_3 + 1/2\cdot (a_3)^2\cdot B_3 + \alpha = \delta_2 \\ e39\cdot (a_3)^3 + (a_3)^2\cdot A_3 + a_3\cdot B_3 = H39 \\ e310\cdot (a_3)^2 + 2\cdot a_3\cdot A_3 + B_3 = H310 \\ e311\cdot a_3 + 2\cdot A_3 = H311 \end{cases}\right| \rightarrow \begin{cases} H39 = a29\cdot A_2 + b29\cdot B_2 + c29\cdot C_2 + d29\cdot D_2 \\ H310 = a210\cdot A_2 + c210\cdot C_2 \\ H311 = a211\cdot A_2 + b211\cdot B_2 + c211\cdot C_2 + d211\cdot D_2 \end{cases}$$

$$A_3 = P/4D_f \quad \text{(B61)}$$

It is observed that a single 3rd order equation in the unknown a_3 can be extracted from the system. Solving this 3rd degree equation will linearise the system and find the remaining unknowns. Thus, considering the second and third equations

from the system of equations (B61) and expliciting in terms of A_3, the fourth equation from the same system we obtain:

$$\begin{cases} e39\cdot(a_3)^3+(a_3)^2\cdot A_3+a_3\cdot B_3=H39 \\ e310\cdot(a_3)^2+2\cdot a_3\cdot A_3+B_3=H310 \\ e311\cdot a_3+2\cdot A_3=H311\rightarrow A_3=-\dfrac{e311}{2}\cdot a_3+\dfrac{H311}{2} \end{cases} \quad \text{(B62)}$$

Replacing A_3 in the second expression from the system described by equations (B62) and expliciting it in terms of B_3, we have:

$$\begin{aligned} &e310\cdot(a_3)^2-e311\cdot(a_3)^2+H311\cdot a_3+B_3=H310\Leftrightarrow \\ &B3=(e311-e310)\cdot(a_3)^2-H311\cdot a_3+H310 \end{aligned} \quad \text{(B63)}$$

As observed before in Section B2.5 from this Appendix, $e310=\dfrac{1}{2}\cdot e311$,

simplifies equation (B63) into:

$$B_3=\frac{1}{2}\cdot e311\cdot(a_3)^2-H311\cdot a_3+H310 \quad \text{(B64)}$$

The complete system (B62) is now:

$$\begin{cases} e39\cdot(a_3)^3+(a_3)^2\cdot A_3+a_3\cdot B_3=H39 \\ A_3=-\dfrac{e311}{2}\cdot a_3+\dfrac{H311}{2} \\ B_3=\dfrac{1}{2}\cdot e311\cdot(a_3)^2-H311\cdot a_3+H310 \end{cases} \quad \text{(B65)}$$

Finally, replacing the two previously found expressions in terms of A_3 and B_3, into the first equation of system (B65) we achieve to a 3rd order equation in terms of the unknown a_3.

$$\begin{aligned} &e39\cdot(a_3)^3-\frac{1}{2}\cdot e311\cdot(a_3)^3+\frac{H311}{2}\cdot(a_3)^2-H311\cdot(a_3)^2+H310\cdot a_3+\frac{1}{2}\cdot e311\cdot(a_3)^3=H39 \\ &e39\cdot(a_3)^3+\frac{H311}{2}\cdot(a_3)^2-H311\cdot(a_3)^2+H310\cdot a_3=H39 \\ &e39\cdot(a_3)^3-\frac{1}{2}\cdot H311\cdot(a_3)^2+H310\cdot a_3-H39=0 \end{aligned} \quad \text{(B66)}$$

Step 3:

Once a_3 is found from the previous last equation, A_3, B_3, α and P can be found by solving the following straight forward equations:

$$\begin{cases} A_3 = -\dfrac{e311}{2} \cdot a_3 + \dfrac{H311}{2} \\ B_3 = \dfrac{1}{2} \cdot e311 \cdot (a_3)^2 - H311 \cdot a_3 + H310 \\ \alpha = \delta_2 - e38 \cdot (a_3)^4 - 1/3 \cdot (a_3)^3 \cdot A_3 - 1/2 \cdot (a_3)^2 \cdot B_3 \\ P = A_3 \cdot 4D_f \end{cases} \tag{B67}$$

APPENDIX C

MATLAB® scripts

C1. Modelling of an indented fully-backed beam sandwich

C1.1 Definition of the sandwich material properties and segment wise parameters

C1.2 Linear and bilinear load-deflection curves and face sheet bending failure load prediction

C1.3 Elastic-perfectly-plastic load-deflection curve and face sheet bending failure load prediction

C1.4 Bilinear-perfectly-plastic load-deflection curve

C1.5 Comparison of critical load predictions at face bending skin failure

C2. Defining the compression foam behaviour

C2.1 Elastic Perfectly Plastic function (MATLAB® *M-file EPPmodel.m*)

C2.2 Bilinear function (MATLAB® *M-file EEmodel.m*)

C2.3 Bilinear Perfectly Plastic function ((MATLAB® *M-file EEPPmodel.m*)

This appendix contains a collection of the principal MATLAB scripts implemented for modelling the indentation curve of fully-backed sandwich beams using the segment-wise model described in chapter II. Scripts for solving the closed form analytical solutions derived for the case of foams exhibiting compression behaviours of the type elastic, elastic-perfectly-plastic, bilinear and bilinear-perfectly-plastic are here transcript using the XPS core and PBT face sheet sandwich as case study. Analytical solutions to derive the critical load at which flexural failure of the sandwich skin occurs are as well transcript for the case of an EPP and BL foam compression behaviour.

C1. Modelling of an indented fully-backed beam sandwich

C1.1 Definition of the sandwich material properties and segment-wise parameters

```
%% BEAM INDENTATION ANALYSIS
% Sandwich I8 - Thermotec: Core XPS 40Kg/m3 (28mm) + SkinTec PBT (0.8mm)
% THREE SEGMENTS - COMPARISON BETWEEN EPP ANALYTICAL MODEL; EE ANALYTICAL MODEL,
EEPP ANALYTICAL MODEL and EXPERIMENTAL DATA
% SW1 [0;0.3787] ; SW2 ]0.3787;4.5393]
%% VARIABLE DEFINITION
clc; close all; clear all
sp=0.36;                    % [MPa]
Ec=11.62;                   % [MPa]
ep=sp/Ec;                   % [mm/mm]
b=29.74;                    % [mm]
tf=0.8;                     % [mm]
tc=28;                      % [mm]
If=(b*tf^3)/12;             % [mm^4]
Ef=15800;                   % [MPa]
Df=Ef*If;                   % [N*mm^2]
% Fitting of k1, k2, q2
k1=16.243;                  % [MPa]
q1=0;                       % [N/mm]
k2=1.0555;                  % [MPa]
q2=6.1281;                  % [N/mm]
q3=sp*b;                    % [N/mm]
delta1=0.3787;              % [mm]
delta2=4.5393;              % [mm]
lam1=(k1/(4*Df))^0.25;      % [mm^-4]
lam2=(k2/(4*Df))^0.25;      % [mm^-4]
sf=434;                     % [MPa]


data=[lam1;lam2;q2;q3;k1;k2;Df;delta1;delta2];
```

C1.2 Linear and bilinear load-deflection curves and face sheet bending failure load prediction

```
%% BILINEAR (BL or EE) ANALYTICAL MODEL
%--- Load-deflection curve for the first elastic segment ---%
We1=0:0.01:delta1;
Pel=8*Df*(lam1^3)*We1;
```

```
%--- Load-deflection curve for the second elastic segment ---%
EEdata=[lam1;lam2;q2;k2;Df;delta1];
size=320;
for x=1:1:size
    a2=x/10-0.1;
    [disp, force, A1]=EEmodel(EEdata,a2);
    alfa2(x)=disp;
    aa(x)=a2;
    P(x)=force;
end
%% -- Load Pf at skin bending failure acc. our developed expression for BL -- %
for x=1:1:size
    a2=x/10-0.1;
    [disp, force, A1]=EEmodel(EEdata,a2);
    f1=k1*delta1;
    f2=k2*delta2+q2;
    F=a2*(f1+f2)/2;
    xf=(a2/3)*((f1+2*f2)/(f1+f2));
    Pf(x)=(sf*b*tf^2)/(3*a2)-((4*Df*lam1^2*A1)/a2)-2*F*((xf/a2)-1);
end
figure(6)
axes1 = axes('LineWidth',2.5,'FontWeight','bold','FontSize',14);
xlim([0 30])
ylim([0 2e3])
box('on');grid('on');hold('all');
plot(aa,P,'-.b',aa,Pf,'r','LineWidth',2);
legend('\bf\fontsize{14}eqs.(3.22-3.24)','\bf\fontsize{14}eqs.(3.35)',-1)
xlabel('Half length (a2) of plastic zone [mm]')
ylabel('Load P[N]')
set(legend,'Location','SouthEast');
%title('Critical load Pf at top skin bending failure')
%
SS=abs(P-Pf);
i=find(SS==min(SS));
Pfailure=min(P(i),Pf(i));
```

C1.3 Elastic-perfectly-plastic load-deflection curve and face sheet bending failure load prediction

```
%% VARIABLE DEFINITION (S.I)
...
lam1=(k/(4*Df))^0.25;      % [mm^-4]
q2=sp*b;                   % [N/mm]
delta1=sp*tc/Ec;           % [mm]
sf=434;                    % [MPa]
...
%%
%%
EPPdata=[lam1;q2;Df;delta1];
size=400;
for x=1:1:size
    a2=x/10-0.1;
    [A1, disp, force]=EPPmodel(EPPdata,a2);
    alfa2(x)=disp;
    P(x)=force;
    Pf(x)=(sf*b*tf^2)/(3*a2)+(q2*a2)-(4*Df*lam1^2*A1)/a2;
    aa(x)=a2;
end
%% -- Load Pf at skin bending failure acc. our developed expression for EPP case
-- %
figure(6)
axes1 = axes('LineWidth',2.5,'FontWeight','bold','FontSize',14);
xlim([0 80])
ylim([0 2e3])
```

```
box('on');grid('on');hold('all');
% plot(aa,Pf,'k');
plot(aa,P,'k',aa,Pf,'r');
xlabel('Half length (a2) of plastic zone [mm]')
ylabel('Load P[N]')
title('Critical load Pf at top skin bending failure')
%
SS=abs(P-Pf);
i=find(SS==min(SS));
Pfailure=min(P(i),Pf(i))
```

C1.4 Bilinear-perfectly-plastic load-deflection curve

```
%% EEPP ANALYTICAL MODEL
%--- Load-deflection curve for the first elastic segment ---%
We1=0:0.01:delta1;
Pel=8*Df*(lam1^3)*We1;
figure(1)
box('on');grid('on');hold('all');
plot(We1,Pel,'b','MarkerSize',3,'LineWidth',2);
legend('\bf\fontsize{14}1st elastic segment for EPP & EE',-1)
xlabel('Mid-span displacement [mm]');
ylabel('Load [N]');
set(legend,'Location','SouthEast');
grid on;

%--- 2nd elastic segment and 3rd plastic plateau ---%
for x=1:1:320
    a2=x/10-0.1;
    [disp, force]=EEmodel(data,a2);
    alfa2(x)=disp;
    P2(x)=force;
    if alfa2(x)>delta2, break, end
end
a2u=a2;
figure(2)
box('on');grid('on');hold('all');
plot(alfa2,P2,'b','MarkerSize',3,'LineWidth',2);
legend('\bf\fontsize{14}2nd elastic segment for EE & EEPP',-1)
xlabel('Mid-span displacement [mm]');
ylabel('Load [N]');
set(legend,'Location','SouthEast');
grid on;

for x=1:110
    a2=a2u-x/10;
    a(x)=a2;
    [disp, force]=EEPPmodel(data,a2);
    alfa3(x)=disp;
    P3(x)=force;
    if alfa3(x)>30, break, end
end
figure(3)
box('on');grid('on');hold('all');
plot(fliplr(alfa3),fliplr(P3),'b','MarkerSize',3,'LineWidth',2);
legend('\bf\fontsize{14} "Plateau" segment for EEPP',-1)
xlabel('Mid-span displacement [mm]');
ylabel('Load [N]');
set(legend,'Location','SouthEast');
grid on;

%--- total curve BLPP ---%
d=[We1 alfa2 alfa3]
Pw=[Pel P2 P3]
figure(4)
```

```
box('on');grid('on');hold('all');
plot(d,Pw,'b','MarkerSize',3,'LineWidth',2);
legend('\bf\fontsize{14}EEPP model',-1)
xlabel('Mid-span displacement [mm]');
ylabel('Load [N]');
set(legend,'Location','SouthEast');
grid on;
```

C1.5 Comparison of critical load predictions at face bending skin failure

The script refers to the material described in the first row of table 2.3 (section 2.3; chapter II).

```
%% PREDICTED INDENTATION FAILURE LOADS FOR SANDWICH BEAMS WITH R130 PVC
FOAM CORES AND GRP SKINS
% Sandwich 1 - Core R130 PVC (25mm) + Skin GRP (GF/Polyester resin) (3.0
mm)
clc;close all;clear
%% VARIABLE DEFINITION (S.I)
sp=3.06;                        % [MPa]
Ec=197;                         % [MPa]
ep=sp/Ec;                       % [mm/mm]
b=40;                           % [mm]
tf=3.0;                         % [mm]
tc=25.0;                        % [mm]
If=(b*tf^3)/12;                 % [mm^4]
Ef=18000;                       % [MPa]
Df=Ef*If;                       % [N*mm^2]
k=(Ec*b)/tc;                    % [MPa]
lam=(k/(4*Df))^0.25;            % [mm^4]
L=300;                          % [mm]
sf=250;                         % [MPa]

% ------------------------------------------------------%
%% SODEN'S ANALYTICAL MODEL (RPP)
%Foundation modulus for an attached foundation:
K=(4/(3^0.5))*(2/3)^0.25;
%Foundation load per unit length (N/mm):
q=sp*b;
for x=(1:1:150);
    y=x/10-0.1;
    y1(x)=y;
    Psoden(x)=K*b*(tf^(3/4))*(sp^(3/4))*(Ef^0.25)*(y1(x)^0.25);
end
figure(1)
plot(y1,Psoden,'k','linewidth',2)
xlabel('Deflection,[mm]')
ylabel('Load,[N]')
title('Sodens Indentation Model')
%
%%Failure top skin load (Pf) at local bending, according Soden
%for an elastic beam firmly attached to a rigid plastic (crushable)
foundation
Pf_soden=(4/3)*b*tf*((sf*sp)^(1/2))

% ------------------------------------------------------%
%% ZENKERT'S MODEL (EPP)
```

```
% Zenkert - Elastic Winkler foundation
%--- Load-deflection curve on elastic zone ---%
% Wec-deflection for onset core crushing(We(xe=0)=alfa)
Wec=sp*tc/Ec;
% We(xe) - elastic deflection
We=0:0.01:Wec;
P=8*Df*(lam^3)*We;
Pc=(2*sp*b)/lam

% Zenkert - Perfectly plastic foundation
%--- Load-deflection curve on plastic zone ---%
% a - half length of plastic zone (0=<a<=L/2)
size=100;
for x=1:1:size
    a=x-1;
    aa(x)=a;
    M(:,:,x)=[((a^2)/(4*Df)),a,-lam;a/(2*Df),1,2*(lam^2);(2*Df)^-1,0,-
2*(lam^3)];
    Q(:,x)=[(sp*b*a^3)/(6*Df)-
lam*ep*tc,(sp*b*a^2)/(2*Df),(sp*b*a)/Df+2*(lam^3)*ep*tc]';
    X(:,x)=(M(:,:,x)^-1)*Q(:,x);
    alfa(x)=ep*tc+(sp*b*a^4)/(24*Df)-(X(1,x)*a^3)/(12*Df)-(X(2,x)*a^2)/2;
    Pf(x)=(sf*b*tf^2)/(3*a)+(sp*b*a)-(4*Df*lam^2*X(3,x)/a);
end
%
% -- Load-Deflection Curve (elastic field + plastic field) -- %
alfatot=[We,alfa];
alfatot=alfatot(1:100);
Pzen=[P,X(1,:)];
Pzen=Pzen(1:100);
figure(5)
plot(alfatot,Pzen,'ok','LineWidth',1)
xlabel('Deflection [mm]')
ylabel('Load P[N]')
title('Zenkert Indentation Model')

% ------------------------------------------------------%
% -- Load Pf at skin bending failure acc. our developed expression
(applied to the EPP case) -- %
figure(6)
plot(aa,X(1,:),'k',aa,Pf,'r');
xlabel('Half length (a) of plastic zone [mm]')
ylabel('Load P[N]')
title('Critical load Pf at top skin bending failure')
%
SS=abs(X(1,:)-Pf);
i=find(SS==min(SS));
Pfailure=min(X(1,i),Pf(i))
%

% ------------------------------------------------------%
%% BENDING TOP SKIN FAILURE LOAD acc. SHUAEIB
for x=1:1:650
    a=x/10-0.1;
    a1=(L/2)-a;
    z=lam*a;
    zz(x)=z;
    z1=lam*a1;

    % 1st relation curve for P vs a
```

```
    N1(x)=2*(z^3)*(sinh(z1)^2+sin(z1)^2)+3*(sinh(z1)*cosh(z1)-
sin(z1)*cos(z1))*(2*(z^2)-1)-6*z;
    D1(x)=(z^2)*(sinh(z1)^2+sin(z1)^2)+2*z*(sinh(z1)*cosh(z1)-
sin(z1)*cos(z1))-(cosh(z1)^2+cos(z1)^2);
    Q1(x)=(3*lam)/(2*sp*b);

    P1(x)=N1(x)/(D1(x)*Q1(x));

    % 2nd relation curve for P vs a
    Mf=sf*b*tf^2/6;

    A(x)=(sinh(z1)*cosh(z1)-sin(z1)*cos(z1))/(sinh(z1)^2+sin(z1)^2);
    B(x)=(sinh(z1)^2-sin(z1)^2)/(sinh(z1)^2+sin(z1)^2);
    N2(x)=((2*Mf*lam^2)/(sp*b))+z^2+2*z*A(x)+B(x);
    D2(x)=z+A(x);
    Q2(x)=lam/(sp*b);

    P2(x)=N2(x)/(D2(x)*Q2(x));
end

figure(1)
axes1 = axes('LineWidth',2.5,'FontWeight','bold','FontSize',14);
xlim([0 9])
ylim([0 1e4])
box('on');grid('on');hold('all');
plot(zz,P1,'k',zz,P2,'r','MarkerSize',3,'LineWidth',2);
xlabel('Half length (a) of plastic zone [mm]')
ylabel('Load P[N]')
title('Critical load Pf at top skin bending failure')

SH=abs(P2-P1);
i=find(SH==min(SH));
Pf_Shuaeib=min(P2(i),P1(i))

%% COMPARISON BETWEEN TOP SKIN CRITICAL LOAD (Pf) TO BENDING acc THE
MODEL USED
% Percentage diference for our developed expression and Shuaeib´s method
D1=((Pf_Shuaeib-Pfailure)/Pf_Shuaeib)*100
%
% Percentage diference for Soden´s and Shuaeib´s method
D2=((Pf_Shuaeib-Pf_soden)/Pf_Shuaeib)*100
%
% Percentage diference for Soden´s and ours method
D3=((Pf_soden-Pfailure)/Pf_soden)*100
%%
```

C2. Defining the compression foam behaviour

C2.1 Elastic Perfectly Plastic function (*EPPmodel.m*)

```
function [A1,disp, force]=EPPmodel(EPPdata,a2)

% EPPdata=[lam1;q2;Df;delta1];
lam1=EPPdata(1,1);
q2=EPPdata(2,1);
Df=EPPdata(3,1);
delta1=EPPdata(4,1);
```

```
a23=(a2^3)/3;b23=(a2^2)/2;d23=1;

a14=lam1;a24=(a2^2);b24=a2;

a15=-(2*lam1^2);a25=2*a2;b25=1;

a16=(2*lam1^3);a26=2;

B=[delta1+((q2*a2^4)/(24*Df));...
    ((q2*a2^3)/(6*Df))-lam1*delta1;...
    ((q2*a2^2)/(2*Df));...
    2*(lam1^3)*delta1+((q2*a2)/Df)];

A=[0 a23 b23 d23;...
    -a14 +a24 +b24 0;...
    -a15 a25 b25 0;...
    -a16 a26 0 0];

X=A\B;
disp=X(4,1);
A2=X(2,1);
A1=X(1,1);
a210=2;
force=2*Df*a210*A2;
```

C2.2 Bilinear function (*EEmodel.m*)

```
function [disp, force]=EEmodel(data,a2)

% data=[lam1;lam2;q2;q3;k1;k2;Df;delta1;delta2];

lam1=data(1,1);
lam2=data(2,1);
q2=data(3,1);
k2=data(6,1);
Df=data(7,1);
delta1=data(8,1);

a23=(exp(-lam2*a2))*sin(lam2*a2);
b23=(exp(-lam2*a2))*cos(lam2*a2);
c23=(exp(lam2*a2))*sin(lam2*a2);
d23=(exp(lam2*a2))*cos(lam2*a2);

a14=lam1;
%b14=-lam1;
a24=(-lam2*exp(-lam2*a2))*(sin(lam2*a2)-cos(lam2*a2));
b24=(-lam2*exp(-lam2*a2))*(sin(lam2*a2)+cos(lam2*a2));
c24=(lam2*exp(lam2*a2))*(sin(lam2*a2)+cos(lam2*a2));
d24=(-lam2*exp(lam2*a2))*(sin(lam2*a2)-cos(lam2*a2));

a15=-(2*lam1^2);
a25=(-2*lam2^2)*(exp(-lam2*a2))*cos(lam2*a2);
b25=(2*lam2^2)*(exp(-lam2*a2))*sin(lam2*a2);
c25=(2*lam2^2)*(exp(lam2*a2))*cos(lam2*a2);
d25=(-2*lam2^2)*(exp(lam2*a2))*sin(lam2*a2);

a16=(2*lam1^3);
%b16=(2*lam1^3);
a26=(2*lam2^3)*(exp(-lam2*a2))*(sin(lam2*a2)+cos(lam2*a2));
b26=(-2*lam2^3)*(exp(-lam2*a2))*(sin(lam2*a2)-cos(lam2*a2));
c26=(-2*lam2^3)*(exp(lam2*a2))*(sin(lam2*a2)-cos(lam2*a2));
d26=(-2*lam2^3)*(exp(lam2*a2))*(sin(lam2*a2)+cos(lam2*a2));

a29=lam2; b29=-a29;c29=a29;d29=a29;
```

```
b14=-lam1; b16=2*lam1^3;

B=[delta1+(q2/k2); -b14*delta1; 0; b16*delta1; q2/k2; 0];
A=[0 a23 b23 c23 d23 0; a14 -a24 -b24 -c24 -d24 0;...
    -a15 a25 b25 c25 d25 0; -a16 a26 b26 c26 d26 0;...
    0 0 1 0 1 -1; 0 a29 b29 c29 d29 0];

X=A\B;
A2=X(2,1);
B2=X(3,1);
C2=X(4,1);
D2=X(5,1);
a210=2*lam2^3;
force=2*Df*a210*(A2+B2+C2-D2);

disp=X(6,1);
```

C2.3 Bilinear Perfectly Plastic function (*EEPPmodel.m*)

```
function [disp, force]=EEPPmodel(data,a2)

lam1=data(1,1);
lam2=data(2,1);
q2=data(3,1);
q3=data(4,1);
k1=data(5,1);
k2=data(6,1);
Df=data(7,1);
delta1=data(8,1);
delta2=data(9,1);

b13=1;
a23=(exp(-lam2*a2))*sin(lam2*a2);
b23=(exp(-lam2*a2))*cos(lam2*a2);
c23=(exp(lam2*a2))*sin(lam2*a2);
d23=(exp(lam2*a2))*cos(lam2*a2);
r23=-q2/k2;

a14=lam1;
b14=-lam1;
a24=(-lam2*exp(-lam2*a2))*(sin(lam2*a2)-cos(lam2*a2));
b24=(-lam2*exp(-lam2*a2))*(sin(lam2*a2)+cos(lam2*a2));
c24=(lam2*exp(lam2*a2))*(sin(lam2*a2)+cos(lam2*a2));
d24=(-lam2*exp(lam2*a2))*(sin(lam2*a2)-cos(lam2*a2));

a15=-(2*lam1^2);
a25=(-2*lam2^2)*(exp(-lam2*a2))*cos(lam2*a2);
b25=(2*lam2^2)*(exp(-lam2*a2))*sin(lam2*a2);
c25=(2*lam2^2)*(exp(lam2*a2))*cos(lam2*a2);
d25=(-2*lam2^2)*(exp(lam2*a2))*sin(lam2*a2);

a16=(2*lam1^3);
b16=a16;
a26=(2*lam2^3)*(exp(-lam2*a2))*(sin(lam2*a2)+cos(lam2*a2));
b26=(-2*lam2^3)*(exp(-lam2*a2))*(sin(lam2*a2)-cos(lam2*a2));
c26=(-2*lam2^3)*(exp(lam2*a2))*(sin(lam2*a2)-cos(lam2*a2));
d26=(-2*lam2^3)*(exp(lam2*a2))*(sin(lam2*a2)+cos(lam2*a2));

b17=1;

b28=1;
d28=b28;
r28=-q2/k2;

a38=1/3;
b38=1/2;
```

```
c38=1;
d38=c38;
e38=-q3/(24*Df);

a29=lam2;
b29=-a29;
c29=a29;
d29=a29;
e39=-q3/(6*Df);

a210=-2*lam2^2;
c210=-a210;
a310=2;
b310=1;
e310=-q3/(2*Df);

a211=2*lam2^3;
b211=a211;
c211=a211;
d211=-a211;
a311=2;
e311=-q3/Df;

b212=1;
d212=b212;
r212=-q2/k2;

d313=1;
c314=1;
a315=2;

% STEP 1 - Linear subsystem to find the unknowns A1;A2;B2;C2;D2
B=[delta1+(q2/k2); -b14*delta1; 0; b16*delta1; delta2+(q2/k2)];
A=[0 a23 b23 c23 d23; a14 -a24 -b24 -c24 -d24;...
    -a15 a25 b25 c25 d25; -a16 a26 b26 c26 d26;...
    0 0 1 0 1];
X=A\B;
A1=X(1,1);
A2=X(2,1);
B2=X(3,1);
C2=X(4,1);
D2=X(5,1);

% STEP 2 - Solving the 3rd degree equation to find a3
H39=a29*A2+b29*B2+c29*C2+d29*D2;
H310=a210*A2+c210*C2;
H311=a211*A2+b211*B2+c211*C2+d211*D2;

x=solve('e39*x^3-(0.5*H311)*x^2+H310*x-H39','x');
% eval(a3);
% eval(imag(a3))
eval(x);

%a3=eval(x);
a3=eval(real(x(2,1)));

% STEP 3 - Solution of the unknowns A3, B3, alfa and P
A3=(-e311/2)*a3+H311/2;
B3=0.5*e311*a3^2-H311*a3+H310;
disp=delta2-e38*a3^4-(1/3)*a3^3*A3-0.5*a3^2*B3;
force=A3*4*Df;
```

APPENDIX D

ABAQUS® scripts

D1. Indentation on a fully-backed beam sandwich

D1.1 Main file: Sandwich indentation input file (*2Dindentation.inp*)

D1.2 Include file: Face sheet material definition (*material.inp*)

D1.3 Include file: Flat support analytical surface definition (*supportAS.inp*)

D1.4 Include file: Cylindrical indenter analytical surface definition (*indenterAS_D25.inp*)

D1.5 Include file: Contact definitions (*contact-02.inp*)

D2. TPB test on a beam sandwich employing a non-linear foam core

D2.1 Main file: Sandwich beam model (*model_03.inp*)

D2.2 Include file: Cylindrical indenter and supports *(supports_impactorTPB-L230.inp)*

D2.3 Include file: Contact definitions *(contact-01.inp)*

D3. Mullins effect on a PA Zotek® foam slab model

D3.1 Main file: Polyamide foam input file (*PA_uniaxial_compress.inp*)

D3.2 Include file: Mullins test data - 1x3 cycles (*Mullins_calibrate_testdata.inp*)

D3.3 Include file: Contact definitions (*contact.inp*)

D3.4 Include file: Flat indenter and flat support (*impactor.inp*)

This appendix is a collection of the main scripts regarding the ABAQUS numerical simulations. These simulations in particular have been carried out in order to model the behaviour of the sandwich beams employing thermoplastic low density foam cores, as designed in this work (see chapter III and IV). For these sandwich materials the thermoplastic foam exhibits a highly non-linear compressive behaviour which has been associated with a hyperelastic behaviour. The purpose of the numerical analysis carried out was then to investigate the suitability of using the HYPERFOAM formulation from the ABAQUS library of materials to simulate the behaviour of the Zotek Polyamide foam used as a core material. Three behaviours in particular have been considered by the numerical simulation: indentation of a fully-backed sandwich beam, three-point bending of a sandwich beam and repeated compression of a pure foam slab.

In order to minimise the length of the scripts while maintaining the essential information of their structure, those repetitive lengthy parts related to nodes and elements definitions have been partially omitted. Foam experimental fitting data corresponding to flatwise, shear and Mullins characterization is as well partially omitted.

D1. Indentation on a fully-backed beam sandwich

D1.1 Main file: Sandwich indentation input file (*2Dindentation.inp*)

```
*HEADING
CONCENTRATED LOAD APPLIED ON A SANDWICH SUPPORTED ON A FLAT PANEL - INDENTATION TEST - 2D
MODEL
**
*** ---------- Sandwich Model ---------- ***
** Skins: TEPEX PA Twill Balanced 0°/90° ; Thickness=2mm per skin -
** Core: PA foam 50Kg/m3 (Zotefoams) ; thickness 10mm ----------
** Plane strain elements - CPE4 - Skin and core ----------
**
*** ---------- 2D MODEL DATA ---------- ***
*PREPRINT,MODEL=YES
*NODE
       5,          0.0          ,  0.0               ,  0.0
      62,          0.0          ,  13.796            ,  0.0
 ........

      601050,   56.25        ,  11.176953      ,  0.0
      601051,   53.75        ,  11.176953      ,  0.0
      601052,   52.5         ,  11.176953      ,   0.0

*ELEMENT,TYPE=CPE4,ELSET=CORE
    1849,     1965,     1967,     1961,     1962
    1850,     1967,     1956,     1957,     1961
........

*ELEMENT,TYPE=CPE4,ELSET=LOWER_SKIN
    4212,     2253,    600120,    600109,     2252
    4231,    600148,    600149,    600145,    600144
........

*ELEMENT,TYPE=CPE4,ELSET=UPPER_SKIN
```

```
     5791,    600532,    600529,    600496,    600497
     5790,    600531,    600528,    600529,    600532
......
**
*** NODE UPPER_SKIN PARA OUTPUT
*NSET, NSET=NOUT_UPPER_SKIN
62,
**
*** NODE FORCED CONTACT
*NSET, NSET=NBEAM2
3419,3783,3844,600702
**
*NSET, NSET=N-SYMM
       5,       62,       63,     1556,     1943,     1944,     1945,     1946,
    1947,     2108,     2109,     2110,    600001,    600002,    600401,    600402,
   600403,    600864
**
*** ELEMENTO UPPER_SKIN PARA OUTPUT
*ELSET, ELSET=EOUT_UPPER_SKIN
     5697,
**
*** TOP_ELEMENT_UPPERSKIN
*ELSET, ELSET=TOP_ELEMENT_UPPERSKIN
     5689,     5691,     5697,     5699,     5708,     5710,     5716,     5718,
     5724,     5726,     5732,     5734,     5740,     5742,     5748,     5750,
     5756,     5758,     5764,     5766,     5768,     5772,     5776,     5780,
     5784,     5788,     5792,     5796,     5803,     5807,     5811,     5815,
     5819,     5823,     5827,     5831,     5835,     5839,     5840,     5844,
     5848,     5852,     5859,     5863,     5867,     5871,     5875,     5879,
     5883,     5887,     5891,     5895,     5899,     5903,     5904,     5908,
     5912,     5916,     5923,     5927,     5931,     5935,     5939,     5943,
     5947,
**
*ELSET, ELSET=BOTTOM_ELEMENT_LOWERSKIN
     4127,     4129,     4133,     4135,     4139,     4141,     4145,     4147,
     4151,     4153,     4157,     4159,     4163,     4165,     4169,     4171,
     4199,     4202,     4204,     4214,     4217,     4220,     4223,     4226,
     4229,     4232,     4235,     4238,     4241,     4244,     4247,     4250,
     4253,     4256,     4259,     4262,     4265,     4268,     4271,     4274,
     4277,     4280,     4283,     4286,     4289,     4292,     4295,     4298,
     4301,     4304,     4307,     4310,     4313,     4316,     4319,     4322,
     4325,     4328,     4334,     4337,     4340,     4343,     4346,     4349,
     4352,
**
*** ---------------------- SECTION DEFINITIONS ------------------------------- ***
****
*ORIENTATION, NAME=LOCAL
1.0, 0.0, 0.0, 0.0, 1.0, 0.0
1,0
** SANDWICH LAYERS - Solid sections for both core and skins
*SOLID SECTION,ELSET=UPPER_SKIN,MATERIAL=TEPEX_PA102_Twill,ORIENTATION=LOCAL
30.0,
*SOLID SECTION,ELSET=CORE,MATERIAL=ZOTEK_PA_FOAM,ORIENTATION=LOCAL
30.0,
*SOLID SECTION,ELSET=LOWER_SKIN,MATERIAL=TEPEX_PA102_Twill,ORIENTATION=LOCAL
30.0,
**
***  ---------------------- CORE MATERIAL ------------------------------------- ***
*MATERIAL, NAME=ZOTEK_PA_FOAM
*DENSITY
 5.0e-11,
** To change the strain energy function order, change the N parameter.
*HYPERFOAM,N=2,TEST DATA INPUT
*UNIAXIAL TEST DATA
** nominal stress(MPa), nominal strain(dimensionless) - COMPRESSION TEST DATA - PRIMITIVE CURVE **
-0.0004, -0.0006
-0.0005, -0.0009
-0.0006, -0.0015
-0.0007, -0.0018
-0.0008, -0.0022
-0.0010, -0.0025
-0.0013, -0.0028
-0.0016, -0.0031
-0.0019, -0.0034
........
*SIMPLE SHEAR TEST DATA
```

```
** nominal shear stress(MPa), nominal shear strain(dimensionless) **
0.0015,    0.0000
0.0015,    0.0002
0.0016,    0.0003
0.0016,    0.0004
0.0016,    0.0006
0.0016,    0.0008
0.0017,    0.0009
0.0018,    0.0011
0.0019,    0.0012
0.0020,    0.0014
0.0020,    0.0015
0.0021,    0.0017
.......
*** ------------------------------- INCLUDE FILES ---------------------------- ***
*INCLUDE, INPUT=database/material.inp
*INCLUDE, INPUT=database/SupportAS.inp
*INCLUDE, INPUT=database/indenterAS_D25.inp
*INCLUDE, INPUT=database/contact-02.inp
**
*** ---------------------- STEP AND BOUNDARIES DATA -------------------------- ***
**
*** ------------------------------- STEP 1 ----------------------------------- ***
*STEP,NLGEOM,INC=1000
Step 1: Contact step
*STATIC,DIRECT
0.5,1.0,,
*BOUNDARY,TYPE=DISPLACEMENT,OP=NEW
N-SYMM,XSYMM
** RB_FLATSUPPORT
RB_FLATSUPPORT,1,2
RB_FLATSUPPORT,6,6
** RB_INDENTER
RB_INDENTER,1,1
RB_INDENTER,6,6
RB_INDENTER,2,2
** FIXED BEAM FORCED CONTACT
NBEAM2, 1,2
*END STEP
**
*** ------------------------------- STEP 2 ----------------------------------- ***
*STEP,NLGEOM,INC=1000
Step 2: loading step
*STATIC,DIRECT
0.02,1.0,,0.02
*BOUNDARY,TYPE=DISPLACEMENT,OP=NEW
N-SYMM,XSYMM
** RB_FLATSUPPORT
RB_FLATSUPPORT,1,2
RB_FLATSUPPORT,6,6
** RB_INDENTER
RB_INDENTER,1,1
RB_INDENTER,6,6
RB_INDENTER,2,2,-6.0
**
*** --------------------- OUTPUT DATA STEP 2 ------------------- ***
**
*OUTPUT,FIELD,FREQUENCY=5
*NODE OUTPUT
U,
*ELEMENT OUTPUT
S,
E,
LE,
NE,
**
**
*OUTPUT,HISTORY
*ELEMENT OUTPUT,ELSET=EOUT_UPPER_SKIN
S22
E22,
LE22,
NE22,
*NODE OUTPUT,NSET=RB_INDENTER
RF,
U,
```

```
*ENERGY OUTPUT,ELSET=EOUT_UPPER_SKIN
ALLDMD
*END STEP
**
```

D1.2 Include file: Face sheet material definition (*material.inp*)

```
**
** --- Skins Material Definition -- **
** --- TEPEX dynalite 102-RG600(x)/47% - PA6 Balanced Twill 0°/90° (BondLaminates);
** --- Thickness=2mm per skin ---
**
** ---------- SKIN ---------- **
*MATERIAL, NAME=TEPEX_PA102_Twill
*DENSITY
  1.8e-9,
*ELASTIC, TYPE=ENGINEERING CONSTANTS
  20210.0, 4000.0, 20210.0,   0.35,     0.17,     0.17,   1709.0,  3100.0
** <E1>     <E2>    <E3>     <niu12>   <niu13>   <niu23>   <G12>   <G13>
   1709.0
** <G23>
**
**
```

D1.3 Include file: Flat support analytical surface definition (*supportAS.inp*)

```
**
*** FLAT SUPPORT USED ON THE INDENTATION SANDWICH TEST ***
*** MODELED AS 2D LINE - ANALYTICAL RIGID SURFACE ***
**
*SURFACE, TYPE=SEGMENTS,NAME=FLATSUPPORT
START,  0.0, 0.0
LINE, 80.0, 0.0
**
*NODE
699993, 37.5, 0.0, 0.0
*NSET, NSET=RB_FLATSUPPORT
699993,
**
*RIGID BODY, ANALYTICAL SURFACE=FLATSUPPORT, REF NODE=699993
**
```

D1.4 Include file: Cylindrical indenter analytical surface definition (*indenterAS_D25.inp*)

```
**
*** CYLINDRICAL INDENTOR USED ON THE INDENTATION SANDWICH TEST ***
*** MODELED AS 2D CIRCUNFERENCE - D25 mm  - ANALYTICAL RIGID SURFACE ***
**
*SURFACE, TYPE=SEGMENTS,NAME=INDENTER,FILLET RADIUS=0.001
START, 12.5, 27.316
CIRCL,  0.0, 14.816, 0.0, 27.316
**
*NODE
699991,  0.0         ,  27.316          ,  0.0
*NSET, NSET=RB_INDENTER
699991,
**
*RIGID BODY, ANALYTICAL SURFACE=INDENTER, REF NODE=699991
**
```

D1.5 Include file: Contact definitions (*contact-02.inp*)

```
**
*** CONTACT SURFACE DATA - 2D INDENTATION SANDWICH TEST ***
**
*SURFACE,NAME=S_TOP_ELEMENT_UPPERSKIN,TRIM=YES
TOP_ELEMENT_UPPERSKIN,
**
*SURFACE,NAME=S_BOTTOM_ELEMENT_LOWERSKIN,TRIM=YES
BOTTOM_ELEMENT_LOWERSKIN
**
**
*SURFACE INTERACTION, NAME=STEEL_PLASTIC
*SURFACE BEHAVIOR,AUGMENTED LAGRANGE
**
** FRICTION COEFFICIENT FOR STEEL-POLYAMIDE AROUND 0.2
*FRICTION
0.2
**
**
*CONTACT PAIR,INTERACTION=STEEL_PLASTIC
S_TOP_ELEMENT_UPPERSKIN,INDENTER
**
*CONTACT PAIR,INTERACTION=STEEL_PLASTIC,ADJUST=0.0
S_BOTTOM_ELEMENT_LOWERSKIN,FLATSUPPORT
**
```

D2. TPB test on a beam sandwich employing a non-linear foam core

Only the files related to the SPAM 230 mm are reproduced.

D2.1 Main file: Sandwich beam model (*model_03.inp*)

```
*HEADING
FLEXURAL PROPERTIES OF THE SANDWICH - 3 POINT BENDING TEST
**
*** ---------- Sandwich Model ---------- ***
** Skins: TEPEX PA Unidirectional 0° ; Thickness=4x0.5mm per skin -
** Core: PA foam 50Kg/m3 (Zotefoams) ; thickness 30mm ----------
** SPAM L=230 mm ----------
**
*** ---------- MODEL DATA ---------- ***
*PREPRINT,MODEL=YES
*NODE
        5,   0.0          ,  0.0          ,  0.0
       10,  0.0          ,  25.4         ,  0.0
       59,  244.0        ,  25.4         ,  0.0
.....
......
*ELEMENT,TYPE=S4,ELSET=LOWER_SKIN
     9326,    602489,    602492,    602494,    602488
     9327,    602488,    602494,    602495,    602487
.....
.....
*ELEMENT,TYPE=C3D8R,ELSET=CORE
    45159,    637097,    637103,    637099,    637093,    603620,    603614,    603613,
   603618
    45160,    637105,    637108,    637107,    637106,    603546,    603687,    603692,
   603547
.......
.......
*** ELEMENTO UPPER_SKIN PARA OUTPUT
*ELSET, ELSET=EOUT_UPPER_SKIN
8490
```

```
**
*** NODE FACE 4 PARA OUTPUT
*NSET, NSET=NOUT_UPPER_SKIN
601424
*** NODE FACE 6 PARA OUTPUT
*NSET, NSET=N_LVDT
602439
**
**
*** BEAM NODES TO FORCE CONTACT ON STEP1
*NSET, NSET=NBEAM1
624727,624671,635059,635003
*NSET, NSET=NBEAM2
626260,626316,636592,636648
.....
.....
*** ---------- SECTION DEFINITIONS ---------- ***
****
** SANDWICH LAYERS - 2Shell sections (2 plies) + 1solid section(1 core)
**
*SHELL SECTION, ELSET=UPPER_SKIN, COMPOSITE, LAYUP=UPPER_SKIN
2.0, 3, TEPEX_PA102_UD, 0.0, lamina_2
**
*SOLID SECTION,ELSET=CORE,MATERIAL=ZOTEK_PA_FOAM
**
*SHELL SECTION, ELSET=LOWER_SKIN, COMPOSITE, LAYUP=LOWER_SKIN
2.0, 3, TEPEX_PA102_UD, 0.0, lamina_1
......
.....
*** ---------- INCLUDE FILES ---------- ***
*INCLUDE, INPUT=database3/material.inp
*INCLUDE, INPUT=database3/Supports_impactorTPB-L230.inp
*INCLUDE, INPUT=database3/contact-01.inp
**
*** ---------- STEP AND BOUNDARIES DATA ---------- ***
**RESTART,WRITE,FREQUENCY=5
*** ---------- STEP 1 ---------- ***
*STEP,NLGEOM
Step 1: contact step
*STATIC,DIRECT
0.5,1.0,,
*BOUNDARY,TYPE=DISPLACEMENT,OP=NEW
** RB_SUPPORT
RB_LEFT_SUPPORT,1,6
RB_RIGHT_SUPPORT,1,6
** RB_IMPACTOR
RB_IMPACTOR,1,6
** FIXED BEAM FORCED CONTACT
NBEAM1,1,3
NBEAM2,1,3
*END STEP
*** ---------- STEP 2 ---------- ***
*STEP,NLGEOM,INC=1000
Step 2: loading step
*STATIC,DIRECT
0.02,1.0,,0.02
*BOUNDARY,TYPE=DISPLACEMENT,OP=NEW
** RB_SUPPORT
RB_LEFT_SUPPORT,1,6
RB_RIGHT_SUPPORT,1,6
** RB_IMPACTOR
RB_IMPACTOR,1,2
RB_IMPACTOR,4,6
RB_IMPACTOR,3,3,-5.0
.....
*** ---------- OUTPUT DATA STEP 2 ---------- ***
**
*OUTPUT,FIELD,FREQUENCY=5
*NODE OUTPUT
U,
*ELEMENT OUTPUT
S, E, LE, NE,
**
*OUTPUT,HISTORY
*ELEMENT OUTPUT,ELSET=EOUT_UPPER_SKIN
S33, E33, LE33, NE33,
```

```
*NODE OUTPUT,NSET=RB_IMPACTOR
RF, U
*NODE OUTPUT,NSET=N_LVDT
U,
*END STEP
```

D2.2 Include file: Cylindrical indenter and supports (*supports_impactorTPB-L230.inp*)

```
**
** CILYNDRICAL IMPACTOR (d=10mm) AND SUPPORTS (d=25mm) **
** SPAN DISTANCE BETWEEN SUPPPORTS L=230 mm **
**
*NODE
     5000,  123.71010071663,  -12.3         ,  40.498463103929
     5041,  123.71010071663,  37.7          ,  40.498463103929
     5446,  12.235238063782,  -12.3         ,  -1.025927171386
     5510,  12.235238063782,  37.7          ,  -1.025927171386
....
....
*ELEMENT,TYPE=R3D4,ELSET=IMPACTOR
     7373,    600090,    600079,    600080,    600089
     7372,    600088,    600090,    600089,    600087
     7371,    600089,    600080,    600023,    600022
....
.....
*ELEMENT,TYPE=R3D4,ELSET=LEFT_SUPPORT
     7532,    600258,    600260,    600255,    600256
     7533,    600260,    600251,    600252,    600255
     7534,    600244,    600245,    600261,    600259
.....
.....
*ELEMENT,TYPE=R3D4,ELSET=RIGHT_SUPPORT
     7636,    600380,    600382,    600377,    600378
     7637,    600382,    600373,    600374,    600377
     7638,    600366,    600367,    600383,    600381
.....
.....
**
*RIGID BODY, REF NODE =     599991, ELSET = IMPACTOR
*RIGID BODY, REF NODE =     599992, ELSET = LEFT_SUPPORT
*RIGID BODY, REF NODE =     599994, ELSET = RIGHT_SUPPORT
**
*NSET, NSET=RB_IMPACTOR
   599991,
*NSET, NSET=RB_LEFT_SUPPORT
   599992,
*NSET, NSET=RB_RIGHT_SUPPORT
   599994,
**
```

D2.3 Include file: Contact definitions (*contact-01.inp*)

```
*** - CONTACT SURFACE DATA - ***
**
*SURFACE, TYPE=ELEMENT, NAME=S_UPPER_SKIN,TRIM=YES
UPPER_SKIN,SPOS
*SURFACE, TYPE=ELEMENT, NAME=S_LOWER_SKIN,TRIM=YES
LOWER_SKIN,SPOS
**
*SURFACE, NAME=RB_LEFT_SUPPORT, TYPE=ELEMENT
LEFT_SUPPORT,SPOS
*SURFACE, NAME=RB_RIGHT_SUPPORT, TYPE=ELEMENT
RIGHT_SUPPORT,SPOS
*SURFACE, NAME=RB_IMPACTOR, TYPE=ELEMENT
IMPACTOR,SPOS
**
*SURFACE INTERACTION, NAME=SUPPORT_STEEL_PLASTIC
**SURFACE BEHAVIOR,AUGMENTED LAGRANGE
```

```
*SURFACE BEHAVIOR,PENALTY=LINEAR,NO SEPARATION
** FRICTION COEFFICIENT FOR STEEL-POLYTHENE AROUND 0.2
*FRICTION
0.2
**
**
*SURFACE INTERACTION, NAME=IMPACTOR_STEEL_PLASTIC
*SURFACE BEHAVIOR,PENALTY=LINEAR
*FRICTION
0.2
**
*CONTACT PAIR,INTERACTION=IMPACTOR_STEEL_PLASTIC,TYPE=SURFACE TO SURFACE,ADJUST=0.0
S_UPPER_SKIN,RB_IMPACTOR
**
*CONTACT PAIR,INTERACTION=SUPPORT_STEEL_PLASTIC,TYPE=SURFACE TO SURFACE,ADJUST=0.0
S_LOWER_SKIN,RB_LEFT_SUPPORT
**
*CONTACT PAIR,INTERACTION=SUPPORT_STEEL_PLASTIC,TYPE=SURFACE TO SURFACE,ADJUST=0.0
S_LOWER_SKIN,RB_RIGHT_SUPPORT
**
```

D3. Mullins effect on a PA Zotek® foam slab model

D3.1 Main file: Polyamide foam input file (*PA_uniaxial_compress.inp*)

```
*HEADING
 HYPERFOAM TEST - UNIAXIAL COMPRESSION WITH MULLINS EFFECT - C3D8R - N=2
**
** with rigid bodies - flat indenter and flat support **
** with files Include "impactor.inp; contact.inp and Mullins_calibrate_testdata.inp "**
**
** --- Core:
** --- PA foam 50Kg/m3 (Zotefoams);
** --- Thickness 30mm ----
** --- 3 x1 strain cycles - Applied loads 110, 170, 390 N
**
*** ----------------------- MODEL DATA ------------------------ ***
*PREPRINT,MODEL=YES
*NODE,NSET=NCUBE
       8,  2.0033333333333,  0.0          ,  27.710666666667
       9,  4.0066666666667,  0.0          ,  27.710666666667
......
** FLAT INDENTER SURFACE NODES
*NSET, NSET=N_FACE4
     233,     235,     237,     239,     241,     243,     245,     247,
     249,     251,     253,     255,     257,     259,     261,     263,
     294,     295,     311,     327,     343,     359,     375,     391,
     407,     423,     439,     455,     471,     487,     503,     519,
.......
** FLAT SUPPORT SURFACE NODES
*NSET, NSET=N_FACE6
     232,     234,     236,     238,     240,     242,     244,     246,
     248,     250,     252,     254,     256,     258,     260,     262,
     264,     267,     297,     313,     329,     345,     361,     377,
......
** LOAD APPLICATION SURFACE ELEMENTS
*ELSET, ELSET=EL_FACE4
     240,     255,     270,     285,     300,     315,     330,     345,
     360,     375,     390,     405,     420,     435,     450,     465,
     480,     495,     510,     525,     540,     555,     570,     585,
     600,     615,     630,     645,     660,     675,     690,     705,
.......
** FLAT SUPPORT SURFACE ELEMENTS
*ELSET, ELSET=EL_FACE6
     226,     241,     256,     271,     286,     301,     316,     331,
     346,     361,     376,     391,     406,     421,     436,     451,
     466,     481,     496,     511,     526,     541,     556,     571,
     586,     601,     616,     631,     646,     661,     676,     691,
     706,     721,     736,     751,     766,     781,     796,     811,
......
```

```
*ELEMENT,TYPE=C3D8R,ELSET=CUBE
      226,      232,      204,        8,      234,      264,      265,      266,
      267
      227,      204,      205,        9,        8,      265,      268,      269,
      266
      228,      205,      206,       10,        9,      268,      270,      271,
.......
*** OUTPUT ELEMENT FACE 4
*ELSET, ELSET=EOUT_FACE4
270
**
*** OUTPUT NODE FACE 4
*NSET, NSET=NOUT_FACE4
237
**
*SOLID SECTION,ELSET=CUBE,MATERIAL=FOAM
**
** ---------------------------- MATERIAL DATA ---------------------- **
*MATERIAL, NAME=FOAM
*DENSITY
 5.0e-11,
** To change the strain energy function order, change the N parameter.
*HYPERFOAM,MODULI=LONG TERM,N=2,TEST DATA INPUT
*UNIAXIAL TEST DATA
** nominal stress(MPa), nominal strain(dimensionless) - COMPRESSION TEST DATA - PRIMITIVE CURVE **
-0.000026, -0.000011
-0.000051, -0.000021
-0.000820, -0.000286
-0.001412, -0.000546
......
*MULLINS EFFECT,TEST DATA INPUT
*INCLUDE, INPUT=database/Mullins_calibrate_testdata.inp
**
*** -------------------- INCLUDE FILES ---------------------- ***
*INCLUDE, INPUT=database/impactor.inp
*INCLUDE, INPUT=database/contact.inp
**
*** -------------------- STEP AND BOUNDARIES DATA ---------- ***
**RESTART,WRITE,FREQUENCY=5
**
*** -------------------------- STEP 1 ---------------------- ***
*STEP,NLGEOM,INC=20
Step 1: Uniaxial Compression to 16% strain (110 N)
*STATIC,DIRECT
.05, ,.05,.05
*BOUNDARY,TYPE=DISPLACEMENT,OP=NEW
** RB_SUPPORT
RB_SUPPORT,1,6
** RB_IMPACTOR
RB_IMPACTOR,2,6
RB_IMPACTOR,1,1,-4.7843
**
........
*END STEP
**
*** ---------------------------- STEP 2 ---------------------- ***
**
*STEP,NLGEOM,INC=20
Step 2: 1st strain unloading
*STATIC,DIRECT
.05, ,.05,.05
*BOUNDARY,TYPE=DISPLACEMENT,OP=NEW
** RB_SUPPORT
RB_SUPPORT,1,6
** RB_IMPACTOR
RB_IMPACTOR,2,6
RB_IMPACTOR,1,1,0.0
**
.......
*END STEP

*** ---------------------------- STEP 3 ---------------------- ***
**
*STEP,NLGEOM,INC=20
Step 3: Uniaxial Compression to 41% strain (170 N)
*STATIC,DIRECT
```

```
.05, ,.05,.05
*BOUNDARY,TYPE=DISPLACEMENT,OP=NEW
** RB_SUPPORT
RB_SUPPORT,1,6
** RB_IMPACTOR
RB_IMPACTOR,2,6
RB_IMPACTOR,1,1,-12.28429
**
.......
*END STEP

*** ---------------------------- STEP 4 ---------------------- ***
**
*STEP,NLGEOM,INC=20
Step 4: 2nd strain unloading
*STATIC,DIRECT
.05, ,.05,.05
*BOUNDARY,TYPE=DISPLACEMENT,OP=NEW
** RB_SUPPORT
RB_SUPPORT,1,6
** RB_IMPACTOR
RB_IMPACTOR,2,6
RB_IMPACTOR,1,1,0.0
**
.........
*END STEP

*** ---------------------------- STEP 5 ---------------------- ***
**
*STEP,NLGEOM,INC=20
Step 5: Uniaxial Compression to 66% strain (390 N)
*STATIC,DIRECT
.05, ,.05,.05
*BOUNDARY,TYPE=DISPLACEMENT,OP=NEW
** RB_SUPPORT
RB_SUPPORT,1,6
** RB_IMPACTOR
RB_IMPACTOR,2,6
RB_IMPACTOR,1,1,-19.78429
**
.......
*END STEP

*** ---------------------------- STEP 6 ---------------------- ***
**
*STEP,NLGEOM,INC=20
Step 6: 3rd strain unloading
*STATIC,DIRECT
.05, ,.05,.05
*BOUNDARY,TYPE=DISPLACEMENT,OP=NEW
** RB_SUPPORT
RB_SUPPORT,1,6
** RB_IMPACTOR
RB_IMPACTOR,2,6
RB_IMPACTOR,1,1,0.0
**
......
*END STEP
```

D3.2 Include File: Mullins test data - 1x3 cycles (*Mullins_calibrate_testdata.inp*)

```
** ---------------------------------------------------------------------------
** ---- Mullins Calibration - Test data - Core Material ------------
** ---------------------------------------------------------------------------
** --- Core:
** --- PA foam 50Kg/m3 (Zotefoams);
** --- Thickness 30mm ------
** --- 3 x 1 strain cycles - Applied loads to 110, 170, 390 N
**
** -- Stabilized cycles (last for each strain level) ---
**
```

```
** -- 1st Strain Level – Load to 110 N  -------
**
*UNIAXIAL TEST DATA
** nominal Stress(MPa), nominal Strain (dimensionless)
-0.000026, -0.000011
-0.000051, -0.000021
-0.000820, -0.000286
-0.001412, -0.000546
-0.002125, -0.000822
....
**
** -- 2nd Strain Level – Load to 170 N -------
**   ,
*UNIAXIAL TEST DATA
** nominal stress(MPa), nominal Strain (dimensionless)
-0.000458, -0.018115
-0.000975, -0.018393
-0.001484, -0.018670
-0.002030, -0.018948
.....
**
** -- 3rd Strain Level – Load to 390 N -------
**
*UNIAXIAL TEST DATA
** nominal stress(MPa), nominal Strain (dimensionless)
-0.000001, -0.083267
-0.000240, -0.083545
-0.000468, -0.083822
-0.000693, -0.084100
-0.000926, -0.084379
-0.001173, -0.084656
.....
```

D3.3 Include file: Contact definitions (*contact.inp*)

```
*** - CONTACT SURFACE DATA - ***
**
*SURFACE, TYPE=ELEMENT, NAME=S_FACE4,TRIM=YES
EL_FACE4
*SURFACE, TYPE=ELEMENT, NAME=S_FACE6,TRIM=YES
EL_FACE6
**
*SURFACE, NAME=RB_SUPPORT, TYPE=ELEMENT
FLAT_SUPPORT,SPOS
*SURFACE, NAME=RB_IMPACTOR, TYPE=ELEMENT
FLAT_IMPACTOR,SPOS
**
**
*SURFACE INTERACTION, NAME=METAL_FOAM
*FRICTION
0.20
**
**
**SURFACE BEHAVIOR,AUGMENTED LAGRANGE
**
**
*CONTACT PAIR,INTERACTION=METAL_FOAM,TYPE=SURFACE TO SURFACE,ADJUST=0.0
S_FACE4,RB_IMPACTOR
**
*CONTACT PAIR,INTERACTION=METAL_FOAM,TYPE=SURFACE TO SURFACE, ADJUST=0.0
S_FACE6,RB_SUPPORT
**
```

D3.4 Include file: Flat indenter and flat support (*impactor.inp*)

```
*** - FLAT INDENTER AND LOWER SUPPORT PLATE - ***
**
*NODE
    99991,  0.0          ,  31.91         ,  32.345
```

```
    99992,  0.0          ,  -3.09         ,  32.345
    99993,  0.0          ,  31.91         ,  -2.655
    99994,  0.0          ,  -3.09         ,  -2.655
    99995,  30.05         ,  31.91         ,  32.345
    99996,  30.05         ,  -3.09         ,  32.345
    99997,  30.05         ,  31.91         ,  -2.655
    99998,  30.05         ,  -3.09         ,  -2.655
    99999,  30.05         ,  14.41         ,  14.845
    88888,  0.0          ,  14.41         ,  14.845
**
*NSET,NSET=RB_IMPACTOR
99999
*NSET,NSET=RB_SUPPORT
88888
**RIGID ELEMENTS R3D4 TO DEFINE THE SQUARE PLATES
*ELEMENT,TYPE=R3D4,ELSET=FLAT_IMPACTOR
   500002,    99995,    99997,    99998,    99996
*ELEMENT,TYPE=R3D4,ELSET=FLAT_SUPPORT
   500001,    99991,    99992,    99994,    99993
*RIGID BODY,REF NODE=RB_IMPACTOR,ELSET=FLAT_IMPACTOR
*RIGID BODY,REF NODE=RB_SUPPORT,ELSET=FLAT_SUPPORT
**
```

PUBLICATIONS

Amorim J, Pitarresi G. *Investigation on the behaviour of fully thermoplastic composite sandwich beams under concentrated loads*. ETDCM09, Experimental Techniques and Design in Composite Materials Conference, September 2009, Vicenza, Italy.

Amorim J, Pitarresi G. *Investigation on the indentation behaviour of sandwich beams using crushable and hyperelastic foam cores*. In: Proceedings of ICEM14 Conference. Poitiers (France), July 2010. DOI:10.1051/epjconf/20100624002.

Pitarresi G, **Amorim J**, Arena A. *Analisi del comportamento ad indentazione in travi sandwich in composito con anima in schiuma polimerica*. In: Proceedings of XXXIX AIAS Conference. Maratea, September 2010. AIAS 2010 – 124.

Pitarresi G, **Amorim J**. *Indentation of sandwich beams with foam cores exhibiting non-linear compressive behaviour*. J Sandw Struct Mater. (submitted)

BIBLIOGRAPHIC REFERENCES

[1] Allen HG. Analysis and design of structural sandwich panels. London: Pergamon Press; 1969.

[2] Plantema FJ. Sandwich construction. New York: Wiley; 1966.

[3] Stamm K, Witte H. Sandwichkonstruktionen. Wien: Springer; 1974.

[4] Zenkert D. An introduction to sandwich construction. London: Chameleon Press Ltd; 1995.

[5] Vinson JR. The behaviour of sandwich structures of isotropic and composite materials. Technomic Publ, Lancaster PA (1999).

[6] Pitarresi G. Strutture sandwich – cenni sul comportamento meccanico di strutture sandwich in materiale isotropo e composito, Università degli studi di Palermo, dipartimento di Meccanica; Gennaio 2007.

[7] DIAB Sandwich Handbook (2003), Sandwich Concept, available at www.diabgroup.com, last access on February 2008.

[8] Gough GS, Elam CF, de Bruyne ND. The stabilization of a thin sheet by a continuous supporting medium. J Roy Aero Soc 1940;44:12-43.

[9] Williams D, Leggett DMA, Hopkins HG. Flat sandwich panels under compressive end loads. A.R.C., R&M 1987, 1941.

[10] Vinson JR. Sandwich structures. Appl Mech Rev 2001;54(3):201-214.

[11] Marguerre K. The optimum buckling load of a flexibly supported plate composed of two sheets joined by a light weight filler, when under longitudinal compression. D.V.L. (ZWB UM 1360/2), October 1944; 11 p. 5 figs.

[12] Hoff NJ. Bending and buckling of rectangular sandwich plates. N.A.C.A. Technical Note 2225, November 1950.

[13] Flügge W. Determination of optimum dimension of sandwich panels. La Recherche Aeronautique 1949; 7.

[14] Eringen AC. Bending and buckling of rectangular sandwich plates. Proceedings of the first U.S. National Congress of Applied Mechanics, ASME, New York, 1952, pp. 381-390.

[15] March HW. Behaviour of a rectangular sandwich panel under uniform lateral load and compressive edge load. Forest Products Laboratory Report 1834, September 1952.

[16] Ericksen WS. Supplement to effects of shear deformation in the core of a flat rectangular sandwich panel. Forest Products Laboratory Report 1583-C, March 1956.

[17] March HW. Effects of shear deformation in the core of a flat rectangular sandwich panel: 1, buckling under compressive end load: 2, Deflection under uniform transverse load. Forest Products Laboratory Report 1583, August 1955.

[18] Raville ME. Deflection and stresses in a uniformly loaded simply supported, rectangular sandwich plate. Forest Products Laboratory Report 1847, 1955.

[19] Anon. Materials, properties and design criteria part II, sandwich construction for aircraft. *Military Handbook 23* (ANC-23), Department of the Air Force Research and Development Command; Department of the Navy, Bureau of Aeronautics; and the Department of Commerce Civil Aeronautics Administration, 2nd Edition, 1955.

[20] Reissner E. The effect of transverse shear deformation on the bending of elastic plates. J Appl Mech (*Transactions of the ASME*) 1945; 12:A69-A77.

[21] Libove C, Batdorf SB. A general small – deflection theory for flat sandwich plates. *NACA TN 1526*, 1948, also in *NACA* report 899.

[22] Mindlin RD. The influence of rotary inertia and shear on flexural motions of isotropic, elastic plates. J Appl Mech (*Transactions of the ASME)* 1951; 18:31-38.

[23] Vinson JR, Shore S. Bibliography on methods of structural optimization for flat sandwich panels. Naval Air Engineering Center Report, NAEC-ASC-1082, April 15, 1965.

[24] Vinson JR, Shore S. Methods of structural optimization for flat sandwich panels. Naval Air Engineering Center Report, NAEC-ASC-1083, April 15, 1965.

[25] Vinson JR, Shore S. Design procedures for the structural optimization for flat sandwich panels. Naval Air Engineering Center Report, NAEC-ASC-1084, April 15, 1965.

[26] Vinson JR, Shore S. Structural optimization of corrugated core and web core sandwich panels subjected to uniaxial compression. Naval Air Engineering Center Report, NAEC-ASC-1109, May 1967.

[27] Vinson JR, Shore S. Structural optimization of flat corrugated core sandwich panels under in-plane shear loads and combined uniaxial compression and in-plane shear loads. Naval Air Engineering Center Report, NAEC-ASC-1110, July 1967.

[28] McCoy TT, Vinson JR, Shore S. A method for weight optimization of flat truss core sandwich panel under lateral loads. Naval Air Engineering Center Report, NAEC-ASC-1111, July 1967.

[29] Hoff NJ. Monocoque, sandwich and composite aerospace structures. Technomic Publ, Lancaster PA (1986).

[30] Ha KH. Finite element and sandwich construction: A critical review. In *Sandwich Constructions I – Proceedings of the first International Conference on Sandwich Construction*. Editors, Olsson KA and Reichard RP, EMAS Publications, United Kingdom, 1989; 69-84.

[31] Bert CW. Part I, Shock and vibration digest. 1991;23:3-14; Part II, Shock and vibration digest. 1991;23:19-21.

[32] Noor AK, Burton WS, Bert CW. Computational models for sandwich panels and shells. Appl Mech Rev 1996;49(3):155-199.

[33] Fairbairn W. An account of the construction of the Britannia and Conway Tubular Bridges. John Weale *et al*., London, 1849.

[34] EconCore, Economic Core and Panel Technologies, available at www.econcore.com, last access on December 2010.

[35] Zenkert D, Shipsha A, Persson K. Static indentation and unloading response of sandwich beams. Compos Part B 2004;35:511-522.

[36] ABAQUS Version 6.9 documentation collection, ©Dassault Systèmes, 2009.

[37] Li B, Gu YD, English R, Rothwell G, Ren XJ. Characterisation of nonlinear material parameters of foams based on indentation tests. J Mater Design 2008; doi:10.1016/j.matdes.2008.09.040.

[38] Steeves CA, Fleck NA. Collapse mechanisms of sandwich beams with composite faces and a foam core, loaded in three-point bending part I: analytical models and minimum weight design. Int J Mech Sci 2004;46(4):561-583.

[39] Steeves CA, Fleck NA. Collapse mechanisms of sandwich beams with composite faces and a foam core, loaded in three-point bending part II: experimental investigation and numerical modelling. Int J Mech Sci 2004;46(4):585-608.

[40] Tagarielli VL, Fleck NA, Deshpande VS. Collapse of clamped and simply supported composite sandwich beams in three-point bending. Compos Part B 2004;35:523-534.

[41] Gibson LJ, Ashby MF. Cellular solids - Structure and Properties. Pergamon Press, Oxford, 1988.

[42] Triantafillou T, Gibson L. Failure mode maps for foam core sandwich beams. Materials Science and Engineering 1987;95:37-53.

[43] Triantafillou T, Gibson L. Minimum weight design of foam core sandwich panels for a given strength. Materials Science and Engineering 1987;95:55-62.

[44] Lingaiah K, Suryanarayana BG. Strength and stiffness of sandwich beams in bending. Experimental Mechanics 1991;31(1):1-7.

[45] Teotokoglou E. Analytical determination of the ultimate strength of sandwich beams. Applied Composite Materials 1996;3:345-353.

[46] Chen C, Harte A-M, Fleck N. The plastic collapse of sandwich beams with a metallic foam core. International Journal of Mechanical Sciences 2001;43(6):1483-1506.

[47] Hoff NJ, Mautner SE. Buckling of sandwich type panels. Journal of the Aeronautical Sciences 1945;12(3):285-297.

[48] Abrate S. Localized impact on sandwich structures with laminated facings. Appl Mech Rev 1997;50(2):69-82.

[49] Schwarts-Givli H, Frostig Y. High-order behaviour of sandwich Panels with a bilinear transversely flexible core, Composite Structures 2001;53(1):87-106.

[50] Koissin V, Shipsha A. Residual dent in locally loaded foam core sandwich structures: analysis and use for NDI. Compos Sci Technol 2008;68:57-74.

[51] Steeves, Fleck NA. Material selection in sandwich beam construction. Scripta Materialia 2004;50:1335-1339.

[52] Petras A, Sutcliffe MPF. Indentation resistance of sandwich beams. Compos Struct 1999;46:413-424.

[53] Frostig Y, Baruch M, Vilnay O, Sheinman I. High-order theory for sandwich-beam behavior with transversely fIexible core. J Eng Mech-ASCE 1992;118(5):1026-1043.

[54] Frostig Y. Classical and high-order computational models in the analysis of modern sandwich panels. Compos Part B 2003;34:83-100.

[55] Petras A, Sutcliffe MPF. Indentation failure analysis of sandwich beams. Compos Struct 2000;50:311-318.

[56] Sokolinsky VS, Shen H, Vaikhanski L, Nutt SR. Experimental and analytical study of nonlinear bending response of sandwich beams. Compos Struct 2003;60: 219-229.

[57] Kim J, Swanson SR. Design of sandwich structures for concentrated loading. Compos Struct 2001;52:365-373.

[58] Shen H, Sokolinsky VS, Nutt SR. Accurate predictions of bending deflections for soft-core sandwich beams subject to concentrated loads. Compos Struct 2004;64:115-122.

[59] Saadati M, Sadighi M. Indentation in lightweight composite sandwich beams. Proc IMechE Part G: J. Aerosp. Eng. 2009;223:825-835.

[60] Abot JL, Daniel IM, Gdoutos EE. Contact law for composite sandwich beams. J. Sandw. Struct. Mater 2002;4(2):157-173.

[61] Koissin V, Shipaha A, Rizov V. The inelastic quasi-static response of sandwich structures to local loading. Compos Struct 2004;64:129-138.

[62] Thomsen OT. Analysis of local bending effects in sandwich plates with orthotropic face layers subjected to localised loading. Compos Struct 1993;25(1-4):511-520.

[63] Thomsen OT. Theoretical and experimental investigation of local bending effects in sandwich plates. Compos Struct 1995;30(1):85-101.

[64] Lee SM, Tsotsis TK. Indentation failure behavior of honeycomb sandwich panels. Compos Sci Technol 2000;60:1147-1159.

[65] Yang M, Qiao P. Nonlinear impact analysis of fully backed composite sandwich structures. Compos Sci Technol 2005;65:551-562.

[66] Soden PD. Indentation of composite sandwich beams. J Strain Anal Eng 1996;31(5):353–360.

[67] Shuaeib FM, Soden PD. Indentation failure of composite sandwich beams. Compos Sci Technol 1997;57:1249-1259.

[68] Minakuchi S, Okabe Y, Takeda N. ‘‘Segment-wise model’’ for theoretical simulation of barely visible indentation damage in composite sandwich beams: Part I-Formulation. Compos Part A 2008;39:133-144.

[69] Lim TS, Lee CS, Lee DG. Failure modes of foam core sandwich beams under static and impact loads. J Compos Mater 2004;38(18):1639-1662.

[70] Sadighi M, Pouriayevali H. Quasi-static and low-velocity impact response of fully backed or simply supported sandwich beams. J Sandw Struct Mater 2008;10(6):499-524.

[71] Rizov VI. Non-linear indentation behavior of foam core sandwich composite materials—A 2D approach. Comp Mater Sci 2006;35:107–115.

[72] Zingone G. Limit analysis of a beam in bending immersed in an elasto-plastic medium. Mechanica 1968;3:48-56.

[73] Green RJ. Penetration of beams on plastic foundation. In *Proc. Am. Soc. Civ Eng. 97*, No. Em6, December 1971, pp. 1769-1772.

[74] Minakuchi S, Okabe Y, Takeda N. ‘‘Segment-wise model’’ for theoretical simulation of barely visible indentation damage in composite sandwich beams: Part II-Experimental verification and discussion. Compos Part A 2007;38:2443-2450.

[75] Gdoutos EE, Daniel IM. Nonlinear stress and deformation behaviour of composite sandwich beams. Applied Mechanics and Materials 2008;13,14:91-98.

[76] Yoon KJ, Kim CK, Park HC. Nonlinear flexural deflection of thermoplastic foam core sandwich beam. J Compos Mater 2002;36(13):1529-1539.

[77] ASTM C365-03, Standard test method for flatwise compressive properties of sandwich cores, ASTM International, December 2003.

[78] Gnip IJ, Kersulis VI, Vaitkus SI, Vejelis S. Assessment of Strength under Compression of Expanded Polystyrene (EPS) Slabs. Materials Science (Medziagotyra) 2004;10:326-329.

[79] Gnip IJ, Kersulis VI, Vaitkus SI. Predicting the deformability of expanded polystyrene in short-term compression. Mechanics of composite Materials 2005;41(2):105-108.

[80] Rizov VI, Shipsha A, Zenkert D. Indentation study of foam core sandwich composite panels. Compos Struct 2005;69:95-102.

[81] Bond-Laminates GmbH, available at: www.bond-laminates.com, last access on October 2010.

[82] IQ Tec Germany GmbH, available at: www.iq-holding.com, last access on October 2010.

[83] Fagerberg L. Wrinkling of sandwich panels for marine applications. Doctoral Thesis (2003); KTH Aeronautical and Vehicle Engineering (ISSN 1651-7660).

[84] Evonik Industries, available at: www.rohacell.com, last access on October 2010.

[85] Zotefoams plc, available at: www.zotefoams.com, last access on October 2010.

[86] AIREX AG, available at: www.corematerials.3acomposites.com, last access on October 2010.

[87] ASTM D 3093/D 3039M-00, Standard test method for tensile properties of polymer matrix composite materials, ASTM International, July 2000.

[88] BS-EN-ISO 14125:1998. Fibre-reinforced plastic composites: determination of flexural properties; British Standard.

[89] Li QM, Mines RAW, Birch RS. The crush behaviour of Rohacell-51WF structural foam. International Journal of Solids and Structures 2000;37:6321-6341.

[90] Branner K. Capacity and lifetime of foam core sandwich structures. Doctoral Thesis (1995); DTU Department of Naval Architecture an Offshore Engineering Technical University of Denmark (ISBN 87-89502 32-9).

[91] UNI EN ISO 3386-1:2000. Materiali polimerici cellulari flessibili, Determinazione delle caratteristiche sforzo-deformazione in compressione, Materiali a bassa massa volumica; Norma Italiana.

[92] ASTM C273-00, Standard test method for shear properties of sandwich core materials, ASTM International, March 2000.

[93] ASTM C393-00, Standard test method for flexural properties of sandwich constructions, ASTM International, April 2000.

[94] Pitarresi G. Private communiacation (2010). Università degli studi di Palermo, dipartimento di Meccanica.

[95] Rizov VI. Elastic–plastic response of structural foams subjected to localized static loads. J Mater Design 2006;27:947-954.

[96] Rizov VI. Low velocity localized impact study of cellular foams. J Mater Design 2007;28:2632-2640.

[97] Rizov VI. Failure behavior of composite sandwich structures under local loading. J Arch Appl Mech 2009;79:205-212.

[98] Mines RAW, Alias A. Numerical simulation of the progressive collapse of polymer composite sandwich beams under static loading. Compos Part A 2002;33:11-26.

[99] MSC Marc technical paper. Nonlinear finite element analysis of elastomers. ©2000 MSC Software Corporation.

[100] Mills NJ, Gilchrist A. Modeling the indentation of low density polymer foams. Cell Polym 2000;19:389-412.

[101] Lyn G, Mills NJ. Design of foam crash mats for head impact protection. The Engineering of sport 2002;4:1-6.

[102] Mills NJ, Fitzgerald C, Gilchrist A, Verdejo R. Polymer foams for personal protection: cushions, shoes and helmets. Compos Sci Technol 2003;63:2389-2400.

[103] Liang G, Chandrashekhara K. Neural network based constitutive model for elastomeric foams. J Eng Struct 2008;30:2002-2011.

[104] Ogden RW. Recent advances in the phenomenological theory of rubber elasticity. Rubber Chemistry and Technology 1986;59:361-383.

[105] Mullins L. Effect of Stretching on the Properties of Rubber. Journal of Rubber Research 1947;16:275–289.

[106] Ogden RW, D. G. Roxburgh. A Pseudo-Elastic Model for the Mullins Effect in Filled Rubber. Proceedings of the Royal Society of London, Series A 1999;455:2861–2877.

[107] Dorfmann A, Ogden RW. A constitutive model for the Mullins effect with permanent set in particle-reinforced rubber. International Journal of Solids and Structures 2004;41:1855-1878.

[108] Ugural AC. Stresses in plates and shells. Singapore: McGraw-Hill International Editions;1999.